AN EVALUATION OF 1-3 CONNECTIVITY COMPOSITE TRANSDUCERS FOR AIR-COUPLED ULTRASONIC APPLICATIONS

Anthony Gachagan

Submitted in December 1996
for the degree of Doctor of Philosophy

Ultrasonics Research Group
Department of Electronic and Electrical Engineering
The University of Strathclyde
204 George Street, Glasgow, G1 1XW
Scotland, United Kingdom

LIST OF CONTENTS

ACKNOWLEDGEMENTS

I would like to thank my supervisor Professor Gordon Hayward, founder of the Ultrasonics Research Group at the University of Strathclyde, for his guidance, support and patience throughout the duration of this Thesis. Initially, I was employed to bolster the URG football squad (and occasionally, research into air-coupled ultrasound). Although initially successful (without Gordon's presence in the team), I now find myself in the position where I cannot guarantee selection in the old crock's team. This spiralling downfall should be attributed to years of great managerial and tactical advice from Gordon Hayward.

Within the Ultrasonics Group, three subgroups have evolved and require separate thanks :

- *the first airborne division consists of Stephen Kelly (master of the capacitive transducer and a bad influence on social occasions), Walter Galbraith (the hydrophone guru and calming influence both on and off the field), Roger Farlow (an expert in electronics, but usually only for two days a week) and Graham Benny (the baby of the group, but a major contributor with beam profiling and beer analysis).*
- *from the other members of the group (riff-raff), specific thanks must go to Jeremy Bennett, Paul Reynolds and Phillipe Perrot for assistance above and beyond the call of duty. Mention has to be made of the good friendships that have developed with both past and present group members, who have collectively ensured a special environment in which to escape from the pressures of Thesis writing and work.*
- *thanks also to both Tommy McCunnie and George Brown for their manufacturing skill and expertise and for supporting my legendary claim to be 'practically stupid'.*

Outwith the University, I would like to thank John McGarritty for his timely intervention in 1991, when he introduced me to Gordon Hayward and for encouragement to complete this Thesis. Also, thanks to Professor David Hutchins and Bill Wright, at Warwick University, for utilising several of my piezocomposite designs in their experiments.

Special thanks must go to my wife, Carole, for her neverending support and supply of encouraging sarcastic comments. Together with our baby daughter, Jodie, they may have prolonged the writing of this Thesis, but they have ensured I had a damn good time away from the pressures of work. Also, thanks to my mum, dad, Margaret Anne, Richard and Patricia for all their support and encouragement throughout my life.

ABSTRACT

Conventional ultrasonic non-destructive evaluation techniques require some form of liquid coupling between the piezoelectric transducer and the sample under inspection to facilitate mechanical energy transfer. Under automated conditions, maintaining a consistent couplant layer can constitute a problem and is manifest in slower scanning rates. To improve scanning speed the ultrasound should ideally propagate across an intermediate airgap. This possibility has been inhibited by the lack of a suitable transducer technology to overcome the practical difficulties inherent in the air medium. The large acoustic impedance mismatch, between a piezoelectric element and air, and the large air attenuation factor ensures both poor sensitivity and resolution characteristics. This Thesis advances transducer technology, enabling these problems to be challenged effectively.

Initially, the Thesis describes the creation of a wideband characterisation methodology for air-coupled ultrasonic transducers operating in the range 100kHz - 2MHz. The proposed technique utilises piezopolymer transducers in both transmission and reception modes and despite the obvious measurement difficulties, good agreement between theory and experiment is illustrated. Results are presented on the characterisation of both electrostatic and 1-3 connectivity piezocomposite devices, in which the inherent narrowband nature of the piezocomposite transducer demonstrates considerable potential for airborne applications. Subsequently, the performance of air-coupled 1-3 connectivity piezocomposite transducers is investigated using both uni-dimensional and finite element modelling techniques. Experimental verification of these techniques enables the finite element approach to be used as the benchmark for evaluation of practical transducer configurations. Consequently, a series of design guidelines are presented for practical air-coupled composite transducer systems. For many applications, the conventional method to improve system resolution, through attachment of a backing block, produces an unacceptably low system sensitivity. Hence, an alternative approach is proposed, utilising strong coupling between the fundamental thickness mode and the first lateral resonance in a 1-3 piezocomposite. Finite element analysis has been employed in the design of a laterally-coupled composite receiver and a -6dB bandwidth of 150% at a centre frequency of 1MHz is presented. Finally, the new transducer design techniques were applied to three different airborne non-destructive testing applications. Successful detection of various defects in carbon-fibre reinforced composite plates is demonstrated.

LIST OF SYMBOLS

The following is a list of symbols referred to throughout this Thesis. All symbols relating to piezoelectric operation comply with the IEEE standard on piezoelectricity [1]. Localised expressions are defined in the text as required.

Symbol	*Definition*	*Unit*
c_{xy}	*elastic stiffness constant*	*Pa or* Nm^{-2}
e_{xy}	*piezoelectric stress constant*	Cm^{-1}
h_{xy}	*piezoelectric charge constant*	Vm^{-1} *or* NC^{-1}
k_{xy}	*piezoelectric coupling coefficient*	
k_t	*thickness mode coupling coefficient*	
f_n	*frequency of minimum impedance*	*Hz*
f_m	*frequency of maximum impedance*	*Hz*
$\varepsilon^S_{33}/\varepsilon_0$	*relative dielectric constant, laterally clamped*	
ε	*permittivity*	Fm^{-1}
ε_0	*permittivity of free space*	$8.854x10^{-12}$ Fm^{-1}
C_0	*transducer static capacitance*	*F*
Z_A	*specific acoustic impedance*	*MRayl*
Y	*Young's modulus*	Nm^{-2}
σ	*Poisson Ratio*	
ρ	*density*	kgm^{-3}
f	*frequency*	*Hz*
λ	*wavelength*	*m*
c	*speed of sound*	ms^{-1}
v_l	*mechanical bulk wave velocity in the thickness direction*	ms^{-1}
P	*pressure*	*Pa or* Nm^{-2}
T	*temperature*	*K*
α	*attenuation*	Npm^{-1} *or* dBm^{-1}
F	*force*	*N*
t	*time*	*s*
T_T	*transducer thickness transit time*	*s*

Symbol	*Definition*	*Unit*
I	*current*	A
V	*voltage*	V
C	*capacitance*	F
L	*inductance*	H
R	*resistance*	Ω
Z	*impedance*	Ω
S_{RX}	*receive sensitivity of the transducer*	VPa^{-1}
S_{TX}	*transmit sensitivity of the transducer*	PaV^{-1}

Superscripts :

^{D} *: constant electric displacement*

^{E} *: constant electric field*

^{S} *: constant strain conditions*

Axis convention :

The following axis convention has been used throughout this Thesis and is relevant to the 'xy' subscript in the above symbol list.

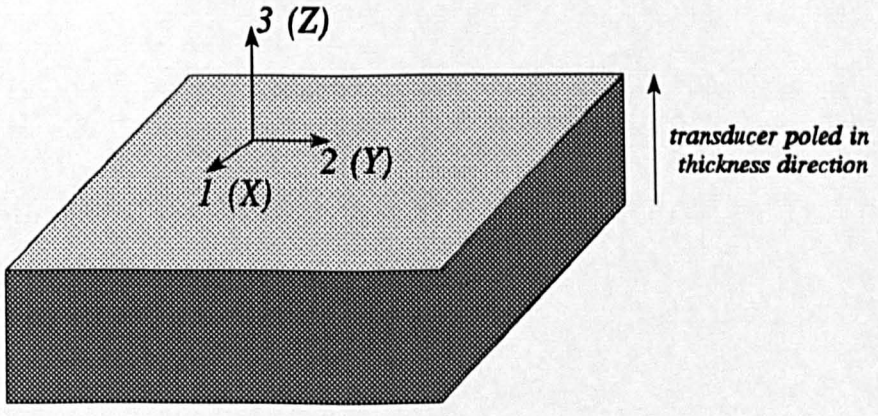

1 and 2 are 'lateral' directions
3 is the 'thickness' direction

CHAPTER 1

INTRODUCTION

ABSTRACT

The requirement for ultrasonic techniques applicable to through air operation, and a brief synopsis of the fundamental difficulties in the design of robust and reliable airborne ultrasonic systems are described. Within this context, the aims of this Thesis and subsequent contributions to the field of airborne ultrasound are presented. Finally, a short overview of the content of each Chapter is presented.

1.1 BACKGROUND

Ultrasonic techniques have found widespread application in the fields of non-destructive evaluation (NDE), biomedical analysis, materials characterisation and underwater systems. Indeed, this brief list may be extended to encompass general instrumentation, whenever the generation and detection of mechanical energy is required. In the case of NDE, there is an increasing requirement for more rapid and accurate inspection of component structures, often in conjunction with a high degree of automation. Examples include the aerospace, nuclear and nautical industries, where detailed manufacturing and in-service inspections of relatively large samples are necessary. Conventional ultrasonic NDE, involving some form of piezoelectric transducer, requires a thin film of liquid coupling fluid between probe and test specimen to facilitate mechanical energy transfer. The requirement for adequate couplant monitoring and fluid irrigation, while maintaining close probe contact, can often constitute a restricting factor, especially under automated conditions. In many cases, the alternative solutions are impractical. These include immersion testing, whereby the probe and test specimen are inserted in a fluid bath, or the use of a localised water jet for the provision of an acoustic path between probe and sample.

Ideally, the ultrasonic energy should propagate over an intermediate air gap which may be varied according to surface geometry and scanning application. However, with conventional piezoceramic probes, the resultant sensitivity and resolution is extremely poor, as a result of attenuation in air and the mechanical mismatch at the transducer and test component air boundaries. Alternative technologies such as optical or magnetic generation and detection of ultrasonic energy may suffer additional restrictions. Most recent developments in through air transducer technology have involved improving existing piezoceramic, piezopolymer and electrostatic transducer configurations.

The primary limitation in an air-coupled piezoelectric system is the energy losses which arise as a consequence of the large acoustic impedance mismatch at the transducer/air and air/sample boundaries. Figure 1.1 illustrates this problem at the four principal

boundaries for a conventional piezoceramic air-coupled through-transmission system. The insertion loss for this system can be calculated from the product of transmission and reflection coefficients at each boundary [2]. For the solid/air boundaries shown in the Figure, an insertion loss of -173dB can be calculated. This figure demonstrates an approximate 140dB reduction in system sensitivity when compared to an identical configuration operating under water load. Also, many NDE applications involve minimum scan speed criteria, which necessitates an ultrasonic system to operate without recourse to signal averaging or any off line post-processing techniques to maximise system signal-to-noise ratio. This problem is accentuated through the slow velocity of sound in air, compared to conventional liquid or gel coupling, which is manifest in extended propagation delays between the transmit and receive elements of a NDE system. Consequently, data should be acquired under single shot conditions. This requires a good signal-to-noise ratio (SNR) for the detected signal, but the combination of the acoustic mismatch problem and the large airborne attenuation factor [3], especially at frequencies in the Megahertz range, inevitably creates poor SNR conditions.

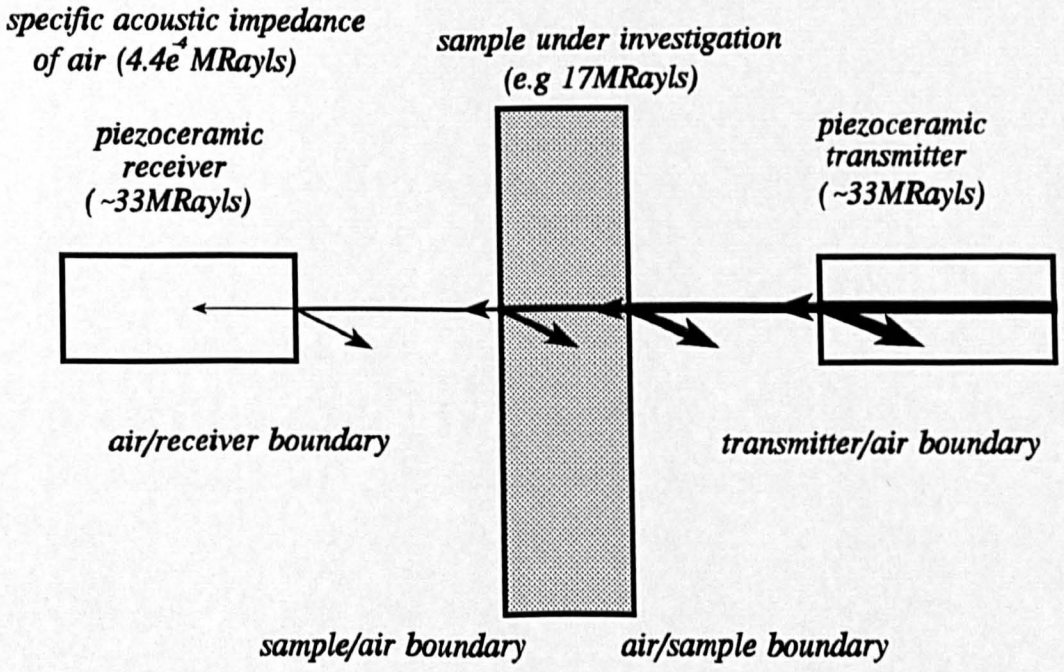

Figure 1.1 Influence of losses at solid/air boundaries for a piezoceramic NDE system

The low SNR conditions inherent in an air-coupled ultrasonic system cannot be recovered by improvements in transducer technology alone, but a comprehensive evaluation of each component in the ultrasonic system is required. Thus, advances in appropriate transducer technology, techniques to improve the acoustic impedance mismatch at the transducer/air boundaries and the design of dedicated transmission and reception circuitry must be considered collectively. This Thesis addresses the transducer problem, specifically involving 1-3 piezocomposite configurations, comprising an array of active piezoceramic rods embedded within an inactive polymer phase.

1.2 Aims and Contributions of Thesis

1.2.1 Aims of Thesis

- To develop a characterisation technique for air-coupled transducers, using standard laboratory equipment. This technique should provide the capability to:
  - provide standard characterisation data to enable comparison between various transducer technologies. This necessitates the acquisition of the transmit voltage response and open circuit voltage response for devices operating in either transmission or reception mode, respectively.
  - calculate the system insertion loss for practical transducer arrangements.

- Evaluate the 1-3 connectivity piezocomposite transducer technology for practical airborne applications.

- Investigate the design of a wideband air-coupled ultrasonic receiver with sufficient bandwidth to complement the high resolution afforded by laser generation.

- Demonstrate practical applications for the theoretical air-coupled transducer designs introduced in this Thesis.

1.2.2 Contributions to the Field of Airborne Ultrasound

- A versatile methodology is presented for the characterisation of the impulse response for air-coupled transducers operating in the frequency range 50kHz - 2MHz. This technique utilises broadband piezopolymer transducers for the transmission and reception of airborne ultrasound. Close correlation between experimental and simulated responses, incorporating the influence of airborne attenuation, substantiates this as a practical technique for the comparison of different air-coupled technologies.

- An experimental approach to measure the two-way system insertion loss for practical air-coupled pitch-catch transducer configurations is proposed. This measurement technique includes the influence of airborne attenuation and therefore is directly representative of the realistic system performance for air-coupled NDE applications.

- A combination of theoretical modelling and experimental analysis is used to predict and assess the performance of 1-3 piezocomposite transducers for operation in an air-coupled environment. Both finite element and uni-dimensional techniques are employed to evaluate transmission and reception characteristics, including the influence of mechanical matching and damping, over the complete volume fraction range, for operating frequencies in the region of 500kHz. Subequently, this modelling approach is utilised to produce a set of practical design guidelines for 1-3 composite transducers for airborne applications.

- A wideband 1-3 connectivity piezocomposite receiver has been designed by utilising a unique property of the transducer structure, whereby close coupling between the fundamental thickness and first lateral resonances effectively extends the bandwidth. The performance of the laterally-coupled composite receiver is shown to compare favourably with a conventional wideband electrostatic transducer.

- The 1-3 connectivity piezocomposite transducer design guidelines presented in this Thesis have been incorporated into three practical non-destructive evaluation applications. These systems demonstrate the successful detection of defects in carbon-fibre reinforced polymer composite materials, as found in the aerospace industry.

1.2.3 Publications to Date Arising as a Result of this Thesis

(a) Journal Publications

Gachagan A, Hayward G, Kelly SP, Galbraith W, 'Characterisation of air coupled transducers', IEEE Transactions on Ultrasonics Ferroelectrics and Frequency Control, 1996, Vol 43(4), pp 678-689

Hayward G and Gachagan A, 'An evaluation of 1-3 connectivity composite transducers for air coupled applications', Journal of the Acoustical Society of America, Vol 99(4), 1996, pp 2148 - 2157

Wright WMD, Hutchins DA, Hayward G and Gachagan A, 'Polymer composite material characterisation using a laser/air-transducer system', Ultrasonics, 1996, Vol 34(8), pp 825-833

Hutchins DA, Wright WMD, Hayward G, Gachagan A, 'Air-coupled piezoelectric detection of laser-generated ultrasound', IEEE Transactions on Ultrasonics Ferroelectrics and Frequency Control, 1994, Vol.41, No.6, pp.796-805

(b) Conference Proceedings

Wright WMD, Hutchins DA, Hayward G and Gachagan A, 'Ultrasonic imaging using laser generation and piezoelectric air-coupled detection', Ultrasonics, Vol 34(2-5), 1996, pp405-409

Wright WMD, Hutchins DA, Gachagan A, Hayward G, 'Evaluation of fiber-reinforced composites using noncontact laser air-transducer system', Review of Progress in Quantitative Nondestructive Evaluation, 1995, Vol.14, Ch.312, pp.1333-1340

Gachagan A, Bennett JT, Hayward G, 'A finite-element modelling approach into the influence of mechanical matching and damping in 1-3 piezocomposites', Proceeding of IEEE Ultrasonics Symposium, Cannes, 1994, pp.995-998

Gachagan A, Galbraith W, Hayward G, 'Wide-band characterization of air coupled transducers', Proceeding of IEEE Ultrasonics Symposium, Cannes, 1994, pp.483-486

Gachagan A, Hayward G, Wright WMD, Hutchins DA, 'Air coupled piezoelectric detection of laser-generated ultrasound', Proceeding of IEEE Ultrasonics Symposium, Baltimore, 1993, pp.651-654

Hayward G, Gachagan A, Hamilton R, Hutchins DA, Wright WMD, 'Ceramic-epoxy composite transducers for noncontacting ultrasonic applications', New Developments in Ultrasonic Transducers and Transducer Systems, 1992, Ch.29, pp.49-56

1.3 Overview of Thesis

Chapter 2 : Air Transducer Technology

This Chapter presents a review of several air transducer technologies and appraises the individual attributes of each approach. From this review, electrostatic and 1-3 connectivity piezocomposite designs are considered as the two principal candidates for the airborne applications. Subsequently, a theoretical evaluation of the fundamental properties of 1-3 connectivity piezocomposite transducers illustrates their suitability for application into low acoustic impedance media. The manufacturing processes used to construct these two transducer designs are described.

Chapter 3 : Characterisation of Air-Coupled Transducers

This Chapter describes a theoretical and experimental study for determination of the through-air system impulse response and insertion loss characteristics for air-coupled transducers. Wideband piezopolymer transducers (PVDF) were designed to operate in both transmission and reception modes and very close agreement between experimental and uni-dimensional modelling results are reported. An investigation into the field profile for air-coupled disc transducers illustrates that the peak value of the spatial response does not correspond to the magnitude of the conventional near-far field boundary. This peak magnitude occurs at a position closer to the source and is considered to be more realistic, from a practical applications viewpoint, for the air separation distance utilised in the characterisation process. Subsequently, the wideband response for a selection of 1-3 connectivity piezocomposite and electrostatic transducers were evaluated. To complement the investigation, relative performances for narrowband operation are also presented under transmission and transmit-receive conditions. The methodology is shown to provide a convenient and robust procedure for comparison of through-air transducers operating in the frequency range 50kHz to 2 MHz. The practical considerations reported in this Chapter are applied to all experimentation in the remainder of the Thesis.

Chapter 4 : A Theoretical Evaluation of 1-3 Connectivity Composite Transducers

A combination of theoretical modelling and experimental analysis is used to predict and assess the performance of 1-3 composite transducers for operation in an air-coupled environment. Specifically, finite element analysis, supported by linear systems modelling, is employed to evaluate transmission and reception characteristics over the complete volume fraction range, for operating frequencies in the region of 500kHz. The theoretical approach is then extended to assess the influence of mechanical matching and backing on transducer sensitivity and bandwidth, with a view towards verifying the models for more practical arrangements. Generally, the finite element technique is shown to agree well with, and hence confirm, the linear systems approach. Where this is not the case, the former is used as the benchmark for experimental comparisons.

Chapter 5 : Improving the Bandwidth of 1-3 Connectivity Composite Receivers using Mode Coupling

An novel approach to extend the bandwidth of 1-3 piezocomposite transducers is proposed utilising strong coupling between the fundamental thickness mode and the first lateral resonance. Finite element modelling techniques are employed to evaluate the influence of mode coupling on the electromechanical coupling factor, surface dilation quality and transducer receive sensitivity and bandwidth. The theory is verified under water loaded conditions and then extended to air-coupled composite transducer designs. A laterally-coupled composite receiver is constructed and its air-coupled performance assessed using a thickness mode composite and a wideband electrostatic device.

Chapter 6 : Through Air Applications for 1-3 Piezocomposites

This chapter describes three examples of NDE systems to which air-coupled 1-3 connectivity piezocomposite transducers have been applied. A pulsed laser has been used to generate ultrasonic transients in samples of metal and fibre-reinforced polymer composite material. These have been detected using both thickness mode and laterally-coupled composite designs and examples of imaged defects in polymeric materials are given. Two rapid scanning systems have incorporated piezocomposite transducer technology for NDE applications. An air-coupled composite transduction system has

been utilised for the generation and detection of Lamb waves. Through which, real-time images of defects in both metallic and carbon-fibre plates have been produced. The second application is a prototype through-transmission system to investigate defects in a variety of composite materials.

Chapter 7 : Conclusions and Suggestions for Further Work

The Thesis ends with a review of the conclusions from each Chapter. Subsequently, from the foundation of the work presented in this Thesis, a collection of suggestions for further work is proposed.

CHAPTER 2

AIR TRANSDUCER TECHNOLOGY

ABSTRACT

There are at present various transducer designs proposed for the generation and detection of ultrasonic energy in an air-coupled environment. Therefore, work in this field has encompassed several technologies : piezoceramic, piezopolymer, piezocomposite, electrostatic, optical and magnetic. These devices have been utilised in proximity sensing, thickness gauging and non-destructive evaluation for a diverse range of materials. This Chapter will present a review of these air transducer technologies, evaluating the individual attributes of each approach. Electrostatic and piezocomposite designs are considered as the two principal candidates for the airborne applications. Subsequently, a theoretical evaluation of the fundamental properties of 1-3 connectivity piezocomposite transducers will illustrate their suitability for application into low acoustic impedance media.

2.1 REVIEW OF AIR-COUPLED ULTRASOUND

2.1.1 Piezoceramics

(a) Applications in Non-Destructive Evaluation

Conventional piezoceramic transducers have been described for application in general NDE [4], non-contact thickness measurements [5], non-destructive inspection of composite materials [6,7] and paper roughness measurements [8]. Deka utilised a double matching layer composition, using low density polystyrene foam as the outer layer [4]. Operating at a frequency of 450kHz, a pitch-catch transducer arrangement was described through which several NDE applications were demonstrated : the detection of holes and a major delamination in a rolled aluminium sheet; Lamb wave techniques were utilised to detect delaminations and resin rich areas in steel sheets ; and proximity sensing and gauging using a low excitation voltage (10V). Yang et al described the use of a 1MHz air-coupled transducer to measure the thickness of paint coating for use in the automobile industry [5]. Under pulse-echo conditions, the transducer resolved the paint thickness to within 25μm. Both Rogovsky [6] and Chimenti and Fortunko [7] have illustrated the application of focused piezoelectric transducers for non-destructive evaluation of composite materials. Neither paper detailed the design of the transducer employed for their study, but the results reported are considered important. Both these papers imply that piezoceramic transducers were used and hence, their work is included within this section. Rogovsky utilised both dry-contact and air-coupled systems to evaluate the integrity of 0.5 - 6.0cm thick composite plates [6]. A through transmission system using wheel probes was shown to detect defects, with dimensions 0.5cm diameter, at an operating frequency of 600 - 700 kHz, although the scanning speed was low (6-10cms^{-1}). The air-coupled transducer systems used both through transmission and single sided pitch-catch configurations, at an operating frequency of 400kHz. The systems operated with increased scan speeds (25-50cms^{-1}), which is comparable to a water jet NDE system, and detected defects down to 6.35mm diameter. Chimenti and Fortunko [7] demonstrated the NDE of pre-impregnated graphite-epoxy lamina (approximately 0.15mm thick) using a pair of air-coupled 500kHz focused piezoelectric transducers, in a through transmission configuration. Results were presented in which

the quality of the 'prepreg' was determined as a function of the adhesion between the epoxy and the graphite fibres. Also, an interesting proposal to increase the energy transfer into the sample was described. A 25dB enhancement in energy transfer was predicted by transmitting the ultrasound at an angle and matching the phases of the incident longitudinal wave and the generated plate wave in the sample. Focussed transducers were also utilised by Stor-Pellinen and Luukkala to measure paper roughness [8]. This technique employed a pulse-echo transducer configuration, operating between 500kHz and 4MHz, where paper roughness was calculated from the reduction in amplitude of the detected signal.

(b) Methods to Improve the Acoustic Impedance Mismatch

Thickness mode piezoceramic transducers possess a specific acoustic impedance of approximately 33MRayl which results in a large acoustic impedance mismatch for airborne applications (the specific acoustic impedance of air is 430Rayl). The sensitivity of these devices can be enhanced by the application of mechanical matching layers to the transducer front face. Such matching layer configurations can be designed using Equation 2.1, where Z_A is the specific acoustic impedance of the transducer, Z_L is the specific acoustic impedance of the load medium and Z_{iOPT} is the specific acoustic impedance of the i^{th} layer of an n-layer matching set [9].

$$Z_{iOPT}=(Z_A^{(n+1-i)}.Z_L^{i})^{\frac{1}{n+1}} \qquad \textbf{(2.1)}$$

For a single matching layer condition, the intermediate matching material should possess a specific acoustic impedance of 0.12MRayl. Available materials with an acoustic impedance close to this value, e.g. balsa wood or cork [10], are highly attenuative. Therefore, partial matching is the preferred approach in practise. Fox et al [11,12] bonded RTV silicone rubber, specific acoustic impedance of approximately 1.0MRayl, onto PZT5H piezoceramic. Acoustic range measurement systems with operating frequencies of 1, 2 and 8MHz were described. The lower frequency devices operated over a 400mm range with an accuracy of ±0.5mm. Whereas, the 8MHz transducer operated over a range of 0.5mm, with a resolution of 0.2μm, and employed an angled buffer, attached between the front face and the matching layer, to increase transducer

bandwidth by inhibiting reflections from re-entering the piezoceramic. To improve the accuracy of measurement based upon time of fight criteria, Hickling and Marin [13] compensated for the dependence of the speed of sound with variation in temperature and perpendicular distances up to 250mm were measured with an accuracy of ±0.1mm.

The problems associated with the manufacture of a material with an acoustic impedance lower than 1.0MRayl has been addressed by several research groups. One methodology through which this has been achieved being the introduction of pockets of air into a material possessing a relatively low acoustic impedance, between approximately 1-3MRayl. The problem associated with this method is that the attenuation and/or scattering of the ultrasonic signal in the material is significantly increased. Yano et al [14] loaded the RTV silicone rubber material with a low density microshpere filler, producing a material with a specific acoustic impedance of 0.3MRayl. This material was utilised as the outer layer in a double matching layer configuration, where the intermediate layer had an acoustic impedance of 5MRayl. Khuri-Yakub et al [15] utilised a similar transducer configuration and proposed the use of silica aerogels, measured acoustic impedance of 0.1MRayl, for further transducer designs. Similarly, Gerlach et al [16] suggested the employment of SiO_2 aerogels and supported the suggestion that a 0.1MRayl material could be fabricated. This paper discussed the use of matching layers with an acoustic impedance gradient, that is, the acoustic impedance of the transducer at one end reducing to the load media at the other. Unfortunately, their application had a medical basis and the matching layer presented was matched to human skin, i.e 1.5MRayl. Although silica aerogels have an excellent potential, Schiller et al reported that very careful handling is necessary and manufacturing is expensive for the tolerances required for construction of good matching layers [10]. Both Schiller et al [10] and Stor-Pelinen et al [17] have utilised balsa wood matching layers, which has a specific acoustic impedance of 0.08MRayl. However, the acoustic matching benefit is compromised by the high attenuation in this material. More recently, developments by Fletcher and Thwaites [18] and Haller and Khuri-Yakub [19] have utilised improved manufacturing approaches to introduce a regular array of air pores into a material. The former proposed a regular array of horn shaped air paths through a low acoustic

impedance material. This design reduced the acoustic impedance of the material, whilst providing acoustical amplification for the sound pressure wave. However, this approach was limited by the manufacturing process utilised, restricting the manufacture of multi-horn matching plates to an operating frequency of 100kHz. The latter approach utilised a micromachined 1-3 Kapton/air composite material, capped at both faces using 56μm tape. In contrast to the former technique, matching layers for operation at frequencies around 1MHz are attainable by this approach. It was suggested that by adjusting the volume fraction to approximately 0.05%, a 0.1MRayl matching layer could be fabricated. Although this value was not realised, a 2dB improvement was shown by a manufactured 1-3 Kapton/air composite layer over a reference PZT5H transducer incorporating a RTV silicone rubber matching layer. In common to all of these techniques is the requirement for good and reliable bonding techniques when applying these layers, as discussed in [17].

The acoustic mismatch problem associated with piezoceramic transducers has encouraged several other methods to facilitate energy transfer into air. Kiełczyński et al [20] fabricated a transducer by embedding a piezoceramic ring in a low impedance elastic material. Thus both the thickness and radial vibrations of the ring couple into the elastic material, where the amplitude of the vertical vibrations on the radiating surface reaches a maximum in the centre of the disc. These devices operated below 250kHz, but demonstrated good bandwidth. The addition of a radiating membrane, Babič [21], to the cylindrical part of a ceramic disc was utilised to couple the radial vibrations into transverse vibrations on the front membrane. The membrane employed was described as an aluminium can, with a wall thickness of 1mm, surrounding a ceramic disc and produced a multi-modal transducer operating around 200kHz. Okada et al described a technique to improve the output drive performance for ultrasonic distance sensors, operating between 20 - 40 kHz [22]. An annular piezoceramic element is used to relieve the strain between the active ceramic and the passive vibration metal plate, when driven under high voltage. An exponential horn, bonded onto the vibration plate, was utilised to amplify the radiated sound. This design was reported to increase the maximum sound pressure levels by between 5 - 20dB, compared to commercially available transducers.

Dabirikhah and Turner [23] proposed a design similar to that of Babič, where a passive polymer is formed into a conical shell and bonded to a ceramic disc or ring. By appropriate choice of wall thickness and cone angle, vibrations in the ceramic are coupled into the cone in the form of plate wave or Lamb modes. The devices can be designed to operate at the thickness or radial mode associated with the ceramic and have been shown to transmit and receive a 1.2MHz ultrasonic signal across a 45mm airgap. Seyed-Bolorforosh described a novel approach in which a piezoelectrically inert 1-3 connectivity composite matching layer was manufactured in the host piezoceramic block [24]. This integrated construction method was intended to find application as a medical ultrasonic transducer and would not be applicable for air-coupled work due to the minimum achievable acoustic impedance for the matching layer being constrained by the mechanical properties of the polymer filler phase.

The above methodologies have been proposed to enhance the acoustic energy transfer between a piezoceramic element and an air load. However, they can also be employed for most piezoelectric technologies which may exhibit better acoustic matching to air, relative to the high specific acoustic impedance of the piezoceramic.

2.1.2 Piezopolymers

Piezopolymer materials offer attractive options for airborne ultrasound by means of improved mechanical matching, good bandwidth potential, and the ability to be configured as a flexible membrane. The main restriction to the use of piezopolymer is the low dielectric constant ($\varepsilon_r \approx 10$) and electromechanical coupling co-efficient ($k_t \approx 0.2$) associated with this material resulting in poor transmission performance. However, the lightweight nature of the material supports its use in acoustic ranging and imaging for robotics applications. Schoewald and Martin [25] utilised 110μm thick polyvinylidene flouride (PVDF) film to produce a 1cm x 2cm transducer operating below 20kHz. Recently, Fiorillo has employed PVDF for robotic applications, where the operational frequencies of the transducers have been increased up to 380kHz [26]. Differing design approaches have been utilised to enhance the performance of PVDF : the use of multi-layered piezopolymer assemblies was estimated to increase system sensitivity [27] ; and

an array of PVDF elements, constructed to operate at two distinct frequencies (60 and 86 kHz), was shown to enhance spatial resolution when compared to images obtained from analogous single operating frequency devices [28].

2.1.3 Optical Methods

Optical methods of generating and detecting ultrasonic energy can theoretically provide better accuracy and resolution because the optical wavelengths are significantly smaller than those attainable by ultrasound propagating through an air medium. This improvement is due to the highly attenuative nature of air restricting the operating frequencies of ultrasonic propagation of more than a few millimeters to below 2MHz and the lesser effect of variations in temperature, pressure and humidity in the propagating channel on optical methods. Unlike conventional techniques, for optical based ultrasound both the efficiency of the transduction process and the spatial distribution of the resulting ultrasonic waves are strongly influenced by the characteristics of the material being inspected.

Laser generated ultrasound is well documented as a good wideband source of ultrasonic energy [29,30]. The main two methods of producing ultrasound are thermoelastic generation, where a substrate is heated in a transient fashion, and ablation, where a coating applied to the surface prior to irradiation is evaporated. The former is considered a good source of shear energy, whereas the latter produces higher amplitude longitudinal waves. The detection of ultrasound is achieved through interferometric methods, where mechanical displacement on the surface of the sample is converted into an electrical signal [31,32]. The sensitivity of these detectors is strongly dependent on the quantity of light that is reflected from the material surface. However, even with a highly polished, highly reflective surface these devices are not as sensitive as conventional piezoceramic transducers [33]. Therefore, fundamentally, these systems are limited by the requirement for a highly absorptive surface during ultrasonic generation and a reasonably reflective surface for ultrasonic detection.

The research effort into optical methods of ultrasonic generation/detection has focused

mainly on the non-destructive evaluation of composite materials commonly found in the aerospace industry : Monchalin described laser generation and detection of ultrasound for on-line thickness gauging in the steel industry and inspection of contoured composite panels [34] ; and Dewhurst et al have utilised a through transmission system and employed digital signal processing techniques to detect 3mm x 3mm defects in 10mm thick carbon fibre composite materials [35]. Sensitivity improvements for optical systems have been suggested by narrowing the bandwidth of the generated ultrasonic wave using a tone burst of laser pulses [36] or by using an array of optical fibres through which shear and surface ultrasonic waves could be generated [37].

Conventional NDE techniques, utilising optical technology, require the sample under consideration to be moved and the transmission/detection system to be fixed [35,38]. This could restrict their scope for NDE applications. However, McKie et al [39] have designed a system incorporating a mirror within the scan head to allow rapid scanning of composites. Here, variations in the angle of the mirror manoeuvre the incident laser pulse across the sample and subsequently, the reflected pulse is deflected back to a receiving interferometer system. Thus, large areas of composite can be scanned without the necessity to move either the optical system or the sample. In addition, an enhancement in system performance has been achieved through the suppression of 'scanning noise', which has been characterised by unpredictable variations in the sensitivity of the receiver system. However, it should be noted that the experiments described in this paper utilised a paint coating on the surface of the sample to improve signal-to-noise ratio (SNR).

2.1.4 Electrostatic Transducers

Electrostatic or capacitive transducers possess considerable potential for airborne operation, since the vibrating membrane is well coupled to the load medium. They consist of a metallised polymer membrane, stretched across a conductive backplate, to which a bias voltage is usually applied. This voltage draws the film tightly over the backplate resulting in pockets of air trapped between the membrane and the backplate. Under application of an AC stimulus, these air pockets can be forced to vibrate through

which the generation of ultrasound is realised. They demonstrate good bandwidth potential due to their non-resonant nature and a high degree of damping between the membrane and the backplate. Another prominent feature is that these transducers are essentially reversible, in that they exhibit an equivalent performance characteristic when operating either in transmission or reception [40]. In the design of a capacitive transducer, the membrane film thickness, bias voltage and the quantity, dimensions and distribution of the air pockets dictate the beam profile, frequency response and sensitivity of the device [40,41]. As a consequence, the transducer design engineer has difficulty interpreting the interplay of the various operating mechanisms. Although potential modelling approaches have been proposed, there is a lack of a definitive strategy : Mattila et al represented the transducer (with v-grooved backplate) as an electrical equivalent circuit and predicted transmission, reception and pulse-echo performance characteristics at an operating frequency of approximately 50kHz [42] ; finite element modelling has been used to estimate the transducer resonant frequency (again with v-grooved backplates) to a reasonable degree of accuracy, although bandwidth was significantly underestimated [43] ; Haller and Khuri-Yakub extended Mason's theory to account for the geometry of their micromachined device and the resultant equivalent circuit was used to predict electrical impedance, displacement at the front face and insertion loss [44] ; and through using an electrical equivalent circuit and incorporating mechanical stiffness effects, electrical admittance and transmit sensitivity have been predicted to within 10% of experimentally measured results over the frequency range 50 - 500kHz [45].

Repeatability in manufacture is of primary importance with regard to formulating a theoretical analysis for electrostatic transducers. This has been achieved through several approaches in which the backplate has been designed to comprise of a specific pattern of air pockets : Mattila et al [42] and Rafiq and Wykes [46] have utilised periodic 'v' shaped grooves ; Suzuki et al [47], Schindel et al [40], Haller and Khuri-Yakub [44] and Anderson et al [45] have used micromachining techniques ; and Hutchins et al [48] have utilised a laser-machined aluminium backplate.

A significant proportion of the work presented has employed electrostatic transducers with operational centre frequencies of 100kHz [42,46] and 500kHz [45,49], where approximately a 100% bandwidth, measured at the -6dB points, has been attained. At these frequencies the transducers have sufficient sensitivity to permit their application in an air-coupled environment. However, very recent micromachined devices have been reported with operating frequencies in the 1 - 10MHz range. Schindel and Hutchins have demonstrated the employment of a capacitive device, with a -6dB bandwidth between 170kHz and 1.9MHz, for various measurements and NDE applications [50]. These authors also reported an electrostatic transducer, comprising of 2.5μm Mylar film, operating at frequencies beyond 4MHz [40]. Although it should be noted that the fragile nature of this thin membrane demands great care for both handling and operation and consequently, questions its operational robustness in industrial environments. Haller and Khuri-Yakub described the manufacture of a 1.9MHz device using silicon surface micromachining [44]. This device was reported to operate with a slightly higher insertion loss compared to a conventional piezoceramic device, but with a better bandwidth characteristic. Although, it should be noted that the measured bandwidth of 20% is low when compared to other capacitive transducer designs. Ladabaum et al [51] have reported electrostatic transducers operating up to 11MHz, using the fabrication techniques described by Haller and Khuri-Yakub [44]. The large air attenuation factor in the megahertz frequency range, between 75 and 85 dB/mm at 20MHz [52], may inhibit their practicality for NDE applications and hence, the realistic operating range of these devices will be in the order of a few millimetres.

Early work by Luukkala and Meriläinen used air-coupled electrostatic transducers to generate plate waves within thin metal sheets at an operational frequency of 100kHz [53]. Using a 'pitch-catch' configuration on one side of the sample, the fundamental antisymmetric Lamb wave detected the presence of both holes and a laminar flaw within aluminium sheets. Recently, Hutchins and Schindel have reported several possible application areas for the advanced micromachined electrostatic devices. A through transmission system was demonstrated to detect both Teflon inclusions (down to 6.35mm square) and impact damage in a 2.2mm thick unidirectional carbon fibre-

reinforced composite plate, at an operating frequency of approximately 500kHz [49]. Using both pulse-echo and through transmission configurations, topographic images of a pcb board were presented and the regular array of 2mm diameter holes was effectively illustrated [50]. In both experiments the transmitting ultrasound was focused onto the material under investigation using a concave optical lens. The transducers utilised in these applications featured an approximate 1.7MHz bandwidth in pitch-catch mode operation. Another through transmission system utilised toneburst excitation to detect defects within carbon-fibre reinforced polymer plates [54]. The toneburst was produced at the through-thickness resonance of the plate under investigation to improve system sensitivity. The wideband nature of the electrostatic devices would enable a single transducer pair to evaluate materials of different thickness. Lamb wave tomographic techniques have been employed to detect a defect in a 0.69mm thick aluminium plate. A pitch-catch transducer configuration was used and the detection of a 8mm half thickness defect was illustrated.

A final point of note is the construction of an electrostatic transducer using an electret film [48]. This material is permanently polarised and is stretched over a laser machined aluminium backplate. The backplate consists of a regular array of 50μm holes. The device demonstrated an excellent bandwidth characteristic, which was centred around 1MHz and extended beyond 2.5MHz. This transducer structure presents significant potential for industrial applications as they have no requirement for a large d.c. bias voltage.

2.1.5 Piezocomposite Devices

A composite transducer, with improved mechanical matching to air, can be manufactured by loading a conventional piezoceramic material with a low acoustic impedance polymer filler. Several ceramic-epoxy composite transducer configurations can be constructed and examples of these are illustrated by Möckl et al [55]. The two principal designs employed for airborne applications are 2-2 connectivity [55], which consist of strips of piezoceramic sandwiched between a passive polymer material, and 1-3 connectivity [2], where a regular 2-D array of ceramic pillars is embedded in a passive polymer matrix.

The sandwich-layer transducer, or 2-2 connectivity composite, uses the piezoelectric d_{31}-effect present in thin rectangular ceramic plates to couple energy into the polymer, through which improved acoustic matching to air is achieved. The transducer properties can be varied by altering the geometric dimensions and the number of layers in the device, where operating centre frequencies below 200kHz and -3dB bandwidths of approximately 80% have been reported [55,56,57]. This transducer design has been utilised in proximity sensing and object identification applications. Möckl et al [55] have presented a 2.5% ceramic volume fraction composite, through which a 30dB gain in electroacoustic efficiency compared to conventional piezoceramics has been described.

The 1-3 connectivity composite transducer utilises a passive polymer matrix, separating active piezoceramic pillars, to reduce lateral clamping in the piezoceramic phase and hence, to promote the electromechanical coupling co-efficient, k_t, towards the higher k_{33} coupling factor, improving efficiency of the composite by up to 40% [58]. This factor combined with a reduced acoustic impedance, due to loading the ceramic with a low impedance polymer filler, encouraged their use in air-coupled applications.

The Ultrasonics group at the University of Strathclyde are currently involved in several air-coupled projects utilising 1-3 connectivity piezocomposite transducer technology. A feasibility study conducted by Hayward and Gorfu [59] revealed potential advances in airborne ultrasonic technology. A series of composite transducers were evaluated for air operation at frequencies between 250kHz and 1.5MHz, using voltage excitation levels down to 50V. Through transmission airborne signatures were demonstrated on a number of solid samples, including glass, aluminium and carbon fibre composite plates ranging from 3mm to 50mm in thickness. Further work by Reilly and Hayward [60] produced a through transmission 'C' scan image for a damaged carbon fibre composite sample, which compared reasonably with a corresponding scan acquired using conventional water loading. The modelling work presented in Chapter 4 of this Thesis, formed the basis for two NDE applications [2,61,62]. Firstly, a two transducer pulse-echo system was employed to generate and detect Lamb waves in thin plates of carbon fibre composite and aluminium, through which detection and imaging of defects has been

demonstrated [2,61]. Secondly, large SNR has been achieved, in real time, for ultrasonic transmission/detection through a 22m thick honeycomb structure [62]. Each technique has demonstrated good resolution in the detection of impact damage (down to 10J) and PTFE inclusions (down to 6mm diameter) in carbon fibre reinforced composite plates. A more comprehensive description of this work can be found in Chapter 6 'Through-Air Applications for 1-3 Composite Transducers'.

2.1.6 Electromagnetic Acoustic Transducer

An electromagnetic acoustic transducer (EMAT) [63] requires the test specimen to be electrically conducting and moreover, only very small separation distances between the probe and test specimen may be tolerated. For ultrasonic generation, a current transient is passed through the coil, which induces an eddy current in the surface of the sample. A Lorentz force is established, due to the presence of the static magnetic field, which causes ultrasonic waves to be radiated. In reception, ultrasonic waves at the surface of the specimen cause the movement of the conducting material within the magnetic field. This leads to eddy current generation which can then be detected by the coil. Detection of a particular type of ultrasonic wave can be optimised through varying the coil and magnetic field geometry.

A summary of various EMAT systems has been described by Maxfield et al [64]. This paper detailed principal practical factors in the design of EMAT transducers and suggested thickness gauging and elevated temperature NDE as potential applications areas. Unfortunately, the EMAT operating as a transmitter provides both a poor bandwidth coupled with low sensitivity. Hence, this has restricted the utilisation of complete EMAT non-contact systems. This problem has been addressed by Hirao et al [65], where improved system sensitivity has been demonstrated by utilising narrowband excitation conditions. This system was reported to operate at 10MHz, with a separation distance of 2mm between the transducer and the sample.

2.1.7 Hybrid Systems

Over recent years, several publications have detailed air-coupled ultrasonic systems combining the different technologies described above. A common feature present in the majority of these designs is the use of laser generated ultrasound. Thus, maintaining good wideband source characteristics, but replacing interferometric detection with more sensitive transducer designs. At present, piezoelectric, electrostatic and EMAT detectors have been utilised and a brief summary is presented below.

Wang et al [66] employed laser generation and a focused 1.0MHz piezoceramic receiver, incorporating a low acoustic impedance matching layer. The laser beam (modulated acousto-optically) is focused onto the sample surface, with the air transducer situated at an angle and on the same side of the sample in order to collect the ultrasonic echo. This system was utilised to measure the thickness of thin films with a reasonable degree of accuracy. Several papers have been produced through the work undertaken for this Thesis, in conjunction with the expertise in laser generation of ultrasound associated with the Ultrasonics Group at Warwick University. This collaboration combined both narrowband [67] and wideband [68,69] 1-3 composite receivers, in the detection of longitudinal, shear, Rayleigh and Lamb waves generated by an incident laser beam in metals and composite materials. Details of this application are described in Chapter 6.

The utilisation of an electrostatic receiver has been investigated by Wright et al [70]. This work used a micromachined capacitance transducer, operational centre frequency of approximately 500kHz, for the detection of longitudinal, shear, Rayleigh and Lamb waves. This combination is theoretically well matched due to the wideband nature of both technologies. Although, to complement the high resolution afforded by laser generation, a capacitive device with a higher operational frequency would be desired.

As previously discussed, in Section 2.1.6, EMAT transducers are more optimally employed as ultrasonic detectors and this characteristic has been utilised by Taylor et al [71], Edwards et al [72] and Hutchins et al [73]. Both Taylor and Edwards designed an annular EMAT receiver, through which a laser beam was directed, and detected the

longitudinal echoes from the sample. The former approach required Cepstral processing to obtain the periodicity from the acquired time signals and subsequently, the inspection of diffusion bonds was illustrated. The latter characterised waveforms through thick metallic samples (up to 25mm thick). The third approach, generated Lamb waves in thin aluminium plates. Two different receiver designs were adopted to enable the detection of either antisymmetric or symmetric Lamb wave modes and the subsequent imaging of defects was illustrated.

Another hybrid system arrangement has been adopted by Safaeinili et al through which the characteristic parameters for a composite plate can be determined [74]. This approach has utilised a focussed piezoceramic transmitter and a wideband electrostatic device in reception to enable the calculation of angular position for the generation of Lamb waves and both longitudinal and shear velocities in composite plates.

2.1.8 Summary

The performance of thickness mode piezoceramic transducers may be enhanced significantly by incorporation of multiple matching layers or the addition of a radiating membrane to facilitate energy transfer into air. However, it is difficult to obtain the optimal degree of improvement owing to the relatively high mechanical impedance of piezoceramic materials. For optical systems, there is usually a requirement for a high quality surface finish and although laser generation is well established, detection sensitivity is relatively low. In the case of EMAT's, there is a requirement for the test specimen to be electrically conducting and moreover, only very small separation distances between probe and test specimen may be tolerated. Electrostatic transducers possess considerable potential for airborne operation, since the vibrating membrane is well coupled to the load medium and the recent introduction of a micromachined backplate has enabled repeatability in manufacture. Piezopolymer and piezoceramic-epoxy composite materials also offer attractive options for airborne ultrasound by means of improved mechanical matching. Also, in the case of the piezopolymers, the ability to be configured as a flexible membrane can be of benefit, although application may be restricted due to its low dielectric constant. Consequently, electrostatic and

piezocomposite designs are considered as the two principal candidates for the airborne applications, in the megahertz range.

Two review papers, presented at the 1994 and 1995 IEEE Ultrasonics International Symposiums, are excellent sources of the current air-coupled transducer technology [75,76]. These papers are complimentary in that they report on work undertaken in both Europe [75] and the USA [76]. These papers cover a selection of technologies and describe several practical applications for the present air-coupled transducer designs. Earlier review papers concentrated on piezoelectric transducer designs [6,57], but hold valuable information with regard to NDE applications [6].

2.2 Suitability of 1-3 Composites for Air Applications

2.2.1 Introduction

Piezocomposite transducers incorporate active piezoceramic elements within a passive polymer phase, to yield enhanced piezoelectric properties with respect to the parent ceramic. These devices are expressed in terms of the connectivity of each phase (the representation corresponds to connectivity in the ceramic phase, followed by the polymer phase), where this refers to the number of orthogonal directions in which each particular phase is continuous [77]. The common connectivity patterns and applications are as follows : 0-3 connectivity transducers are effective in hydrophone applications [78]; 1-3 connectivity devices are utilised in numerous application areas, for example, medical [79], imaging [80] and NDE [81]; 2-2 connectivity composites have been employed in airborne robotic systems [54]; and 3-3 connectivity devices have been reported for imaging and NDE applications [82]. Although each of these transducer configurations have merit, the 1-3 connectivity piezocomposite structure is by far the most efficient and versatile. Consequently, it was chosen for this study.

With reference to Figure 2.1, 1-3 composites offer considerable advantages for airborne operation when compared to standard piezoceramic materials. Mechanical stiffness may be adjusted by an appropriate choice of filler material and ceramic volume fraction [83]. Moreover, further design optimisation is possible by varying ceramic rod shape and distribution, an aspect which is critical at the low volume fractions required for some airborne applications [84]. Other parameters which must be taken into consideration for operation into air include mechanical matching and backing, in addition to the form of electrical stimulation in transmission and electrical loading in reception. These aspects are important for most applications since a low signal to noise situation invariably exists. As a result of the inherent structural complexity and large number of constructional and operational variables, design understanding and possible optimisation of 1-3 connectivity composites for air-coupled operation is not a straightforward matter. The design process would benefit greatly from the availability of an accurate computer simulation model.

For many applications the theoretical behaviour for 1-3 connectivity composites is now

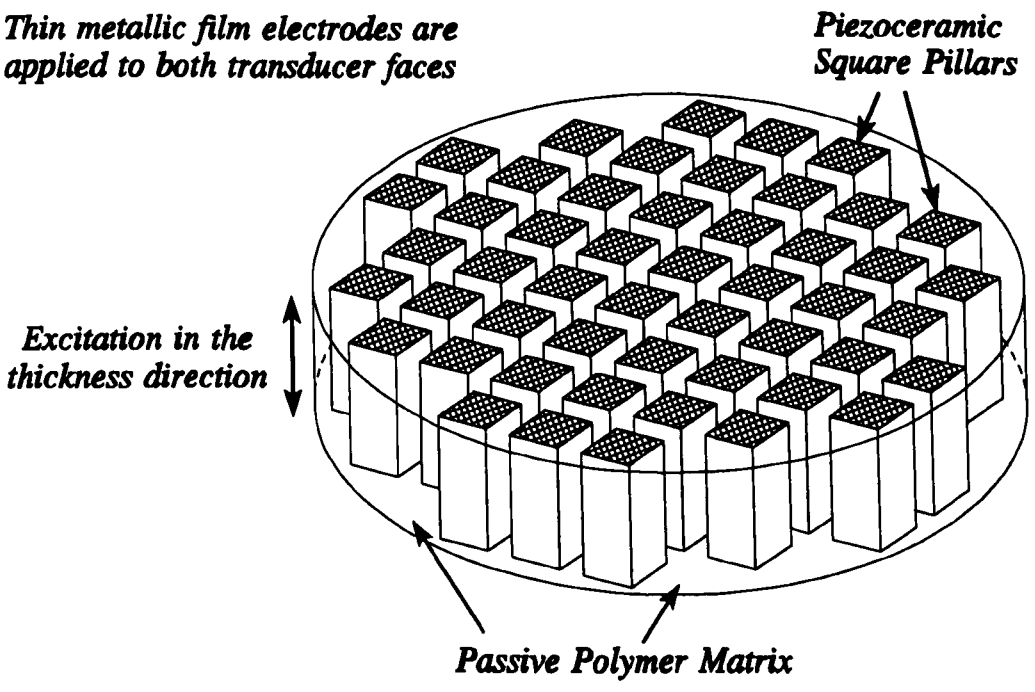

Figure 2.1 Standard construction for a 1-3 connectivity piezocomposite

reasonably well documented (see for example [58] and [83-85]). Provided that the ceramic pillars are sufficiently tall, with low inter-pillar spacing, composite transducer behaviour may be predicted well via one-dimensional (1-D) theories [58,85]. However this approach can be difficult to justify at the extremes of ceramic-polymer volume fraction where inter pillar (or internal modes within the ceramic) resonances can corrupt the desired thickness mode. Furthermore, manufacturing constraints do not always permit the proper geometry for 1-D operation and more computationally intensive methods are required for prediction of composite performance [84].

2.2.2 Fundamental Evaluation of Principal Properties of 1-3 Composites

The introduction of a modelling strategy for 1-3 connectivity transducers, by Smith et al [83], enabled the generation of computer models for the prediction of composite transducer behaviour. This modelling approach requires the simultaneous solution to the piezoelectric-elastic equations for both active and passive phases in the composite transducer, resulting in a single set of equivalent thickness mode parameters. For a given ceramic/polymer composite configuration, the specific acoustic impedance, Z_A, the

thickness mode electromechanical coupling factor, $\overline{k_t}$, and the bulk wave velocity in the thickness direction, $\overline{v_t}$, of a composite transducer can be expressed in terms of Smith's equivalent parameters, $\overline{c_{33}^E}$, $\overline{\varepsilon_{33}^S}$, $\overline{h_{33}}$, and $\overline{e_{33}}$ as described in Equations 2.2 and 2.3. Here, the density of the composite, $\overline{\rho}$, is derived from the equilibrium densities of the ceramic, ρ^c, and filler materials, ρ^f, as in Equation 2.4.

$$\overline{k_t} = \overline{h_{33}} / \sqrt{(\overline{c_{33}^D} / \overline{\varepsilon_{33}^S})} \qquad \overline{Z_A} = \sqrt{\overline{c_{33}^D}\,\overline{\rho}} \qquad \overline{v_t} = \sqrt{\overline{c_{33}^D} / \overline{\rho}} \tag{2.2}$$

Where;

$$\overline{c_{33}^D} = \overline{c_{33}^E} + (\overline{e_{33}})^2 / \overline{\varepsilon_{33}^S} \qquad \overline{h_{33}} = \overline{e_{33}} / \overline{\varepsilon_{33}^S}$$

$$\overline{\varepsilon_{33}^S} = v\left[\frac{\varepsilon_{33}^S + 2(e_{31}^2)}{c(v)}\right] + (1-v)\varepsilon_{11} \qquad \overline{e_{33}} = v\left[e_{33} - 2e_{31}\frac{c_{13}^E - c_{12}}{c(v)}\right] \tag{2.3}$$

and

$$\overline{\rho} = v\rho^c + (1-v)\rho^f \qquad c(v) = c_{11}^E + c_{12}^E + \frac{v(c_{11}+c_{12})}{(1-v)} \tag{2.4}$$

The bar symbol denotes a composite parameter, v represents the volume fraction of piezoelectric ceramic in the composite and all other symbols have their usual meaning as defined in [1]. In this notation the superscripts E and S are used for ceramic constants only.

This one dimensional modelling approach requires the piezoceramic pillars to have a low width-to-height ratio (aspect ratio) and sufficiently fine lateral pillar spacing in order to promote homogeneous behaviour from the composite. Through implementation of the above Equations, it is possible to obtain characteristic responses for 1-3 composite transducers, assuming the above geometrical constraints, over the entire ceramic volume fraction range. For the purposes of reviewing the behaviour of 1-3 composites, a PZT5A piezoceramic and CIBA-GEIGY CY1301/HY1300 epoxy combination, operating at 500kHz, has been analysed. The relevant parameters employed in these calculations can

be found in Appendix A. From this evaluation, the electromechanical coupling co-efficient, k_t and specific acoustic impedance, $\overline{Z_A}$, are of particular relevance to air-coupled performance and are presented in Figures 2.2 and 2.3, respectively. From Figure 2.2, it can be observed that the electromechanical efficiency of the composite transducer approaches the value for k_{33} (=0.7) for the ceramic and is relatively constant over the volume fraction range 30% to 80%. At the extremities, the values for k_t have fallen due to either lateral clamping by the polymer, at high volume fractions, or through the elastic loading of the surrounding polymer, in the lower volume fraction range. At the intermediate volume fractions, a combination of both elastic and lateral clamping ensures that k_t does not attain the actual value of k_{33}. The estimated specific acoustic impedance, shown in Figure 2.3, confirms the ability of these composite transducers to realise a better match to air, when compared to conventional piezoceramics. For the PZT5A/hard set composite, an essentially linear acoustic impedance range between 5 - 28MRayl has been predicted, although this could be reduced further through application of a lower acoustic impedance polymer filler.

Unfortunately, it is not possible to simultaneously optimise all of the parameters in a 1-3 composite. This is illustrated through the linear relationship between volume fraction and relative permittivity shown in Figure 2.4, where the higher volume fraction devices exhibit the higher driving capacity. Thus, a compromise is obvious between good acoustic impedance matching to air at lower volume fractions, and the higher electrical permittivity required for driving purposes, manifest at the higher volume fractions.

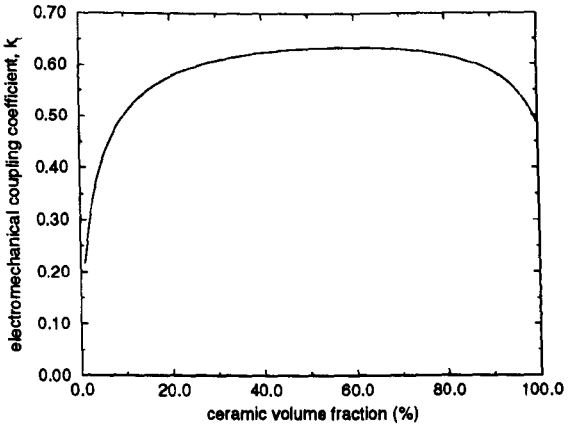

Figure 2.2 Variation in electromechanical coupling coefficient predicted by Smith's model

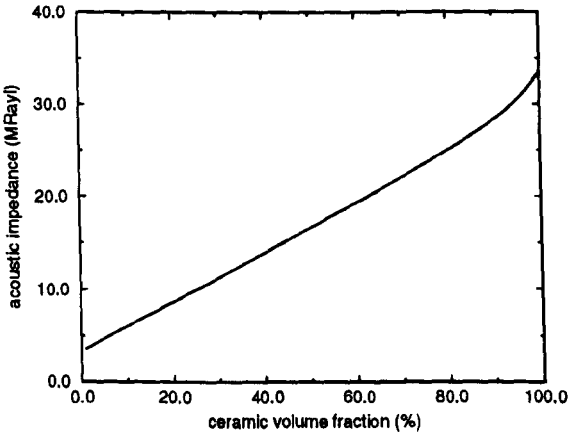

Figure 2.3 Specific acoustic impedance as a function of ceramic volume fraction, as predicted by Smith's model

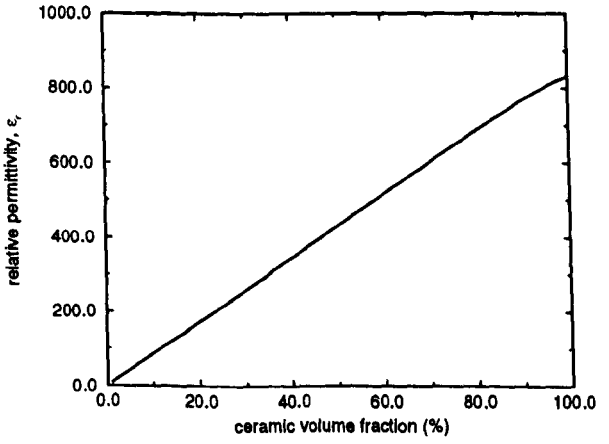

Figure 2.4 Relative permittivity for 1-3 composites, predicted by Smith's model

2.2.3 Adopted Simulation Approach

Firstly, the 1-D equivalent thickness parameters described in Equations 2.2, 2.3 and 2.4 are incorporated within a linear systems model of the transducer system [86]. This approach permits convenient simulation of transducer structure (including backing and matching), electrical loading and the influence of air propagation for both transmission and reception. Provided that the composite vibrates uniformly in the thickness or height dimension, behaving as an effective homogeneous medium, excellent results can be achieved [85]. For those situations incompatible with a 1-D approximation, a finite element approach is employed to perform a harmonic analysis of composite behaviour in the air environment. This approach has been used extensively by Hossack and Hayward [84] and Hayward and Bennett [87] for assessment of composite characteristics and the methodology is described within these References. The finite element analysis involved calculation of the surface pressure at discrete frequency steps with the excitation signal delivered from an ideal voltage generator. Both of these modelling approaches will be used extensively throughout this Thesis.

The air transducer characterisation, described in Chapter 3, has utilised piezopolymer and piezocomposite transducers with the uni-dimensional modelling approach. The composite devices employed have approximated good thickness mode operation and excellent results have been obtained. In Chapter 4, a dual approach has been chosen for the theoretical evaluation of 1-3 composite transducers for through-air applications, over the complete volume fraction range. Generally, the finite element technique is shown to agree well with, and hence confirm, the linear systems approach. Where this is not the case, the former has been used as the benchmark for experimental comparisons. Investigation into mode coupling within a composite transducer, Chapter 5, has exclusively utilised the finite element technique. Through this Thesis, the limitations of the linear systems model are highlighted where relevant.

2.2.4 Manufacture of 1-3 Composite Transducers

Throughout this Thesis, selection of constituent materials for the composites was made on the basis of availability and consistency, ease of manufacture and accurate documentation of parameters for simulation purposes. Consequently, PZT5A ceramic and a relatively stiff polymer, CIBA-GEIGY CY1301/HY1300 were chosen, although it was recognised that both materials may be sub-optimal with respect to through-air operation. However, a small selection of composites were manufactured using PZT5H ceramic to enlarge the scope of the air transducer characterisation, described in Chapter 3.

The manufacturing method utilised to construct the 1-3 connectivity composite transducers was the standard 'dice and fill' technique [88]. Here, a series of parallel cuts are made into a prepolarised piezoceramic. The parallel slots in the ceramic are filled using a suitable polymer. The ceramic/polymer combination has a second series of cuts made, perpendicular to the first and again, the polymer filler material is used to fill the parallel slots. The resultant diced ceramic/polymer composite is then lapped to attain the appropriate centre frequency, after which, each device is electroded using a thin layer of conductive epoxy, as illustrated in Figure 2.1. A holder is constructed from a mild steel tube, incorporating a BNC socket within the end cap, and the transducer positioned within the holder for ease of mounting. The general transducer arrangement is shown in Figure 2.5. It should be noted that, the front face of the composite and the casing are connected to ground to ensure good electrical screening.

When required, a backing block or matching layer was added to the transducer structure, with a view towards increasing bandwidth and/or sensitivity. This enabled the modelling to be verified for more practical arrangements. A perspex backing block was utilised due to ease and consistency of manufacture and concise parameter information, as detailed in Appendix A. A variety of matching layer materials have been examined and are described, as required, throughout this Thesis. It should be noted that the transducer arrangement shown in Figure 2.5 illustrates a two matching layer system bonded onto the active piezocomposite layer.

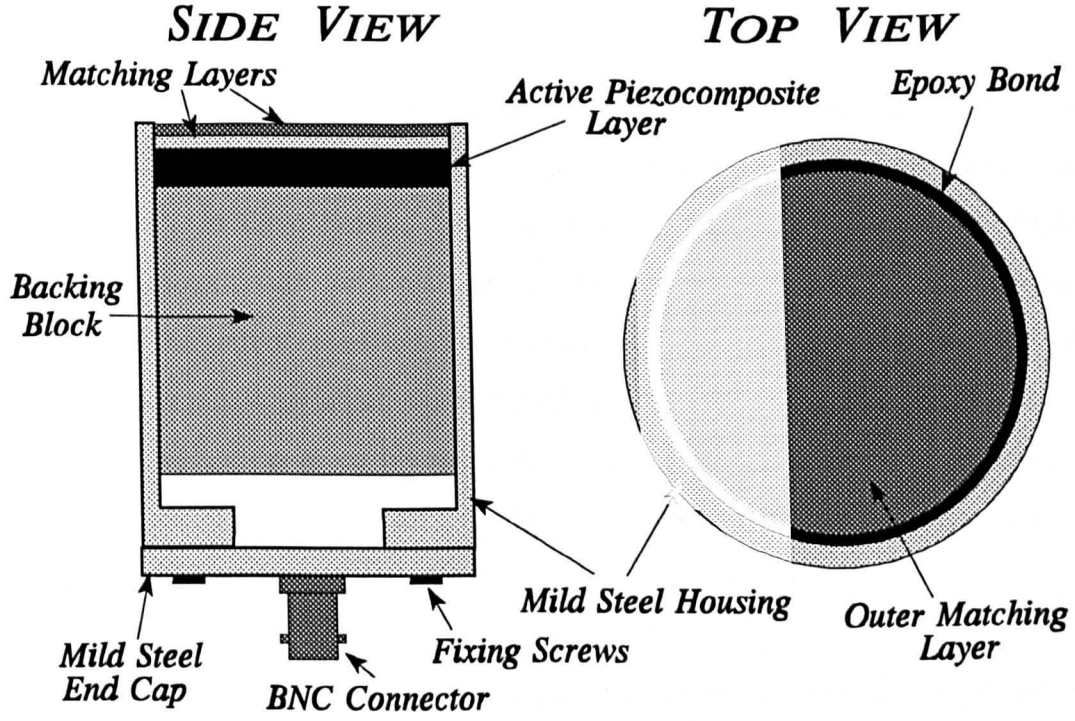

Figure 2.5 Piezocomposite transducer construction

The manufacturing equipment utilised in the Ultrasonics Laboratory, at the University of Strathclyde, imposes practical limitations on the dimensions of a 1-3 composite transducer. Therefore, only simple geometries can be constructed using parallel cuts. Although a range of saw blade widths are available, 0.17mm up to 1.00mm, it is difficult to manufacture long, thin pillars at the extremities of the volume fraction range. This will be detailed, when appropriate, throughout this Thesis. Advances in manufacturing techniques (injection moulding [89] and lost mould [90]) are being utilised to construct more complicated geometries, possessing a finer lateral spatial scale. Therefore, the simulation work presented here has been utilised to estimate the optimum 1-3 composite transducer configurations, with a view towards future design of composite transducer systems.

2.3 Electrostatic Transducer Manufacture

Due to the potential of these transducers for air-coupled operation, a selection of capacitive devices have been constructed to differing specifications. The manufacturing tools at Strathclyde have limited the transducers to comprise of random roughness backplates, although this was seen as a restriction principally for manufacturable repeatability. Aluminium, steel and brass materials have been used for backplates, where a variation in average roughness was achieved using a commercial lapping and polishing machine. To evaluate a more comprehensive selection of electrostatic devices, three different thicknesses of mylar film (2.5μm, 3.5μm and 5.0μm) have been used as vibrating membranes.

The basic transducer design is shown in Figure 2.6. Here, aluminium coated mylar film was pre-tensioned between two aluminium rings to support the vibrating membrane. The membrane support ring was bolted to an aluminium holder containing a removable perspex plug to insulate the backplate from the rest of the transducer assembly. Three screws allow the membrane to be brought into contact with the backplate and tension can be adjusted as required. The bias and excitation signals are applied to the backplate via a BNC connection which also provides a ground return for the housing assemblies. The aluminium support rings are each 4.0mm thick and the tension screw heads protrude by 0.5mm, hence this arrangement results in a minimum 4.5mm air separation between the active vibrating membrane and a test sample or receiving transducer.

It is important to describe the interconnection between the bias voltage, the transducer and the driving electronics, as in transmission, or the pre-amplifier, as in reception. Figure 2.7 illustrates the electrical connections required to isolate the connecting electronics from the bias voltage (HT). The high voltage rating capacitor effectively blocks the bias voltage from the terminals of the connecting electronics. This electrical arrangement was housed in a screened steel casing and is required for every experiment involving electrostatic transducers.

Finally, it should be noted that no attempt was made to describe the theory of operation for electrostatic devices. At the time of writing no convenient theoretical model was available, although a potential approach is described comprehensively in [45].

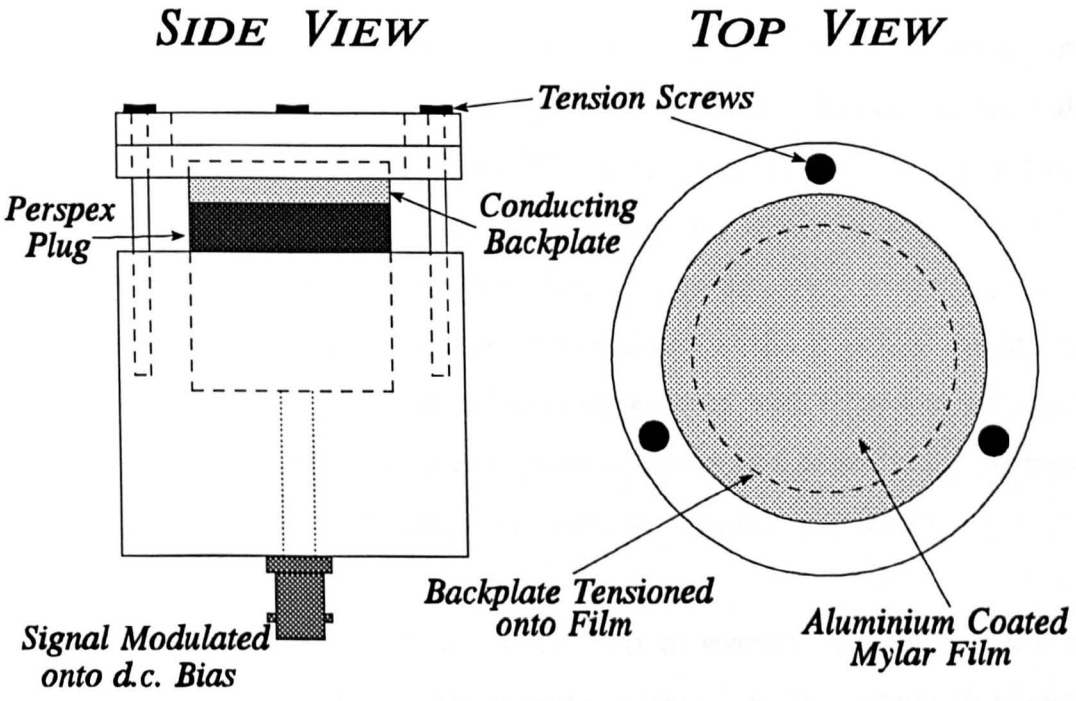

Figure 2.6 Electrostatic transducer construction

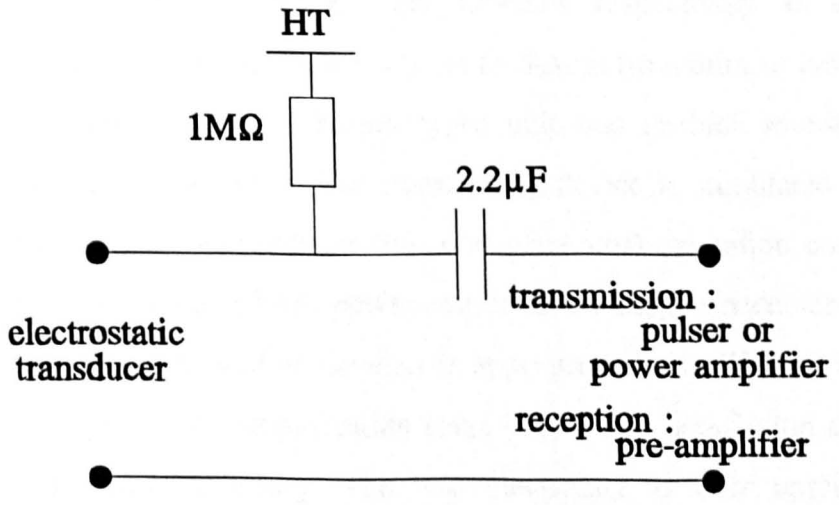

Figure 2.7 Blocking Capacitor arrangement required for electrostatic experimentation

2.4 Experimental Arrangement

The experimental layout utilised throughout this Thesis is shown in Figure 2.8. The transducer performance is examined under two different operating conditions, corresponding to transmission and reception modes of operation. For each experimental phase, a precision manipulator (capable of 1μm resolution) was utilised to carefully align both the transmit and receive transducers. The transmitting device is positioned using the X and Y axis of the manipulator. In addition, the rotational alignment of the transmitter, with respect to the reception device, was necessary to ensure that the transducer faces were parallel. The detector is attached to the Z-axis of the precision manipulator which was employed to maintain consistency with respect to propagation distances. With the transmitter/receiver alignment correct, indicated by the position of maximum received signal, both transducers were then locked in position.

For the Thesis, it was necessary to perform all experimentation in a constrained environment to ensure consistency with respect to attenuation [3]. A standards laboratory was utilised to conduct all the air-coupled experimentation described in the Thesis. This laboratory provided a controlled environment, in which the temperature and relative humidity were maintained at 20°C±2° and 40%±5% respectively. In addition, the experimental system, was housed within a glass enclosure (to minimise the influence of air currents) containing a digital thermo-hygro unit that enabled monitoring of air temperature and relative humidity. The transmitting device is stimulated under either wideband (pulser unit) or narrowband (function generator) excitation conditions. For some narrowband excitation, a 50dB power amplification stage is necessary to drive the transmitting device and this will be detailed as appropriate in the Thesis. The receiving transducer may require a pre-amplification stage before data acquisition and again this will be detailed where necessary. The bias electronics is only applicable to the electrostatic transducer experiments. Specific details of driving and detection electronics are described where necessary throughout the Thesis.

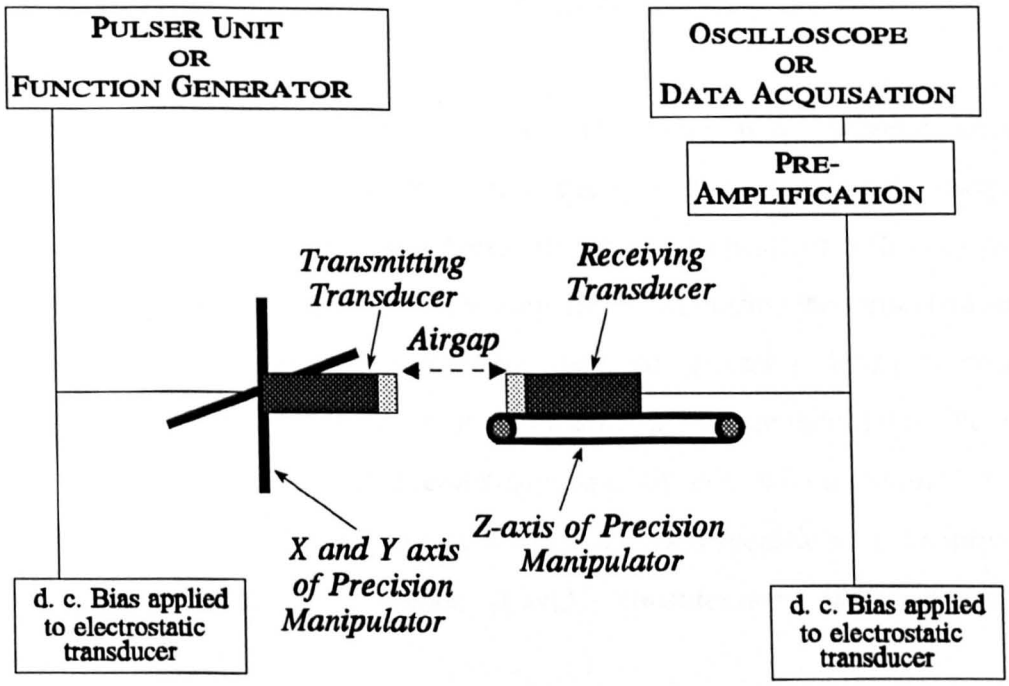

Figure 2.8 Experimental arrangement utilised throughout the Thesis

2.5 Conclusions

A review of the predominant technologies associated with airborne ultrasonic generation/detection has described the relative merits of each approach. Consequently, electrostatic and piezocomposite transducers are considered most suitable for operation in air-coupled ultrasonic systems. Unfortunately, there is a limited theoretical knowledge concerning the electrostatic technology. However, this matter is being addressed at present by several research groups. Well defined modelling methodologies have been reported for 1-3 connectivity piezocomposite transducers, which coupled with an increased electromechanical coupling co-efficient and lower specific acoustic impedance, compared to conventional piezoceramic, provides considerable potential for airborne ultrasound applications.

CHAPTER 3

CHARACTERISATION OF AIR-COUPLED TRANSDUCERS

ABSTRACT

This Chapter describes a theoretical and experimental study for determination of the through-air system impulse response, insertion loss and characteristic field profile for air-coupled transducers. Wideband piezopolymer transducers (PVDF) are employed in both transmission and reception modes and their behaviour assessed by means of mathematical modelling and experiment. Specifically, a linear systems model approach, modified to include the influence of attenuation in the propagation medium, was used to design suitable PVDF transducers for wideband operation in air. Suitable devices were then manufactured for determination of the transmission and reception response characteristics of piezocomposite and electrostatic transducers when operating in the air environment. Within the characteristic field profile for air-coupled disc transducers, the influence of airborne attenuation ensures the conventional near-far field boundary is not observed and hence, a restricted operational field exists. These factors are significant for the correct operation of an air-coupled device and experimentally acquired field characteristics are used to position the transducer system. A range of transducers was evaluated, including 1-3 connectivity composites of different ceramic volume fraction and mechanical matching conditions, in addition to electrostatic devices of varying design. To complement the investigation, relative performances for narrowband operation are also presented under transmission and transmit-receive conditions. Despite the obvious measurement difficulties, good agreement between theory and experiment was observed and the methodology is shown to provide a convenient and robust procedure for comparison of through-air transducers operating in the frequency range 50kHz-2MHz.

3.1 INTRODUCTION

Considerable research effort has produced several ultrasonic transducer calibration techniques, examples of which include tone burst testing [91], thermal equivalent calorimetric method [92], time delay spectrometry [93], reciprocity calibration [94], vector calibration [95] dynamic calibration [96] and beam profiling [92,97]. These procedures each possess relative merits for the calibration of transducers in a water loaded environment, but they lose robustness in the transition to air-coupled transducer operation. Principal reasons include the very short wavelengths, the high attenuation in air and the insensitivity of available transducers. Therefore, these constraints have restricted air-coupled transducer characterisation to devices with operating frequencies below 150kHz [98], although recently Anderson et al [45] have reported characterisation of electrostatic transducers using standard microphone air calibration techniques. However, despite the advances made in air transducer technology, there is at present a lack of suitable calibration tools for characterisation and evaluation of air-coupled systems operating in the important range 250kHz and 2MHz.

The principal transducer parameters of interest are the transducer operational impedance profile, the impulse response when the device is operated either as a transmitter or a receiver and the characteristic beam profile. The impedance profile enables the determination of the resonant modes within the transducer, hence the electrical and mechanical resonances particular to a mode can be extracted and consequently the electromechanical coupling coefficient associated with the mode can be obtained. These parameters are utilised to verify that the transducer will operate at the desired frequency and that the electromechanical coupling efficiency of the device is sufficient. The impulse response of the transducer will characterise the sensitivity and operational bandwidth of the transducer when employed as an ultrasonic source or detector. This information can be acquired by utilising Erikson's tone burst testing method [91], but the process is time consuming and maintaining a stable experimental environment presents a problem, especially in air. The nature of the ultrasonic field of the transducer defines the suitability for a device to operate in a given ultrasonic system [99]. This

field profile is of particular importance in an air-coupled system due to the highly attenuative nature of air, resulting in a restricted operating range.

This Chapter will discuss the use of piezopolymer transducers (PVDF) to measure the transmission and reception response of air-coupled transducers, over the frequency range 0.25MHz - 2MHz, under both wideband and narrowband operating conditions. PVDF transducers were designed through a uni-dimensional modelling technique [86] to operate either as a transmitter or as a receiver and to possess unipolar, planar and broadband characteristics for air-coupled operation. Due to the low signal to noise ratio (SNR) in air, the piezopolymer devices were first evaluated in a water environment using a calibrated hydrophone [100], in order to validate the simulation approach. The model was then extended to predict the corresponding performance in air, where the influence of the frequency dependent attenuation was included to yield realistic simulation results. The experimental field profile for an air coupled transducer, operating around 500kHz, has been acquired using a standard hydrophone in conjunction with a precision manipulator, capable of 1μm resolution. The short wavelengths and high attenuation factor ensures that the traditional near/far field boundary is not established in an air environment. Hence, the positioning of air transducers is of paramount importance and the measured field profiles are used to evaluate the optimum transducer position for the characterisation process.

Two different types of air transducer were considered. Firstly, a range of 1-3 connectivity composite devices of differing microstructure and under different mechanical matching conditions was evaluated with respect to transmission, reception and transmit-receive performance. To complement this study, a range of wideband electrostatic transducers was also evaluated under similar operating conditions. Here manufacturing aspects such as bias voltage, membrane thickness and backplate roughness were varied and experiments performed to extract the same performance parameters.

3.2 THICKNESS MODE MODELLING

The modelling strategy for 1-3 connectivity transducers by Smith et al [58], described in Section 2.2.2, enabled the generation of computer models for the prediction of composite transducer behaviour. The thickness mode parameters were modified according to the composite volume fraction to obtain an equivalent uni-dimensional response. Hayward and Hossack [85] combined this modelling strategy with a linear systems modelling approach [86] to generate a comprehensive computer model. This computer model has the facility to investigate the influence of electrical stimulation in transmission, electrical loading in reception and the inclusion of mechanical matching and/or damping, to predict impedance, transmission, reception and pulse-echo characteristics for piezoceramic, piezocomposite and piezopolymer transducer performance as a function of the operating environment. Hence, the model can be used to produce transducer characteristics such as centre frequency, bandwidth and sensitivity and present this information as either the time or frequency domain plots. Throughout, care was taken to ensure that the composite pillar dimensions and spacings were compatible with homogenous operation. For the devices under consideration, this constrained the minimum pillar aspect ratio (width to height) to approximately 0.1 [87]. A more detailed description of this modelling approach can be found in Appendix B.

To enhance accuracy, the equivalent thickness mode parameters of each transducer were measured (as far as possible) according to the IEEE Standard on Piezoelectricity [1], prior to insertion within the model. This involves measurement of the transducer thickness, weight and electrical and mechanical resonances to yield the device velocity, density, electromechanical coupling factor, acoustic impedance, h_{33}, e_{33}, C_{33}^{D} and C_{33}^{E}. In addition, the capacitances at a frequency lower than the lowest resonance (0.01 or less of measured f_m) and at a frequency higher than the principal natural resonances (greater than twice f_n) are required to calculate the dielectric permittivities at constant stress, ε_r^t , and constant strain, ε_r^s , respectively.

3.3 THE EXPERIMENTAL APPROACH

3.3.1 Experimental Arrangement

The experimental equipment was maintained constant throughout with the six basic elements shown in Figure 3.1. Here each component is expressed in either electrical or mechanical terms and provides individual building blocks through which the experiment can be defined in terminology suitable as input for the linear systems model. The electrical stimulation circuit is represented by an equivalent T-network, represented by Z_1, Z_2 and Z_3. Here each impedance can be configured as an RLC circuit connected either in series or in parallel. The cabling effects are modelled as a inductor/capacitor combination, where the capacitance, C_C, is connected across the cable and the inductor, L_C, is a series impedance. Each piezoelectric device is simulated using a set of equivalent thickness mode parameters, but in electrical terms it is represented by the operational impedance, Z_T. The operating medium is considered as a mechanical interface at the front face of the transducer and the appropriate attenuation factor will be applied to the propagating pressure wave. Two methods of detection are employed throughout this paper, firstly the resistor/capacitor parallel combination of an oscilloscope and secondly the effective resistive load of a pre-amplifier stage, possessing a 90dB gain. Combining these various components enables the experimental environment to be simulated accurately by the linear systems model.

The influence of cabling was approached from three different aspects. Firstly, in the case when a piezoelectric receiver is under investigation, the cabling effects are ignored. For the purpose of this experiment, the detector can be deemed to be directly connected into the input stage of the pre-amplifier, because the detector and the pre-amplifier were housed together to ensure that lead lengths were minimised. Secondly, the membrane hydrophone was supplied with cable and connector attached and hence, manufacturers specifications have been used [101]. Finally, for all other cases, the influence of cabling effects can be significant. Therefore, for the purposes of this paper the cable connected to the PVDF device remained constant. The values utilised for C_C and L_C were calculated from manufacturers specifications and basic transmission line theory. The

cable employed has a characteristic impedance of 50Ω and a capacitance stated as 70pF per meter length, which translates into a capacitance of 84pF for the 1.2m cable length used. Transmission line theory defines the characteristic impedance as given in Equation 3.1, where Z_o is the impedance, R^C is the resistance, L^C is the inductance, G^C is the conductance and C^C is the capacitance associated with a transmission line.

$$Z_o = \sqrt{\frac{R_C + j\omega L_C}{G_C + j\omega C_C}} \qquad (3.1)$$

Typical values for R^C and G^C are insignificant and hence the equation can be simplified and solved to give a value of 0.21μH for the cable inductance, L_C. This was subsequently confirmed by experimental measurement.

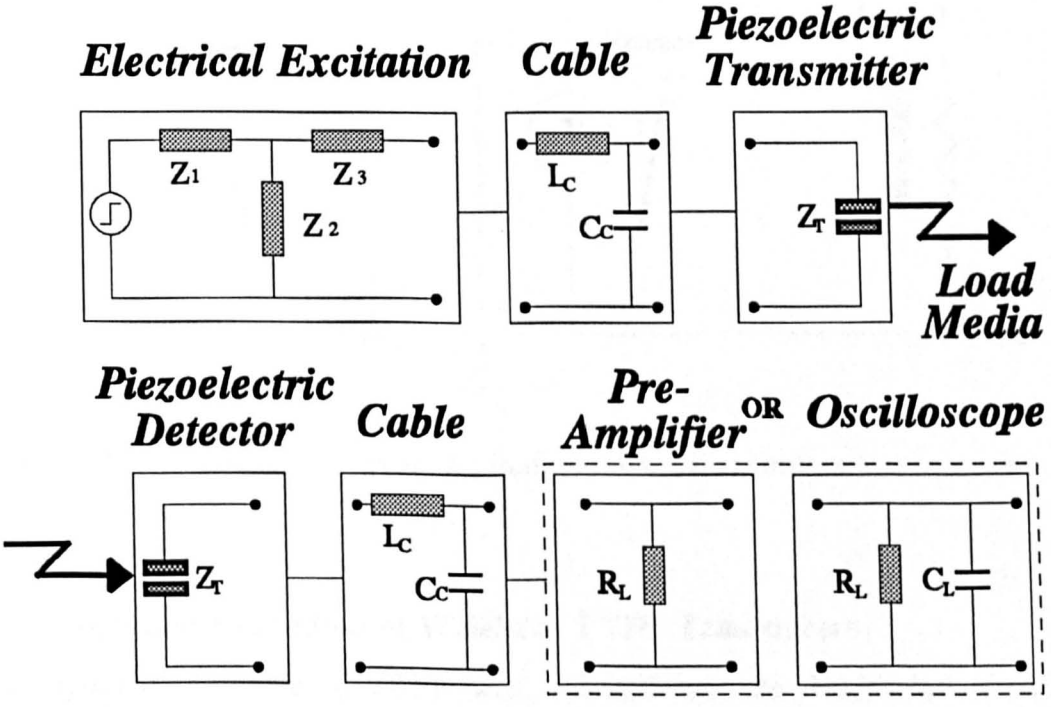

Figure 3.1 Block diagram of the experimental system

Two different means of electrical stimulation have been employed and are depicted in Figure 3.2 : a pulser unit delivering a 200V differentiated step, with a rise time of 10ns, through a configuration of R_O, the on resistance of the MOSFET, C_B, the blocking capacitor and R_E, the damping resistor [102]; and a Panametrics 5052PR pulser/receiver unit producing a pseudo-impulsive forcing function, characterised by a 30ns triangular spike delivered through a low impedance source resistance, R_O. These will be described in the text as the *pulser unit* or the *Panametrics unit*, respectively. The significance of evaluating these two electrical stimulation circuits will be described fully later.

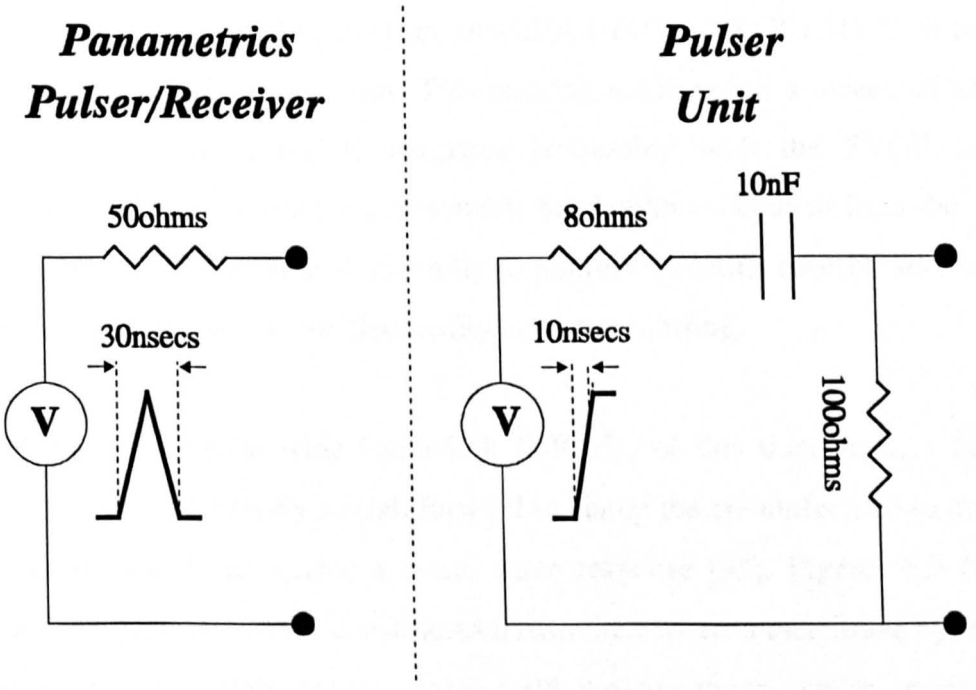

Figure 3.2 Electrical excitation circuits utilised in simulation

3.3.2 Design and Evaluation of Wideband PVDF Transducers

Polyvinylidene Fluoride (PVDF) was selected as the basis for a wideband transmission/reception transducer [103]. Several factors influenced the choice of this material, namely the possession of a high operating frequency coupled with good bandwidth potential and a reasonable acoustic impedance match to air. Importantly, circular PVDF probes can be manufactured to demonstrate minimal edge diffraction and hence approximate well to an ultrasonic plane wave source [99], thereby minimising possible response variations due to aperture diffraction.

(a) Transmission

The application of a PVDF transmitter to generate an approximate planar pressure impulse incident on the front face of a composite receiver was considered. The main restriction to the use of a piezopolymer as a transmitter is the low dielectric constant associated with this material, resulting in a poor drive performance. However, the advantages were considered sufficient to merit investigation. Appendix A details the electromechanical characteristics for the piezopolymer film used to construct a wideband transmission device. A pair of piezopolymer transducers, 20mm in diameter, were constructed from 25μm thick PVDF film and bonded to a 40mm thick perspex backing block. A thin layer, measured to be 3μm, of CIBA-GEIGY CY1301/HY1300 hard set epoxy was used as the bonding agent. This backing medium has a measured acoustic impedance of 3.2MRayls, which compares favourably with the PVDF acoustic impedance of 3.9MRayls, ensuring a reasonable bandwidth is obtained from the device. The backing block was also shaped carefully to minimise internal reverberation and the entire assembly placed within an electrically screened housing.

In addition to the potential wide bandwidth (20MHz) of this transducer, a principal advantage is that it is relatively straightforward to clamp the circumference to minimise edge diffraction and hence create a plane wave response [99]. Figures 3.3 (a) - (f) demonstrate this property for the constructed transmitter, where a membrane hydrophone has been utilised to obtain several axial field measurements, under water loaded conditions. This Figure demonstrates that as the separation between the transducers increases the received pulse shape remains reasonably constant and a decrease in amplitude is evident due to attenuation in the medium.

A PVDF membrane hydrophone [100] was used firstly in a water environment to evaluate the source and confirm the theoretical model. Results were acquired with the PVDF transmitter driven under both pulser and Panametrics excitation and the standard hydrophone connected directly into an oscilloscope. The spectral and temporal responses for the pulser unit, driving the PVDF/hydrophone system, are illustrated in Figures 3.4(a) and 3.4(b), respectively. Corresponding responses for the Panametrics unit are

shown in Figure 3.5(a) and 3.5(b). Under both excitation conditions, it can be seen that the linear systems modelling approach has predicted the system response to a reasonable degree. The influence of the cabling connected to the PVDF transducer has tuned the systems to approximately 15MHz and 20MHz, for pulser and Panametrics excitation respectively.

The linear systems model was then used to investigate the theoretical plane pressure wave generated by the PVDF transmitter when operating directly into air. The simulated transmitted force spectra when the PVDF device operates into both water and air media are illustrated in Figure 3.6(a) and 3.6(b), for pulser and Panametrics excitation respectively. Due to the inefficient energy transfer at the transducer/air boundary, the curves for each medium have been normalised, with a 66dB difference in signal level predicted between water and air loaded conditions. In the absence of propagation attenuation, this reveals that the frequency content does not differ significantly for the two load media. Hence, both systems are capable of producing a pressure wave which would be considered adequate for the simulation of impulse excitation for transducers operating below 2MHz.

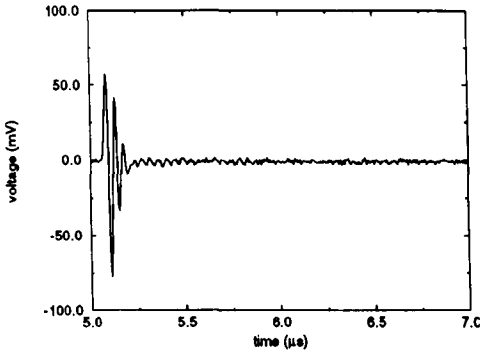

(a) 7.5mm separation

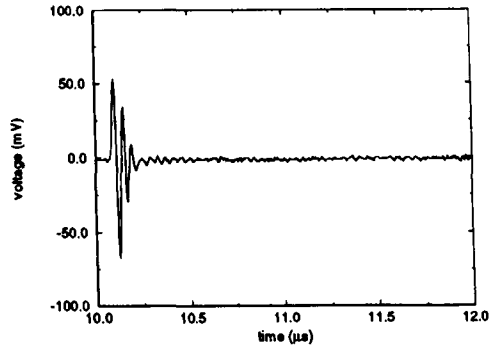

(b) 15mm separation

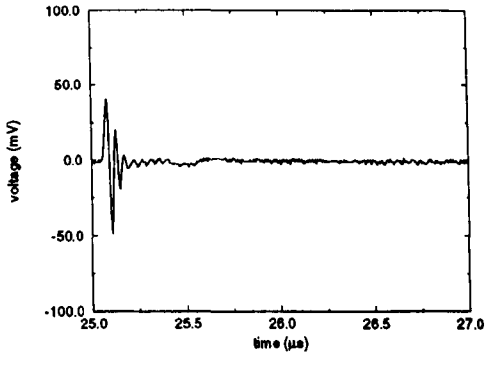

(c) 37.5mm separation

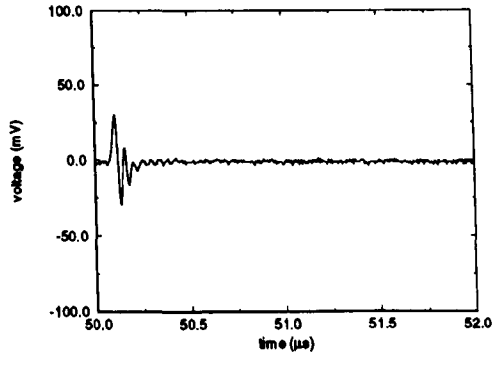

(d) 75mm separation

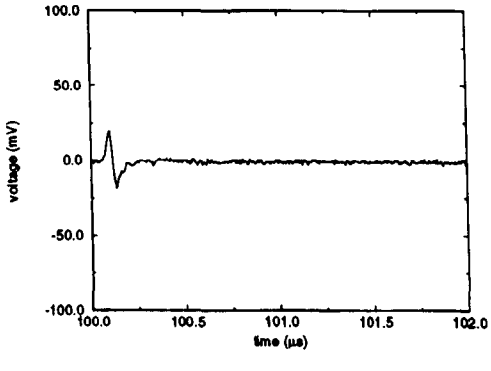

(e) 150mm separation

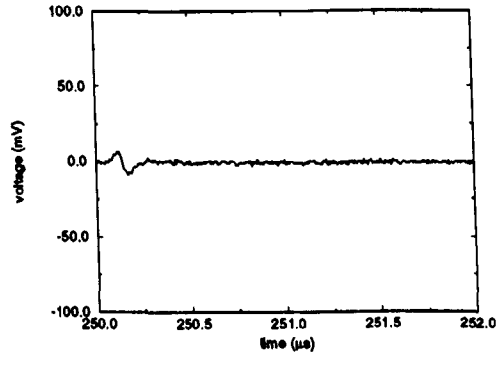

(f) 375mm separation

Figure 3.3 Axial field measurements for the PVDF transmitter, under water loading

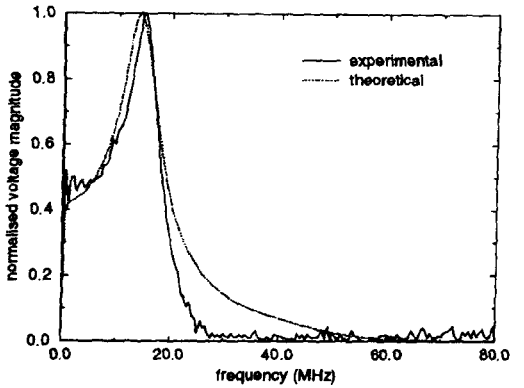

Figure 3.4(a) System frequency response for PVDF transmitter/membrane hydrophone system combination, after differentiated step excitation

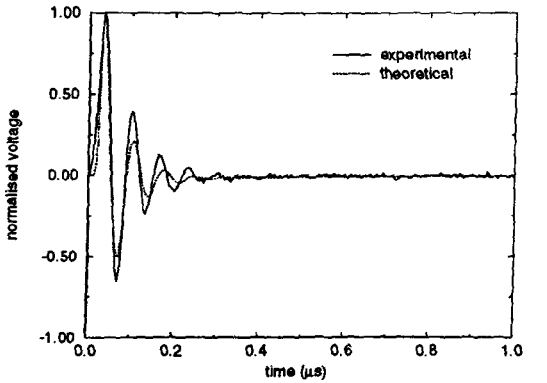

Figure 3.4(b) Time response for PVDF/Hydrophone system after differentiated step excitation

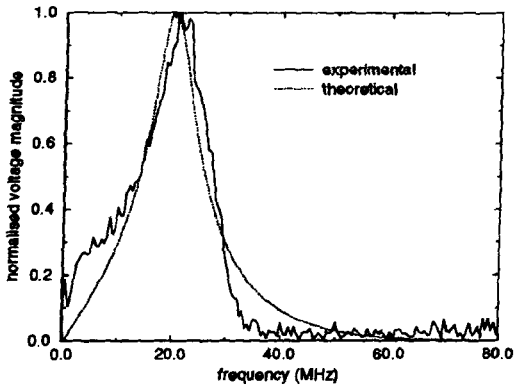

Figure 3.5(a) System frequency response for PVDF transmitter/membrane hydrophone combination after pseudo impulse excitation

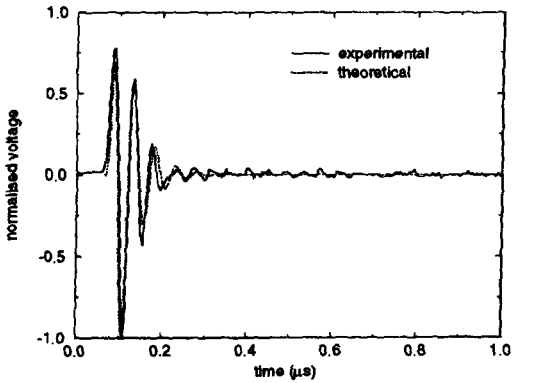

Figure 3.5(b) Time response for PVDF/Hydrophone system after pseudo impulse excitation

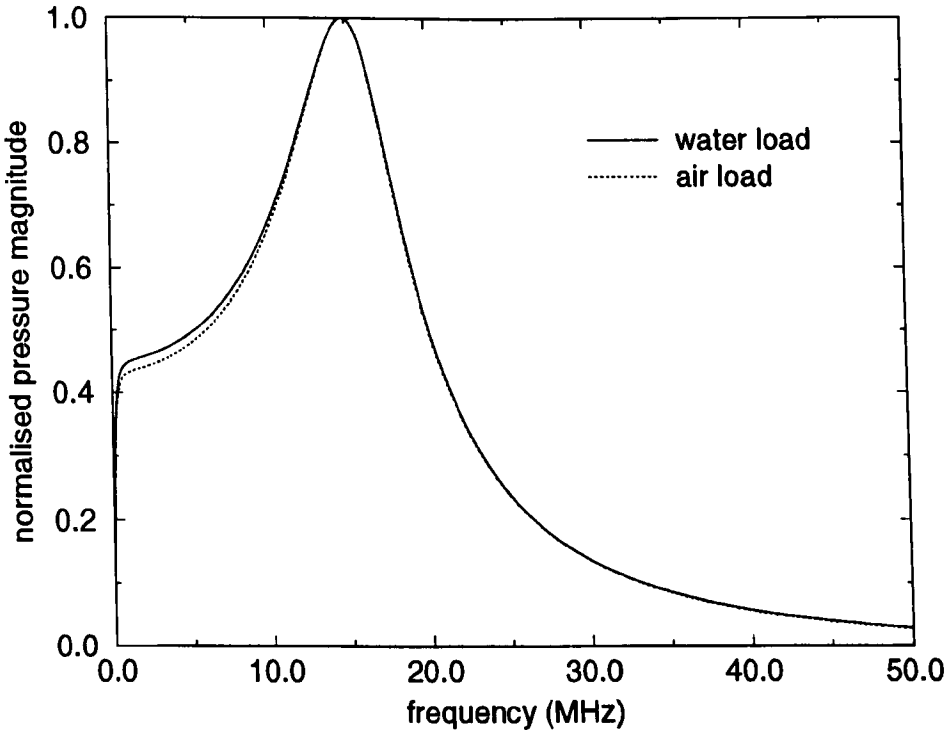

Figure 3.6(a) Predicted PVDF transducer transmission spectra, after differentiated step excitation

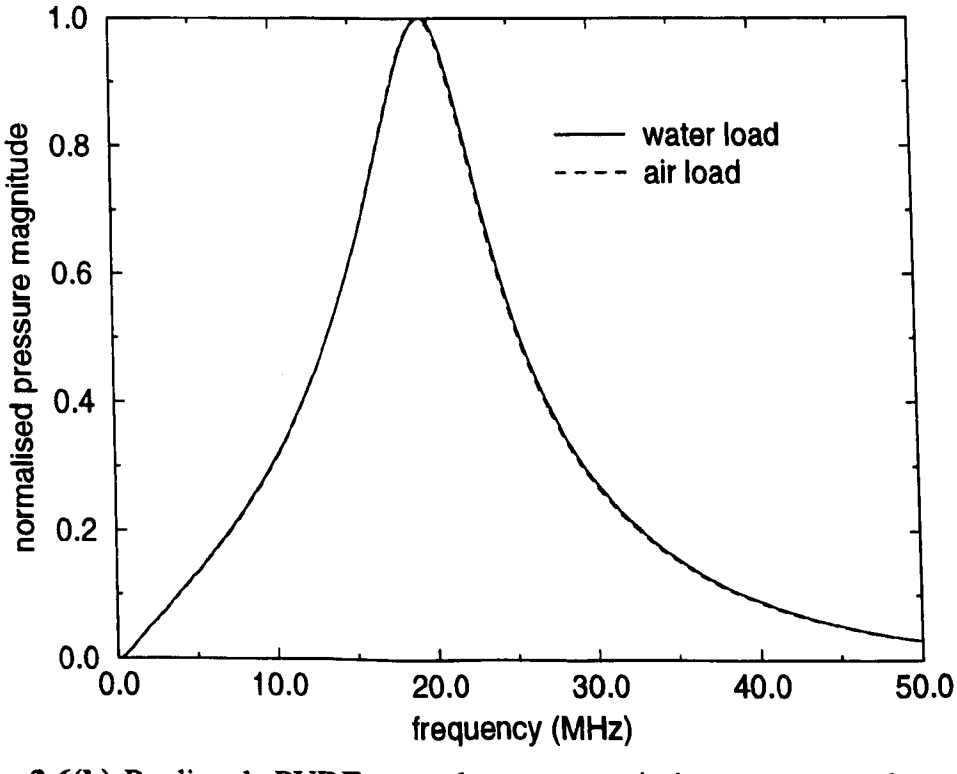

Figure 3.6(b) Predicted PVDF transducer transmission spectra, after pseudo impulse excitation

(b) Reception

For field and calibration measurements, the detection transducer should not interfere with the incident acoustic field and should not distort the pressure profile, either as a consequence of aperture diffraction or frequency response limitations. With its relatively low specific acoustic impedance, the PVDF membrane hydrophone provides a good match to water and may be configured to possess a flat response up to 20 MHz. Its active dimensions are much smaller than the incident wavelength and as such, it is ideally suited for water measurements in the low MHz frequency range. However the situation is quite different in the air environment, where the presence of any physical device will interfere with the acoustic field and the short wavelengths (0.345mm @ 1 MHz) introduce sensitivity problems with the resultant small sensor dimensions. Although non-contact optical systems have been described recently [104] for operation in water, no air calibration data has been reported to the knowledge of the author. Of available hydrophones, the membrane configuration, although by no means ideal, appears to offer the best prospect for air operation and it was thus decided to investigate this relatively low cost route.

A bilaminar PVDF membrane hydrophone [100], supplied by GEC-Marconi [101], with an active area of $0.2mm^2$ and a film thickness of 28μm was studied as a basis for wideband reception to enable absolute pressure measurement. The device was calibrated for immersion use and the relevant data is shown in Table 3.1, from which the wideband properties are apparent. This is confirmed by the linear systems simulations shown in Figure 3.7, which show the hydrophone impulse response when subject to both air and water loading. In these examples the hydrophone was assumed to operate into a resistive load of 1MΩ via different conditions of cable capacitance. Interestingly, the responses in air and water appear to be identical over the critical frequency range 50 kHz to 5 MHz. This somewhat unexpected result is due to the fact that cable capacitance dominates the hydrophone response and the modelling results indicate that apart from overall sensitivity changes, the spectral profiles for air and water are in close agreement for variations in cable capacitance of 20% around the measured hydrophone value of 110pF. Indeed, provided that the electrical loading connected to the hydrophone is

maintained within recommended guidelines (a parallel load resistance greater than 50kΩ and an end of cable capacitance, including any integral cable and connector, greater than 50pF) its response is stated to be 'flat' within ±1dB over the range 50kHz to 20MHz. Subsequently, it was considered possible to use the hydrophone for calibration of absolute pressure in the field of an air-coupled transducer.

Frequency (MHz)	2	3	4	5	10
Sensitivity (nV/Pa)	53	53	53	54	59

Table 3.1 Calibrated data for the standard hydrophone [101]

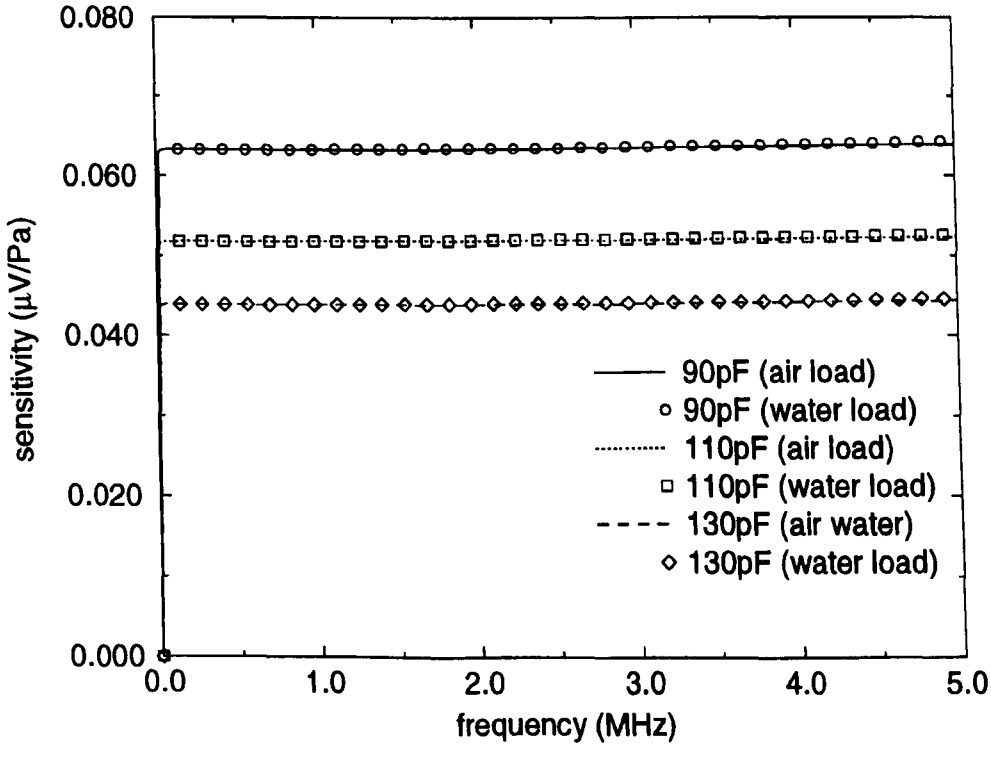

Figure 3.7 Calibrated membrane hydrophone under air and water loading

The generation of flexural waves in the membrane hydrophone can be problematic, especially for air-coupled measurements. These Lamb wave modes will be generated at shallow angles of incidence [105], 10° for the fundamental symmetrical mode (s_0), and consequently, careful alignment of the transmitter and hydrophone is necessary. Interference from the Lamb wave is governed by the group velocity of the Lamb wave in the PVDF membrane and the overall dimensions of the hydrophone. For the

experimentation described in this Thesis, Lamb wave generation did not constitute a problem.

3.3.3 Air Transducer Manufacture

(a) 1-3 Connectivity Composite Transducers

A range of composite transducers were constructed through the methodology described in Section 2.2.4. A selection of the manufactured transducer properties are summarised in Table 3.2, along with that of a 'pure' ceramic transducer. The Table describes each piezoelectric device by specifying the constituent materials, any mechanical matching / damping applied to the device and the electromechanical coupling co-efficient, k_t, as described in Equation 3.2. Where the electrical and mechanical resonances are described as f_m and f_n respectively. Note that no attempt was made to repolarise the composites after the dicing operation and some depolarisation is evident (from the slightly lower than expected values of coupling coefficient) in the measured data. As indicated in the Table, three devices included damping at the rear face, either in the form of a backing block of tungsten loaded epoxy, possessing a measured specific acoustic impedance of 8 MRayls, or perspex (3.2 MRayls). Front face matching layers were bonded to some of the transducers as either a single hard setting epoxy layer or a double loaded silicone rubber matching layer. Unless otherwise stated, the transducer centre frequencies for transmission or reception were measured at 550kHz +/- 10%.

$$k_t^2 = \frac{\frac{\pi f_m}{2f_n}}{\tan\left[\frac{\pi f_m}{2f_n}\right]} \qquad (3.2)$$

(b) Electrostatic Transducers

The basic transducer configuration has been described earlier in Section 2.3. Differences in membrane thickness and backplate roughness resulted in a wide operational frequency range, although, for the majority of transducers, maximum response was produced over the range 450 - 650kHz. Importantly, the most sensitive electrostatic and composite

transducers were centred very close to 600kHz, enabling a more accurate comparison of the two technologies. Details of the various devices are summarised in Table 3.3.

Transducer	Mnemonic	Matching	Backing	k_t
PZT5H	PZT5H	No	No	0.470
20% PZT5A/Hard set	C20	No	No	0.446
20% PZT5A/Hard set	C20B	No	3.2MRayl	0.476
30% PZT5A/Hard set	C30ML	Double	No	0.612
40% PZT5A/Hard set	C40	No	No	0.591
40% PZT5A/Hard set	C40MLB	Single	8MRayl	0.577
60% PZT5A/Hard set	C60	No	No	0.587
60% PZT5A/Hard set	C60B	No	8MRayl	0.586
70% PZT5A/Hard set	C70ML	Double	No	0.570
70% PZT5H/Hard set	C70	No	No	0.622

Table 3.2 Constituent materials for piezoelectric transducers

Material	Mnemonic	Backing Plate	Average Roughness	Bias
5μm mylar	RB5.0	Rough Brass	50μm	250V
5μm mylar	LA5.0	Lapped Aluminium	9μm	250V
5μm mylar	PS5.0	Polished Steel	3μm	250V
3.5μm mylar	RB3.5	Rough Brass	50μm	200V
3.5μm mylar	LA3.5	Lapped Aluminium	9μm	200V
3.5μm mylar	PS3.5	Polished Steel	3μm	200V
2.5μm mylar	RB2.5	Rough Brass	50μm	120V
2.5μm mylar	LA2.5	Lapped Aluminium	9μm	120V
2.5μm mylar	PS2.5	Polished Steel	3μm	120V

Table 3.3 Constituent materials for electrostatic transducers

3.4 Airborne Attenuation

3.4.1 Evaluation of Standard Theory

For the considered range of frequencies, attenuation of the propagating ultrasonic wave within the air environment can be significant. The atmospheric absorption of sound energy has been presented by Bass et al [3] and a methodology proposed for the calculation of the attenuation constant as a function of frequency, where variations in air temperature, pressure and relative humidity, in the propagation channel, are also incorporated. The expression shown in Equation 3.3 has been proposed in [3] for the a calculation of the attenuation constant, α (Npm^{-1}), in air.

$$\alpha = f^2 \{1.84e^{-11}(P_O/P)(T/T_O)^{1/2} + (T_O/T)^{5/2} [(1.278e^{-2}\frac{e^{-2239.1/T}}{f_{r,O}+(f^2/f_{r,O})}) + (1.068e^{-1}\frac{e^{-3352/T}}{f_{r,N}+(f^2/f_{r,N})})] \} \quad (3.3)$$

where f is the frequency (Hz); T is the air temperature (K); T_O = 293.15K; P is the atmospheric pressure (Nm^{-2}); P_O = 1.01325x10^5 Nm^{-2}; and $f_{r,O}$ and $f_{r,N}$ are the rotational relaxation frequencies (Hz) for oxygen and nitrogen, respectively.

A more detailed description of the airborne attenuation theory described by Bass et al is presented in Appendix C.

Bass et al have stated that the algorithm is accurate to +/- 5% over the temperature range 273.15°K-313.15°K; the range of relative humidity 0-100%; the range of frequencies from 50Hz to 10MHz when the pressure is 1 atm; and for pressure from 1 atm down to a few hundredths of an atmosphere. From this information, one important feature to note regarding this theory is that it is restricted to frequencies below 10MHz, but due to the large attenuation in air at these frequencies, between 75 and 85 dB/mm at 20MHz [52], this was not considered to be a serious constraint.

Consequently, this attenuation coefficient is applied to the general form of the absorption equation and the result is shown in Equation 3.4. Here, P is the resultant pressure amplitude after the pressure wave has travelled a distance defined by z, P_o is the initial pressure amplitude at the front face of the transducer and α has been calculated from Equation 3.3. In the following analysis, these Equations were implemented to facilitate comparison between theoretical and experimental data, where the approach simulates a low pass filter.

$$P=P_o e^{-\alpha z} \tag{3.4}$$

3.4.2 Linear Systems Model modified to include Air Attenuation

The modified airborne attenuation theory has been combined within the linear systems model [86] to enable the prediction of the pressure wave incident on the front face of an air-coupled detector. Both of the proposed excitation methods have been examined to estimate their characteristic response in air. Thus, the variation of the intermediate airgap between the PVDF transmitter and a detector has been simulated and the results are illustrated in Figures 3.8(a) and 3.8(b), for differentiated step excitation (pulser unit), and Figures 3.9(a) and 3.9(b), for pseudo-impulsive excitation (Panametrics unit). These Figures illustrate the theoretical frequency spectra and time plots respectively, for different separation distances and assuming no multiple reflections within the gap. Here, the data has been presented relative to the zero air attenuation simulations shown previously in Figures 3.6(a) and 3.6(b). Considerable differences in the frequency content when the pressure wave experiences airborne attenuation is portrayed for both excitation methods. The corresponding time plots show unipolar behaviour and an expansion in pulse width, with increasing airgap separation.

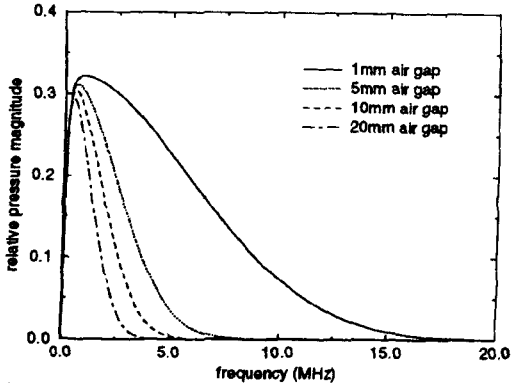

Figure 3.8(a) Predicted spectra for a PVDF transmitter with variation in airgap, after differentiated step excitation (scaled relative to spectra shown in Figure 3.6(a))

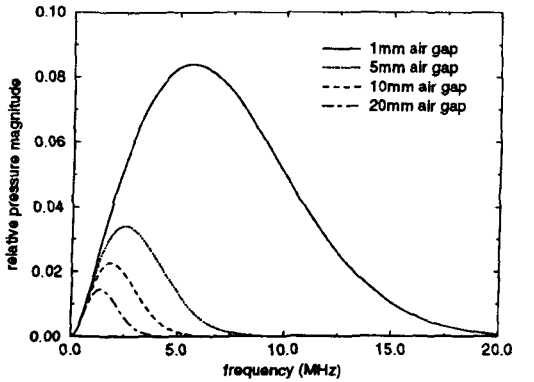

Figure 3.9(a) Predicted spectra for a PVDF transmitter with variation in airgap, after pseudo impulse excitation (scaled relative to spectra shown in Figure 3.6(b))

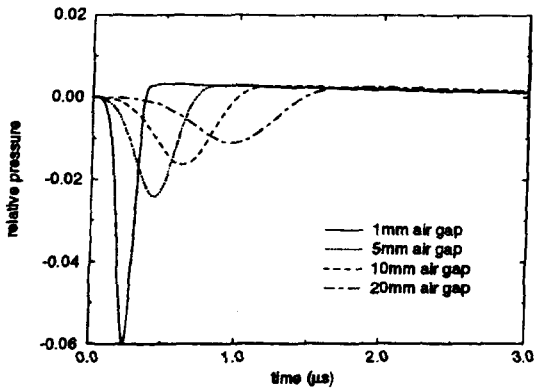

Figure 3.8(b) Corresponding temporal responses for spectra shown in Figure 3.8(a)

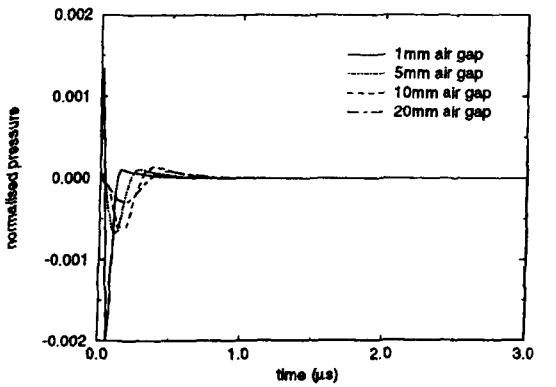

Figure 3.9(b) Corresponding temporal responses for spectra shown in Figure 3.9(a)

Experimental confirmation of these results proved extremely difficult, due to the low sensitivity of both the PVDF transmitters and the membrane hydrophone (active area $0.2mm^2$). However, it was just possible to measure the pitch-catch response of two PVDF devices of identical design, with the pulser unit used to excite the transmitter and the receiver operating directly into the preamplifier. This is shown in Figure 3.10, for an air separation distance of 20mm. Despite a low peak signal level of 5mV and poor SNR, reasonable correlation between theory and experimental data has been achieved. The result is significant since the unipolar nature of the theoretical response is verified by the experiment, inferring validity of the data shown in Figure 3.8(b).

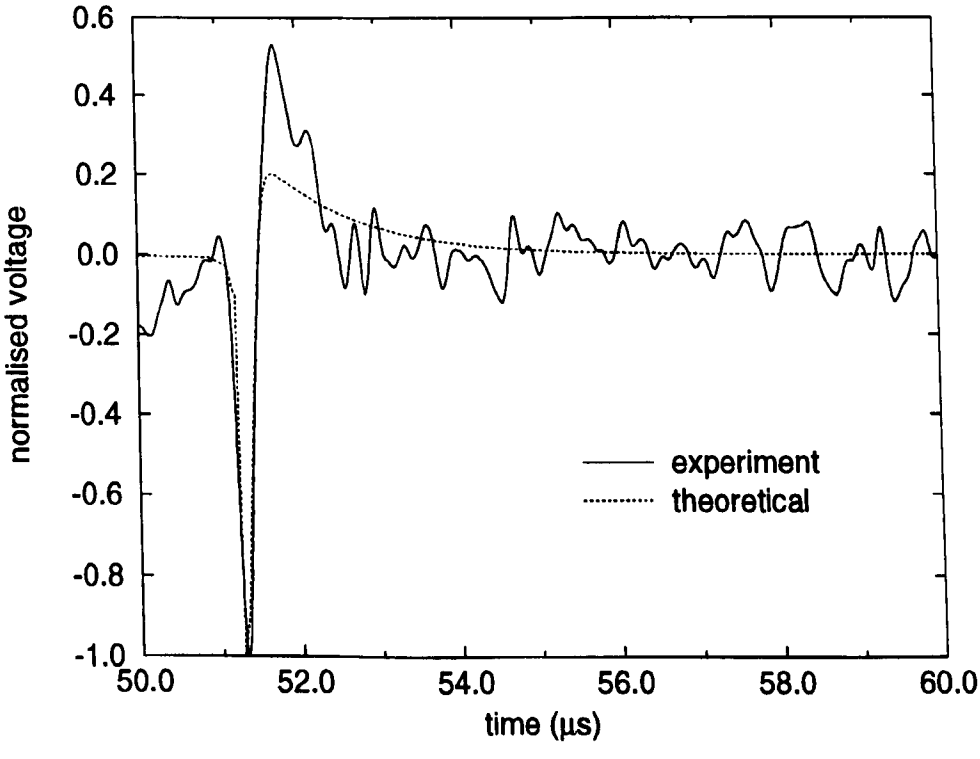

Figure 3.10 Air coupled PVDF transducer pitch-catch system response

However, it is apparent from these results that generation of even an approximate impulsive pressure function is extremely difficult in the air environment and that the gap separation distance can be critical. Moreover, for a valid comparison of different transducers, it is essential that the transmitted force spectrum overlaps that of the receiving devices. To investigate the validity of the proposed wideband transmission systems, the PVDF output was compared theoretically with ideal impulsive excitation applied to the reception device. Figure 3.11 illustrates the predicted normalised response for a damped 20% piezocomposite receiver, (device C20B described in Table 3.2), under

four different stimulation conditions : ideal impulsive excitation (delta function); impulse excitation including the influence of airborne attenuation (delta + air attenuation); the PVDF transmitter/pulser combination including airborne attenuation (pulser + air attenuation); and Panametrics excitation of the transmitter including air attenuation (panam + air attenuation). A separation distance of 20mm between transmitter and receiver was assumed. The low pass characteristic of air attenuation is evident, but the transducer receive impulse response has been reproduced quite well by the PVDF/pulser unit transmission method. This can be explained through analysis of the predicted spectral characteristics shown in Figures 3.8(a) and 3.9(a) for pulser unit and Panametrics excitation respectively. These plots show the main frequency content for the pulser unit case to be concentrated at frequencies below 1MHz, for an air separation distance of 20mm. Whereas, Panametric stimulation produces a spectra with a higher frequency content, but with the main concentration at frequencies above 1MHz. For the receivers presently under evaluation, most operational centre frequencies were in the region of 500kHz, with only two electrostatic devices extending significantly beyond 1MHz. The transmitter spectral characteristics, under pulser unit excitation, were thus considered adequate for air separation distances of approxiamtely 20mm.

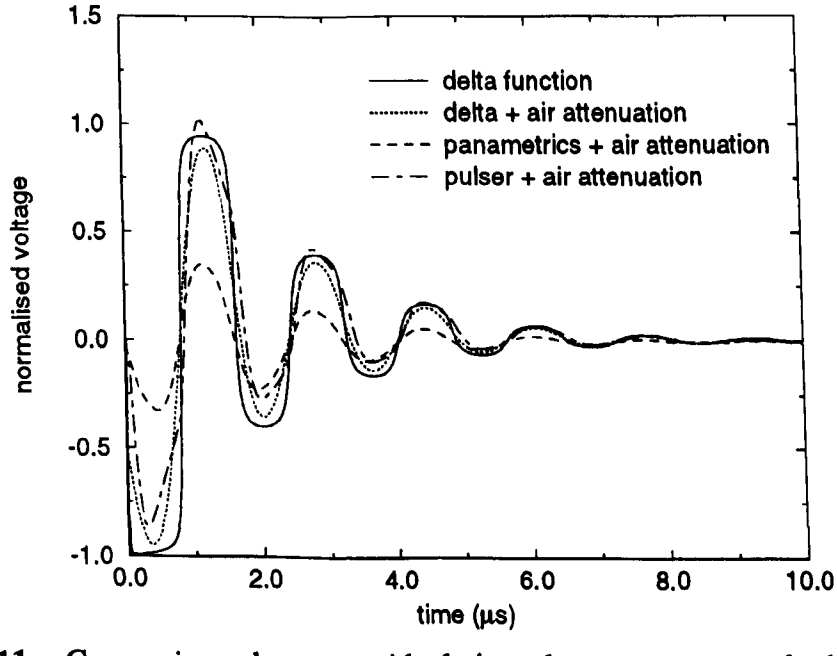

Figure 3.11 Comparison between ideal impulse response and the receiver response under practical stimulation conditions

3.4.3 Evaluation of Modified Modelling Theory for 1-3 Composites

(a) Transmission

The impulse transmission responses for composites C40 and C60B were measured using pulser unit stimulation and the membrane hydrophone. To assess simulation of air attenuation, the separation between transducer and hydrophone was set at 35mm and 17.5mm respectively, with the corresponding transmission response profiles illustrated in Figures 3.12(a) and 3.12(b). In both cases, good agreement between theory and experiment may be observed, with the model predicting correctly the principal features of each configuration.

(b) Reception

The pulser unit/PVDF transducer combination was then used to simulate a broadband transmission for evaluation of the through air reception 'impulse' response for the C20B and C40 devices. The separation distance between the composite under test and the PVDF transmitter was set to 35mm and 17.5mm respectively. The received voltage profiles are shown in Figures 3.13(a) and 3.13(b) and again, good agreement is apparent, with the experimental data appearing to validate the theoretical approach.

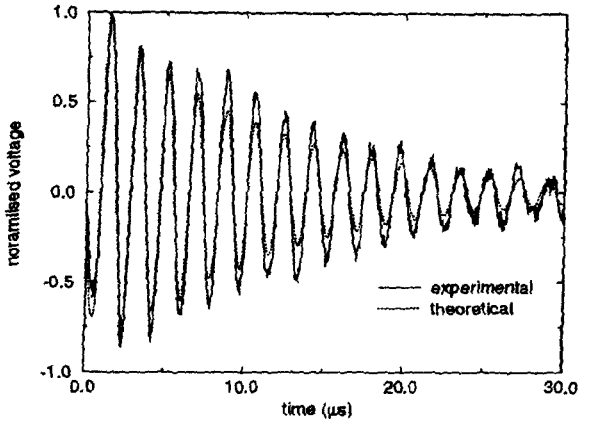

Figure 3.12(a) Transmission response for a 40% piezocomposite

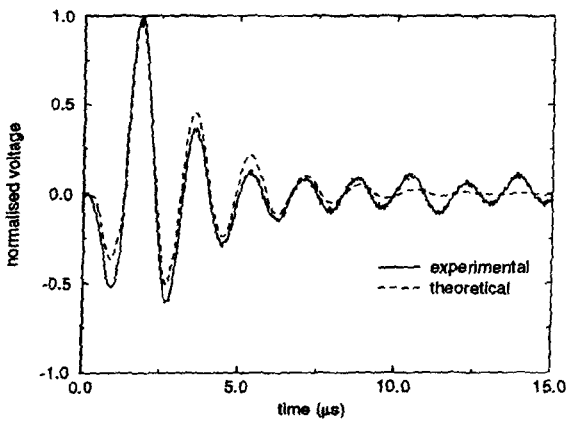

Figure 3.12(b) Transmission response for a damped 60% composite

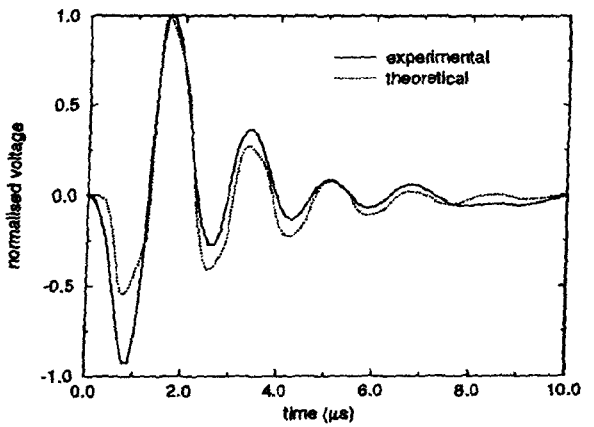

Figure 3.13(a) Receive characteristic for a 20% damped piezocomposite

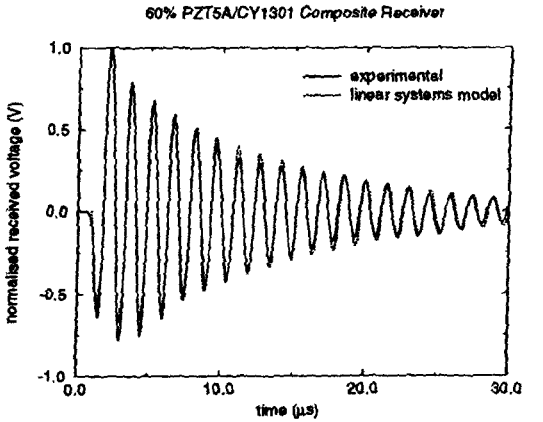

Figure 3.13(b) Receive response for a 40% composite transducer

3.5 Radiated Fields of Air-Coupled Transducers

3.5.1 Introduction

The ultrasonic field profile associated with a transducer is an important feature that can limit system performance, especially in an air environment. Many investigators have analysed the radiated field pattern from ultrasonic transducers operating into a fluid load [106,107] and an excellent review of their work can be found in Reference 99. Three main problems exists for through air ultrasonic propagation. Firstly, the requirement for a calibrated receiver, with sufficient sensitivity and an active area comparable to the sound wavelength in air. Secondly, the short wavelengths will increase the number of maxima and minima associated with the interference pattern between plane and edge wave components. Finally, the influence of airborne attenuation will dominate the ultrasonic field structure limiting propagating distances. The following work will incorporate standard beam profile theory and the influence of airborne attenuation to analyse air-coupled beam profiles. An experimentally acquired axial field profile for an air-coupled composite transducer, operating around 500kHz, will be presented. Consequently, the transducer positioning criteria used in the characterisation process will be proposed.

3.5.2 Theoretical Air-Coupled Acoustic Field Characteristics

Considering the air propagation media using standard theory [106] permits a preliminary guide to the irradiated field structure. This analysis will use Equations 3.5 and 3.6 to assess the near-far field boundary, N, and the angle of divergence of the sound energy, γ_o, respectively. Where, a is the radius of the transducer and λ is the wavelength of the ultrasound.

$$N = \frac{a^2}{\lambda} \tag{3.5}$$

$$\sin\gamma_o = 1.22\,\frac{\lambda}{2a} \tag{3.6}$$

Table 3.4 illustrates the predicted difference in ultrasonic field structure for a 30mm diameter ceramic disc, operating at 500kHz, in both water and air media. For the

purposes of this comparison, the influence of air attenuation has not been included in the analysis. These results illustrate the influence of the smaller wavelength of sound energy in air, where the near-far field boundary is located further from the transducer and the beam divergence is at a shallower angle compared to operation under water load. Although, the narrow beam divergence can be considered a benefit to overall system performance, the location of the near-far field boundary could be a constraining feature due to the influence of airborne attenuation.

	Water Load	Air Load
N	75 mm	326 mm
γ_o	6.5°	1.5°

Table 3.4 Comparison between theoretically predicted behaviour of the ultrasonic field in both water and air media

The on-axial air-coupled field profile of a piston mounted in a rigid infinite baffle can be considered by combining standard theory [106] and the air attenuation theory, discussed in Section 3.4. This theoretical approach has been used to predict the acoustic field behaviour under three different load conditions : a standard water load ; an air load, not incorporating the influence of airborne attenuation ; and with the theory modified to include airborne attenuation. A 30mm disc transducer is assumed to be driven under continuous wave (cw) conditions at an operating frequency of 500kHz. Figure 3.14 illustrates the predicted on-axis directivity profile under these load conditions. The results shown in this Figure compare favourably with the results presented in Table 3.4, for both water and air loads (neglecting the influence of air attenuation). It should be noted that the concept of conventional 'near field' and 'far field' zones is not strictly valid for operation in air, due to the high attenuation, which can dominate the field structure at these frequencies. Consequently, the axial positioning of a air-coupled detector is of critical importance. It should be noted that the limited resolution of the graph disguises the response close to the transducer and total constructive and destructive interference will occur in this region.

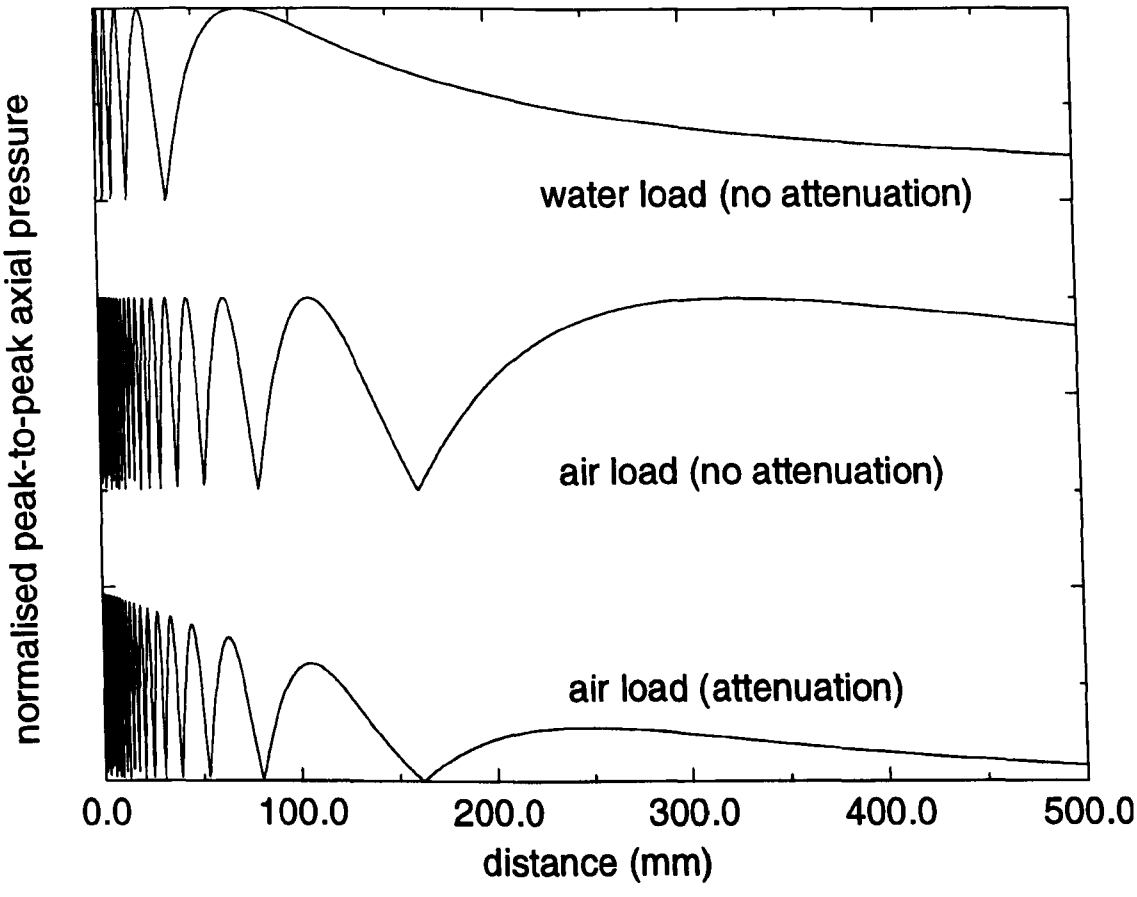

Figure 3.14 On-axis directivity profile for a 30mm disc under cw conditions operating into various load conditions

3.5.3 Experimental Air-Coupled Field Profiles

By utilising an air-coupled transmitter / hydrophone arrangement, it is possible to experimentally measure the on-axial field profile using the apparatus described in Section 2.4. The transmitter is excited using a 10-cycle tone burst, delivered at the transducer centre frequency (496kHz), and 50dB of power amplification. The experimentally acquired field profile for composite device C60, from Table 3.2, is presented in Figure 3.15. In the near field of the transducer a constructive/destructive interference pattern is evident. When combined with the influence of airborne attenuation, which is manifest as the exponential decrease in signal strength as the air separation distance is increased, these attributes unite to modify the concept of a conventional near/far field boundary. Therefore, the peak axial signal strength is closer to the transmitter, at approximately 22.5mm.

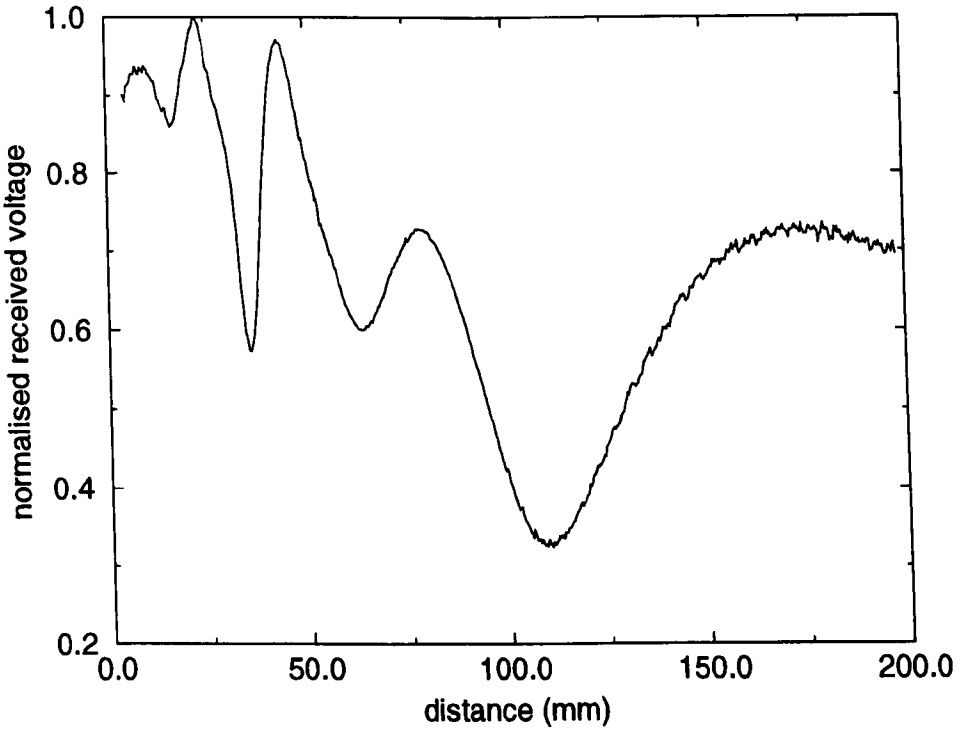

Figure 3.15 Experimentally measured axial field profile for a 60% composite transducer, operating at 496kHz

The axial field profile illustrated in Figure 3.15 differs markedly from the theoretical prediction shown in Figure 3.14 for an air load and including the influence of air attenuation. A lower number of fluctuations due to interference between the plane and edge wave components is evident in the experimentally acquired response. In fact, at a distance of 100mm, an experimental null has been measured, which contradicts the theoretical prediction. To fully evaluate the experimentally measured response both the directivity of the hydrophone and the surface displacement profile for the transmitting device, to ensure plane wave generation, would have to be investigated. In addition, the transducer was driven under tone burst excitation conditions. For the purpose of the Thesis, the principal feature from the experimentally measured axial field profile is the position of maximum pressure, at 22.5mm. Consequently, the separation between the transmit and receive transducers, for the work presented in the Thesis, will correspond to the experimentally measured peaks in the acoustic fields for the range of devices under consideration. This was also considered to be more realistic from an applications viewpoint, where the air separation distance is often required to be as small as possible.

3.6 Characterisation for Air-Coupled Transducers

3.6.1 Evaluation of Wideband Response

(a) Results

To facilitate logical comparison between differing transducer configurations, the power source, transducer shape and surface area, air gap size, air temperature, pressure and relative humidity and the receive electronics were maintained constant for each experiment. Section 2.4 describes the experimental arrangement in more detail. Unless otherwise stated, each transducer was circular with a diameter of 30mm, and as far as possible designed to operate at a median frequency of 550kHz (±10%).

The experimental results for both transmission and reception, are detailed in Table 3.5, with the -3dB bandwidths indicated in parenthesis. To provide additional insight into potential performance, the pulse-echo insertion loss and -6dB bandwidth are also shown in the Table. For transmission evaluation, the hydrophone signal was used to calculate an absolute source pressure level, while open circuit voltage response is used to quantify reception sensitivity. To achieve the latter, it was necessary to calibrate the PVDF transmitter. This was performed in conjunction with the membrane hydrophone by means of the substitution technique [108].

(b) Transmission Analysis

Considering firstly the transmission characteristics, the results indicate that the 70% PZT5A/hard set piezocomposite, incorporating a double front face matching layer, exhibits a 12.2dB improvement in sensitivity over the best electrostatic device, (2.5μm mylar with rough brass backplate), although the piezocomposite bandwidth is considerably lower. However, the very thin membrane proved to be extremely fragile, even under laboratory conditions, and for more robust operation, the 5μm film is recommended. In this case the sensitivity difference is greater at 15.2dB. A reasonably wideband response can be observed for the damped 40% composite transducer, although the sensitivity is reduced as a result of the sub-optimal volume fraction. The actual best composite transmitter is a complex function of constituent materials, centre frequency

and the type of matching layer(s), and the results here are intended only as a guide to absolute variations between different transducer configurations. Chapter 4, 'An evaluation of 1-3 connectivity composite transducers for air-coupled ultrasonic applications', will describe the optimisation of the piezocomposite transducer.

Mnemonic	Transmit Voltage Response (dB re 1μPa/V)	Open Circuit Voltage Response (dB re 1V/μPa)	Pulse-echo Impulse Response	
			Insertion Loss (dB)	B/W (kHz)
PZT5H	116.8 (19kHz)	-210.2 (13kHz)		
C20	115.0 (22kHz)	-200.9 (19kHz)		
C30ML	122.3 (71kHz)	-186.1 (58kHz)	-113.3	5%@600
C40	116.8 (54kHz)	-199.7 (77kHz)		
C40MLB	118.8 (148kHz)	-194.2 (132kHz)	-101.5	25%@394
C60	117.9 (22kHz)	-202.2 (14kHz)		
C70ML	134.6 (62kHz)	-188.8 (41kHz)	-92.3	5%@601
C70	120.5 (24kHz)	-204.5 (15kHz)		
RB5.0	119.4 (242kHz)	-196.3 (322kHz)	-87.0	109%@403
LA5.0	118.0 (293kHz)	-206.6 (348kHz)	-89.9	124%@457
PS5.0	117.5 (311kHz)	-201.8 (375kHz)	-101.5	138%@470
RB3.5	121.1 (329kHz)	-193.7 (483kHz)	-85.0	73%@551
LA3.5	119.3 (486kHz)	-204.1 (556kHz)	-89.3	142%@645
PS3.5	118.6 (587kHz)	-199.1 (590kHz)	-99.5	92%@1220
RB2.5	122.4 (458kHz)	-189.4 (525kHz)	-77.1	126%@597
LA2.5	121.7 (594kHz)	-196.9 (632kHz)	-79.3	168%@672
PS2.5	120.1 (806kHz)	-193.2 (677kHz)	-97.3	90%@1403

Table 3.5 Wideband characterisation for a selection of the transducers described in Tables 3.2 and 3.3

(c) Reception Analysis

The reception data described in Table 3.5 reveal some interesting differences. The best reception sensitivity for the piezocomposites occurs for the lower volume fractions and double matching layer, at -186.1dB re 1V/μPa. This result was expected and further explanation can be found in Chapter 4. Interestingly, this figure is comparable with receiving transducers operating in a water environment. The most sensitive electrostatic device is only 3.3dB lower and the more robust 5μm configurations are at best 10dB down, although in all cases with significantly improved bandwidths. Indeed, conventional methods such as backing, for extending the bandwidth of the resonant, thickness mode devices, are unlikely to yield the wideband performance of the electrostatics. However, the bandwidth may be extended (at the expense of sensitivity) by means of alternative methods, as described in Chapter 5. Throughout, there was some variation in bandwidth across the ranges of both types of transducer. In the case of the piezocomposites, this is due to the different structure (volume fraction, backing and matching layers), in addition to the fact that for the mode of operation described, the transmission and reception sensitivities peak at the frequencies of impedance minimum and maximum respectively [102,109]. For the electrostatic transducers, the variation was due in part to differences in surface roughness, membrane tension and thickness.

(d) Sensitivity-Bandwidths Measurements

It is interesting to compare the sensitivity-bandwidth product for the best electrostatic and composite transducers. In transmission, sensitivity-bandwidth products of 58700 V.Hz, 22300 V.Hz and 33000 V.Hz were calculated for transducers RB2.5, RB5.0 and C70ML, respectively. In addition, values of 211000 V.Hz, 60000 V.Hz and 34000 V.Hz were calculated for transducers RB2.5, RB5.0 and C30ML, respectively, when operating in reception. These results emphasise the significant wideband characteristic of the electrostatic transducer, where a six-fold improvement, comparing devices RB2.5 and C30ML, is evident from the reception data.

(e) Pulse-Echo Analysis

In the wideband pulse-echo tests, the normal reflector was a polished glass block positioned approximately 10mm from the transducer face, with the received voltage taken directly from an oscilloscope of input resistance 1Mohm in parallel with a capacitance of 20pF. The results indicate that the electrostatic devices are far superior with respect to both bandwidth and sensitivity, which is somewhat surprising given the previous data for separate transmission and reception performance. Indeed, for most of the piezocomposites and the piezoceramic transducer, there was insufficient signal to permit accurate measurement. The reasons for this are due primarily to the relatively narrowband nature of the piezocomposites and the fact that the frequency of transmission is significantly different from that which is required to maximise reception response. Furthermore, none of the piezoceramic based devices under consideration were designed specifically for pulse-echo operation and only two are considered at all suitable for air operation (C30ML/C70ML). The sub-optimal matching of the other piezocomposite to give a measurable response (C40MLB), has also resulted in a peak spectral response at the relatively low value of 394kHz, which corresponds to the fundamental resonance of the transducer/matching layer combination. These results serve to illustrate the requirement for extremely careful design of piezoceramic air-coupled transducers. These problems do not arise for the electrostatic devices, although there is considerable variation in the measured pulse-echo centre frequency. An illustration of the temporal and spectral wideband response from RB2.5 is shown in Figure 3.16, from which the enhanced bandwidth of the electrostatic device is evident. This was the most efficient electrostatic device, which is confirmed by the separate transmission and reception results. The centre frequency is very close to 600kHz, facilitating narrowband comparison with corresponding composite designs.

3.6.2 Narrowband Characterisation

(a) Transmit Voltage Response

The best transducers from the previous experiments were then evaluated under narrowband operating conditions. The transmit voltage responses for the RB2.5

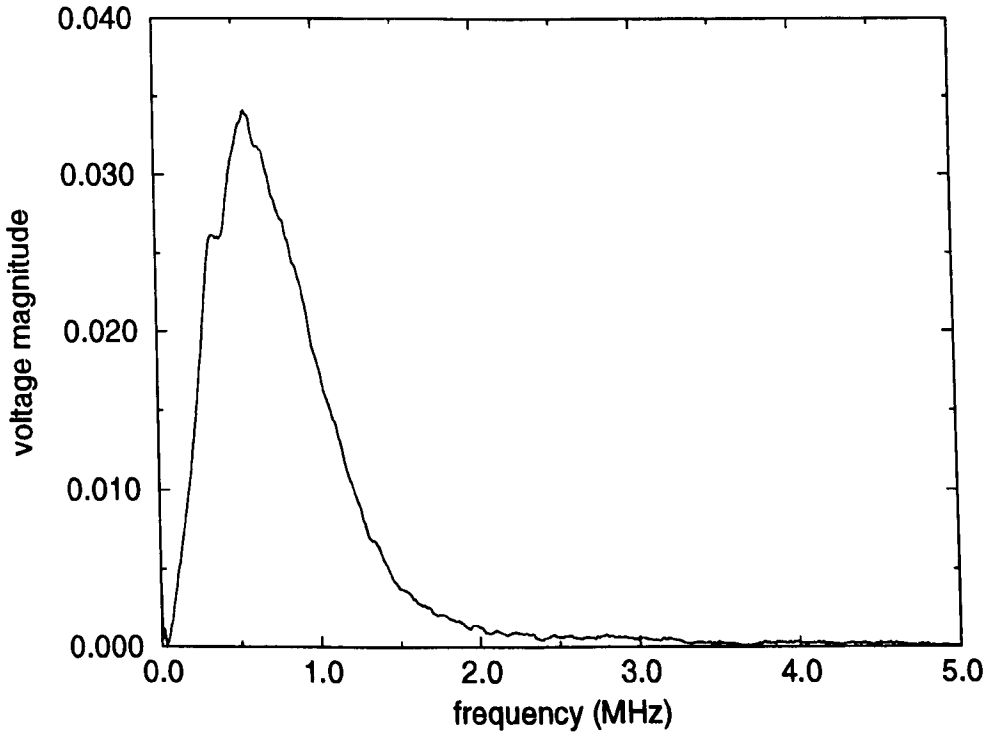

Figure 3.16(a) Pulse-echo spectral response for the 2.5μm mylar electrostatic, with rough brass backplate

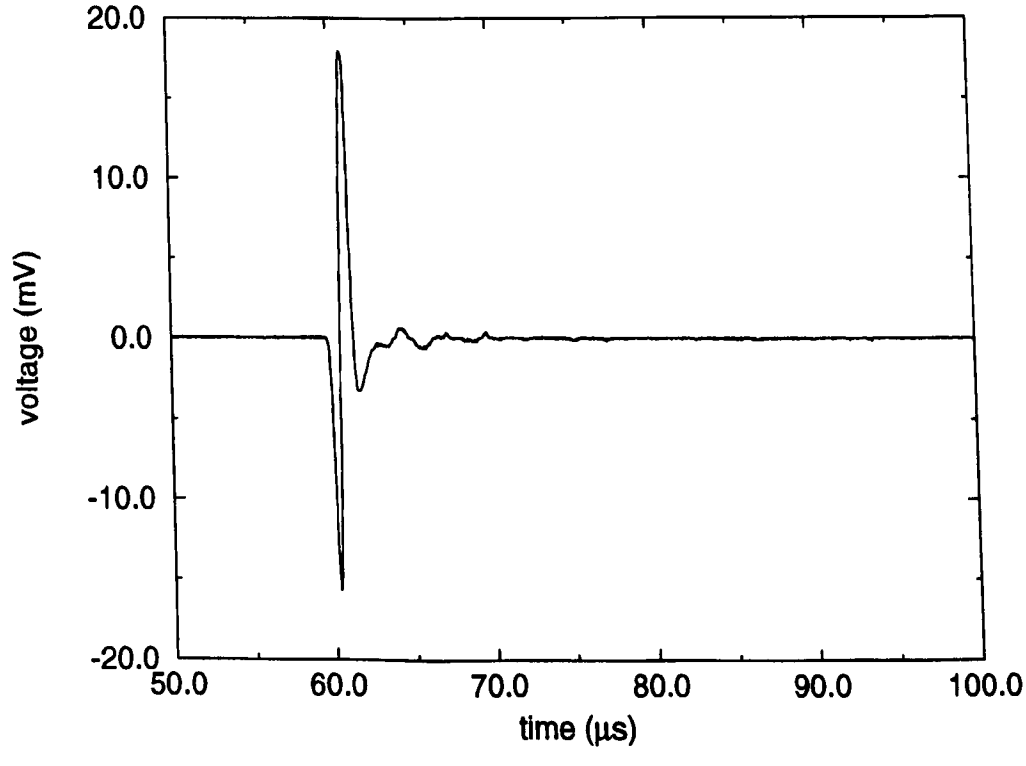

Figure 3.16(b) Pulse-echo time response for the 2.5μm mylar electrostatic, with rough brass backplate

electrostatic and C70ML composite transducers were measured in air using a 20 cycle 600kHz tone burst (75V peak to peak). The gap separation distance was 20mm, with the hydrophone connected directly to the pre-amplification stage. Sensitivity figures of 138.2dB re 1μPa/V and 126.8dB re 1μPa/V were achieved for the composite and capacitive devices respectively, with the difference due to the resonant properties of the composite transducer.

(b) Through Transmission Performance

Narrowband transmit-receive comparisons were also performed using a 20 cycle tone burst (10V peak to peak) by connecting the separate receiving transducer directly into an oscilloscope. In this case, RB2.5, RB5 and C70ML/C30ML transducer pairs were positioned 20mm apart in transmit-receive mode and the transmission frequency adjusted to achieve maximum response. The received temporal responses are illustrated in Figures 3.17(a) - 3.17(c) respectively. It should be noted that the 5μm mylar electrostatic transducer pair operated at approximately 400kHz, whereas the other two combinations employed a 600kHz excitation signal. Also, these signals were acquired in real-time, with no signal averaging applied to the data. The piezocomposite pair demonstrate superior sensitivity over both electrostatic combinations, 22.7dB and 30.9dB respectively. The high SNR associated with the composite pair (greater than 35dB) would enable their application to real-time non-destructive evaluation systems.

Finally, it was interesting to compare the differences in sensitivity when the electrostatic receiver in the transmit-receive experiments was replaced by a composite device. The previous narrowband experiment was repeated using the same RB2.5 electrostatic transmitter but with the C30ML composite as the receiver, as shown in Figure 3.17(d). Here, a 13.6dB improvement in receive sensitivity has been exhibited by the composite detection system. Hence, the resonant nature of the piezocomposite devices has demonstrated superior narrowband sensitivity performance in transmission, reception and pitch-catch modes of operation.

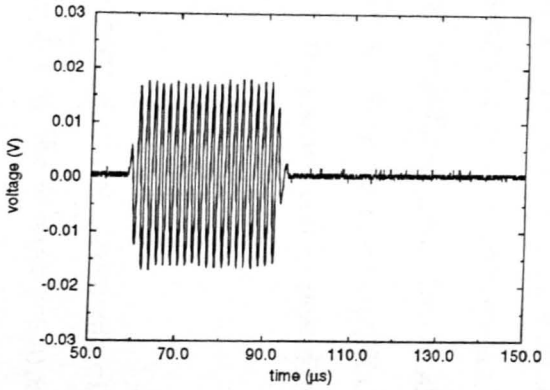

Figure 3.17(a) Narrowband through transmission response for the 2.5μm electrostatic transducer pair

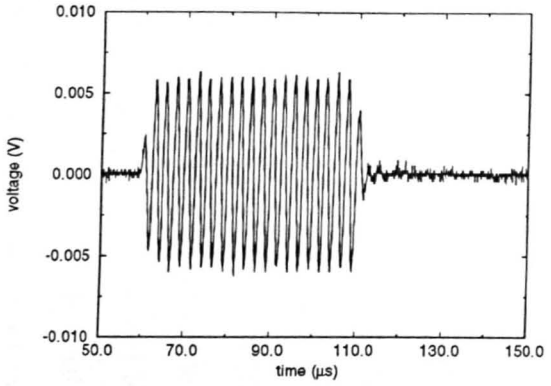

Figure 3.17(b) Narrowband through transmission response for a 5.0μm electrostatic pair

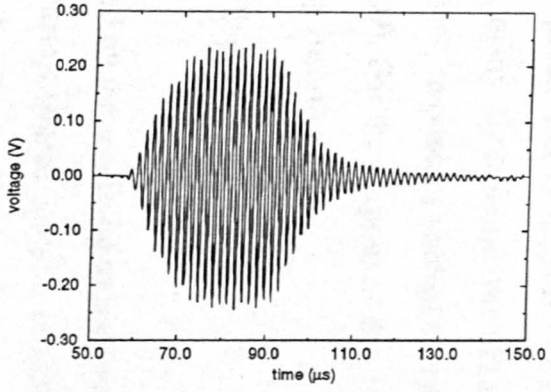

Figure 3.17(c) Narrowband through transmission response for the 70%/30% composite transducer combination

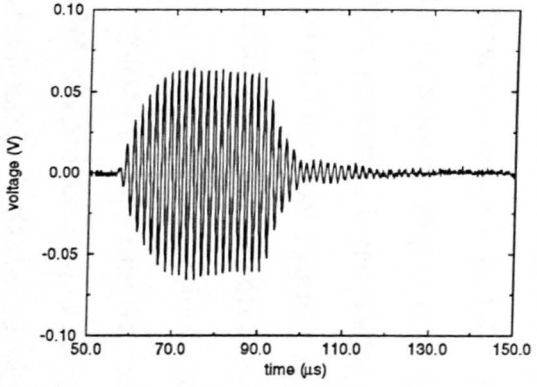

Figure 3.17(d) Narrowband through transmission response for the 2.5μm electrostatic transmitter / 30% composite receiver combination

3.7 System Insertion Loss

Several workers have introduced the concept of insertion loss in an attempt to define a standard comparison between various air transducer designs. In 1983, Fox et al measured a two way insertion loss of 52dB for the pulse-echo response of a PZT5H ceramic transducer, including a RTV silicone rubber matching layer, under electrically tuned conditions [10]. Similarly, Yano et al measured one way insertion loss to compare the relative advantages of several different matching layers for a 1MHz PZT5H device [13], yielding values in the order of 30dB. To characterise a micromachined composite matching layer, Haller and Khuri-Yakub reported a 17dB one way insertion loss for a Kapton/air layer when used with a PZT5H transmitter [19]. Recently, Mattila et al described a two way insertion loss of approximately 46dB for the pulse-echo response from a 50kHz electrostatic transducer with a v-grooved backplate [42]. Unfortunately, these applications of insertion loss differ and there appears to be no standard measurement technique for both two way and one way insertion loss. The well known microwave theory relates the decibel ratio of the maximum available power from the excitation source to the power delivered into a matched load [110]. This approach was employed by Selfridge [111] for comparison of array transducers in ultrasonic imaging. Since the transducers were designed to operate into 50Ω, this definition of two way insertion loss is appropriate. However in many applications the ultrasonic transducers are interfaced quite differently and moreover, maximum voltage reception sensitivity is obtained under open circuit conditions [109]. For the purpose of this work the following definition is used to describe the two way insertion loss.

$$IL=20\log_{10}\left(\frac{V_R}{V_I}\right) \tag{3.7}$$

where V_R is the electrical voltage generated by the receiving transducer into a 1MΩ load and V_I is the voltage produced by the electrical source across a similar load. In practice V_R was measured using an oscilloscope of sufficiently high input impedance (1MΩ in parallel with 20pF) that is known to approximate closely to an open circuit for the transducers under consideration [109].

The two way system insertion loss across a fixed airgap, under both narrowband and wideband excitation, has been evaluated using the best transducers from the experiments in Section 3.6.1. Narrowband excitation utilised a 20 cycle tone burst (10V peak to peak) and the transmission frequency adjusted to achieve maximum response. Whereas, wideband conditions were generated using the pulser unit (240V differentiated step function). In both situations, the receiving transducer has been connected directly into an oscilloscope. For these experiments, RB2.5 and RB5 electrostatic transducer pairs and C70ML/C30ML composite transducer combination were positioned 20mm apart in transmit-receive mode.

The experiments described earlier in Section 3.6.2(b), 'Through-Transmission Performance', have been utilised to evaluate the narrowband insertion loss characteristics, as shown in Figures 3.17(a) - (c). Insertion losses of 50.8dB, 57.2dB and 26.3dB were measured for the RB2.5 and RB5.0 electrostatic pairs and the composite pair respectively. The corresponding insertion losses measured under conditions of wideband excitation were 74.4dB, 81.8dB and 61.3dB supporting the narrowband results and again reflecting the sensitivity gain afforded by the composite transducers. The experimentally acquired through transmission wideband responses are shown in Figures 3.18(a) - (c), for the 2.5μm and 5.0μm electrostatic and composite pairs respectively. However, it should be noted the difference in bandwidth exhibited by each transduction system, where the wideband characteristic of the electrostatic transducer is clearly evident from these Figures.

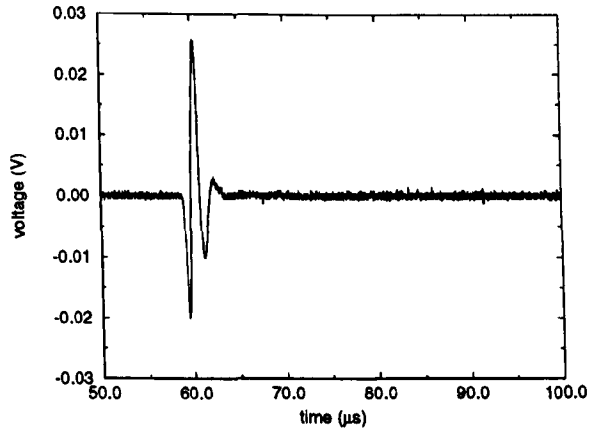

Figure 3.18(a) Wideband through transmission response for the 2.5μm mylar electrostatic transducer pair (rough brass backplate)

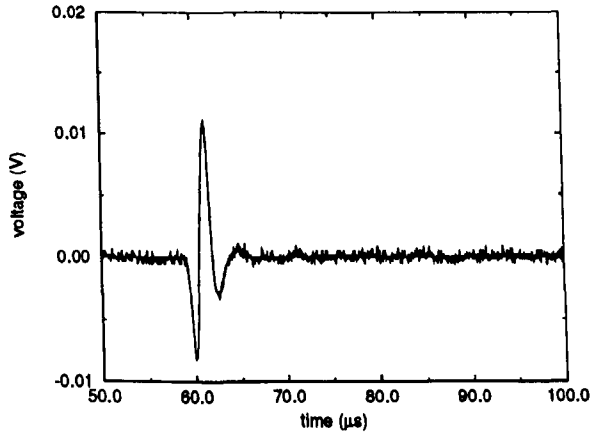

Figure 3.18(b) Wideband through transmission response for the 5.0μm mylar electrostatic transducer pair (rough brass backplate)

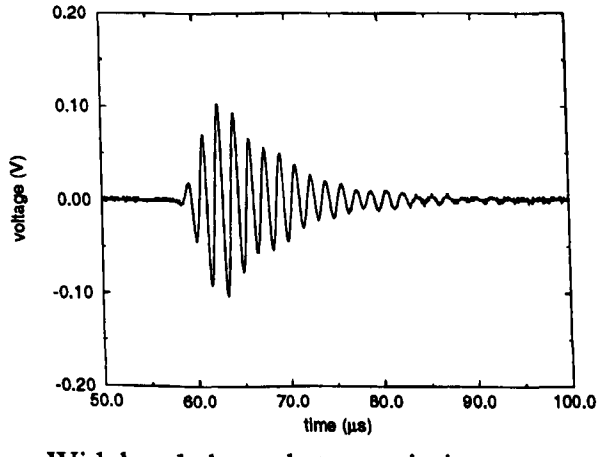

Figure 3.18(c) Wideband through transmission response for the 70%/30% composite transducer combination

3.8 Conclusions

This Chapter has attempted to assess and quantify the performance of different ultrasonic transducers when operating in the air environment at frequencies around 500kHz. The influence of air as a propagation medium has been discussed and good agreement obtained between theory and experiment for both PVDF and piezocomposite transducers. For operation in this frequency regime, it is shown that a properly configured PVDF transmitter approximates well to a wideband source, producing reliable and repeatable results for near range calibration purposes. Interestingly, the PVDF membrane hydrophone, although calibrated initially for use in water, may be applied directly to the air environment, provided that the electrical loading is maintained within certain bounds. Under these conditions, the hydrophone may be used to give quantitative information on through air transmission performance, although SNR is reduced when compared to the water coupled situation. The extent of this reduction is due entirely to the transmitter properties and the influence of attenuation within the air channel.

An experimental comparison of two different transducer technologies has also been conducted. This involved piezocomposite and electrostatic transducers of identical dimensions and operating under similar conditions. It should be noted that no attempt was made to optimise any particular transducer configuration and both types of devices may be subject to improvement. The results indicate that the best sensitivity figures are obtained for piezocomposite transducers, under narrowband operating conditions. However, it is considered unlikely that standard piezocomposite designs will ever match the sensitivity-bandwidth product figures of electrostatic transducers. Importantly, new developments in micro-machined design of electrostatic devices will also provide a significant cost benefit in terms of manufacture. Although techniques such as injection moulding will reduce the volume cost of piezocomposites in the medium term, electrostatic transducers may well have a distinct competitive edge.

CHAPTER 4

A THEORETICAL EVALUATION OF 1-3 CONNECTIVITY COMPOSITE TRANSDUCERS

ABSTRACT

A combination of theoretical modelling and experimental analysis is used to predict and assess the performance of 1-3 composite transducers for operation in an air-coupled environment. Specifically, finite element analysis, supported by linear systems modelling, is employed to evaluate transmission and reception characteristics over the complete volume fraction range, for operating frequencies in the region of 500kHz, and the theory confirmed using the novel experimental techniques described in Chapter 3. The theoretical approach is then extended to assess the influence of mechanical matching and backing on transducer sensitivity and bandwidth, with a view towards verifying the models for more practical arrangements. Throughout, the influence of air propagation is included in the simulation approach and highlighted where this factor is significant. Generally, the finite element technique is shown to agree well with, and hence confirm, the linear systems approach. Where this is not the case, the former is used as the benchmark for experimental comparisons.

4.1 INTRODUCTION

The characterisation process, described in Chapter 3, indicated that 1-3 connectivity piezocomposite transducers have significant potential for airborne applications. The range of composite transducers utilised in this process were not necessarily designed to operate in air. Therefore, an evaluation of 1-3 connectivity composite transducer for airborne operation could facilitate improved transducer designs.

As demonstrated in Chapter 3 excellent results can be achieved through uni-dimensional modelling techniques, provided that the composite vibrates uniformly in the thickness or height dimension, behaving as an effective homogeneous medium. This approach has been employed to assist with the design of a prototype through transmission scanning system, for operation in air [60]. For composite devices exhibiting multi-modal behaviour, the introduction of finite element analysis (FEA) has enabled detailed investigation into the transducer microstructure [84,87]. Consequently, FEA has been utilised to investigate design criteria to promote uni-modal operation through the application of maximum pillar aspect ratio guidelines [87], and enhance the electromechanical coupling coefficient through appropriate choice of ceramic rod shape and distribution [84,87] and polymer filler material [112].

A dual approach has been chosen for the theoretical evaluation of 1-3 composite transducers in through-air applications. The linear systems model of the transducer system [85], described in Appendix B, permits convenient simulation of transducer structure (including backing and matching), electrical loading and the influence of air propagation for both transmission and reception. For those situations incompatible with a 1-D approximation, a finite element approach is employed. The commercially available ANSYS code [113] is used to perform a harmonic analysis of composite behaviour in the air environment. This analysis involves the calculation of surface pressure at discrete frequency steps with the excitation signal delivered from an ideal voltage generator. For the theoretical results shown here, both models are used over the complete volume fraction range.

4.2 FINITE ELEMENT ANALYSIS

The finite element analysis work presented in this Thesis has utilised a software library of routines in the form of a simplified interface to the ANSYS code. A detailed discussion of these programs has been presented by Bennett [114], where the objective was to develop a transparent environment where the ANSYS code could be utilised by users possessing a minimum knowledge base in FEA. Therefore, this Thesis will not examine the fundamental operation of the finite element code, but will apply the models developed by Bennett to investigate the different aspects of behaviour of 1-3 composite, air transducer structures. The approach developed by Hossack and Hayward [84], for the analysis of transmission and reception transducer performance, has been extended by Bennett to incorporate mechanical matching and damping conditions, under both air and fluid loading. A description of the necessary input and output information required for this modelling environment is provided in Appendix D. Here, only the relevant aspects of the FEA modelling technique will be discussed.

Finite element analysis considers the structure under investigation to be an assembly of discrete elements, connected together at a finite number of nodes. The solution is formed from the summation of the interaction between elements in the structure, where each set of elements is considered small enough to enable their behaviour to be assumed to be linear. The overall behaviour of the structure is determined from the collective contribution of each set of elements. Within the ANSYS code, a multi-field solid element and a standard isotropic solid element are employed to model the piezoelectric ceramic and inactive polymer phases, respectively. These are both 8 node brick elements in which three-dimensional nodal displacements are the degrees of freedom for the system. Additionally, each node of the multi-field elements has voltage as the degree of freedom. Within the ANSYS code it is assumed that the device operates into a vacuum. Therefore no addition loading mechanism is required because the specific acoustic impedance of air is close to that of a vacuum, when compared to the relatively high specific acoustic impedance of a composite transducer. Also, the implementation for the finite element technique incorporates ideal impulsive stimulation conditions, as the

ANSYS code cannot readily incorporate accurately the actual electrical stimulation circuitry.

The size of the structure to be modelled is constrained by the available computer memory and determines the processing time required. As a consequence, the analysis of the full transducer structure is only undertaken when a detailed investigation is necessary, for example to determine the influence of plate modes. Hence, only a portion of the composite will be modelled. For this work the composite transducer comprises of square section ceramic pillars embedded periodically in the polymer phase and includes the application of mechanical matching and/or damping. Therefore, the quarter symmetry section, shown in Figure 4.1, is sufficient to analyse the modal behaviour of the composite transducer.

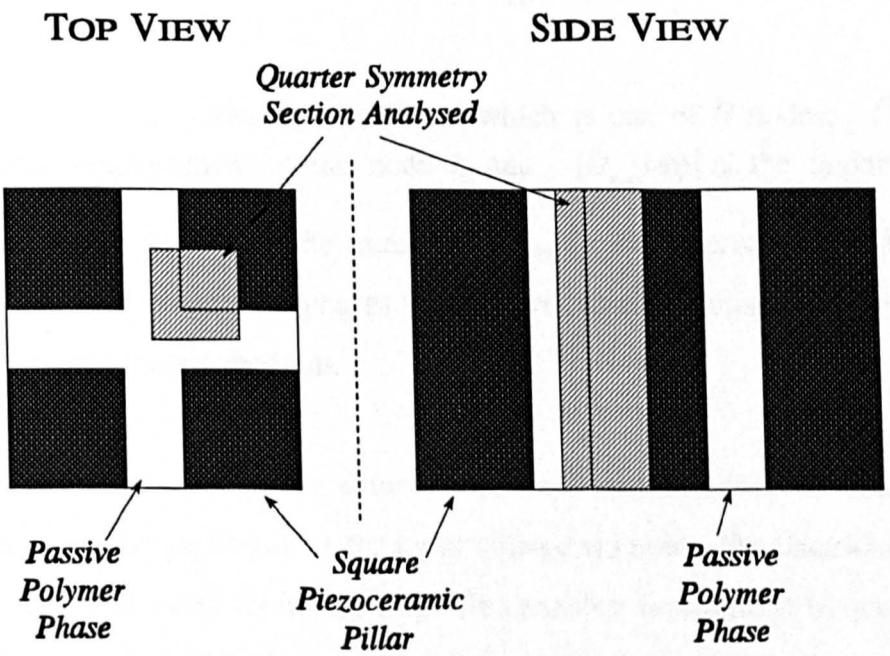

Figure 4.1 Quarter symmetry section employed by FEA

The behaviour of the piezocomposite can be described by different output parameters that are generated from the finite element analysis. As the behaviour of the transducer is required over a band of frequencies and losses in each component are important, harmonic analysis was used. The analysis produces the complex charge, $\hat{Q}(\omega)$, as a

reaction to the input voltage, $\hat{V}(\omega)$, allowing the electrical impedance, $\hat{Z}_T(\omega)$, to be calculated as:

$$\hat{Z}_T(\omega) = \frac{\hat{V}(\omega)A_t}{j\omega\hat{Q}(\omega)A_{exp}} \tag{4.1}$$

where A_t and A_{exp} are the areas of the modelled and physical transducer respectively.

With 1-3 piezocomposites, the displacement across the surface is not constant as the ceramic rods will generally displace with a slightly greater amplitude than the polymer matrix. An indicator of these phenomena is dilation quality, Q_{dil}, which is defined as:

$$Q_{dil}(\omega) = \frac{\sum_{i=1}^{N} \hat{D}_i(\omega)A_i}{A_t\,|\hat{D}_{max}(\omega)|} \tag{4.2}$$

where A_i is the area surrounding the node i which is one of N nodes; $\hat{D}_i(\omega)$ is the complex nodal displacement at the node i; and $|\hat{D}_{max}(\omega)|$ is the maximum nodal displacement on the surface of the transducer. Q_{dil} factors approaching unity indicate uniform surface dilation of both phases and confirm that the composite is operating as an effective homogeneous medium.

The current through the composite structure can be determined from the FEA predicted charge held on the device and since the input voltage is known, the electrical impedance may be calculated at every frequency step. This enables the resonant frequencies of the device to be obtained. The electromechanical coupling coefficient, k_t, of a particular mode may be evaluated, as in Equation 3.2, from its impedance minimum, f_m, and impedance maximum, f_n.

The transducer can be operated in two possible modes: transmission or reception. Under transmission conditions, the complex input voltage, $\hat{V}_{in}(\omega)$, generates the complex average output pressure, $\hat{p}_{out}(\omega)$, across the front face of the transducer giving the

transmit sensitivity, $S_{TX}(\omega)$, as:

$$S_{TX}(\omega) = \left| \frac{\hat{p}_{out}(\omega)}{\hat{V}_{in}(\omega)} \right| \tag{4.3}$$

The receive sensitivity, $S_{RX}(\omega)$, has a similar definition:

$$S_{RX}(\omega) = \left| \frac{\hat{V}_{out}(\omega)}{\hat{p}_{in}(\omega)} \right| \tag{4.4}$$

Here $\hat{V}_{out}(\omega)$ is the complex output voltage generated by the complex pressure, $\hat{p}_{in}(\omega)$ impinging on the whole front surface of the transducer.

The output pressure, $\hat{p}_i(\omega)$, at node i can be calculated from the surface displacement, $\hat{D}_{node}(\omega)$:

$$\hat{p}_i(\omega) = j\omega Z_L \hat{D}_i(\omega) \tag{4.5}$$

where Z_L is the specific acoustic impedance of the load, 400 Rayl for air.

ANSYS requires specific material parameters to analyse the behaviour of a piezoelectric structure. For its application to 1-3 composites, the piezoceramic elements require density, dielectric constants, elastic co-efficient matrix and piezoceramic matrix to be defined, whereas the polymer phase requires the definition of density, Young's modulus and Poisson's Ratio. The combination of these material parameters and the device geometry enable the finite element package to construct the matrices necessary for the computational stage of the analysis. Details of all material properties included with the modelling are presented in Appendix A.

4.3 THE EXPERIMENTAL APPROACH

4.3.1 Experimental Arrangement

This section describes the adopted approach, through which experimental verification of the modelling techniques was achieved. Wideband transducer performance was examined under transmission, reception and pitch-catch modes of operation, in an effort to obtain the impulse response. In practice this involves approximating the true impulse response owing to the bandlimited nature of the drive and receive electronics and the propagation medium, as described in Chapter 3. Since the transducers under investigation were all operating around 500kHz, the techniques employed in Chapter 3 to characterise air-coupled transducers were considered appropriate. Therefore, a standard hydrophone will be utilised to acquire the transmission response and a wideband PVDF transducer was utilised to generate a wideband pressure wavelet for the receiver experiments. In all experiments, the transmitting device was driven by the pulser unit, described in Section 3.3.1, and the receiver element was interfaced to a high gain pre-amplifier (90dB) with an input resistance of 1MΩ and a -3dB bandwidth of 6MHz. It may be noted that all of the circuit parameters, including cabling, were incorporated within the linear systems model. Although, the finite element code only produced the ideal transducer impulse response, for reasons stated previously, this was not expected to constitute a significant problem.

As stated in Section 2.4, it was necessary to perform all experiments in a constrained environment to ensure consistency with respect to air attenuation [3]. Where necessary, the influence of airborne attenuation, Equation 3.3, was used to facilitate comparison between theoretical and experimental data.

4.3.2 Composite Transducer Manufacture

Selection of constituent materials for the composites was made on the basis of availability and consistency, ease of manufacture and accurate documentation of parameters for simulation purposes. Consequently, PZT5A ceramic and a relatively stiff polymer, CY1301/HY1300 were chosen, although it was recognised that both materials

may be sub-optimal with respect to through-air operation. Details of the parameters utilised for these materials can be found in Appendix A. A range of transducers were constructed using the manufacturing process described in Section 2.2.4. At a later stage a perspex backing block and different matching layers were added to the transducer structure, with a view towards verifying the finite element code for more practical arrangements.

Each transducer comprised a square slab of dimensions 12.5mm x 12.5mm and the principal properties are summarised in Table 4.1, where f_m and f_n are defined as the fundamental electrical (impedance minimum) and mechanical (impedance maximum) frequencies respectively. The ceramic pillar aspect ratio (width to height) is critical and must be sufficiently low to minimise the influence of inter-pillar resonances and promote homogeneous operation in the thickness dimension [87]. Unfortunately this constraint was difficult to meet at the lower volume fractions using available slicing equipment and moreover, exact uniformity in transducer centre frequency was not achieved. However the maximum variation of 6% across the volume fraction range was not expected to constitute a problem for experimental evaluation and in any case, all relevant composite dimensions and materials constants were included within the finite element analysis.

volume fraction	10%	20%	30%	40%	50%	60%	70%	80%	90%
height(mm)	2.56	2.73	2.80	2.82	2.77	2.82	2.78	2.77	2.78
aspect ratio	0.19	0.09	0.10	0.14	0.19	0.26	0.40	0.47	0.89
f_m (kHz)	569	559	553	567	568	583	591	592	593
f_n (kHz)	610	627	630	654	662	692	700	705	660
k_t	0.394	0.491	0.518	0.537	0.553	0.586	0.575	0.582	0.476
Static (pF) Capacitance	46.9	87.5	127.8	169.1	215.1	253.2	299.1	341.9	594.6

Table 4.1 : Characteristics of the manufactured range of composite transducers

A comparison between the theoretical and experimental values for thickness mode coupling coefficient is shown in Figure 4.2. Although the trends are similar, it may be noted that measured values are approximately 10% lower across the range. At intermediate volume fractions (20% - 80%) this difference is caused primarily by depolarisation during the slicing process, while at the extremities, errors are introduced by lateral mode interference in the location of f_m and f_n during the impedance analysis.

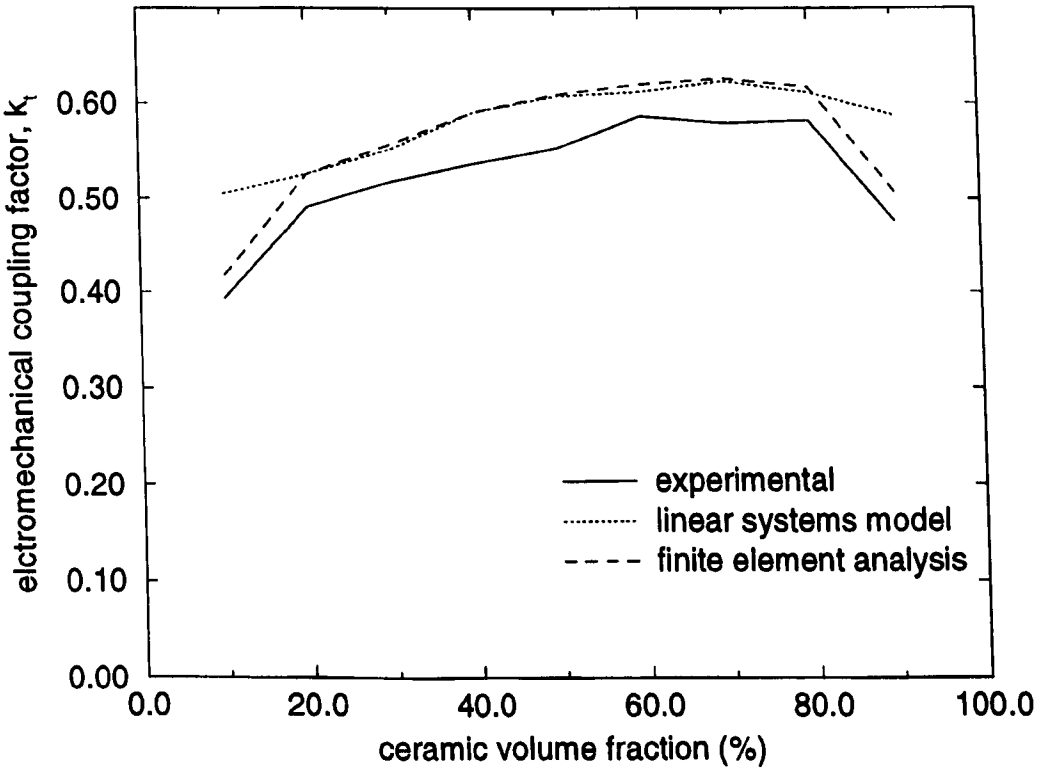

Figure 4.2 Comparison between simulated and experimental values for k_t

The piezoelectric transducer will operate most efficiently at f_m for transmission or f_n for reception. The impedance minimum defines the value for f_m and consequently, when operating in transmission, the frequency for maximum current flow through the transducer. Subsequently, maximum charge will be realised at this frequency, which will result in maximum stress at the transducer faces due to the indirect piezoelectric effect. The mechanical thickness resonance, f_n, for a piezoelectric transducer is defined by the transducer thickness and the longitudinal velocity of sound through the transducer material. Consequently, when operating in reception, the device will tend to naturally vibrate at this frequency. Thus it is apparent that careful consideration of both the

transmit and receive elements for the design of an air-coupled NDE system will be required to maximise system efficiency. The influence of these two parameters on the overall transducer system performance will be highlighted later in this Chapter.

A final point of note concerns the form of pulser used for transducer excitation. This involves deposition of a quantity of charge on the transducer electrodes from a blocking capacitor [102]. Since there is a considerable variation in transducer static capacitance (46.9pF at 10% to 594.6pF at 90%), it was important to ensure that each device was subject to uniform excitation. Practically, this was achieved by maintaining a ratio of 10:1 with respect to blocking and transducer capacitance respectively.

4.4 EXPERIMENTAL RESULTS

4.4.1 Introduction

In the following analysis, the prediction capabilities of both modelling techniques for the manufactured range of 1-3 piezocomposite transducers will be evaluated for transmission, reception and pitch-catch performance. This process will include the application of fixed mechanical matching and damping over the range, in addition to a comparison on the influence of several matching layer combinations to one device. This section is intended to substantiate the application of both modelling approaches and is not to be perceived as a definitive solution. Once validated, these techniques can be employed for evaluation of improved transducer designs for through-air operation.

It should be noted that owing to the very different implementations for the finite element and linear systems models and the fact that ANSYS cannot readily incorporate accurately the actual electrical stimulation circuitry, all results are presented in normalised form, where the peak response (over the volume fraction range) was used to normalise the range of results for each data set.

4.4.2 Impedance Profile

The initial stage in the experimental program was to ensure that modelling techniques employed have the capacity to predict the impedance profiles for the range of manufactured composite devices, detailed in Table 4.1. To demonstrate the effectiveness of each modelling approach, two composite transducer configurations are illustrated : the multi-modal nature of the 90% composite and the 40% transducer, with a Silicone Rubber matching layer bonded to the front face.

The ability of the finite element analysis to successfully predict multi-modal behaviour in a 1-3 piezocomposite transducer is illustrated in Figure 4.3, for the 90% device. The linear systems model will always estimate uni-modal performance for the transducer, but the FEA predicted the two main resonances with good accuracy being observed. From

the Figure it can be seen that the fundamental thickness resonance occurs at 660kHz, with the first lateral resonance, at 760kHz, impinging upon this resonance. The close proximity of these two vibrational modes can be attributed to the aspect ratio (0.89) for the 90% composite lying outwith the maximum pillar aspect ratio (MPAR) criteria (0.55) described by Hayward and Bennett [87]. The experimental profile depicts two smaller resonances at around 500kHz and 575kHz, these represent plate modes within the device. By modelling the entire transducer structure, the finite element approach has predicted the occurrence of these modes within the device to a reasonable degree.

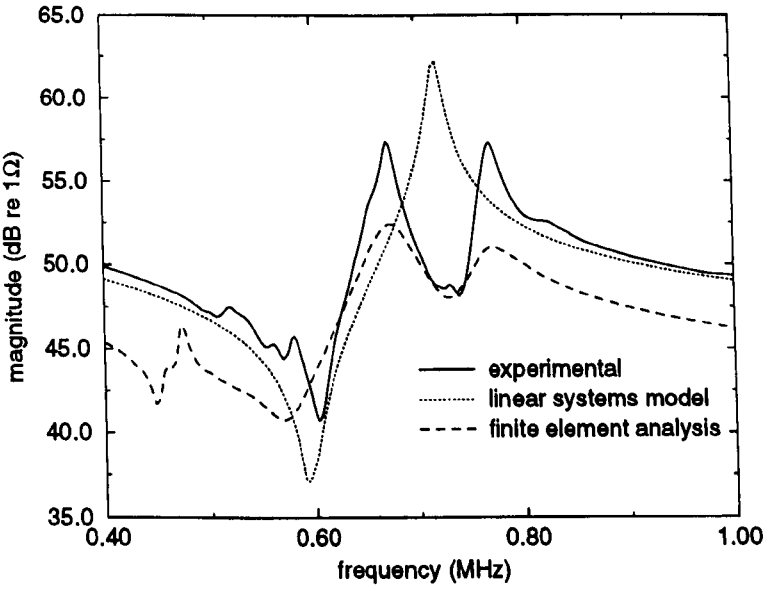

Figure 4.3 Impedance profile for the 90% composite transducer

The impedance profile for the 40% composite transducer, including a 0.43mm thick Silicone Rubber matching layer, is presented in Figure 4.4. Here, the composite transducer is operating as a thickness mode device, with the aspect ratio for the 40% transducer below the MPAR guidelines of 0.3 [87]. Consequently, both modelling techniques have successfully predicted both resonances present in the device. The Figure depicts two resonances associated with this device, the fundamental resonance is that of the actual composite transducer at 630kHz and a second mode at 450kHz which corresponds to the combined transducer and matching layer resonance.

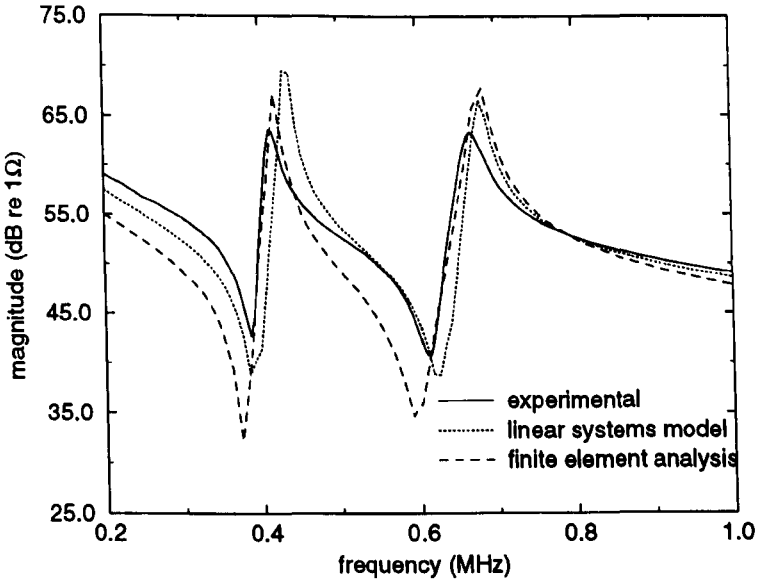

Figure 4.4 Impedance profile for 40% composite, including a silicone rubber matching layer

4.4.3 Transmission Analysis

Normalised transmission levels for the elementary composites (i.e. no matching or backing) are outlined in Figure 4.5, from which good agreement between theory and experiment may be observed. It is evident that 50% to 70% composites possess the best drive performance as a result of the inevitable compromise between coupling coefficient, electrical permittivity and acoustic matching to air.

The experiments were then repeated with the addition of a silicone rubber matching layer at the front face of each transducer. The matching layer possesses an specific acoustic impedance of 1.05MRayls and a thickness of 0.43mm was selected to provide quarter wavelength matching at a frequency of 575kHz, corresponding to the mean of the transducer range. For the relatively wideband conditions, this was considered to approximate uniform matching across the transducer range. The results are shown in Figure 4.6 and again there is reasonable agreement between theory and experiment. A comparison with Figure 4.5 indicates that the peak response has been shifted slightly up the volume fraction range, as a consequence of silicone rubber providing improved acoustic matching at higher volume fraction. Interestingly, for the 70% composite, a 12dB improvement was recorded by inclusion of the matching layer.

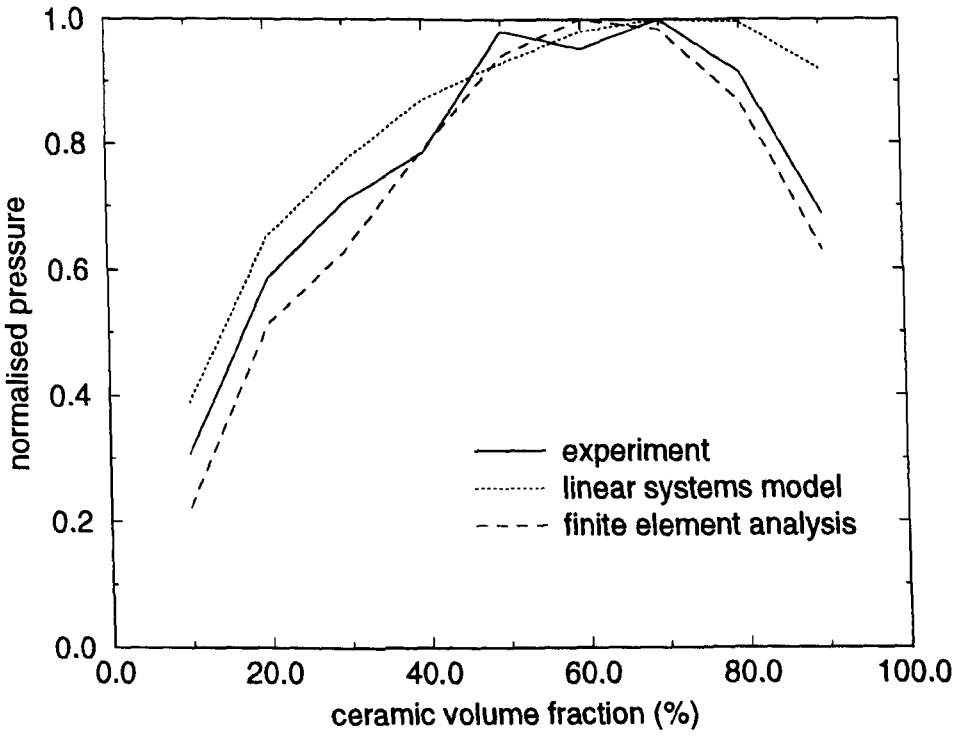

Figure 4.5 Wideband 1-3 composite transmission performance

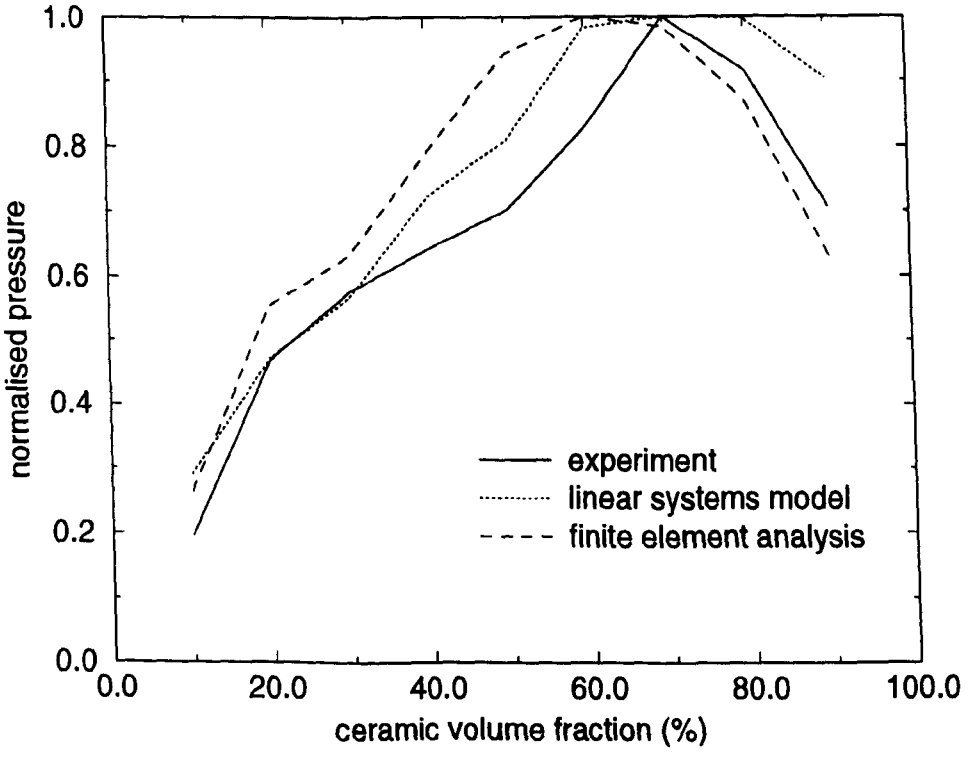

Figure 4.6 1-3 Composite, plus matching layer, transmission performance

A perspex backing block was then bonded to the rear face of each transducer, providing a variable level of damping across the range. At 10% the backing provides 50% damping, while at 90% it is approximately 10% and a corresponding reduction in transducer bandwidth is to be expected. The results are shown in Figure 4.7(a), with similar trend as before although the peak response at 70% has been reduced by 6dB. Figure 4.7(b) illustrates the variation in -3dB bandwidth expressed as a percentage of the transducer centre frequency. The damping example presented here has discriminated against the higher volume fraction devices, but the intention is to illustrate the validity of the modelling approaches not to define an optimum level of damping.

Good agreement was observed between theory and experiment in all cases, with the linear systems model providing an adequate prediction of the trends. Here, the finite element results agree more closely with the experimental data, despite excluding the actual electrical loading. For both modelling techniques, the frequency spectra were modified to include attenuation of air, according to Equation 3.3.

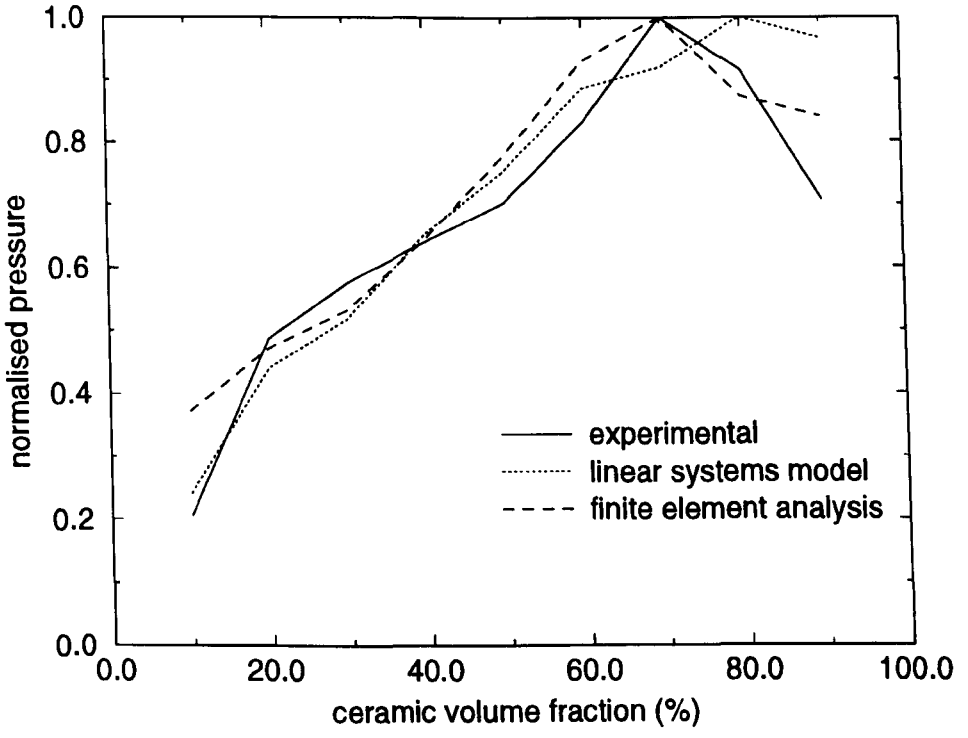

Figure 4.7(a) 1-3 Damped composite wideband transmission performance

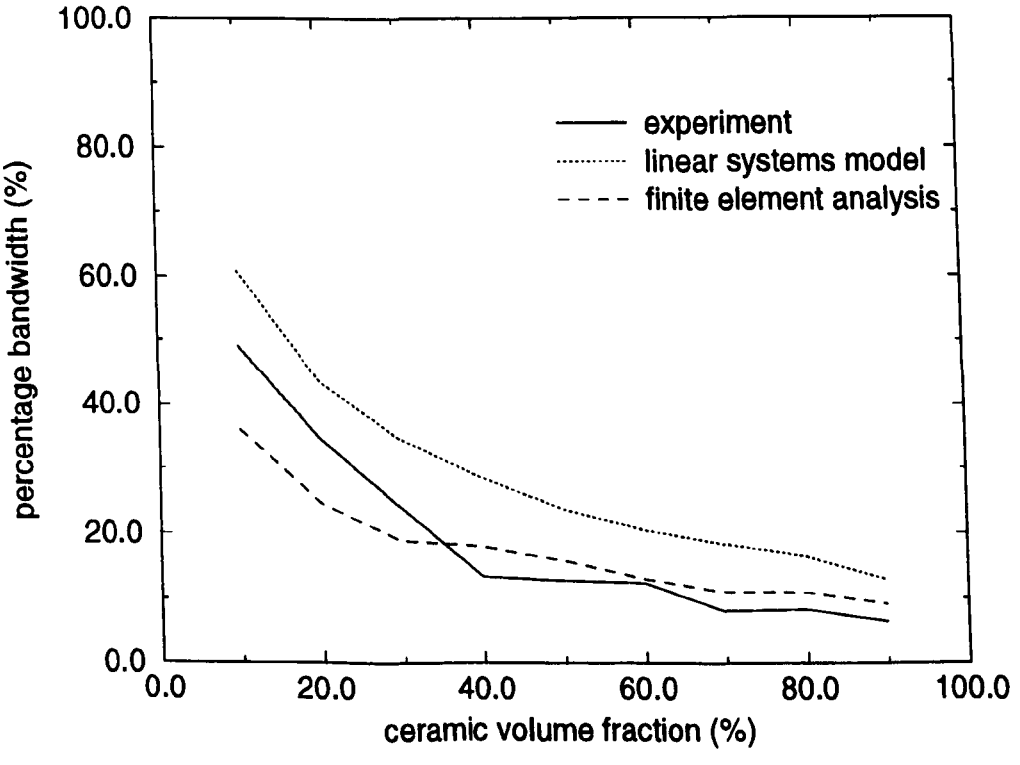

Figure 4.7(b) Percentage bandwidth variation for damped composites

4.4.4 Reception Analysis

Figure 4.8 shows the variation in reception impulse response for the elementary transducers. Since the aspect ratio for the 10% composite is too high for homogeneous operation, the linear systems data has been normalised to the 20% composite, providing good agreement between theory and experiment over the remainder of the range. However, the finite element data and experimental results are in good agreement across the entire range, indicating maximum sensitivity at 20% volume fraction. Interestingly, the sub-optimal behaviour of the 10% device has been predicted well by the finite element model. For completeness, Figure 4.8 shows the finite element results for optimal pillar dimensions, where the maximum pillar aspect ratio (MPAR) compatible with homogeneous operation [87] has been used. These results have been normalised to the predicted performance for the 20% transducer and better agreement with the linear system approach is evident.

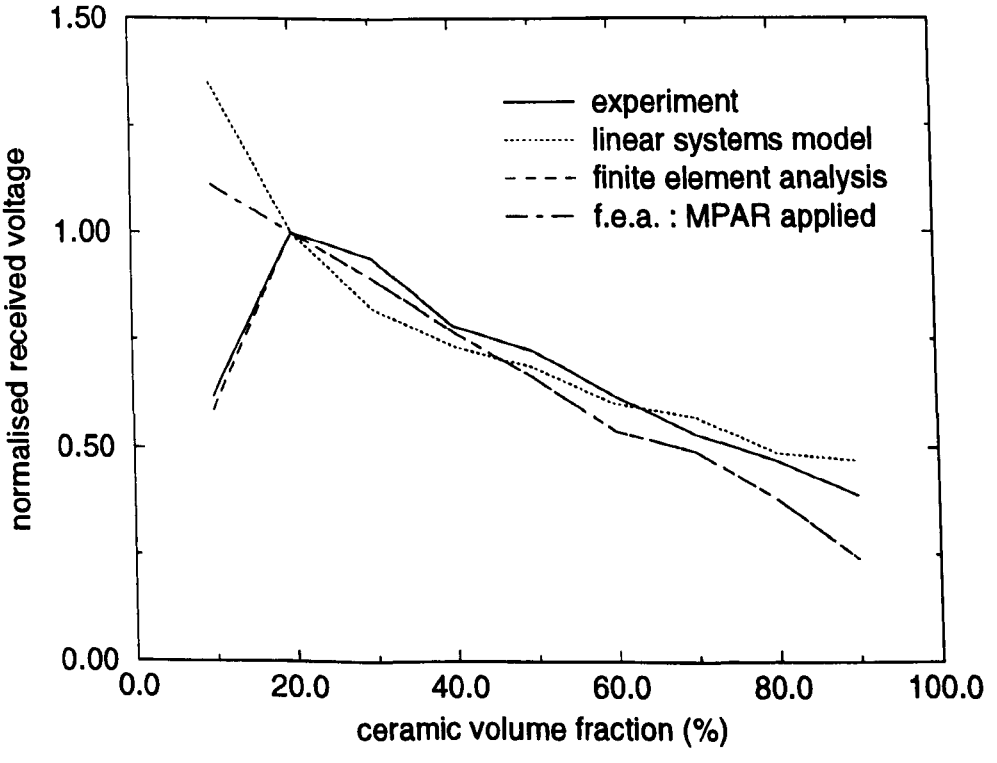

Figure 4.8 Wideband 1-3 piezocomposite reception sensitivity

Owing to the multi-modal behaviour of the experimental 10% composite, the linear systems model was restricted to the range 20% to 90%, for evaluation of mechanical matching and damping in reception. Figure 4.9 illustrates the influence of adding a silicon rubber matching layer and due to this sub-optimal matching, the peak response has been shifted to 40% with a 6dB gain over the unmatched composite at 30% volume fraction. Good agreement is observed between theory and experiment, particularly for the finite element data. Corresponding results for a perspex backing block are shown in Figures 4.10(a) and 4.10(b). As previously discussed in the damped transmission experiment, Section 4.4.3, the level of damping is varied across the volume fraction range. The expected reduction in bandwidth is again obtained, with a corresponding increase in reception sensitivity due the more narrowband nature at higher volume fractions. At 30% a 4db reduction is sensitivity was recorded over the unbacked case.

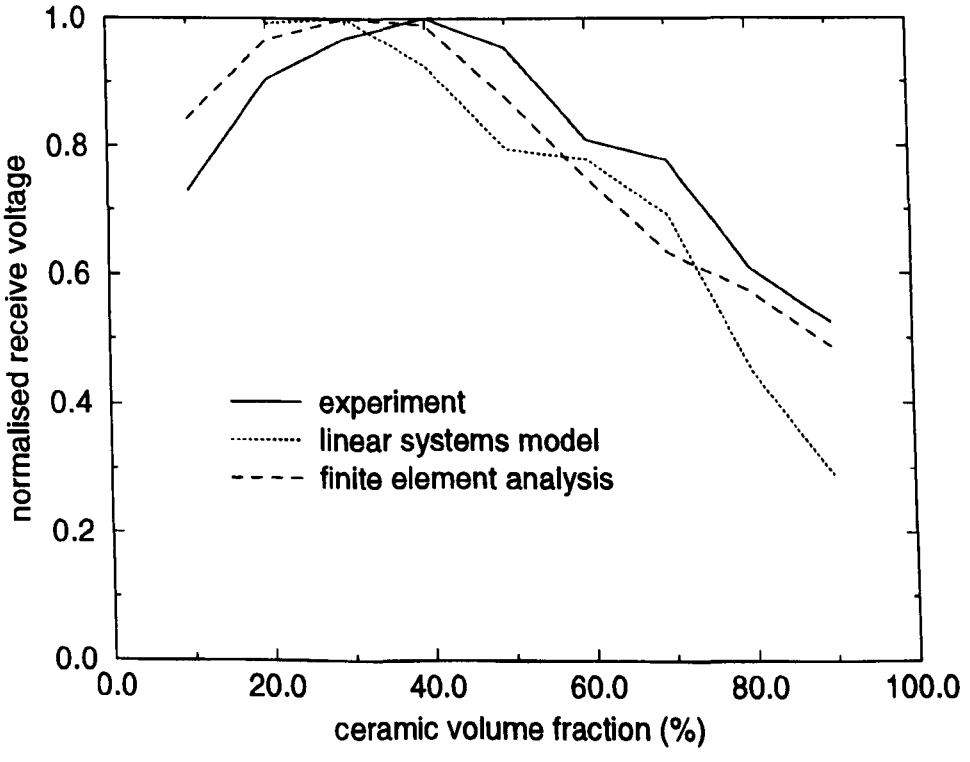

Figure 4.9 Wideband reception sensitivity for 1-3 Composites, plus matching layer

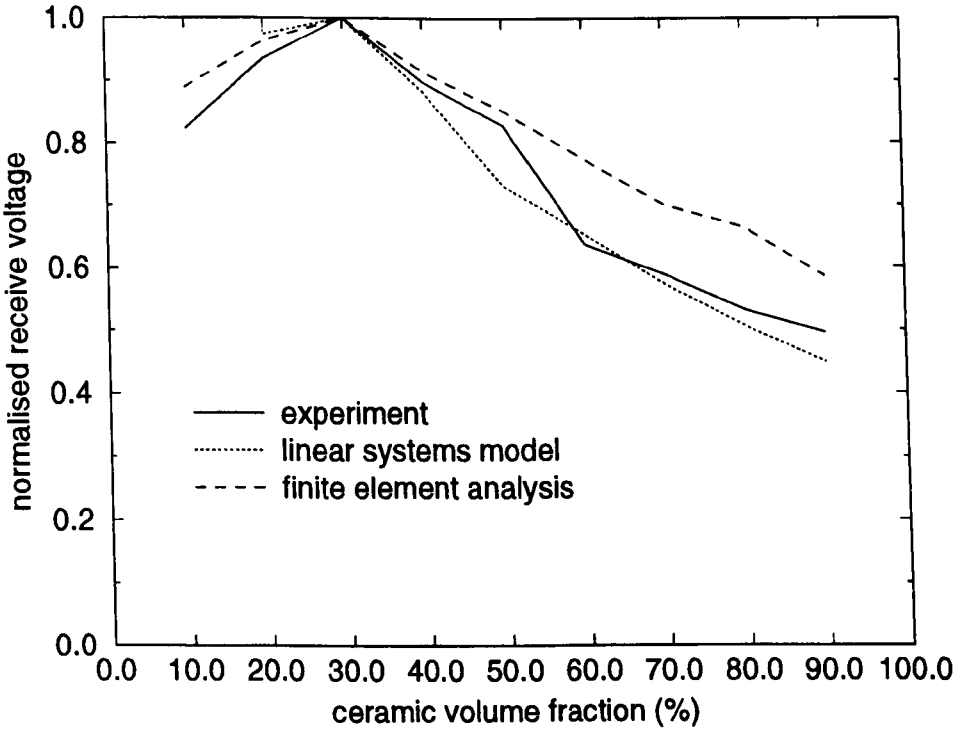

Figure 4.10(a) Damped composite wideband reception performance

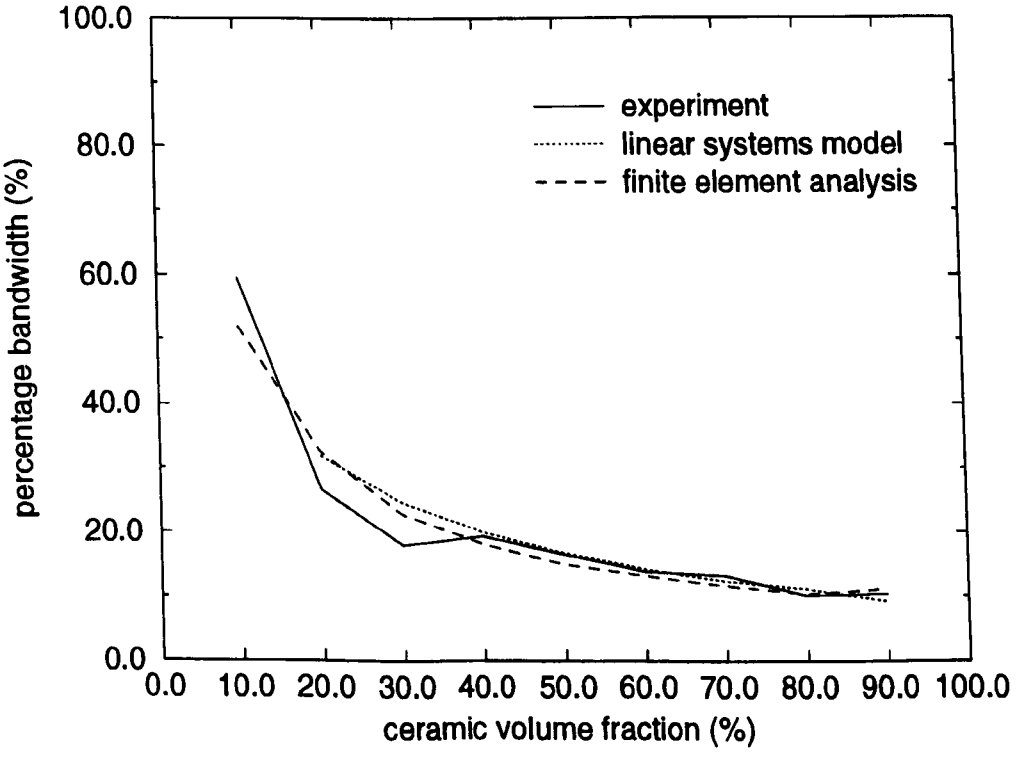

Figure 4.10(b) Percentage bandwidth variation for damped composite receivers

4.4.5 Application of Mechanical Matching Layers

The introduction of matching layer(s) to the front face of an air-coupled 1-3 connectivity piezocomposite transducer was investigated using the materials described in Table 4.2, where their properties have been calculated from velocity and density measurements. A detailed description of the parameters utilised for these materials can be found in Appendix A. The 40% composite transducer was utilised to validate simulation data under these conditions for both transmission and reception. The thickness of each material was designed to approximate quarter wavelength conditions at 610kHz, which represents a compromise between f_m and f_n for this device. In addition to using each material as a single matching layer, a silicone rubber/perpsex matching layer combination was examined. The transducer construction for a two matching layer system is illustrated in Figure 2.5. Figures 4.11(a) and 4.11(b) present this analysis, for transmission and reception respectively, in which the results from each individual structure have been normalised to the performance of the unmatched case, indicated by NOML. Good correlation between theory and experiment may be observed. It should be noted that, in the transmission experiment, the single silicone rubber layer has outperformed the double matching layer condition, as a consequence of the sub-optimal thickness of each layer. As stated in the Introduction, Section 4.4.1, the purpose of this evaluation is to validate the application of the modelling approaches and not as a definitive solution.

Material	Mnemonic	Thickness	Specific Acoustic Impedance
Perspex	PX	1.14mm	3.2MRayls
CY1301-HY1300	HS	1.03mm	2.9MRayls
CY208-HY956	SS	0.77mm	2.2MRayls
Silicone Rubber	SR	0.41mm	1.05MRayls

Table 4.2 : Matching layer materials selected for experimental analysis

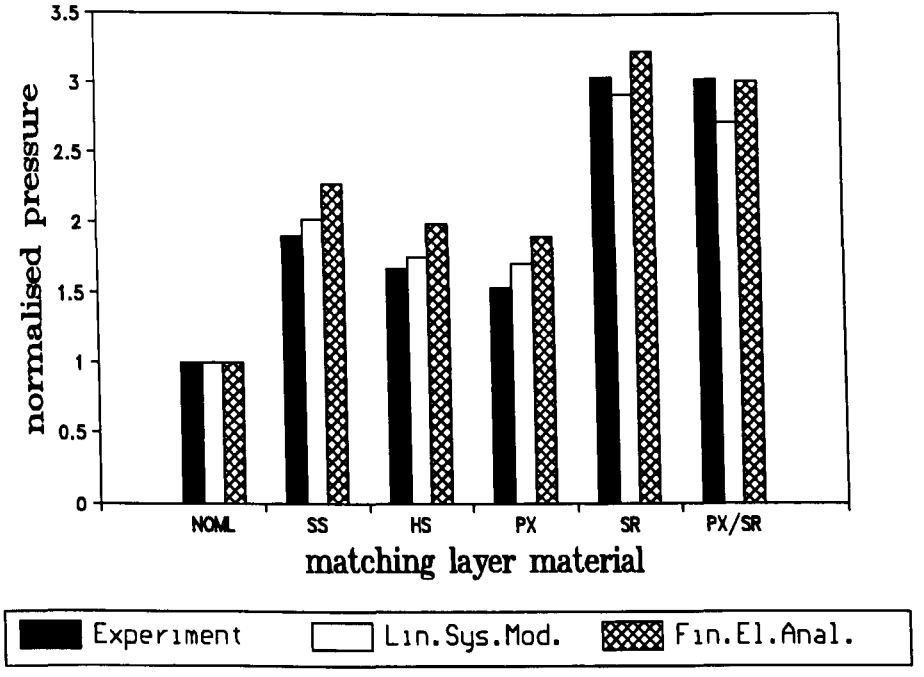

Figure 4.11(a) Transmission performance for a 40% composite under various matching conditions

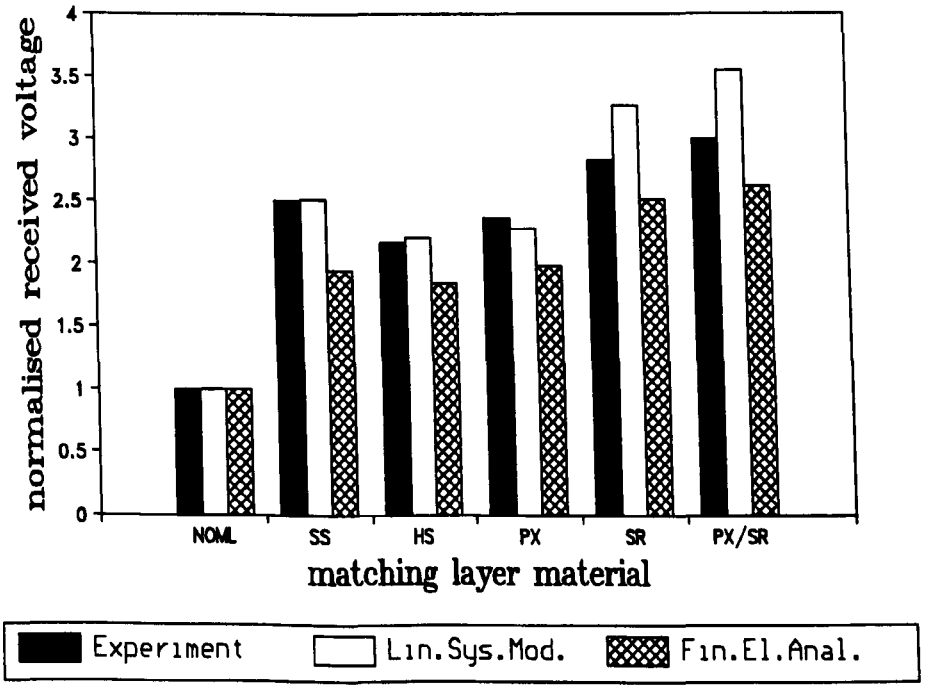

Figure 4.11(b) Reception sensitivity for a 40% composite under various matching conditions

4.5 Optimisation of Composite System Design

4.5.1 Introduction

Section 4.4 experimentally verified the application of both finite element and linear systems modelling techniques for evaluation of air-coupled 1-3 connectivity composite transducers. The FEA has performed well across the entire volume fraction range, including analysis incorporating mechanical matching and damping conditions. Although, the linear systems model produced an inaccurate result for the manufactured 10% composite, it has performed satisfactorily. In this section, the finite element model will be used to evaluate constituent materials, optimal volume fractions in transmission, reception and pitch-catch and practical solutions to the application of mechanical matching and damping. The linear systems model is used sparingly to enable clarity in the Figures.

4.5.2 Constituent Material Selection

For a 1-3 piezocomposite, the active piezoceramic material should possess high permittivity and k_{33}, both of which are found in the Lead Zirconate Titanate (PZT) ceramics. For the purpose of this investigation both PZT5A and PZT5H are utilised. Only two passive materials have been chosen to represent a variation in the polymer filler material properties corresponding to hard set (CIBA-GEIGY CY1301/HY1300) and soft set (CIBA-GEIGY CY208/HY956) epoxies. These material were considered adequate to provide a reasonable selection of potential piezocomposite transducers for air applications. Details of the material parameters included in the analysis can be found in Appendix A. In all FEA simulations, the maximum pillar aspect ratio compatible with homogeneous operation [87] has been used as detailed in Table 4.3.

The material combinations were simulated to evaluate both transmission and reception performance, where the transducers were assumed to operate at 500kHz and designed to promote uni-modal, homogeneous operation. Figures 4.12(a) and 4.12(b) illustrate the finite element analysis results in transmission and reception, respectively. In transmission, the higher permittivity of PZT5H produces a composite with a greater

drive performance, whereas in reception, PZT5A exhibits the better characteristics. In both modes of operation, the lower damping in the hard set epoxy yields superior sensitivity, although at the expense of bandwidth. Hence, a 50% - 70% PZT5H/hard set composite transmitter and a 10% - 30% PZT5A/hard set composite receiver represent the best composite selections from the range of materials.

	ceramic volume fraction	PZT5A/ Hard set		PZT5A/ Soft set		PZT5H/ Hard set		PZT5H/ Soft set	
		height (mm)	aspect ratio	height (mm)	aspect ratio	height (mm)	aspect ratio	height (mm)	aspect ratio
Transmission	10%	2.65	0.05	2.2	0.06	2.625	0.05	2.16	0.06
	20%	2.775	0.09	2.45	0.10	2.73	0.09	2.41	0.10
	30%	2.83	0.09	2.6	0.10	2.8	0.10	2.55	0.10
	40%	2.89	0.13	2.7	0.14	2.85	0.13	2.65	0.14
	50%	2.925	0.18	2.775	0.19	2.9	0.18	2.725	0.19
	60%	2.975	0.25	2.83	0.27	2.935	0.26	2.775	0.27
	70%	3.01	0.37	2.85	0.40	2.985	0.38	2.82	0.40
	80%	3.1	0.46	2.925	0.49	3.085	0.47	2.88	0.50
	90%	3.05	0.53	2.635	0.55	3.05	0.53	2.88	0.55
Reception	10%	3.13	0.04	3.05	0.05	3.2	0.04	3.1	0.04
	20%	3.425	0.07	3.35	0.07	3.5	0.07	3.45	0.07
	30%	3.58	0.07	3.5	0.08	3.685	0.07	3.6	0.07
	40%	3.68	0.10	3.635	0.10	3.8	0.10	3.75	0.10
	50%	3.75	0.14	3.7	0.14	3.885	0.14	3.85	0.14
	60%	3.8	0.20	3.775	0.20	3.95	0.19	3.9	0.19
	70%	3.85	0.29	3.825	0.29	4.0	0.28	3.98	0.28
	80%	3.93	0.37	3.9	0.37	4.085	0.35	4.05	0.36
	90%	3.9	0.51	3.925	0.50	4.075	0.48	4.1	0.48

Table 4.3 Simulated composite transducer dimensions for 500kHz operating frequency

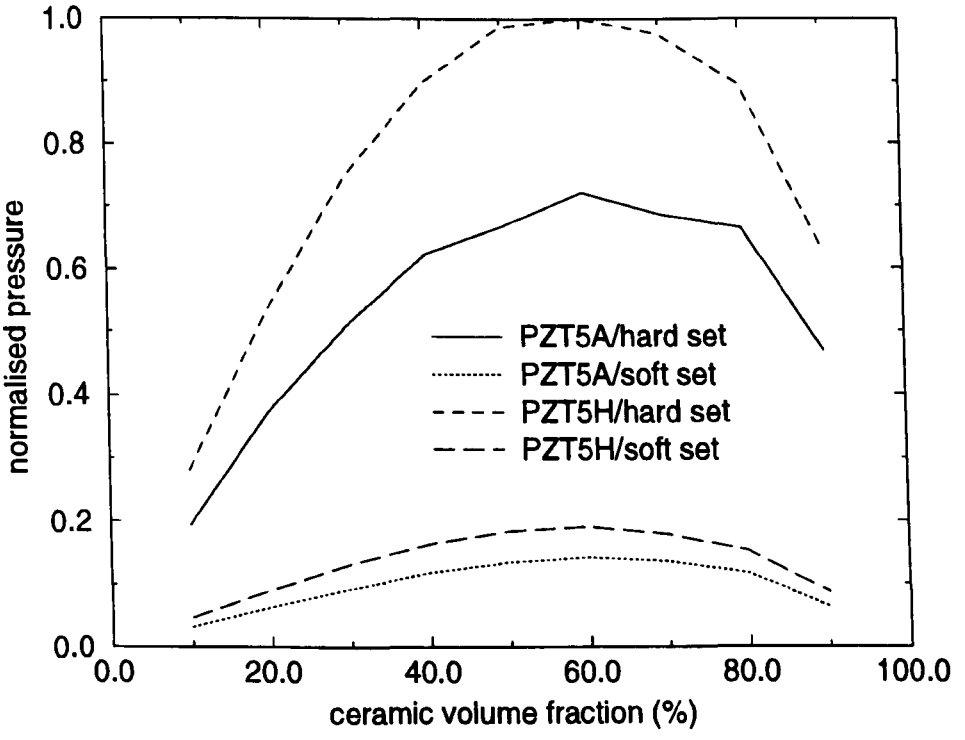

Figure 4.12(a) Influence of constituent materials on composite transmission performance at 500kHz

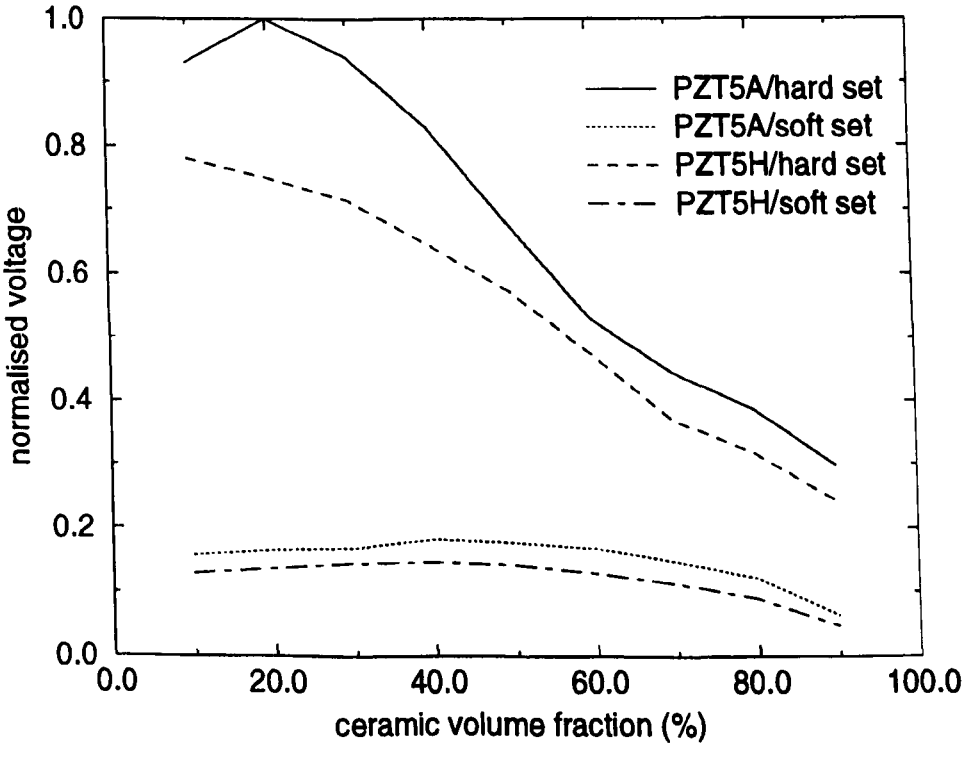

Figure 4.12(b) Influence of constituent materials on composite reception performance at 500kHz

For transmission and reception on separate transducers it is important to realise that under the stated electrical load conditions, peak transmission occurs at f_m, while maximum reception sensitivity at f_n [77]. For efficient composites those frequencies are relatively widely separated and since the transducers in air are inherently narrowband, maximisation of pitch-catch sensitivity requires careful alignment of these frequencies. That is, f_m of the transmitter should ideally coincide with f_n of the receiver. This is demonstrated through a comparison between two differing transducer systems, as illustrated in Figure 4.13, where the system performance for a selection of transducer pairs operating in either pitch-catch or pulse-echo are shown. Here pitch-catch operation employs frequency matching, whereas pulse-echo utilises the same transducer parameters for both the transmitter and receiver. Here, 'pc62' on the horizontal axis corresponds to a frequency matched 60% transmitter and a 20% receiver combination, while 'pe3' represents two identical 30% composites. The simulation selected the best transmission and reception devices from Figures 4.12(a) and 4.12(b) in the pitch-catch case and intermediate volume fractions as in the pulse-echo configuration. Under the frequency matched conditions for a 60% PZT5H/hard set transmitter and a 20% PZT5A/hard set receiver, the finite element analysis has predicted a 30dB improvement over the 30% PZT5A/hard set transducer pair.

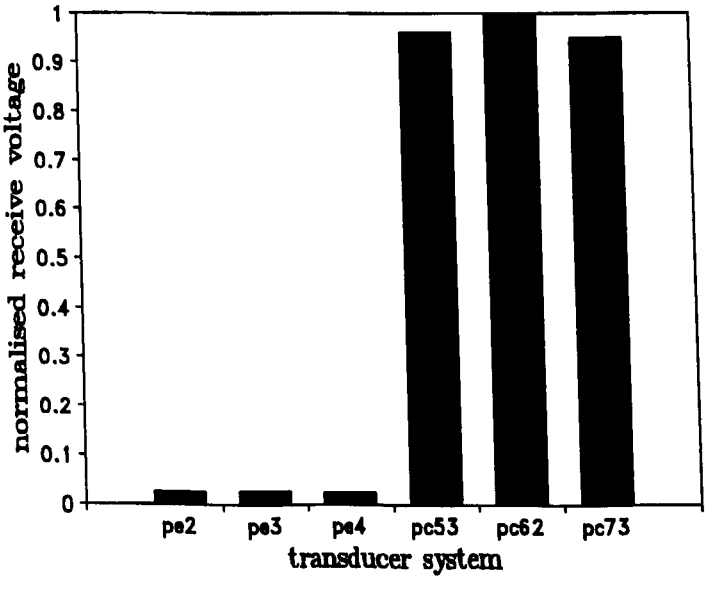

Figure 4.13 Simulated composite transducer system performance

4.5.3 Mechanical Matching Layers

The materials described in Table 4.4, in addition to a selection of the materials from Table 4.2, have been evaluated in a variety of matching layer combinations to assess the improvement in transducer performance for a 60% PZT5H/hard set composite transmitter and a 20% PZT5A/hard set receiver, under quarter wavelength conditions. Properties for materials 1 and 2 in Table 4.4 were extracted from Selfridge [115], while those for material 3 [116] were calculated from density and velocity measurements. Data for materials 4 and 5 were calculated using standard theory. A detailed description of the material parameters utilised can be found in Appendix A. The matching layer configurations were designed using Equation 2.1. For double matching layers, the specific acoustic impedance of the outer layer, either silicone rubber or membrane filter, has been substituted for Z_A to provide a practical matching configuration.

Material	Mnemonic	Thickness	Specific Acoustic Impedance
Tracon 401ST	TR	1.485mm	4.81MRayls
Epon	EP	1.415mm	3.4MRayls
Membrane Filter	MF	0.625mm	0.5125MRayls
Optimum #1	O1	0.25mm	0.09MRayls
Optimum #2	O2	0.225mm	0.077MRayls

Table 4.4 : Additional matching layer materials employed in simulation

Figures 4.14(a) and 4.14(b) show the predicted improvement for the transmitter and receiver, respectively, normalised to the unmatched case, indicated by NOML. For both the transmitter and receiver, the optimum single matching layer case, O1 and O2 respectively, has been included to assess the relative performance of the practical matching layers. The best non-optimum configuration, perspex/membrane filter, is approximately 4dB below the optimum single layer case. Although this combination has been predicted to increase performance by approximately 10% over the single membrane filter layer, it is straightforward to demonstrate that the relative increase in transducer efficiency decreases as the number of layers in a multi-layer configuration increases [9]. Consequently, the improvement in performance predicted for the perspex/membrane

filter combination (16dB in transmission and 15dB in reception), over the unmatched case, is considered to represent a reasonable practical matching layer configuration.

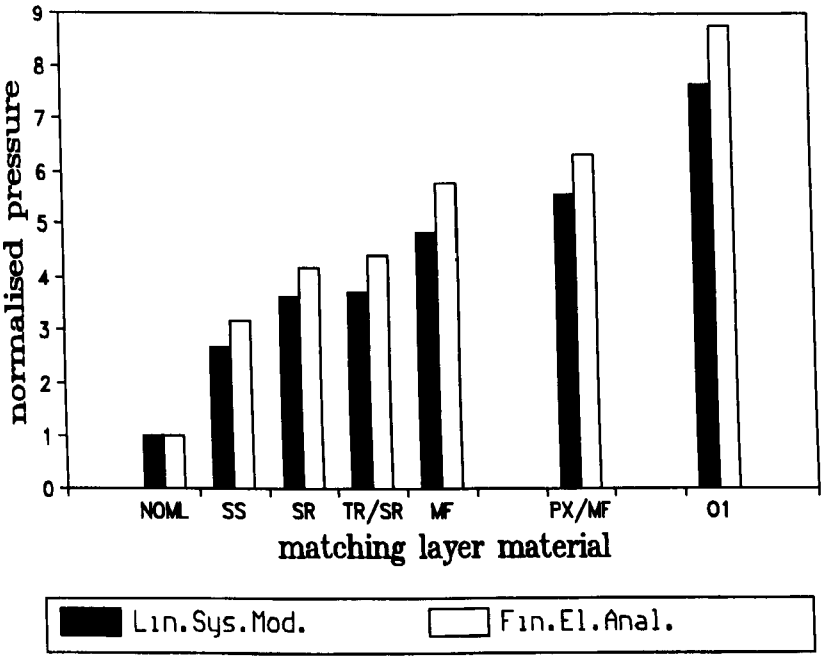

Figure 4.14(a) Application of mechanical matching layers to a 60% PZT5H/hard set composite transmitter

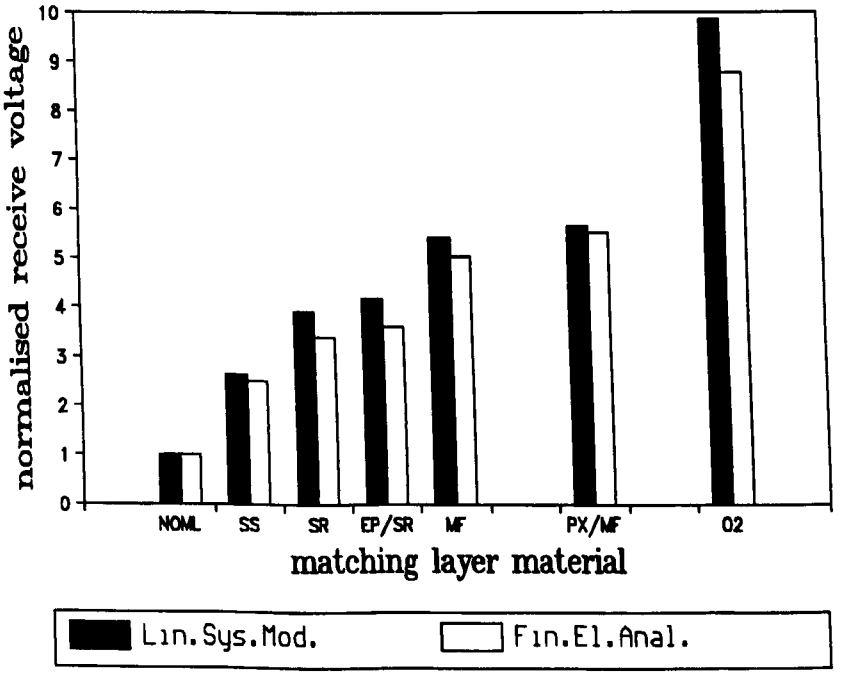

Figure 4.14(b) Application of mechanical matching layers to a 20% PZT5A/hard set composite receiver

4.5.4 Mechanical Damping

System resolution can be improved by applying mechanical damping, to the transducer rear face, to reduce reverberation within the transducer and consequently increase bandwidth. For the purposes of these simulations half and full damping conditions correspond to the specific acoustic impedance of the backing material being equal to 50% or 100% of the transducer impedance respectively. Figure 4.15(a) and 4.15(b) demonstrate the bandwidth and performance characteristics, predicted for a pitch-catch system under both damping conditions. It is assumed that both the transmitting and receiving transducers have the same volume fraction and are frequency matched. Almost 75% bandwidth has been realised with full damping, but the corresponding sensitivity at 20% is 17dB down compared to the undamped case over the volume fraction range. Clearly, the half damping conditions conform to a compromise between the undamped and fully damped cases, where approximately 45% bandwidth can be realised but with a 14.2dB reduction in performance, at 20% volume fraction.

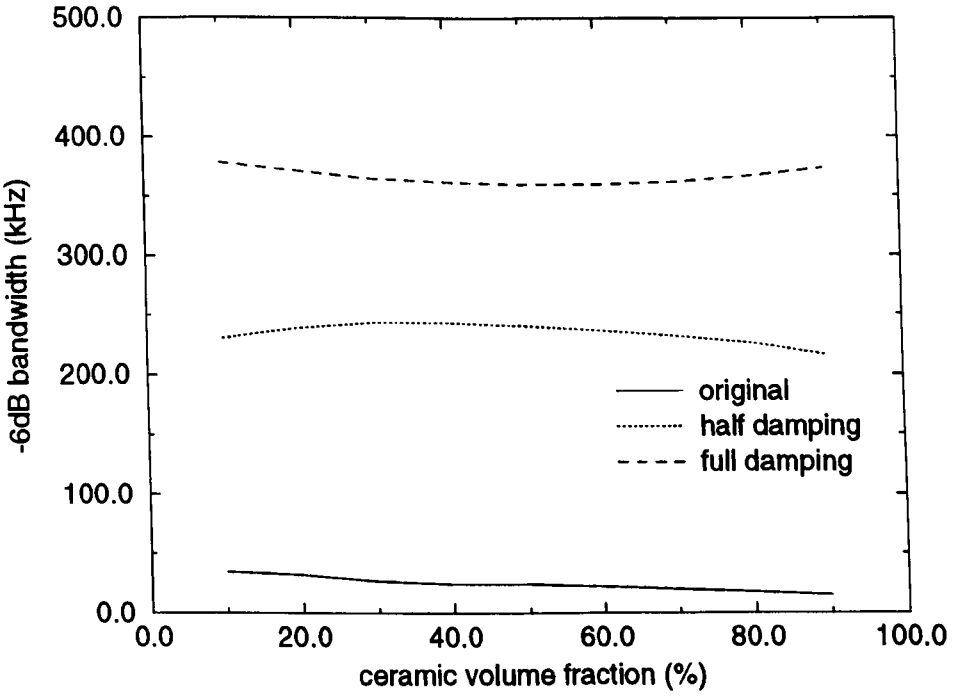

Figure 4.15(a) -6dB bandwidth characteristics of damped composite transducers

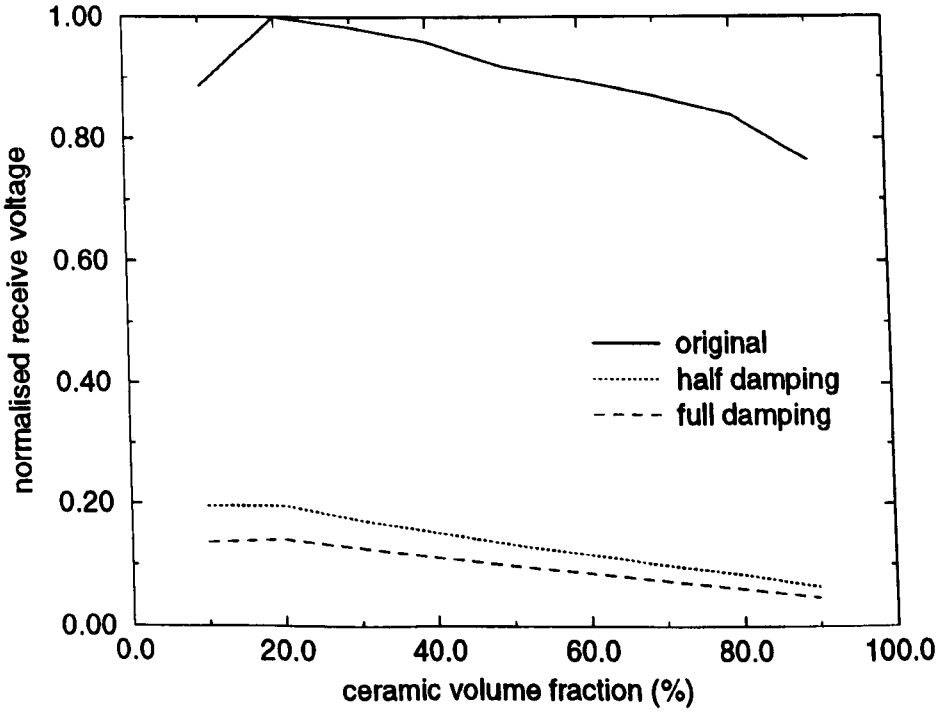

Figure 4.15(b) Sensitivity comparison for damped composite transducers

4.6 CONCLUSIONS

A dual modelling strategy has been evaluated to assess the performance of air-coupled 1-3 connectivity piezocomposite transducers. The finite element approach performs well across the entire volume fraction range, including analysis incorporating mechanical matching and damping conditions. The linear systems technique is also satisfactory, but requires that the composite behaves as an effective homogeneous medium, necessitating conformity with pillar aspect ratio constraints. The major benefit of the uni-dimensional approach is the ability to analyse the problem with a considerably shorter process time. This indicates that the FEA should not be used to the exclusion of the linear systems model, but rather a dual modelling strategy is possible for the design of 1-3 piezocomposite transducer systems.

These models predict that a 50% - 70% composite transmitter and 10% - 30% receiver comprise the basic elements of a through air transducer system. The best transmit performance is as a result of the compromise between the improved acoustic impedance matching as the ceramic volume fraction is reduced and the high coupling efficient and permittivity associated with high volume fraction devices. Whereas, in reception the low acoustic impedance associated with the low volume fraction devices is the overriding factor to establish the optimum transducer configuration. A double matching layer combination of perspex and a microporous membrane filter is estimated to enhance transducer performance by 16dB. Frequency matching of transmitter and receiver permits a sensitivity improvement of 30dB under narrowband conditions. Although wideband operation is achievable by rear face (75%) damping of the composite consequent pulse-echo sensitivity is reduced by 17dB. This is significant because air is an inherently poor medium for the propagation of ultrasound.

CHAPTER 5

Improving the Bandwidth of 1-3 Connectivity Composite Receivers using Mode Coupling

ABSTRACT

System resolution can be improved by applying mechanical damping to the transducer to reduce reverberation within the device and consequently increase its bandwidth. Modelling predicts an improvement in transducer bandwidth, under the influence of mechanical damping, although system sensitivity is severly reduced to produce a desired wideband response. Therefore an alternative approach is suggested, utilising the strong coupling between the fundamental thickness mode and the first lateral resonance in a 1-3 piezocomposite. Conventional composite transducer design requires adequate decoupling between these modes to produce a composite which will behave as a homogeneous medium and possess a good electromechanical coupling efficiency and a high surface dilation quality. However, if a high system bandwidth is desired, then the strong coupling of these modes can be utilised, but this is achieved at the expense of electromechanical coupling efficiency and surface dilation quality. Finite element modelling techniques are employed to evaluate the influence of mode coupling on composite receiver bandwidth, under water loading. The theory was then extended to incorporate air-coupled composite transducer designs. This technique is particularly relevant to airborne detectors as reasonable system sensitivity is maintained in conjunction with a significant improvement in bandwidth. Finally, the air-coupled performance of a laterally-coupled composite receiver is shown to compare favourably with both a thickness mode composite and an electrostatic transducer.

5.1 INTRODUCTION

The resonant modes of vibration within 1-3 connectivity composite transducers are of significant interest for the transducer design engineer. As a result of the regular periodicity of the piezoceramic pillars within this structure, a number of mechanisms exist to support several vibrational modes and hence, the design process becomes more complex. Figure 5.1 depicts a hierarchial representation of the main resonance mechanisms within a 1-3 connectivity piezocomposite structure.

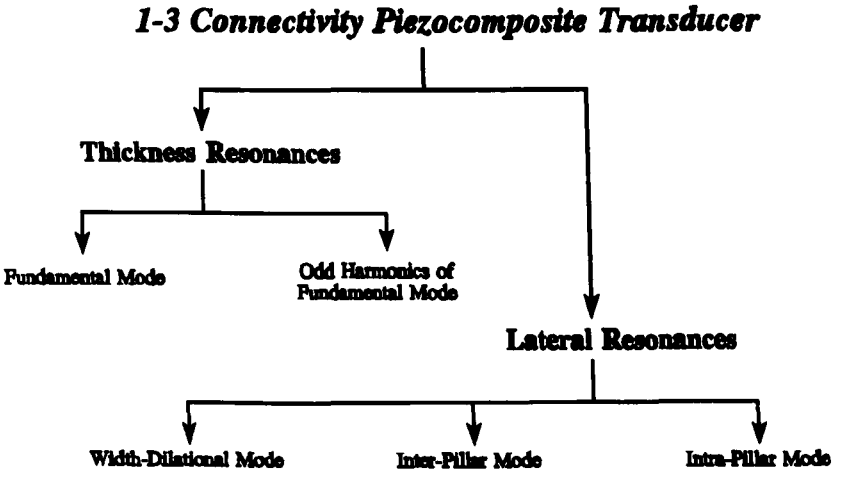

Figure 5.1 Hierarchial representation of vibrational resonance within a 1-3 piezocomposite transducer

The fundamental thickness mode of a composite transducer is a result of the finite thickness of the device and the longitudinal speed of sound within the structure. Further thickness mode resonances occur at the odd harmonics of the fundamental, although with reduced coupling as the mechanical damping increases with frequency. Lateral resonances are identified as mechanical motion in directions *1* and *2*, after excitation in the *3* direction, using the axis convention illustrated on page (xii). The three classifications of lateral vibrational mechanisms are width-dilational, inter-pillar and intra-pillar modes. Width-dilational resonances occur due to the finite lateral dimensions of the transducer in the form of radial modes (disc transducers) or plate modes (plate

transducers). These modes do not normally constitute a design problem because the coupling of these modes is weak within the composite transducer as a consequence of the high damping associated with the polymer phase and, for many applications, their frequency is low compared to the fundamental thickness resonance. Inter-pillar resonances arise due to the periodic spacing of the piezoceramic pillars within the structure and are influenced by the inter-pillar spacing, the pillar shape and the shear velocity in the polymer phase. These vibrational modes present design problems for low ceramic volume fraction composites, where the frequency at which the lateral mode occurs can interfere with the fundamental operating frequency. Intra-pillar resonances are as a consequence of the finite lateral dimensions of the ceramic pillars. These vibrational modes can constitute a design problem for high ceramic volume fraction devices.

Considerable work has been reported about the resonances generated within the 1-3 composite structure. Gururaja et al described the mechanism for each resonance mode observed within a composite transducer and discussed their implication for optimisation of transducer designs [117]. A significant proportion of the published work has focused on the influence of inter-pillar resonances to the design of composite transducers. In order for the composite transducer to operate as a thickness mode device, Smith et al reported that these resonant modes should occur at a frequency at least twice that of the desired thickness mode [83]. Auld and Wang used a theory based on Bragg scattering to predict the resonant frequency of the inter-pillar vibrational mode [118]. This method is particularly relevant to low ceramic volume fraction composite devices. Further work by Auld has designed the inter-pillar spacing to correspond to half the wavelength of a laterally propagating wave [119]. This criteria is applicable to linear array design, where cross coupling between elements is undesirable. Chan et al have described the mode coupling between the lateral and thickness resonances, as the thickness of the transducer was varied [120]. It was concluded, for an example composite transducer, that as the aspect ratio was increased there was a frequency band where strong mode coupling occurred and the transducer should be operated outwith this region. Investigations by finite element techniques into the composite transducer microstructure, by Hossack and

Hayward [84] and Hayward and Bennett [87], have produced a set of design guidelines to promote homogeneous behaviour through the application of the Maximum Pillar Aspect Ratio (MPAR) [87]. This principle enables a composite transducer to be designed with both the inter-pillar and intra-pillar resonances sufficiently removed from the fundamental thickness mode resonance. An alternative technique to suppress the inter-pillar and intra-pillar modes can be achieved by constructing a distributed-period composite structure [121]. Here, the regular periodic distribution of the ceramic pillars is replaced by a distribution of pillar dimensions in which there is no dominant lateral resonance. A different method was proposed by Sherrit et al [122] and Oakley and Marsh [123] in which the polymer phase was removed to form a 1-3 ceramic-air composite transducer and hence, no convenient medium was available to support the lateral vibrational modes. These transducer designs provide enhanced acoustic impedance matching to low acoustic impedance media and improved electromechanical coupling coefficient compared to conventional PZT/hard set polymer composite transducers. Although, the complexity in manufacturing such a device would limit the practical applications.

In the work described, the lateral resonances are viewed as parasitic modes of vibration and hence, effort has concentrated on the separation of these modes from the fundamental thickness resonance. An interesting approach, developed by Bui et al [124], was to design a multifrequency composite transducer which utilised both the thickness and lateral resonances. It was envisaged that these devices would find application in medical systems, where the lower frequency would be used to locate the area for examination and the higher frequency used to obtain a higher resolution image.

The work presented in this Chapter will describe a novel design technique which utilises the inter-pillar resonance to enhance effectively the bandwidth of the composite receiver. As described in Section 4.5.4, when full damping conditions were applied to the rear face of a composite transducer a 17dB decrease in receive sensitivity was predicted under pulse-echo conditions. The associated large inherent losses due to operating in air ensures that this reduction in sensitivity would be unacceptable for any practical

application. The alternative approach presented here will increase the composite transducer bandwidth without significant degradation to the sensitivity. As the ceramic pillar aspect ratio is increased the coupling between the fundamental thickness mode and the first lateral resonance is altered. This is observed in the frequency content for these composite devices, where the two distinct peaks, one each for the thickness and lateral resonance, in the spectra move closer together as the aspect ratio increases. Under strong coupling conditions, when the two resonances are in close proximity, these effectively combine to produce a single broadband peak in the frequency spectrum. The stimulus for this work was to develop an air-coupled piezoelectric receiver with sufficient bandwidth to complement the high resolution afforded by laser generation of ultrasound. Hence, the work presented will concentrate on the wideband composite receiver problem. Results from this hybrid system on both aluminium and carbon-fibre reinforced composite materials are detailed in Chapter 6.

Throughout this investigation a 20% PZT5A/hard set composite receiver has been utilised, in accordance with the specifications in Section 4.5.2. The design of a laterally coupled composite receiver was initially assessed in terms of electromechanical coupling efficiency and dilation quality for a composite transducer using finite element modelling. A constant thickness for the transducer was assumed and the ceramic pillar aspect ratio varied in order to estimate any deterioration in these parameters as the mode coupling conditions were altered. To verify the modelling approach, the fractional bandwidth was predicted for a range of 20% composite receivers, with aspect ratio 0.1 to 0.37, under both undamped and damped conditions. Favourable correlation with experimentally measured results was obtained. The experiment was conducted under water loading conditions and a PVDF transmitter, described in Section 3.3.2(a), was used to generate a wideband ultrasonic signal. The modelling was then extended to analyse the bandwidth improvement for air-coupled composite receiver designs. Consequently, a laterally-coupled composite receiver was manufactured and its air-coupled performance observed to compare well with the received signal acquired by an electrostatic transducer operating under identical conditions.

5.2 Bandwidth Considerations for a Piezocomposite Receiver

5.2.1 The Piezoelectric Receiver

The complex electromechanical operation of a piezoelectric reception element has been successfully analysed using a physically meaningful block diagram format [107]. This methodology is described in Appendix B and demonstrates the factors which influence both primary and secondary piezoelectric action. This approach facilitates a simple bandwidth analysis. Reverberation within the piezoelectric element is transferred into a ringing in the temporal response of the device, where a long time signal is synonymous with a narrower bandwidth. Hence, it is clear that one method to improve the bandwidth is to reduce the extent to which resonant activity contributes to the overall transducer response. This can be achieved by reducing the influence of the reverberation factors through reduction of the reflection coefficients at the faces of the transducer.

5.2.2 Methods to Improve the Bandwidth of Piezoelectric Transducers

(a) Mechanical Damping of Transducer

The application of either mechanical backing or matching [125,126] is the conventional method to enhance bandwidth. Mechanical damping, to the transducer rear face, will reduce reverberation within the transducer and consequently increase bandwidth. This standard approach was adopted for the modelling work described in Chapter 4, where a 75% bandwidth was predicted under pulse-echo conditions, but the corresponding sensitivity was 17dB down compared to the undamped case. Desilets et al described the use of mechanical matching layers to improve transducer bandwidth [126]. The methodology used a quarter-wave matching technique to estimate the optimum acoustic loading impedance for broad-band matching. This approach does not yield the high bandwidth characteristic exhibited by mechanical damping, although good sensitivity performance was reported.

(b) 1-3 Connectivity Piezocomposite Transducers

Alternative methods for improving the bandwidth of a 1-3 piezocomposite transducer have been reported using non-standard geometries for the composite structure [84]. Here, a composite design comprising three different ceramic pillar geometries was analysed using finite element modelling techniques. Each geometry produces a distinct thickness mode resonant peak, due to the different ceramic pillar aspect ratio. The resonant modes couple due to their close proximity and hence, an effective increase in system bandwidth is observed. This method was demonstrated to improve the transducer bandwidth, although it was constrained due to the deterioration of the thickness coupling coefficient as the ceramic pillar aspect ratio is increased. This paper also analysed a second approach, where a composite transducer with a non-uniform thickness was evaluated using finite element modelling [84]. Again an increase in transducer bandwidth was predicted, although the non-uniform vibrating aperture was considered to constitute a problem.

(c) Predictions using Uni-Dimensional Modelling Techniques

Chapter 4 illustrated that the linear systems modelling technique is not suitable for the evaluation of multi-modal transducer structures. Although, it can be used as a guide to optimum, thickness mode, transducer performance. Uni-dimensional modelling was used to estimate the air-coupled receive impulse response for a 20% PZT5A/hard set composite transducer under no damping, half damping (50%), and full damping (100%) conditions (the specific acoustic impedance of the composite is estimated at 8.6MRayl). The undamped transducer was designed to operate at 1.0MHz, which corresponds to a thickness of 1.75mm. The simulation utilised the wideband pressure wavelet generated by the PVDF transmitter, including the influence of airborne attenuation over a 20mm airgap, as described in Chapter 3. This signal is illustrated in Figure 3.9(b). The predicted receive responses are illustrated in Figure 5.2. This Figure demonstrates the influence of the increased damping conditions on the pulse length, where a short single cycle pulse has been predicted for full damping compared to over 25-cycles under no damping conditions. As anticipated, a reduced peak-to-peak receive sensitivity for the 100% damped transducer (-9.4dB) has been predicted compared to the undamped case.

The half damping conditions are a compromise between these two conditions, where a 5-cycle pulse is predicted with a 4.1dB reduction in receive sensitivity.

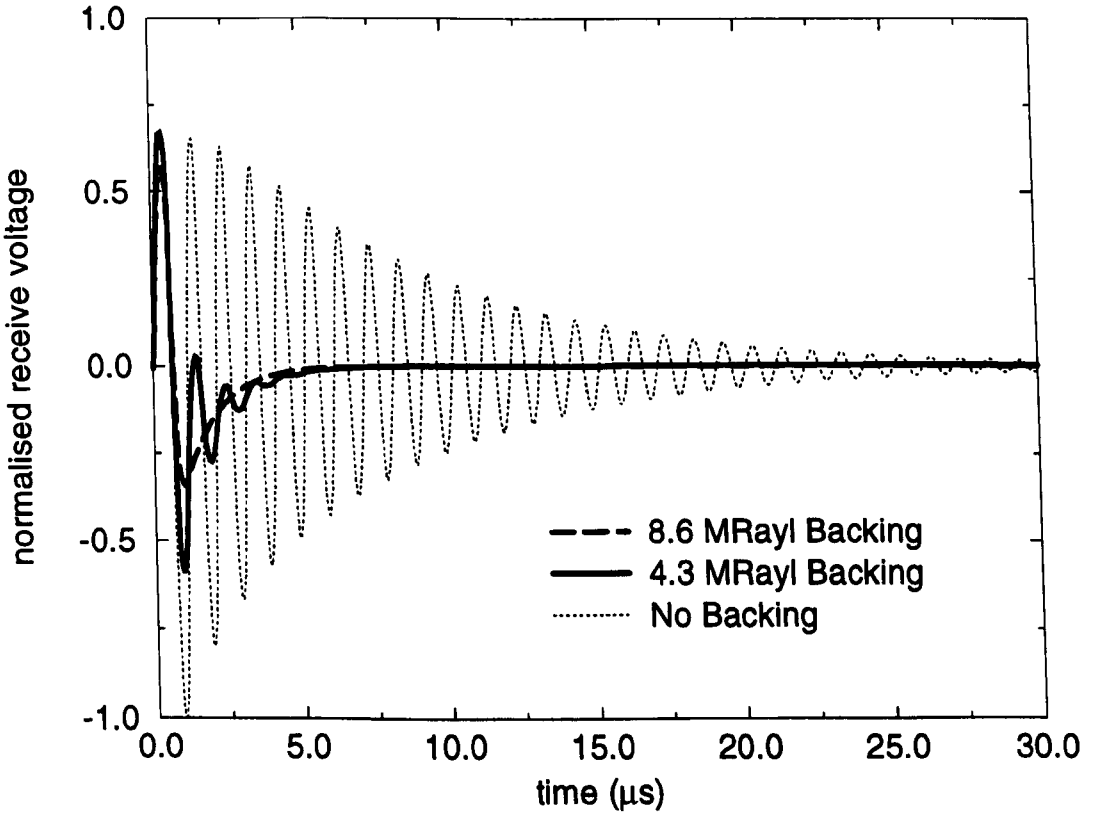

Figure 5.2 Temporal receive responses for a 20% composite under various damping conditions, as predicted by linear systems model

5.3 Influence of Lateral Mode Coupling on Composite Behaviour

5.3.1 Introduction

Finite element analysis is utilised to investigate the mode coupling behaviour of 1-3 connectivity piezocomposite transducers. A range of 20% PZT5A / hard set piezocomposite receivers were constructed, each with a different aspect ratio. The transducers were evaluated under both undamped and half damping conditions, which were chosen to determine the bandwidth improvement for devices with useful sensitivity characteristics. In order to validate the modelling approach, these transducers were evaluated under water load. This methodology was adopted to examine fully the influence of mode coupling on the transducer bandwidth. The modelling could then be applied to air-coupled operation, where the influence of air attenuation will be a limiting factor on the transducer performance.

5.3.2 Range of Composite Transducers Constructed

The results from Section 4.5.2 indicate that a 20% PZT5A/hard set epoxy composite transducer combination will operate well in reception. Hence, the range of receivers constructed used this configuration. The ceramic pillar width (0.22mm) and inter-pillar spacing (0.32mm) have been kept constant and the transducer thickness varied between 0.6mm and 2.2mm, resulting in a spread of aspect ratios from 0.37 to 0.1, respectively. The manufacturing specifications were chosen to support the first lateral mode at approximately 2MHz. Table 5.1 describes the range of transducer constructed. The composite receivers were evaluated under both undamped and approximate half damping conditions. The damping to the transducer rear face was achieved through application of a 40mm thick perspex block, acoustic impedance of 3.2MRayl. The perspex was shaped to inhibit internal reflections within the backing block, as shown in Figure 5.3. This practical arrangement approximates well to half damping conditions, 4.3MRayl, for the 20% composite devices. Each device was housed in a water-proofed aluminium casing.

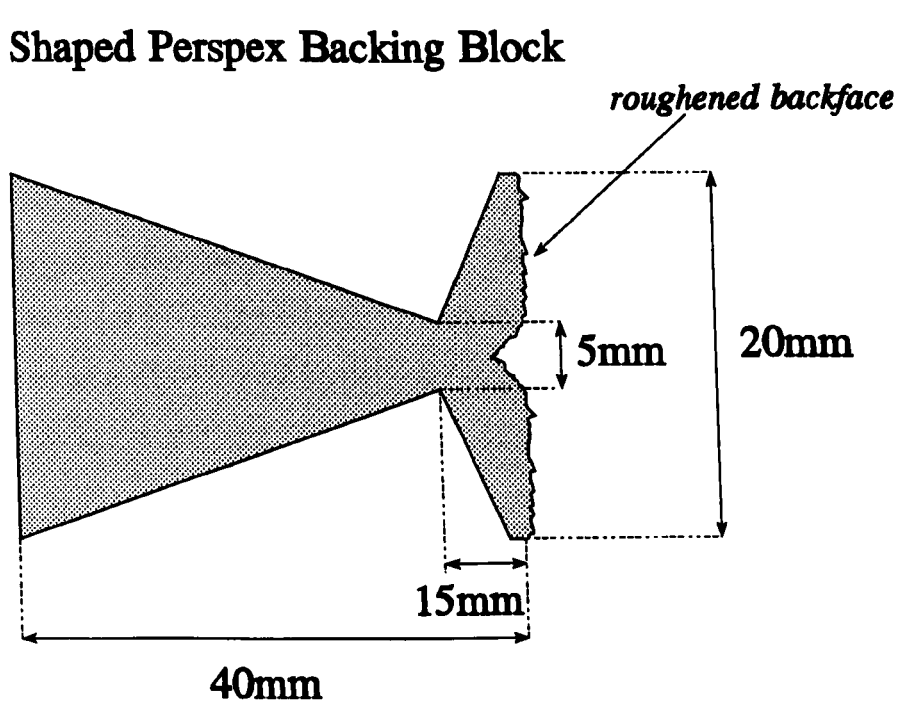

Figure 5.3 Configuration for the shaped perspex backing block

aspect ratio	0.1	0.126	0.141	0.177	0.196
thickness (mm)	2.17	1.74	1.56	1.24	1.12
f_n (MHz)	0.77	0.96	1.13	1.28	1.48
k_t	0.541	0.532	0.534	0.514	0.473
aspect ratio	0.216	0.234	0.262	0.301	0.367
thickness (mm)	1.02	0.94	0.84	0.73	0.61
f_n (MHz)	1.68	1.77	1.82	2.06	2.38
k_t	0.441	0.386	0.375	0.356	0.287

Table 5.1 Properties of manufactured 20% composite transducers

5.3.3 Laterally-Coupled Piezocomposite Impedance Profiles

Initially, the finite element technique has been used to predict the impedance profiles for both damped and undamped composite transducer arrangements. Figure 5.4(a) illustrates the impedance profile for the composite transducer with an aspect ratio of 0.196. Figure 5.4(b) presents the impedance profile for the 0.234 aspect ratio transducer, under perspex damped conditions. Both Figures demonstrate reasonable correlation between the finite element analysis and the experimentally acquired results. These Figures illustrate examples of lateral mode coupling, where the close proximity of both the fundamental thickness and inter-pillar resonance is clearly evident.

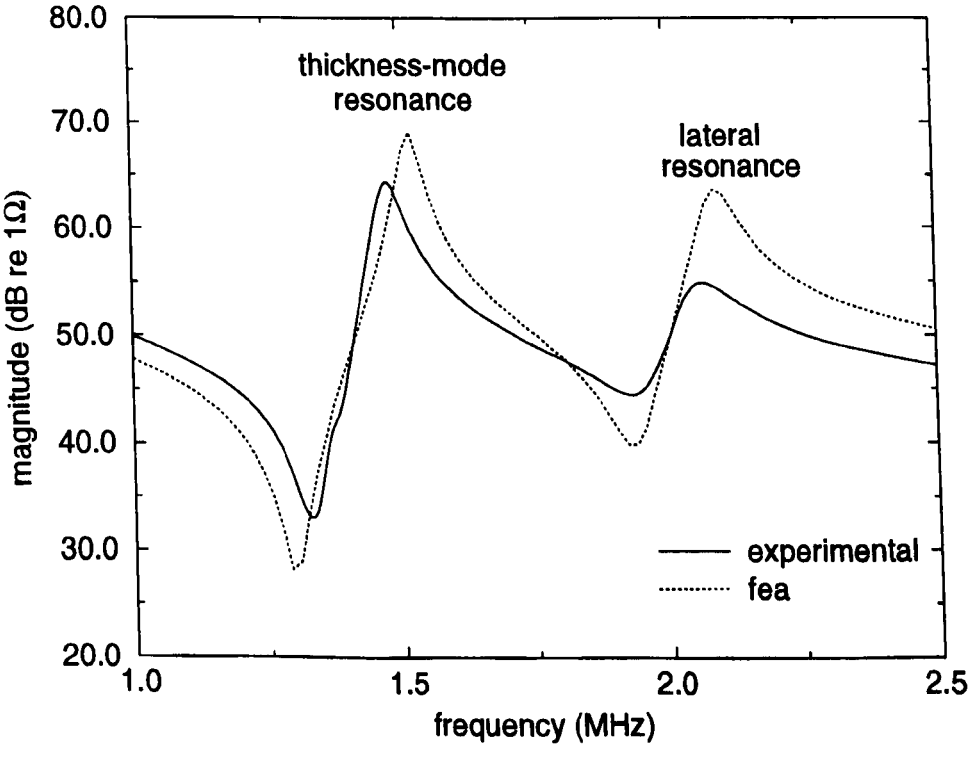

Figure 5.4(a) Impedance profile for the 20% composite transducer, with an aspect ratio 0.196

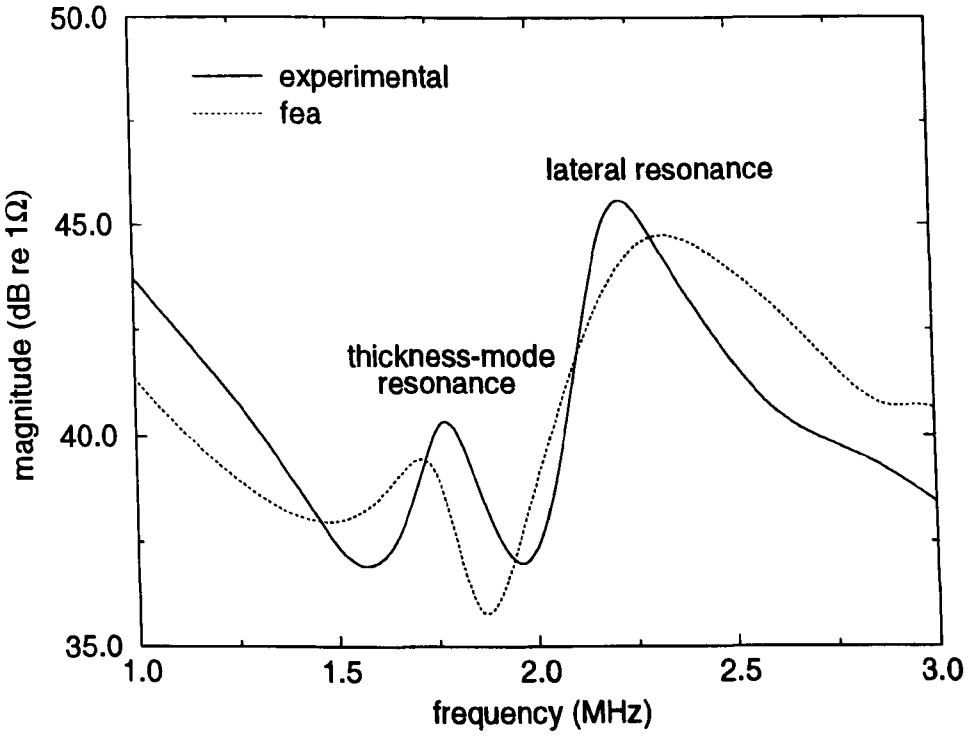

Figure 5.4(b) Impedance profile for a damped 20% composite transducer, with aspect ratio 0.234

5.3.4 Coupling between the Fundamental Thickness and Inter-Pillar Resonances

Hayward and Bennett [87] investigated the coupling between the fundamental resonance and the inter-pillar resonances, using finite element methods, in order to evaluate the Maximum Pillar Aspect Ratio (MPAR) conditions which will permit the composite to behave as a homogeneous medium. For a 20% composite device, the MPAR criteria ensures that the first lateral resonance is at least double the frequency of the fundamental thickness mode when the aspect ratio is less than 0.17.

Using the finite element techniques described in [87], the influence of mode coupling upon the mechanical resonance (f_n), electromechanical coupling coefficient (k_t), described by Equation 3.2, and surface dilation quality (Q_{dil}) at the mechanical resonance, calculated using Equation 4.2, have been predicted. The transducer parameters used in this analysis were consistent with the range of undamped composites described in Section 5.3.2. In contrast to [87], the mechanical resonance has been chosen because the present work is primarily concerned with reception characteristics. The

results of this evaluation are shown in Figures 5.5. Reasonable correlation with experimental data, acquired from range of transducers described earlier, is evident throughout these Figures. Here, the aspect ratio has been varied between 0.1 and 0.4 because as the aspect ratio is increased further the composite transducer exhibits several vibrational modes and thus, identification of the two modes of interest is difficult.

(a) Undamped Composite Transducers

Figure 5.5(a) illustrates the relative positions of the fundamental thickness and first lateral resonances. As anticipated, the frequency of the fundamental thickness mode increases almost linearly as the aspect ratio is increased. When these resonances are well separated, for aspect ratio < 0.2, the lateral resonance remains at a relatively constant frequency. As the aspect ratio is increased, mode coupling then forces the first lateral mode to a higher frequency. The influence of mode coupling on electromechanical coupling efficiency is demonstrated in Figure 5.5(b). Estimated values of k_t, for the fundamental thickness resonance, can be observed to decrease as the aspect ratio increases. In contrast, the coupling efficiency of the lateral mode increases until this resonance is dominant. There is a discrepancy between the experimentally measured and FEA predicted crossover point, as the experimentally acquired values are lower than predicted, perhaps as a consequence of depolarisation during the slicing process. Finally, the dilation quality at the mechanical resonance is presented in Figure 5.5(c), where Q_{dil} is predicted to decrease, with increasing aspect ratio, for both thickness and lateral resonances. In reception, this transducer can only be regarded as operating as an effective homogeneous medium at an aspect ratio below 0.15. Although after an aspect ratio of 0.3 values for Q_{dil} increase for the lateral resonance, which coincides with the crossover in coupling coefficient.

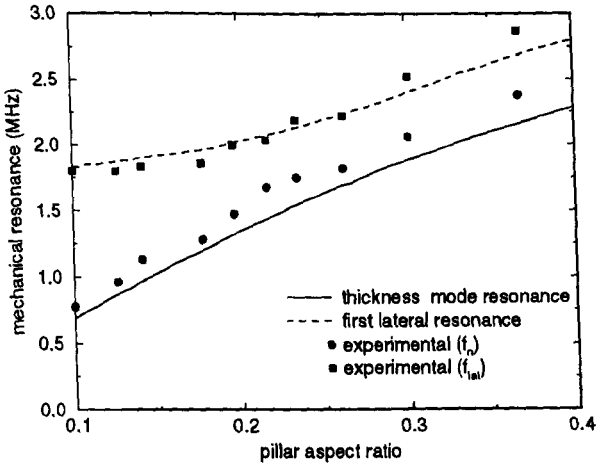

(a) mechanical resonance frequencies

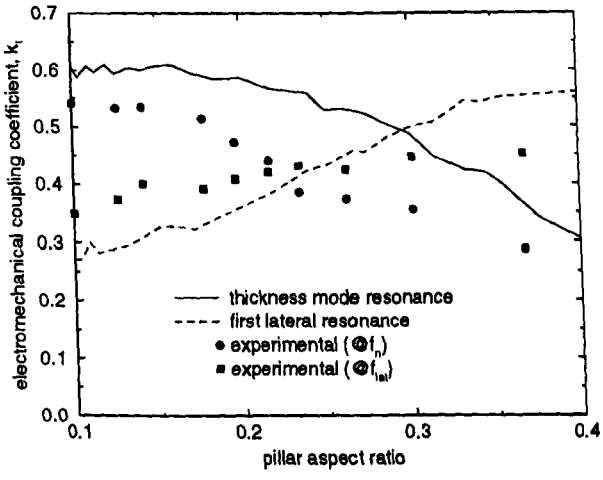

(b) electromechanical coupling coefficient

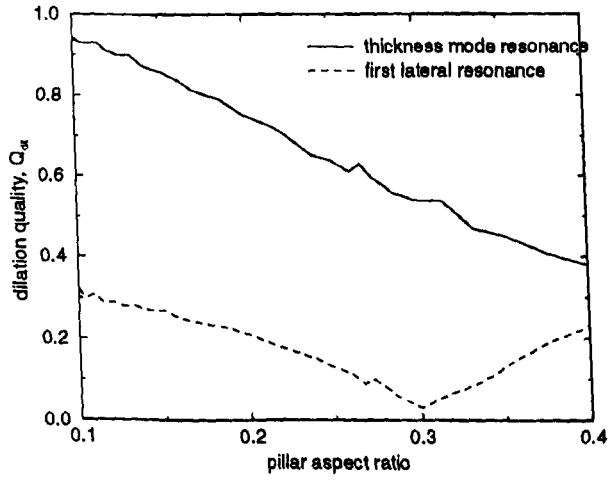

(c) dilation quality at the mechanical resonance

Figure 5.5 Transducer characteristics as a function of aspect ratio for a 20% PZT5A/hard set composite transducer

(b) Damped Composite Transducers

The application of mechanical damping to the rear face of the composite transducer results in a different relationship between the thickness and lateral resonance mechanisms, when compared to the undamped case illustrated in Figure 5.5(a). The mechanical resonances for the range of damped composite devvices are shown in Figure 5.6, where good correlation between theory and experiment has been again been achieved. For an aspect ratio of 0.234, the predicted values for the fundamental thickness and first lateral resonances are separated by only 25kHz for the damped case, compared to approximately 50kHz for the undamped case. Therefore, the application of mechanical damping, to the rear face of the composite, has effectively brought the two modes closer together. There are no experimental entries for the composite transducer with an aspect ratio of 0.367 in this Figure. This is as a result of difficulty in positive identification of the relevant modes.

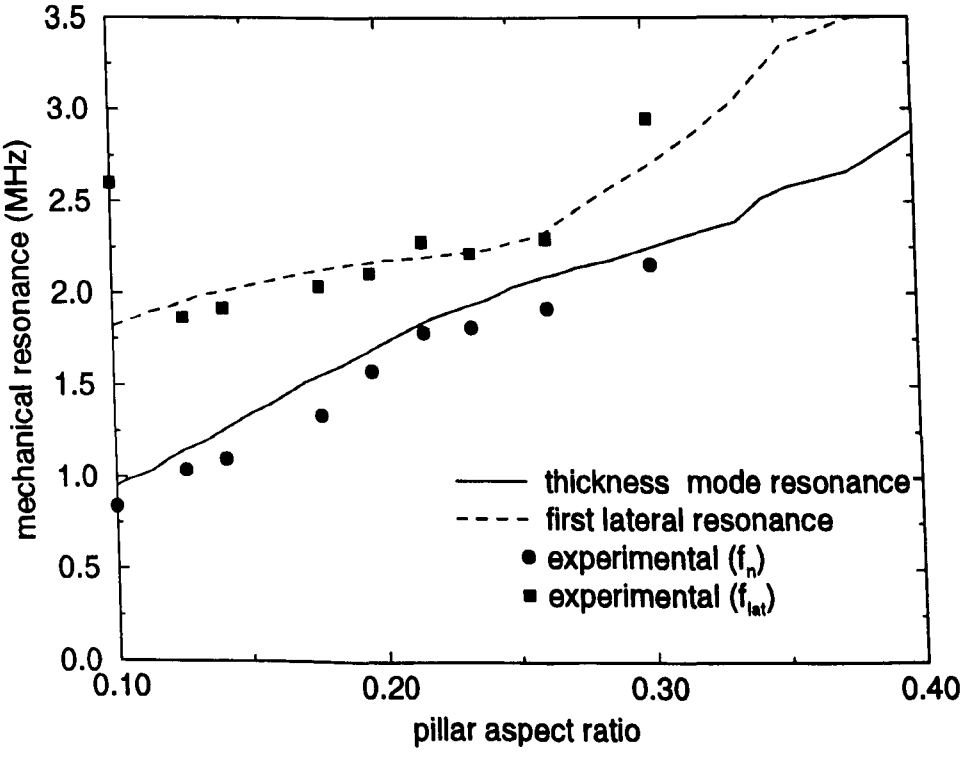

Figure 5.6 Mechanical resonance frequencies as a function of aspect ratio for a 20% damped PZT5A/hard set composite transducer

5.3.5 Experimentation under Water Load

(a) Experimental Arrangement

As a consequence of the high air attenuation factor and high operating frequencies, the modelling was evaluated under water load. A broadband pressure wave was desired to investigate the bandwidth of the composite receivers and the PVDF transmitter, described in Section 3.3.2(a), was considered appropriate. The earlier work utilised two pulser units to drive the PVDF transducer and the corresponding spectral and temporal responses, under water load, are shown in Figures 3.4 and 3.5. For the present range of transducers, operating under water load, either excitation method would simulate approximate impulse conditions. Although for the air-coupled experimentation a different scenario would ensue. The influence of air attenuation upon the two wideband excitation methods was demonstrated in Section 3.4.2 and Figures 3.8(a) and 3.9(a) illustrate the predicted frequency content for different air separation distances. The differentiated step excitation approach was chosen for the work described in Chapters 3 and 4 because the transducers under investigation operated between 500kHz and 1MHz. The current analysis will utilise transducers operating in the frequency range 500kHz to 3MHz. Hence, the Panametrics pulser unit will offer more appropriate excitation conditions in which to evaluate the bandwidth improvement for composite transducers exhibiting mode coupling characteristics. Under this pseudo impulsive excitation technique, the air-coupled PVDF transmitter is estimated to operate with a centre frequency of approximately 1.5MHz for an airgap separation of 20mm.

It should be noted that the finite element code implements the electrical stimulation under ideal impulsive excitation conditions.

(b) Undamped Composite Transducers

The receive sensitivity and bandwidth for the range of transducers, prior to the application of mechanical damping, were acquired experimentally under water load. Reasonable correlation can be observed between the experimental and the corresponding modelled results presented in Figure 5.7. The water load introduces mechanical damping at the transducer front face and hence, increases the device bandwidth over an identical

transducer operating under air loading. It is interesting to note that the uni-dimensional model predicts approximately 27% bandwidth, which is close to both the FEA and experimental results for an aspect ratio of 0.1. As the aspect ratio is increased, the experimental transducer bandwidth peaks at a maximum value of 60% corresponding to an aspect ratio of 0.196. The corresponding receive sensitivity is 3.75dB down compared to the thickness-drive transducer response with an aspect ratio of 0.1. It is interesting to note that both the point of maximum bandwidth, for an aspect ratio of 0.2, corresponds closely with the region of maximum coupling in Figure 5.5(a), where the thickness and lateral resonances are in close proximity, and also to the coupling coefficient crossover point in Figure 5.5(b). In addition, the theoretically predicted point of maximum bandwidth occurs for an aspect ratio of 0.24 corresponds closely with the theoretical point of maximum coupling, as illustrated in Figure 5.5(a).

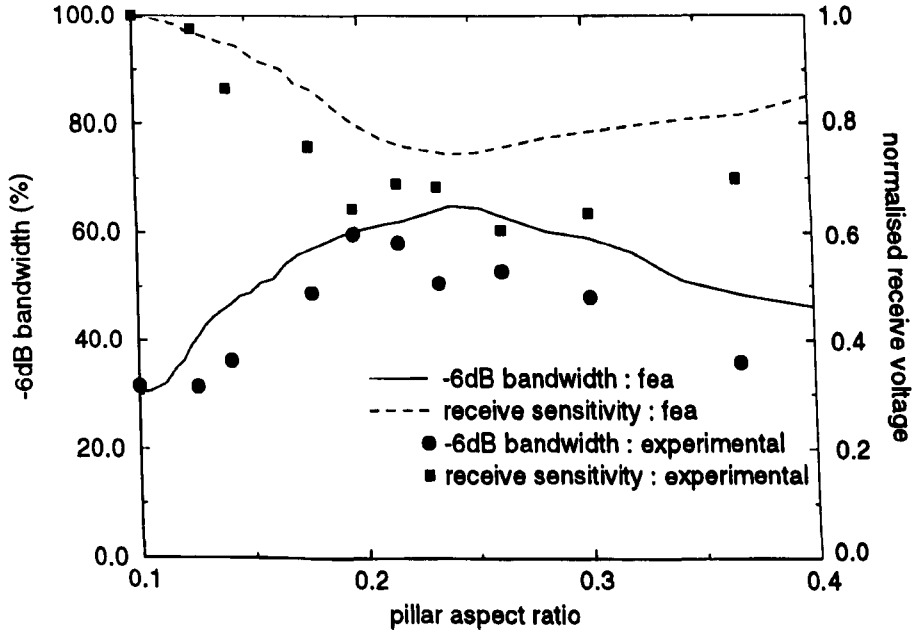

Figure 5.7 Bandwidth and sensitivity characteristics for 20% composite transducers under water loading

(c) Damped Composite Transducers

For this series of experiments the composite transducers were subject to mechanical damping, at the rear face, in the form of a shaped perspex block. Again, the receive sensitivity and bandwidth have been recorded and compared to theoretical predictions. Figure 5.8 illustrates good agreement between theory and experiment. The overall

characteristics shown in this Figure are similar to the results presented in Figure 5.7 for undamped transducers. The bandwidth for a low aspect ratio composite has increased to 66% compared with 31% for the unbacked case. The experimental transducer bandwidth peaks at a value of 116% for an aspect ratio of 0.216 and the subsequent receive sensitivity is reduced by 3.25dB over a device with an aspect ratio of 0.1. In addition, it should be noted that the region of maximum bandwidth, aspect ratio between 0.2 and 0.25, corresponds to the region of maximum coupling shown earlier in Figure 5.6.

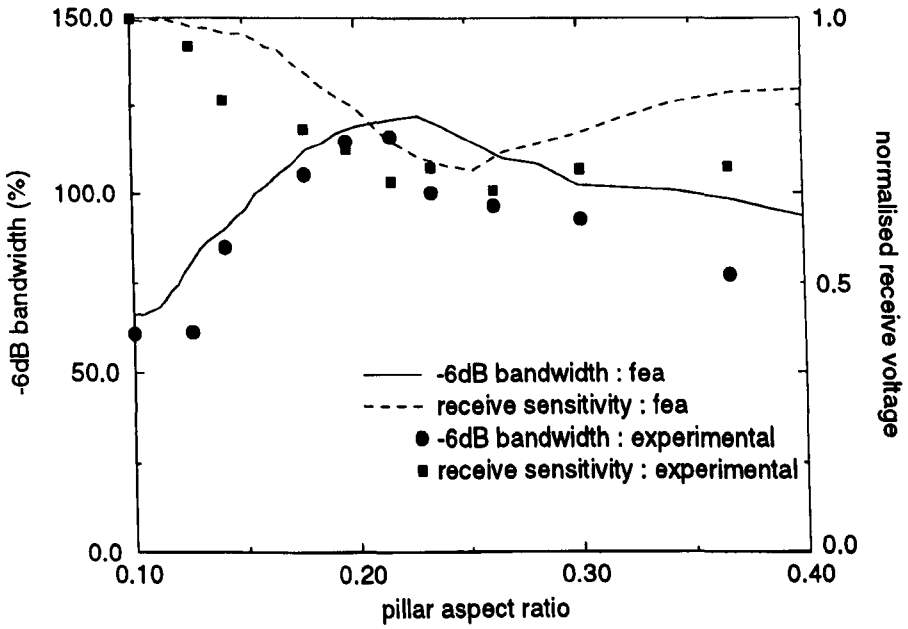

Figure 5.8 Bandwidth and sensitivity characteristics for 20% damped composite transducers under water loading

(d) Experimental Results

The experimentally acquired temporal signals, from the composite receivers with aspect ratio 0.1 and 0.216, are presented in Figure 5.9(a). Here, the lower operating frequency of the 0.1 aspect ratio device is clearly evident and the 66% bandwidth is manifest as the received six cycle pulse. The 0.216 aspect ratio composite has a shorter pulse length, as a consequence of both its higher operating frequency and wider bandwidth. This is illustrated in the corresponding frequency spectra, shown in Figure 5.9(b). The high aspect ratio device has a -6dB bandwidth of 116%, centred around 2.15MHz, whereas the lower aspect ratio composite has a 66% bandwdith centred around 780kHz.

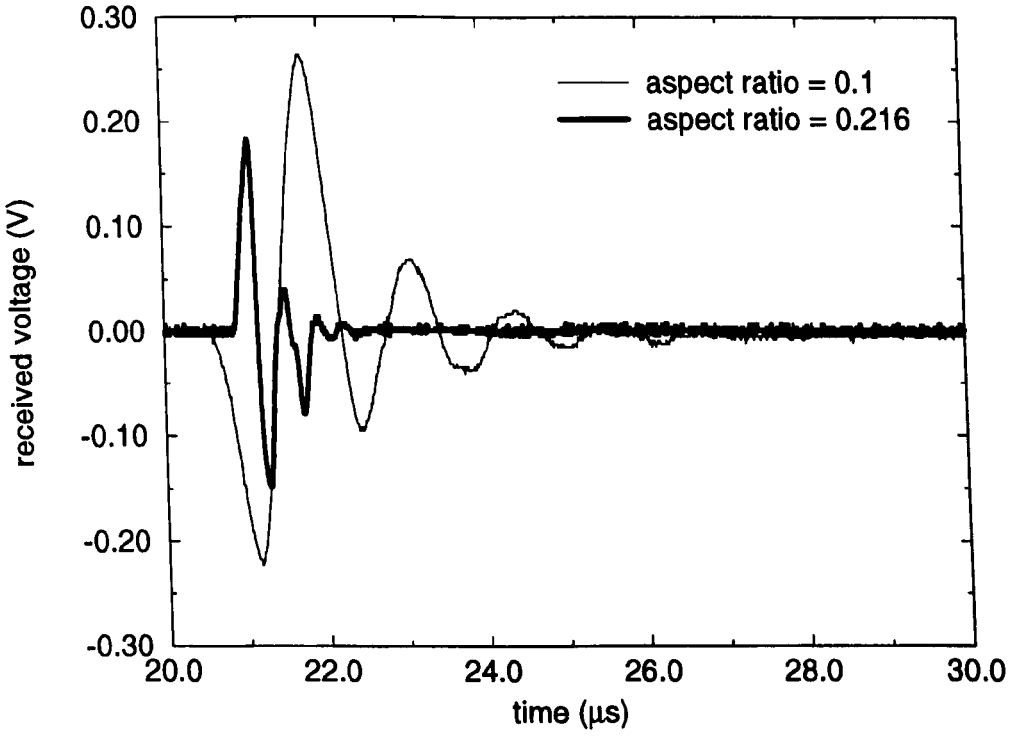

Figure 5.9(a) Experimentally acquired temporal response for transducers, with different aspect ratio, under water load conditions

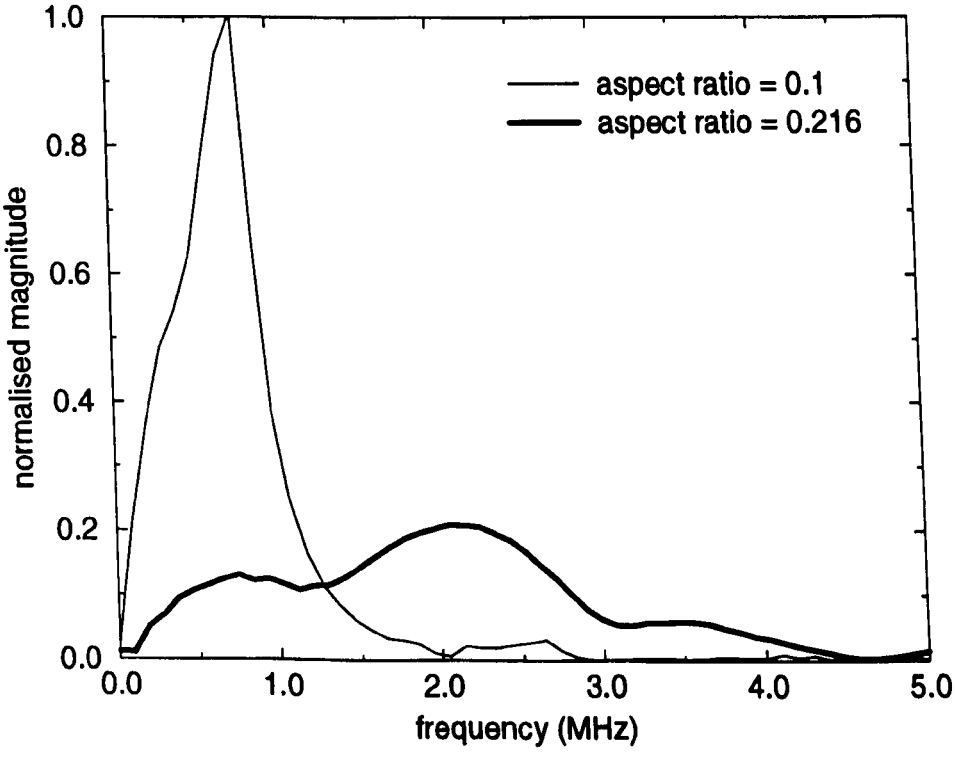

Figure 5.9(b) Corresponding frequency spectra for the temporal responses shown in Figure 5.8(a)

5.4 AIR-COUPLED WIDEBAND PIEZOCOMPOSITE RECEIVER PERFORMANCE

5.4.1 Introduction

Laser generated ultrasound is the main established non-contact source of wideband ultrasonic energy. Corresponding optical detection of this energy requires a highly reflective surface, which is opposite to the requirements for optical generation. This consideration was discussed in Section 2.1.7, where different transducer technologies were presented as alternative ultrasonic receivers to optical interferometric detection [66 - 73]. Hence, the improved bandwidth characteristics of the laterally coupled composite transducer could find application as a wideband air-coupled receiver to complement the high resolution afforded by laser generated ultrasound. Experimentally validated under water load, finite element modelling is now utilised to analyse the bandwidth improvement for air-coupled composite receivers. The results from the modelling will be used to construct a wideband laterally-coupled composite receiver. Initially, the receive characteristics of this device are compared with a thickness drive composite transducer (aspect ratio of 0.1). Finally, the wideband nature of the electrostatic transducer, described earlier in Chapter 3, will be employed to evaluate further the available bandwidth of the laterally-coupled composite.

5.4.2 Finite Element Analysis under Air Load Conditions

(a) Undamped Composite Transducers

Earlier, Figure 5.5(a) illustrated a constant separation between the mechanical resonant frequencies of the fundamental thickness and first lateral vibrational modes for increasing pillar aspect ratio in undamped 20% composite transducers. Therefore without the introduction of damping at either the front or rear face of the transducer, the composite would operate with two independent resonance mechanisms. This phenomenon has been predicted by FEA for the range of 20% composite transducers, with no mechanical damping attached, operating into an air load. Figure 5.10 illustrates the predicted receive sensitivity frequency spectrum for 20% composite transducers with aspect ratio of 0.162 and 0.303. Here, the distinct peaks in the spectra are associated

with the fundamental thickness and first lateral resonances. This trend was predicted for the variation in aspect ratio between 0.1 to 0.4. For the composites with aspect ratio 0.162 and 0.303, their respective -6dB bandwidths are 3.7%, centred around 1.1MHz, and 5.8%, centred around 1.88MHz. Consequently, these devices are not considered to possess adequate bandwidth for application as wideband air-coupled ultrasonic receivers. It should be noted that the results shown in this Figure are for ideal impulse excitation conditions at the transducer front face and hence does not include airborne attenuation. Also, it is interesting to note the second lateral resonance, at around 3MHz, in both the frequency spectra shown in Figure 5.10.

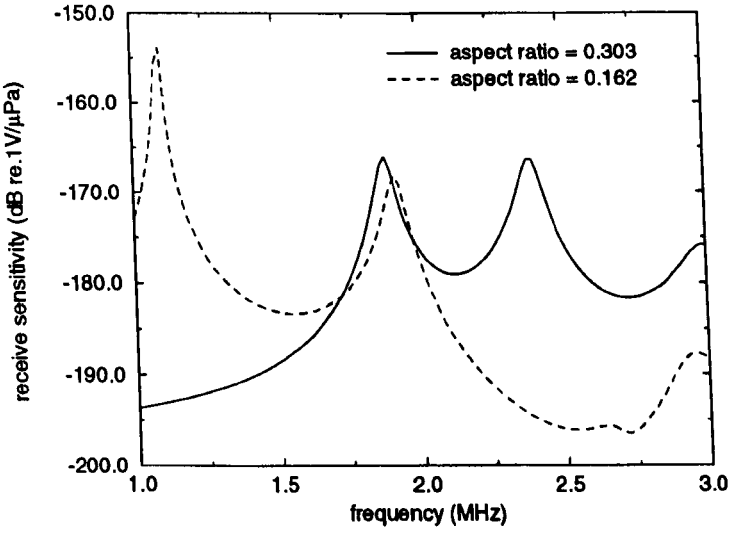

Figure 5.10 FEA predicted spectral content of the receive response for air-coupled 20% composite transducers with different aspect ratio

(b) Damped Composite Transducers

The FEA analysis was repeated with the addition of a perspex block to the transducer rear face. The increased damping of the transducer structure assists in coupling the two vibrational modes of interest together. The subsequent bandwidth and sensitivity variation are shown in Figure 5.11. The percentage bandwidth peaks, at 86%, for an aspect ratio of approximately 0.24, whereas the receive sensitivity is reduced by 3.7dB. This value compares favourably with the 9.4dB reduction in sensitivity, under 100% damping conditions, estimated by uni-dimensional modelling in Section 5.2.2(c). The influence of mode coupling for damped composite transducers was illustrated in Figure 5.6, where mechanical damping effectively brought both the fundamental thickness and

first lateral modes closer together. This phenomenon is manifest in the predicted higher bandwidth for the composite with an aspect ratio of 0.24, as shown in Figure 5.11.

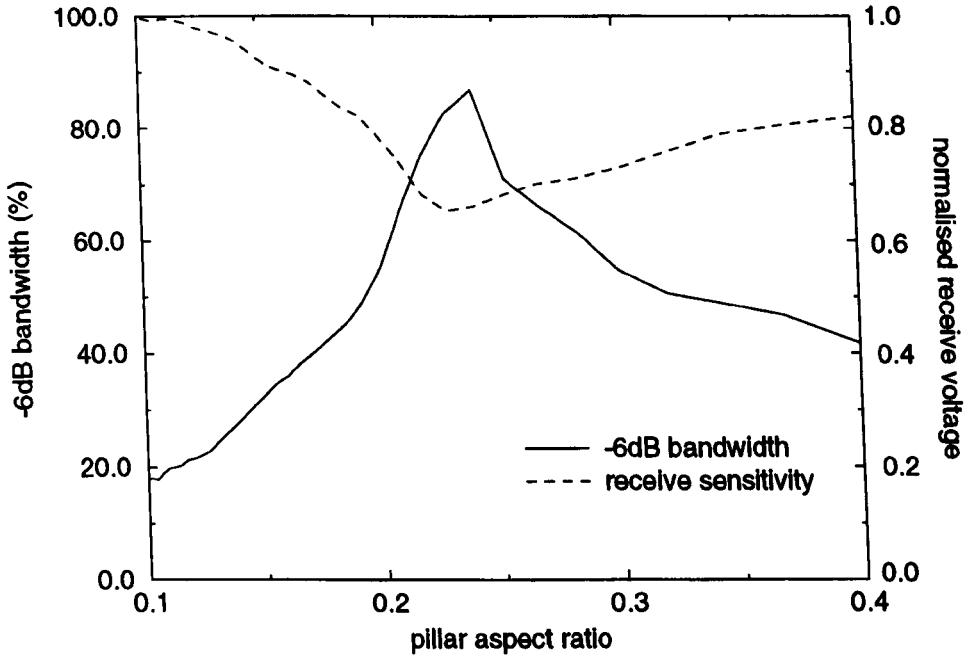

Figure 5.11 Bandwidth and sensitivity characteristics for 20% composite transducers, with varying aspect ratios, under ideal impulsive conditions

5.4.3 Manufacture of Laterally-Coupled Composite for Airborne Applications

(a) Construction of Air-Coupled Composite Receivers

A laterally-coupled composite receiver was constructed using the FEA predicted aspect ratio for maximum bandwidth (0.24) described in the previous Section. To complement the evaluation of this device, a thickness-mode composite was also manufactured. Both transducers were manufactured from a common block of PZT5A and potted from the same mix of CIBA-GEIGY CY1300/HY1301 hard set epoxy. In order to measure the transducer electromechanical coupling efficiency, k_t, mechanical resonances, f_n and f_{lat}, and the device dilation quality, Q_{dil}, and maintain consistency with the results presented in Section 5.3.4(a), the composites have been evaluated prior to the application of mechanical damping to the rear face. Details of the measured transducer properties are presented in Table 5.2. Although the thickness of each device has been maintained constant, the fundamental thickness mechanical resonances are different for each composite. This is a consequence of the coupling between the fundamental and lateral

resonances in the composite with an aspect ratio of 0.244. As anticipated, the electromechanical coupling coefficient for the laterally-coupled composite is down compared to the uni-modal device. Figure 5.12 demonstrates the various resonances within each composite transducer.

composite	thickness	aspect ratio	resonance	mechanical resonance	k_t
thickness-mode	0.9mm	0.108	thickness	1.97MHz	0.525
laterally-coupled	0.9mm	0.244	thickness	1.63MHz	0.386
			lateral	2.11MHz	0.432

Table 5.2 Properties for manufactured 20% PTZ5A/hard set composite receivers

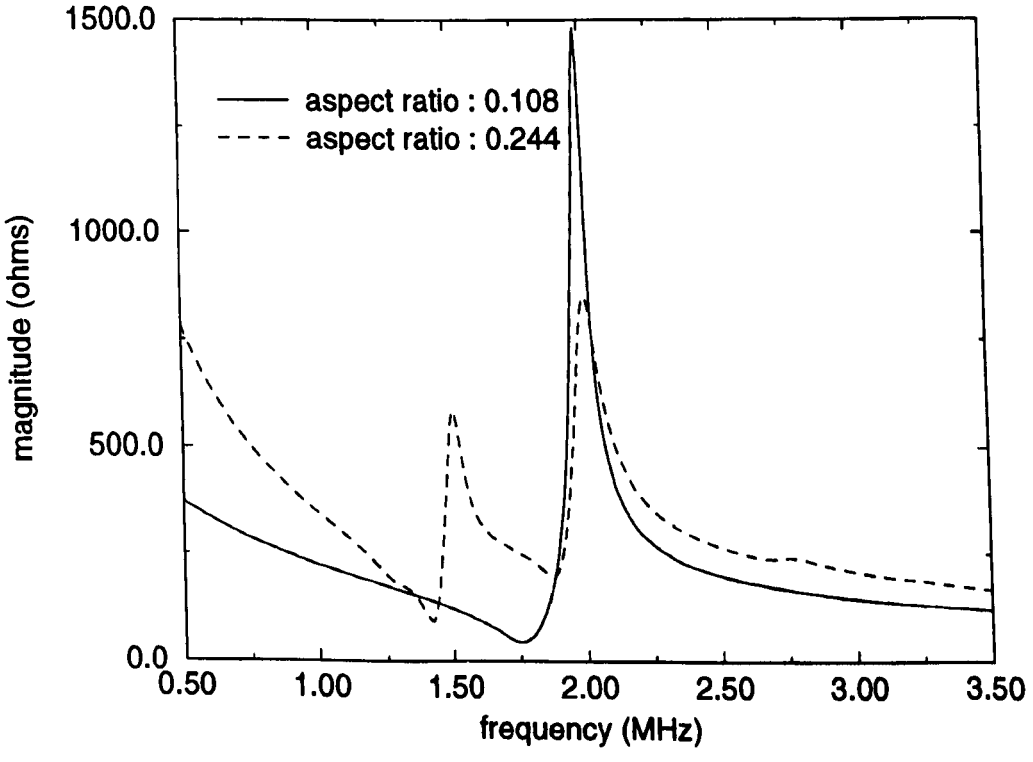

Figure 5.12 Impedance profiles for manufactured 20% composite transducers

(b) Surface Displacement Profiles

It is interesting to compare the surface displacement profiles for the two composite transducers described in Table 5.2. A Polytec single point interferometer (OFV-302) and displacement decoder (OVD-30) have been used to acquire out-of-plane displacement from the surface of the transducers. The focussed spot size from the interferometer was 25μm. The precision manipulator, described in Section 2.4, was utilised to scan the transducer in front of the laser interferometer. The composite transducer with an aspect ratio of 0.108 has a 97μm pillar width and a step size of 30μm was considered adequate to scan the transducer microstructure. These experimentally acquired plots are illustrated in Figures 5.13(a) and 5.13(b), for the 0.108 and 0.244 aspect ratio devices respectively, where the lighter shading indicates a higher surface displacement. In Figure 5.13(a), the attachment to the front face electrode can be seen in the top right hand corner. There is also some fluctuation in the measured data to the left of this point. However, the transducer has a good overall uniformity, which is manifest in the measured dilation quality of 0.79. In fact, it is difficult to differentiate between the piezoceramic square pillars and the epoxy filler material. For the higher aspect ratio composite, shown in Figure 5.13(b), a different response has been acquired. Here, the matrix of piezoceramic square pillars is clearly evident, although adjacent pillars have different displacement values. In addition, the polymer filler material has a lower displacement value, indicated by the darker shading, compared to the ceramic pillars. Clearly, the device is not acting as a homogeneous medium and consequently, the measured dilation quality for this transducer was 0.52.

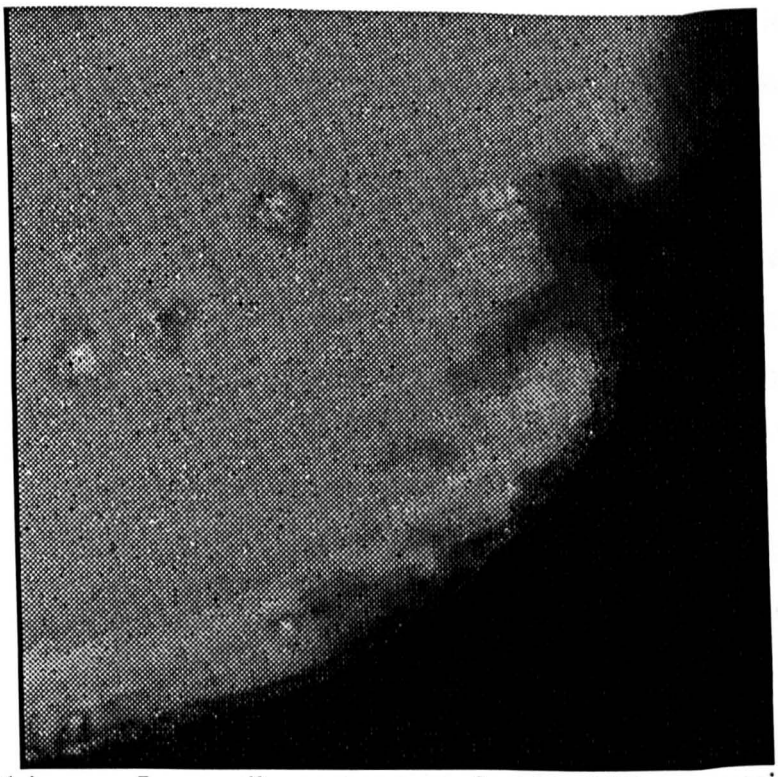

Figure 5.13(a) Laser vibrometer scan for the 20% composite transducer (aspect ratio of 0.108)

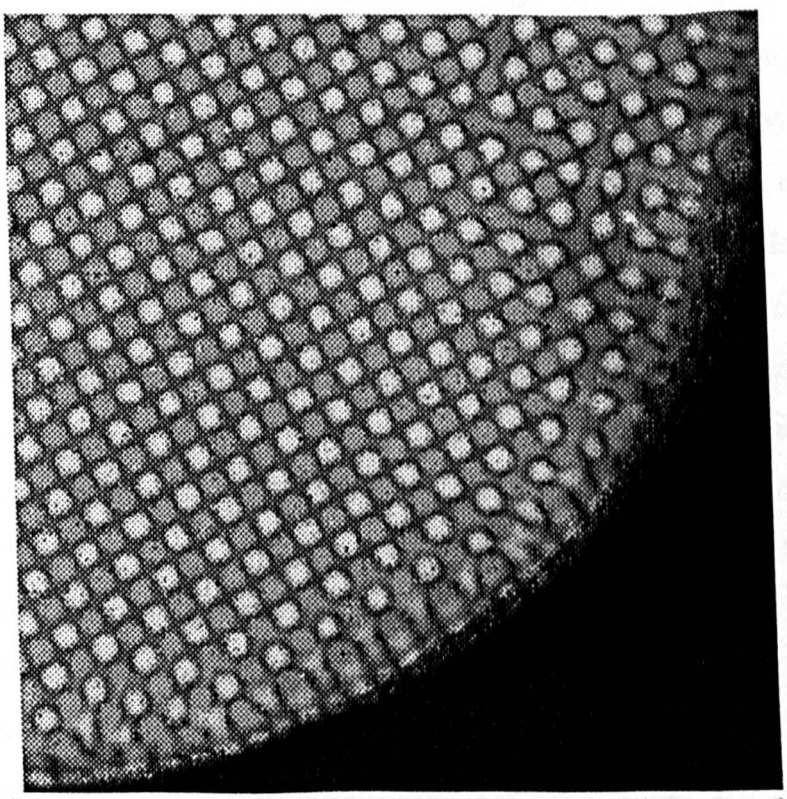

Figure 5.13(b) Laser vibrometer scan for the 20% composite transducer (aspect ratio of 0.244)

(c) Experimental Evaluation of Laterally-Coupled Composite Receiver under Air Load

The receive performance of the laterally-coupled composite was evaluated using the thickness mode composite, described in Table 5.2, and an electrostatic transducer. Comparison between the two composite transducers permitted measurement of the bandwidth improvement of the laterally-coupled receiver. The electrostatic device will facilitate evaluation with a sensitive and wideband air-coupled transducer, as described in Chapter 3. The electrostatic transducer utilised was constructed from 2.5μm Mylar film stretched across a polished steel backplate. This device was chosen due to its inherently large bandwidth and further characterisation details can be found in Chapter 3. A shaped perspex backing block was bonded onto the rear face of the two composite transducers, thus the 0.244 aspect ratio composite construction corresponds to the FEA prediction from Section 5.4.2(b). As described in Section 5.3.4(a), a PVDF transmitter, driven by a Panametrics pulser/receiver unit, was utilised to provide a wideband pressure wavelet at the front face of the air-coupled receivers. The receive sensitivity and bandwidth of the transducers were acquired at an air separation of 20mm.

The receive temporal responses acquired by the three transducers are illustrated in Figure 5.14. The laterally-coupled composite, Figure 5.14(a), has realised an excellent bandwidth in the from of an almost unipolar response. This signal is in excellent agreement with Figure 3.10, which illustrated the experimentally acquired pitch-catch response for an air-coupled PVDF transducer pair. The peak-to-peak received signal level from the thickness drive composite is lower than detected by the laterally-coupled composite. This is a consequence of the realisable bandwidth of the incident pressure wavelet, where the influence of airborne attenuation has reduced the magnitude of frequency components above approximately 1.5MHz. Moreover, the thickness drive composite demonstrates a reduced bandwidth due to the ringing evident in the received signal. The receive sensitivity for the electrostatic transducer, shown in Figure 5.14(c), has outperformed both composite transducers. Reasonable bandwidth is demonstrated, but the acquired pulse is not as compact as the laterally-coupled response.

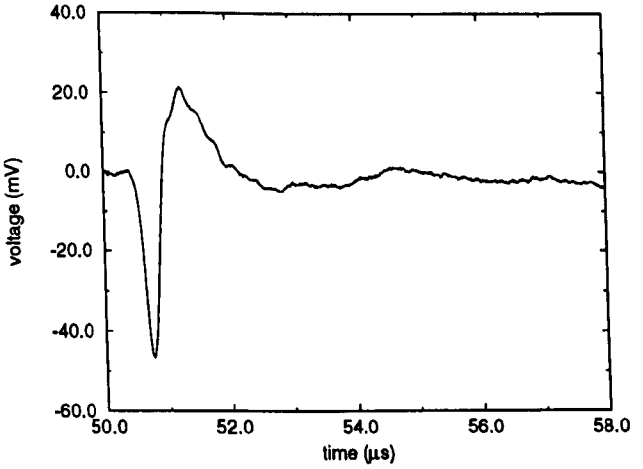

(a) Laterally-coupled composite

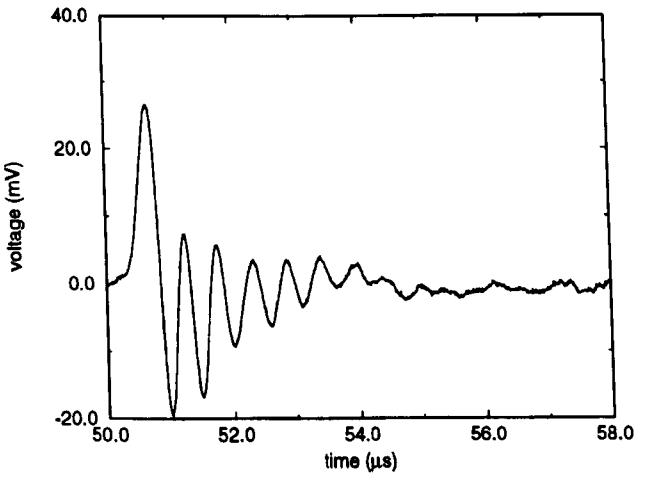

(b) Thickness mode composite

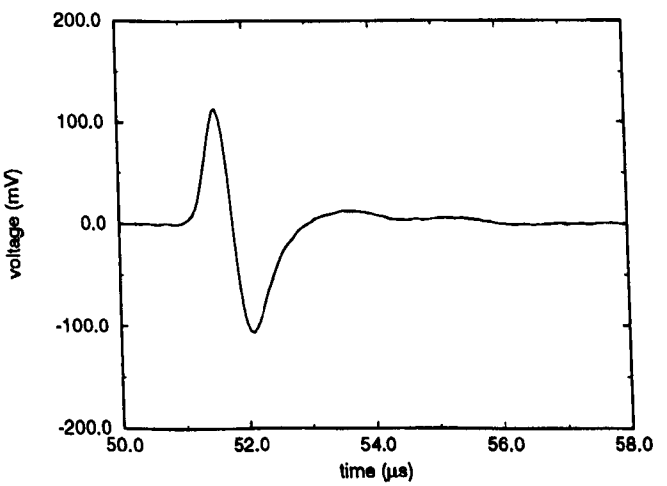

(c) 2.5μm Mylar electrostatic transducer, with polished steel backplate

Figure 5.14 Receive signals acquired by air-coupled wideband transducers

In order to fully appreciate the bandwidth for each of these detectors, Figure 5.15 presents a comparison of the receive spectral characteristics calculated from the signals shown in Figure 5.14. The results shown in this Figure have been normalised in order to facilitate logical comparison of the bandwidth characteristics. The influence of airborne attenuation is evident in the lack of high frequency components above 2.5MHz. The laterally-coupled composite transducer has a better -6dB bandwidth characteristic of 1.5MHz, centred around 1.15MHz, compared to 825kHz, centred around 500kHz, for the electrostatic transducer. The resonant behaviour of the thickness drive composite is illustrated in the spectral peak at approximately 1.8MHz. It should be noted that although the finite element analysis, presented in Figure 5.11, illustrated a percentage bandwidth of 86%, this was evaluated under ideal impulsive conditions. Hence, the frequency spectra for the predicted response was centred around approximately 2MHz. Therefore, the absolute frequency bandwidths are in good agreement.

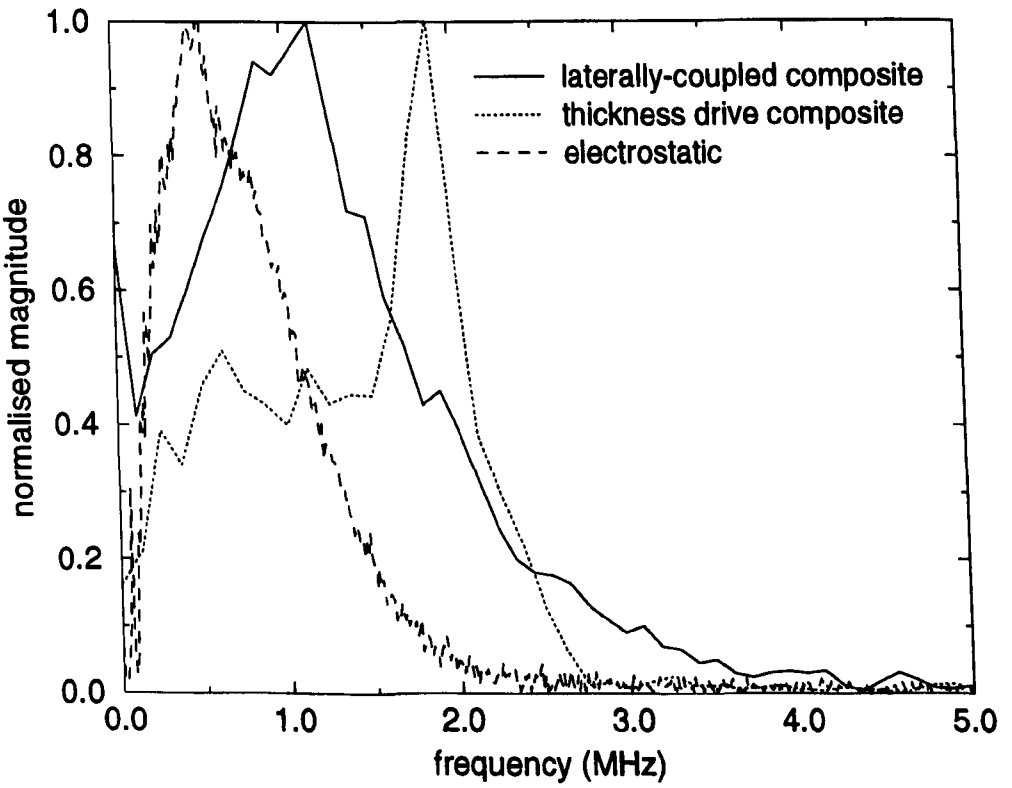

Figure 5.15 Comparison of the spectral characteristics for the detectors under investigation

5.5 LATERALLY-COUPLED PIEZOCOMPOSITE TRANSMITTER

For completeness, the transmit performance of a laterally-coupled composite transducer was investigated using several of the damped 20% devices described earlier in this Chapter. The Panametrics pulser/receiver unit was employed as wideband excitation for the transducers and a standard hydrophone, connected directly to an oscilloscope, was used to detect the generated ultrasonic signals. The experimentation was conducted under water loading.

Finite element modelling was used to investigate the transmit performance of 20% ceramic volume fraction piezocomposites as the pillar aspect ratio is varied between 0.1 and 0.4. The transducer -6dB bandwidth and sensitivity were predicted and are illustrated in Figure 5.16. The modelling has predicted a peak in bandwidth, at an aspect ratio of 0.21, although the subsequent reduction in transducer sensitivity is extremely critical. These trends have also been observed in the experimentally acquired data and, in fact, it was impossible to detect any signal from the 0.367 aspect ratio composite device. For the 0.196 aspect ratio composite, the experimentally measured bandwidth was 86%, around a centre frequency of 1.25MHz, although the received peak-to-peak voltage was approximately 10mV. The temporal and spectral responses for this composite transducer are presented in Figures 5.17(a) and 5.17(b). The low SNR associated with this signal is comparable in magnitude to similar experiments described in Section 3.3.2(a), specifically Figure 3.3(d), using a wideband PVDF transmitter. Using an identical reception arrangement, the peak-to-peak received voltage measured for the PVDF transducer was approximately 15mV. As described in Section 3.4.2, experimental confirmation of the air-coupled PVDF transmit response was extremely difficult, due to the low sensitivity of both the PVDF device and the membrane hydrophone in air. Consequently, the low SNR associated with the 0.196 aspect ratio composite device, under water load, will constitute a problem for transducer operation in air. This is compounded by the modelling predictions from Chapter 4, where the 20% composite transducer is shown to be a poor transmitter of ultrasound for operation into an air load. Consequently, the air-coupled transmit performance of the laterally-coupled composite

proved impossible to detect.

Therefore, although finite element analysis predicts an increase in bandwidth as a result of lateral coupling within a 20% composite transducer, the subsequent reduction in transducer sensitivity ensures that this bandwidth enhancement technique cannot be utilised for the range of 20% composites evaluated in this study.

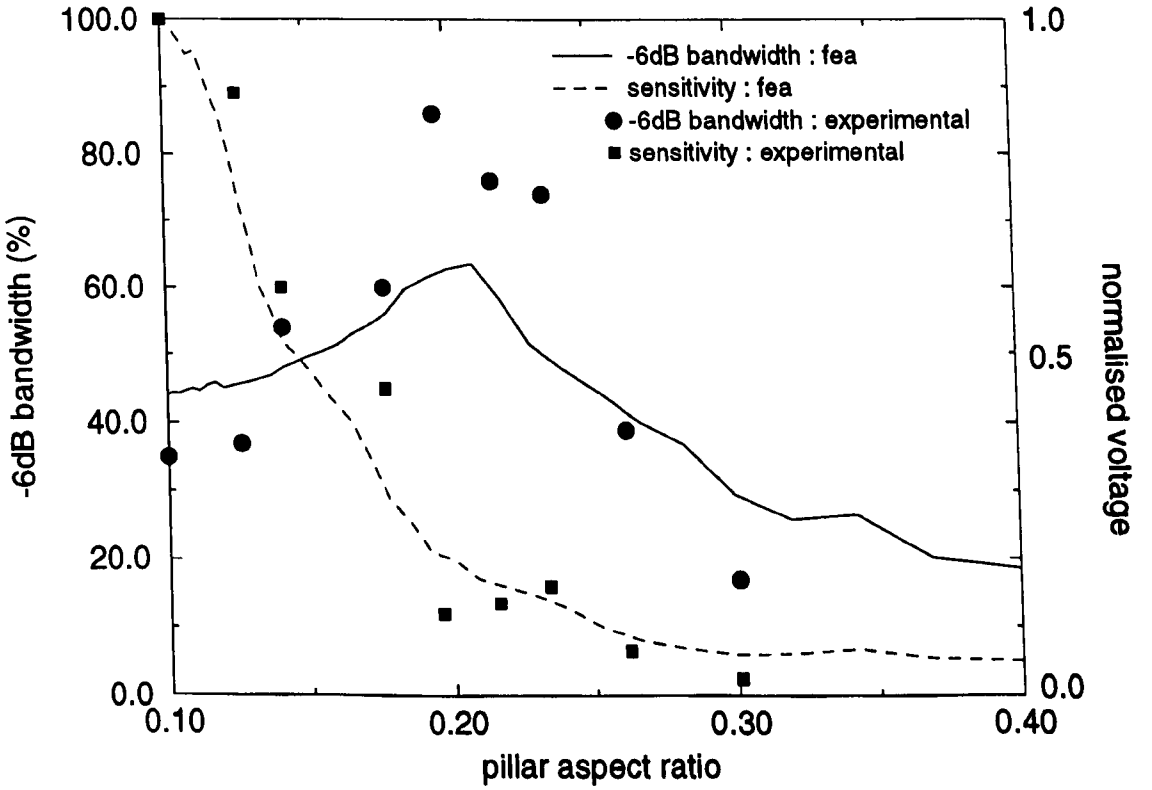

Figure 5.16 Bandwidth and sensitivity characteristics for 20% damped composite transducers, operating in transmission, under water load

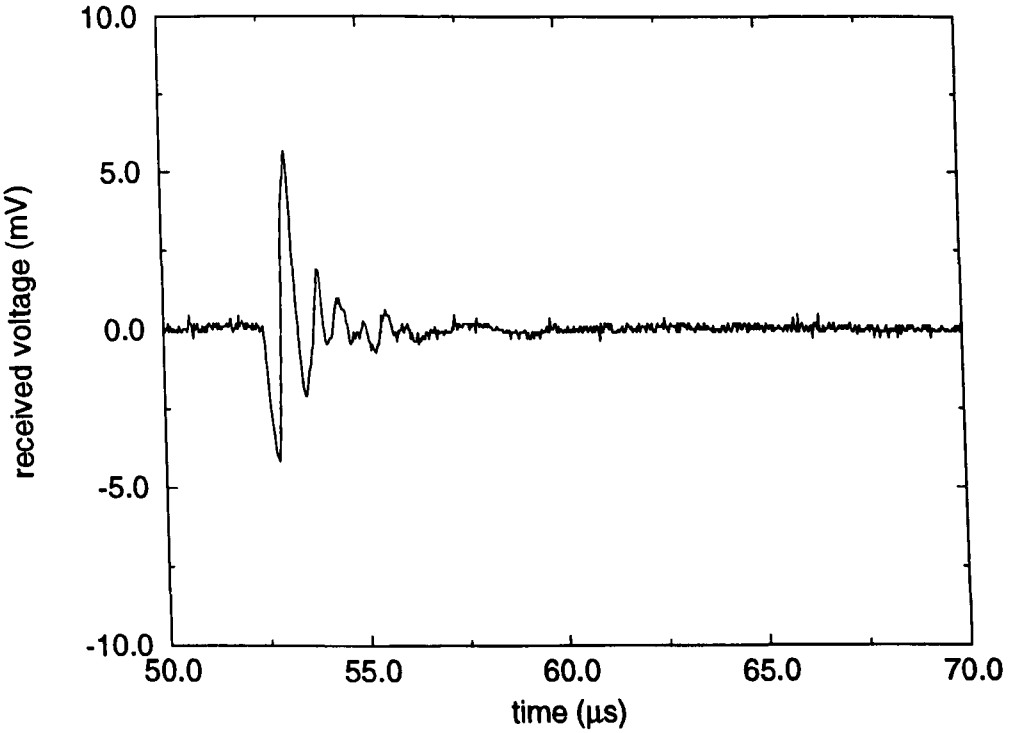

Figure 5.17(a) Signal detected from laterally coupled 20% composite transmitter, aspect ratio of 0.196

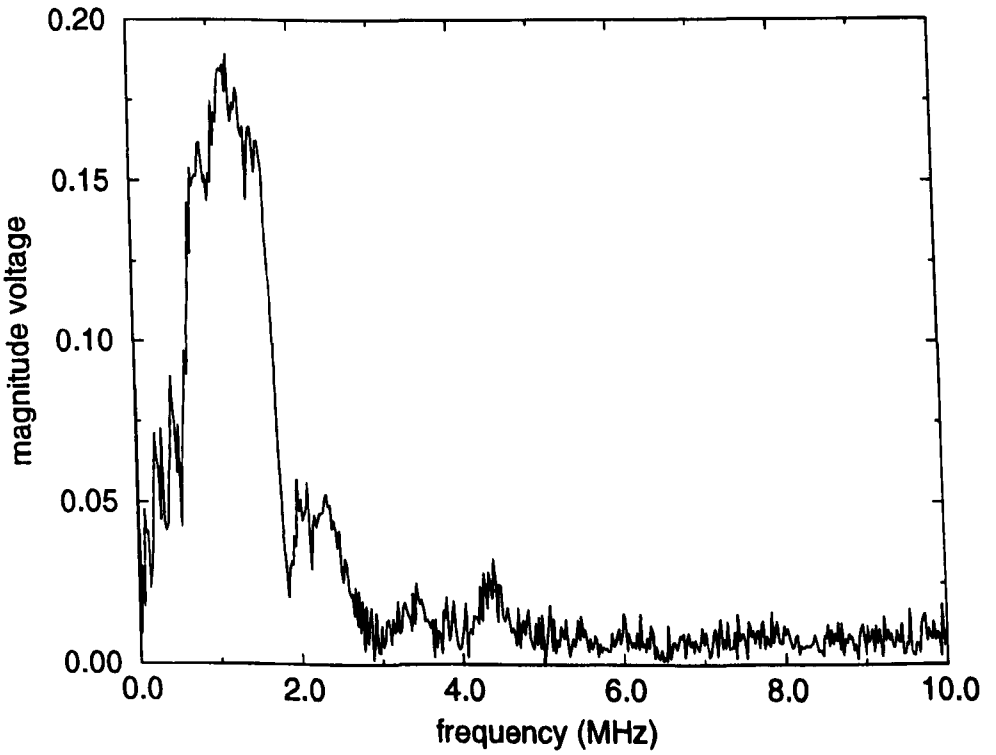

Figure 5.17(b) Spectral response of signal shown in Figure 5.17(a)

5.6 CONCLUSIONS

This Chapter has demonstrated a novel technique to improve the bandwidth for 1-3 connectivity piezocomposite transducers, operating in reception. Strong coupling between the fundamental thickness and first lateral resonances, in a damped composite device, effectively extends the transducer bandwidth characteristic. Finite element analysis has been utilised to investigate this effect, where reasonable correlation was demonstrated with experimentally acquired data, under water load conditions. It is important to note that the maximum bandwidth was obtained in the region of maximum coupling between the fundamental thickness and first lateral resonances and when the electromechanical coupling efficient of both resonant modes are equally strong. In addition, damping applied to the rear face of the transducer enhances the coupling between these two resonant modes. The modelling techniques were then extended to evaluate air-coupled performance and subsequently, a design for a wideband air-coupled composite receiver was proposed.

In order to attain a high bandwidth performance from a piezocomposite transducer, reverberation within the device must be minimised. Conventionally, this is achieved by attaching an appropriate damping medium to the rear face of the device. For the transducers employed in this study, a perspex backing medium was utilised and shown to increase the coupling between the fundamental thickness and first lateral modes. Although, the acoustic mismatch between the piezocomposite transducer and the perspex block will only partially reduce the reverberation and consequently, the characteristic time response should reverberate for several cycles. In fact, the minimum transducer bandwidth is established by the acoustic match between the transducer and the backing medium. Therefore, in order to achieve the bandwidth response demonstrated by the laterally-coupled composite transducer, a secondary effect must take place. As stated earlier, the point of maximum bandwidth corresponds to the region where both resonant modes are equally strong. Consequently, at this point the charge generated by the lateral mode could cancel out the charge due to the thickness-drive reverberation. This hypothesis holds true for the results presented in this Chapter for the range of 20% 1-3

connectivity piezocomposite transducer evaluated. This concept requires a more rigorous investigation to fully evaluate the physical interaction between the thickness and lateral resonances. Unfortunately, the current computing facilities and ANSYS finite element software package, Version 5.0 Vol III was used throughout this Thesis, cannot support this analysis. It is envisaged that this investigation should be undertaken in the near future.

The proposed design for a wideband air-coupled composite receiver was constructed and the bandwidth improvement experimentally verified. This device exhibits a very good -6dB bandwidth characteristic, when compared with both a thickness drive composite and an electrostatic device. Although, the transducer receive sensitivity is approximately a factor of three down on the electrostatic transducer sensitivity. In fact, the detected unipolar response compares very favourably with the predicted pressure wavelet, from a PVDF transmitter, incident of the receiver front face, as described in Chapter 3. Consequently, a innovative method to improve system resolution has been demonstrated which could find application as a wideband air-coupled receiver to complement the high resolution afforded by laser generated ultrasound. The practical aspects of such a system will be described in Chapter 6.

CHAPTER 6

THROUGH AIR APPLICATIONS FOR 1-3 PIEZOCOMPOSITES

ABSTRACT

This Chapter describes three examples of NDE systems to which air-coupled 1-3 connectivity piezocomposite transducers have been applied. The modelling techniques described earlier in this Thesis have been used in the design for each of these NDE systems. A pulsed laser has been used to generate ultrasonic transients in samples of metal and fibre-reinforced polymer composite material. These have been detected using air-coupled 1-3 connectivity piezocomposite transducers. Such a non-contact transduction system was used for detection of longitudinal waves in bulk material, Rayleigh waves at solid surfaces and Lamb waves in thin plates. This system can also be used to image defects in polymeric materials, and examples are given of the detection of defects in fibre-reinforced polymer composites. Within the Ultrasonics Research Group at Strathclyde, a combination of piezocomposite transducers and careful design of the receiving electronics has resulted in a 103dB improvement in SNR compared to a commercial pulser/receiver system. These techniques have been utilised in two rapid scanning system applications. An air-coupled composite transduction system has been utilised for the generation and detection of Lamb waves. Through which, real-time images of defects in both metallic and carbon-fibre plates have been produced. The second application is a prototype air-coupled NDE system to investigate through transmission response for a variety of composite materials. This system has successfully detected 9 PTFE inclusions, of various shape and dimensions, in a 3.7mm thick composite plate.

6.1 Air-Coupled Piezoelectric Detection of Laser Generated Ultrasound

6.1.1 Introduction

The use of pulsed lasers for ultrasonic generation in solid materials has been of recent interest for nondestructive evaluation [29], but a completely non-contacting ultrasonic system also requires a suitable detector. As described earlier in Chapter 2, several technologies have been incorporated as reception devices with this optical source. The most common method is to use some form of optical device [31,32], but an all-optical system needs a sample with a reasonably good reflectivity. Two non-contact methods which could be used if the sample is electrically conducting are capacitance transducers [127], which are most useful as a calibration device, and the electromagnetic acoustic transducer (EMAT) [63]. Recently, both electrostatic devices [48] and piezoelectric designs [66-68] have been utilised to improve both system sensitivity and bandwidth.

A combination of expertise in pulsed laser generation at Warwick University and piezocomposite detectors, designed through the modelling approaches described in Chapters 4 and 5, has provided a distinctive NDE transduction system. The hybrid system comprises essentially a wideband point source coupled with an inherently narrowband receiver of finite aperture. The design goal was to create a reception device of sufficient sensitivity and bandwidth to complement the high resolution afforded by laser generation. Initially, standard air-coupled 1-3 connectivity piezocomposite transducers were used and additional signal processing has been applied to the resultant waveforms to improve system resolution. The wideband composite designs, described in Chapter 5, have also been evaluated in this hybrid system and several NDE scans are presented to demonstrate successful imaging in polymer-based materials.

This collaboration required a significant portion of the work, described in this Section, to be performed at Warwick University. The author is most grateful to Professor D.A. Hutchins and W.M.D.Wright for the experimental data and the resultant images which are presented in this Section.

6.1.2 Experimental Environment

The apparatus used to perform through-transmission waveform capture and imaging is shown schematically in Figure 6.1. Two laser sources were available, either a Q-switched Nd:YAG laser, providing 4ns pulses of 120mJ in the near infra-red, or a pulsed CO_2 laser operating in the far infra-red. The pulses were directed onto the sample, and various optical elements were used to adjust the optical power density to give the desired generation conditions. The samples were either of aluminium (the reference material) or various fibre-reinforced polymer composites. Signals from the detector were amplified using a Cooknell CA6 charge amplifier, digitised, and transferred to a PC for storage and analysis. To detect Rayleigh and Lamb waves, which radiate or 'leak' into air, the air-coupled transducer was displaced from the laser source and rotated to vary the angle between the transducer and the surface.

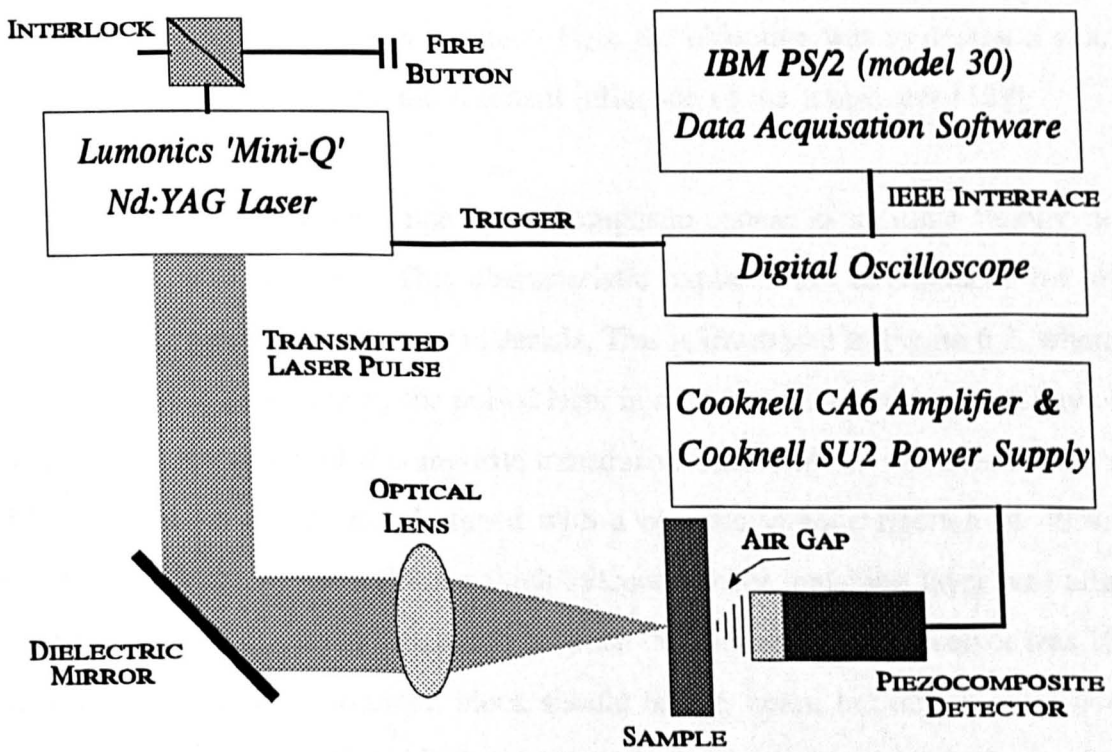

Figure 6.1 Experimental environment for an ultrasonic laser generation/piezoelectric detection system

To permit evaluation of the actual ultrasonic signal generated by the incident laser beam in the sample, a capacitive transducer was placed in contact with the surface of the sample to provide calibration waveforms [127]. The capacitive device, with a bandwidth of 10MHz, consisted of an insulated ball-bearing, to which a 100V d.c. bias was applied. Displacement in the block produced a charge from the transducer, which was fed into a charge amplifier to generate a voltage output.

6.1.3 Application of Standard Piezocomposite Detectors

(a) Introduction

The standard piezocomposite is a resonant device and although extremely efficient for air-coupled operation, the bandwidth is often insufficient to resolve target structural characteristics. This difficulty is further emphasised when used in conjunction with the wideband laser source. Consequently, a range of deconvolution algorithms were implemented, within the Ultrasonics Group at Strathclyde University [128], and assessed for operation with the through air system. Here the objective was to design a suitable deconvolution filter to remove the resonant influence of the transducer [129].

Reverberations within an undamped piezocomposite appear as multiple ringing in the transducer impulse response. This characteristic explains the requirement for signal processing when evaluating thinner materials. This is illustrated in Figure 6.2, where the ultrasonic signals generated by the pulsed laser in a 19.8mm aluminium block have been detected using an air-coupled composite transducer. This detector was constructed from PZT5A / hard set epoxy and designed with a ceramic volume fraction of 40%. The device was unbacked, but a 0.4mm thick silicone rubber matching layer was attached to the front face. The airgap separation between the sample and the receiver was 10mm. The reflections in the aluminium block should be 6μs apart, but due to pulse overlap, scant information regarding block structure is apparent. A reference wavelet was acquired by the contact capacitive device and is presented in Figure 6.3. Within the aluminium block, multiple reflections of both the longitudinal (L, 3L and 5L) and shear (S, 3S and 5S) components may be recognised clearly.

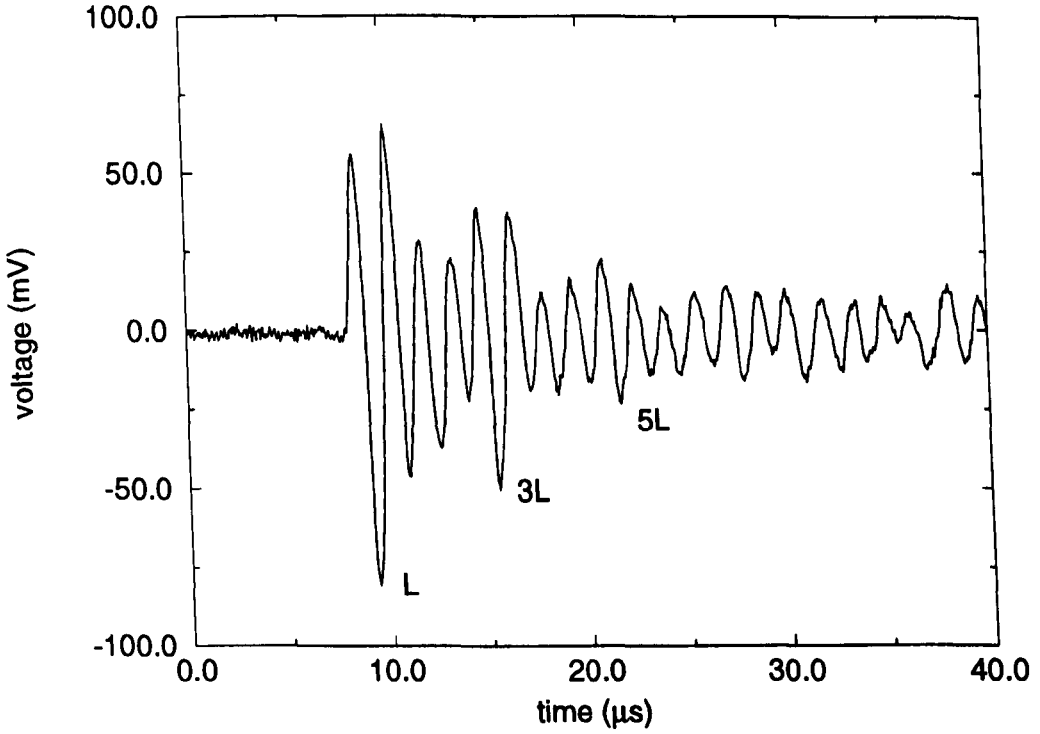

Figure 6.2 Signal received by a resonant 40% composite transducer through 19.8mm aluminium block

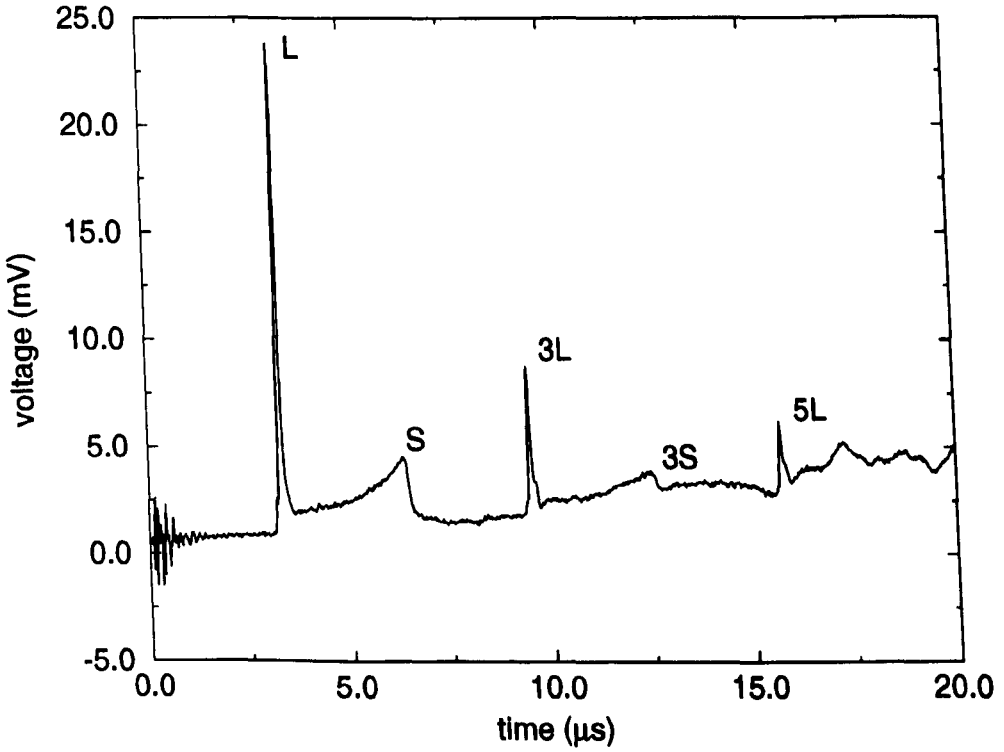

Figure 6.3 Signal received by a capacitive device after laser excitation of an 19.8mm thick aluminium block

In an attempt to identify reflections within the aluminium block, post processing in the form of deconvolution was applied to the data. Adaptive and non-adaptive methods were applied to both simulated and experimental data sets with varying degrees of success. This Chapter will concentrate on the performance of two algorithms : Modified Least Means Squared [130] and Minimum Entropy [131] techniques.

It is well documented that the majority of deconvolution processes requires both the data to exhibit minimum delay characteristics and the distortion wavelet to be spatially invariant and truly representative of the system transfer function [129]. Appendix E explains the signal waveform shape associated with minimum delay characteristics. In ultrasonic applications, this may be achieved in practice through a system consisting of a planar transmission device, for example an apodised piezoceramic transducer [132] and a wideband point source receiver. However, the present configuration incorporates an ultrasonic point source coupled with a finite aperture receiver. Any measured impulse response is thus strongly dependent on the relative spatial configuration, which proved difficult to maintain constant. Moreover, it should be noted that firstly, the data received from the system is of mixed delay characteristics and secondly, the detected waveform shape varies as a function of the thickness of the aluminium block under examination. This later problem is caused by diffraction and spherical wave transmission within the aluminium block. Thus the signal evolves as it propagates through the sample and the spatial invariance condition is no longer valid.

The adaptive technique selected was the 1D Modified Least Means Squared (MLMS) algorithm, which is based on the Adaptive Line Enhancer (ALE) configuration [130]. This approach utilised an autoregressive model, which generates a signal estimate sequence and a weight (tapped delay filter coefficients) sequence to produce an error sequence, i.e. the deconvolved output. This technique permits the signal processing algorithms to follow the evolution of the waveform. The algorithm is relatively straightforward to use and requires only precise adjustment of one parameter (the convergence, μ). The main disadvantage with the method is that the algorithm prefers minimum delay characteristics, which the waveform in question does not exhibit. Thus

the resulting output has a suboptimal resolution capacity.

The nonadaptive technique chosen was the Minimum Entropy Deconvolution (MED) algorithm, proposed by Wiggins [131]. This is an iterative process, which is computationally excessive and consequently very slow. The MED algorithm constructs an inverse filter which will produce the simplest deconvolved signal in accordance with the real data, that is, as a signal constructed from a number of spikes (delta functions) separated by near-zero terms. The technique assumes a non-Gaussian reflectivity function and utilises an optimisation technique to recover both the amplitude and phase information. For this reason the algorithm is more robust to non-minimum phase wavelets, when compared to most of the classical deconvolution algorithms. Although, the approach does require the spatial invariance assumption to obtain the best resolution along the wavelet. One significant advantage of the MED approach is that in addition to providing signal compression, the noise components are reduced. As the MED operator maximises the spikiness of the output traces, it selectively suppresses frequency bands over which the ratio of coherent signal-to-random noise is lowest and thereby emphasizes those bands in which coherent signals dominate.

Further details of the implementation of both of these deconvolution algorithms can be found in Appendix E.

(b) Simulation of Hybrid System

In order to assess the performance of the deconvolution algorithms, the response of the hybrid system was simulated. With reference to Figure 6.4, this system comprises of five main components : ultrasonic wave generation and propagation in the sample, $G(\omega)$; both reverberation within the sample and the transmission characteristic at the sample/air interface $F(\omega)$; influence of airborne attenuation, $A(\omega)$; receive transducer response, $H(\omega)$; and receive amplifier noise figure, $N(\omega)$.

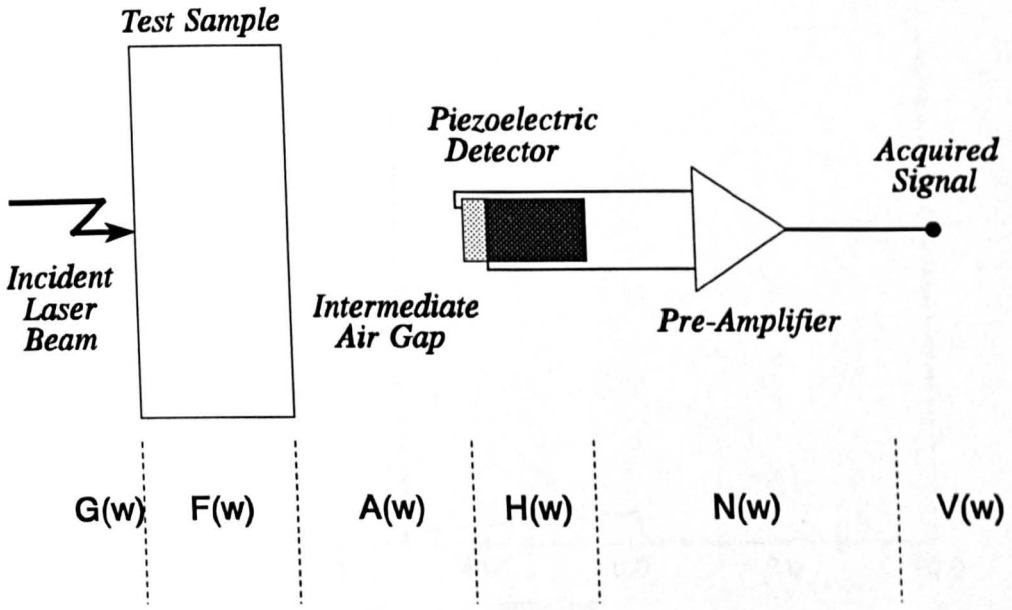

Figure 6.4 Simulation blocks for laser generated and remote piezoelectrically detected ultrasound

An expression for the received voltage, calculated in the frequency domain, is described by Equation 6.1.

$$V(\omega) = G(\omega)\, F(\omega)\, A(\omega)\, H(\omega)\, N(\omega) \qquad \textbf{(6.1)}$$

The incident laser beam generates longitudinal and shear components within the sample [30]. Software has been written by D.A. Hutchins at Warwick University, to compute the displacement waveform in a solid half-space, for a disc shaped source. To determine both the longitudinal and shear components at an observation point in the solid, the programme requires the laser source radius, the type of force acting at the sample front face (the ablation technique used in these experiments was simulated as a normal force), observation distance in the thickness direction and both the longitudinal and shear wave velocities within the solid. The predicted waveform at the rear face of a 19.8mm thick aluminium sample is illustrated in Figure 6.5, where both the longitudinal (L) and shear (S) components can be easily identified.

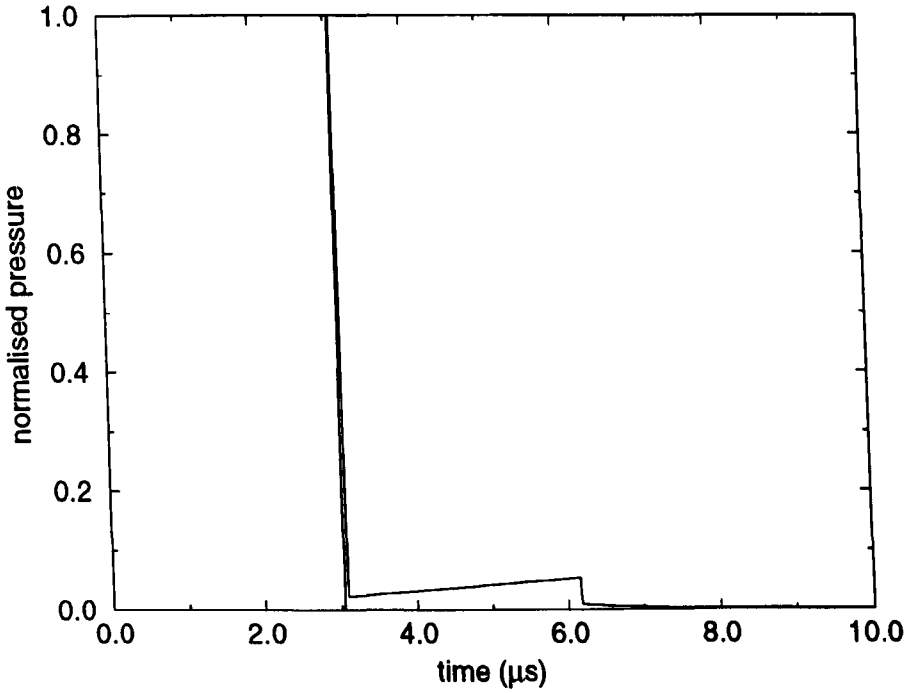

Figure 6.5 Simulated longitudinal and shear wave component in a 19.8mm thick aluminium sample

The velocity of the longitudinal component is greater than twice the shear velocity in aluminium (v_l=6420ms^{-1}, v_s=3040ms^{-1}) [115]. This represents an approximate transit time, t, of 3μs and 6.5μs for the longitudinal and shear waves within a 19.8mm aluminium block. Intuitively, the next signal observed at the rear face of the sample should be the first reflected longitudinal wave. This wave should arrive 6μs after the initial longitudinal component (t=9μs). Due to the difference in shear and longitudinal acoustic velocities, the second reflection of the longitudinal component (t=15μs) should arrive before the first reflected shear wave (t=19.5μs). With reference to the calibration signal, shown in Figure 6.3, it can be observed that a shear reflection occurs approximately at t=12.5μs. This can be explained through mode conversion of the initial shear wave component mode into a longitudinal component at the rear face. Hence, there is no longer a shear component after the first transit time. Effectively, a longitudinal waveform, with the shape shown in Figure 6.5, reflects within the sample with the longitudinal velocity.

A graphical representation of the reflectivity process is illustrated in Figure 6.6. Here, the air media is represented by areas 1 and 3 and the sample by area 2. T_T is the transit time for the waves of force to cross the sample. R_F and R_B are the reflection coefficients for the ultrasonic waves at the front and rear faces of the sample respectively. These coefficients are calculated from the specific acoustic impedance of air, Z_{air}, and the specific acoustic impedance of the sample, Z_A, as shown in Equation 6.2.

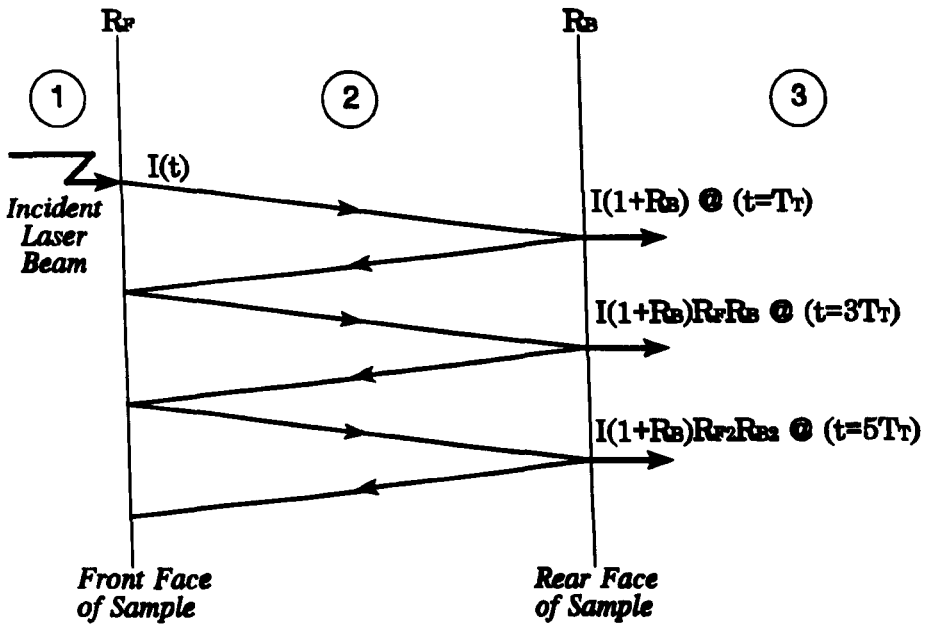

Figure 6.6 Ultrasonic wave generation and propagation within the sample

$$R_F = R_B = \frac{Z_A - Z_{air}}{Z_A + Z_{air}} \tag{6.2}$$

Waves of force entering medium 3 can be represented by the summation of each individual component at times $t = T_T, 3T_T, 5T_T$, etc. This is shown in Equation 6.3.

$$F(t) = I(1+R_B)\,[@t=T_T] + I(1+R_B)R_F R_B\,[@t=3T_T] + I(1+R_B)R_F^2 R_B^2\,[@t=5T_T] \tag{6.3}$$

The influence of loss within the sample can be incorporated through Equation 6.4, where, L is the sample thickness and α is the longitudinal loss factor in the sample.

$$e^{-\alpha L} \tag{6.4}$$

Equation 6.3 can be transformed into the Laplace Domain, including the influence of attenuation within the sample described by Equation 6.4, to yield the solution shown in Equation 6.5.

$$F(s) = I(1+R_B)e^{-sT_\tau}e^{-\alpha L}\sum_{n=0}^{\infty}(R_F R_B)^n e^{-2nsT_\tau}e^{-2n\alpha L} \tag{6.5}$$

where s is the Laplace Complex Variable.

Taking the sum to infinity for this geometric progression and noting that reflection coefficients are equal at both faces, now represented by R, the solution can be expressed as in Equation 6.6.

$$F(s) = \frac{G(s)(1+R)\,e^{-sT_\tau}e^{-\alpha L}}{1-R^2e^{-2sT_\tau}e^{-2\alpha L}} \tag{6.6}$$

Using this reflectivity process, a simulation of the transmitted ultrasonic waveform into the air load has been calculated for the 19.8mm aluminium sample. This predicted response, is illustrated in Figure 6.7, where good correlation with the experimentally acquired reference wavelet, shown in Figure 6.3, is evident.

Transfer functions can be obtained for the detection stages of this system. The influence of airborne attenuation has been discussed in Chapter 3 and a unique solution can be calculated for a particular experimental environment from the airgap separation and atmospheric conditions. The piezoelectric detector is represented by its receive impulse response, which can be calculated through the modelling techniques discussed in Chapter 4. Finally, the transfer function for the amplification stage can be determined from relevant data sheets. Hence, the predicted response from this hybrid system, including the introduction of noise, has been determined and is illustrated in Figure 6.8. Reasonable correlation between the experimentally acquired system response, shown in Figure 6.2, can be observed.

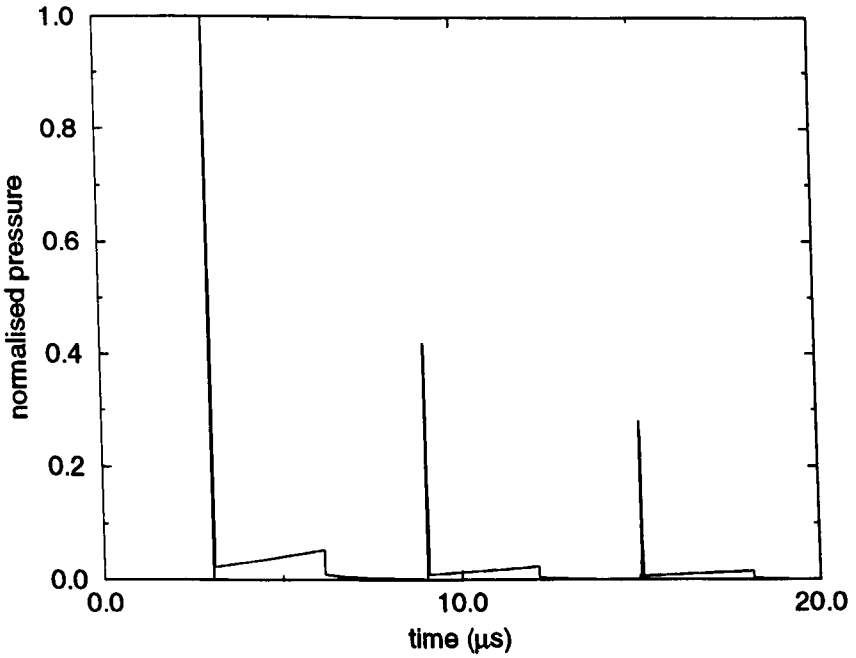

Figure 6.7 Simulated reflectivity function for laser generated ultrasound in a 19.8mm thick aluminium sample

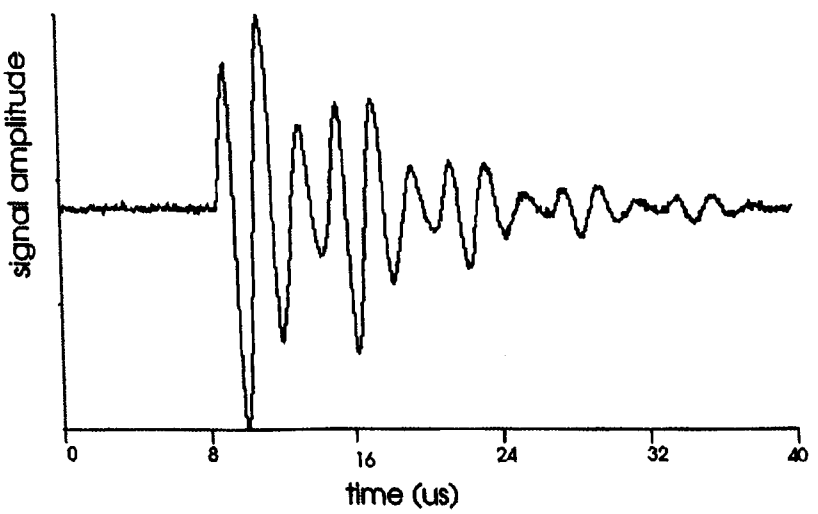

Figure 6.8 Predicted response from the hybrid system, transmitting through a 19.8mm thick aluminium block

(c) Deconvolution Algorithms Applied to Narrowband Hybrid System Response

Initially, the two deconvolution approaches were tested using the simulated data. Figures 6.9 and 6.10 illustrate the performance of the Modified Least Means Squared and Minimum Entropy techniques respectively. In both cases, the main longitudinal components have been clearly resolved. Although both results possess secondary smaller components close to the main longitudinal components. These algorithms are building an inverse filter according to the first signal that they encounter, in this case the longitudinal component, and hence the shear component is not necessarily taken into account. In conclusion, there is a low confidence in the shear nature of the small peaky artefacts. However, the main longitudinal peaks confirm the structure of the reflectivity function.

The deconvolution algorithms were applied to the experimentally acquired data, presented in Figure 6.2. The deconvolved result using the adaptive MLMS algorithm is presented in Figure 6.11. This technique has extracted the first through transmitted pulse and two internal reflection pulses. The result from the nonadaptive approach is illustrated in Figure 6.12. This algorithm has performed quite well, with reasonable signal definition. The deconvolved output shows that the algorithm has decoded the first through transmitted pulse and three internal reflection pulses. In both deconvolved results shear wave mode conversions are present in between the reflection pulses, which could be interpreted as flaw characteristics in an NDE environment. However, given sufficient apriori information, it may be possible to remove such multiples by similar deconvolution procedures.

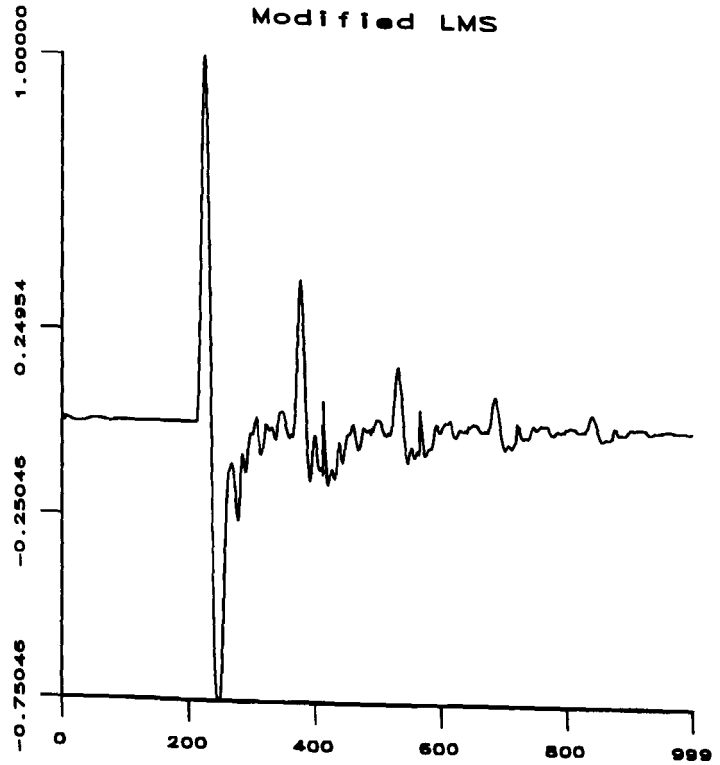

Figure 6.9 Modified least means squared deconvolved result from simulated data

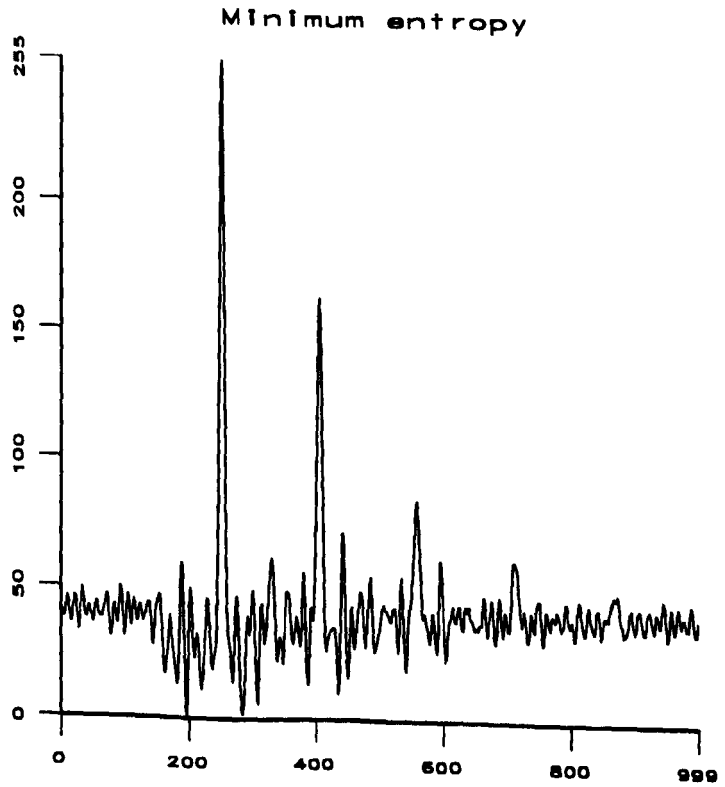

Figure 6.10 Result of Minimum Entropy deconvolution on simulated signal

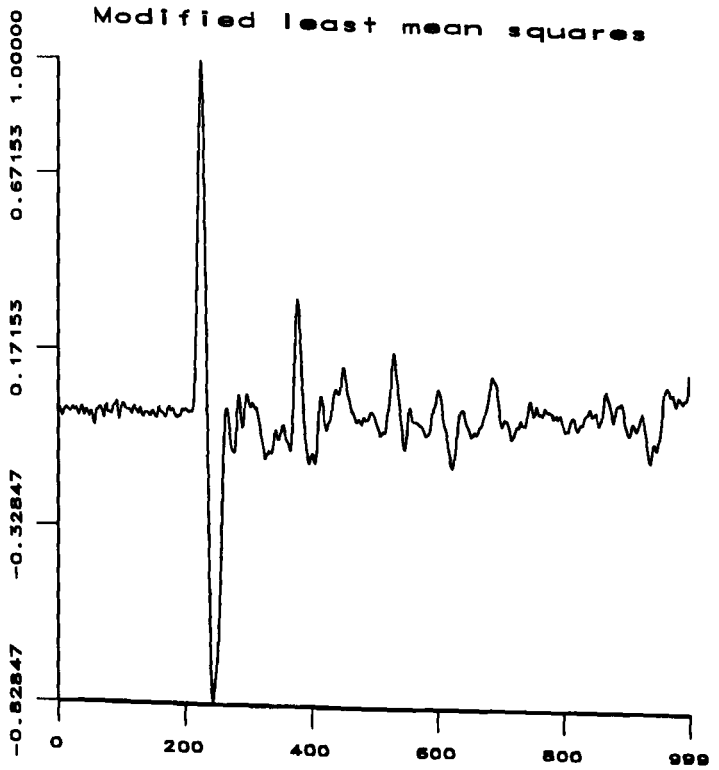

Figure 6.11 MLMS deconvolved result from experimentally acquired data

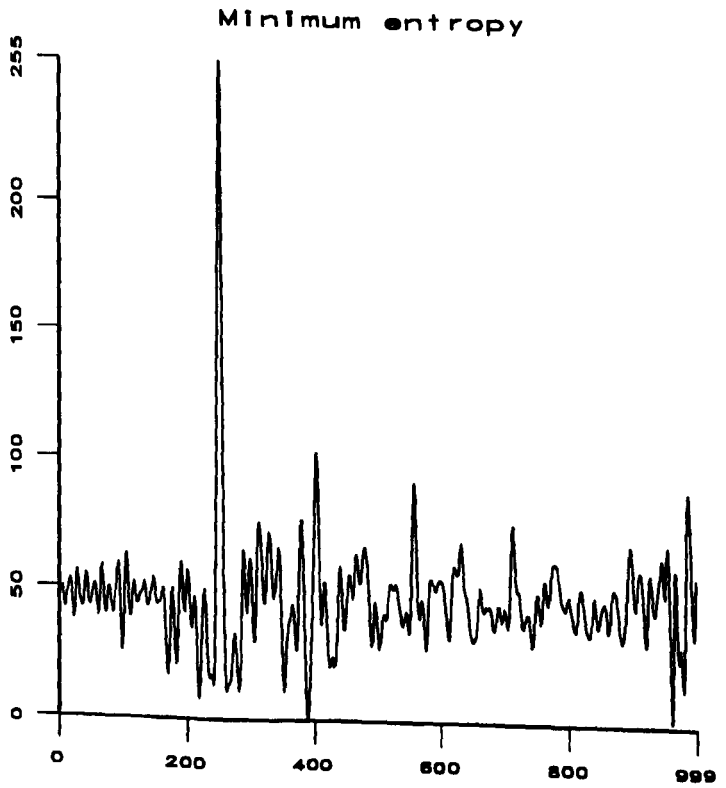

Figure 6.12 Result from ME deconvolution on experimentally acquired data

(d) Detection of Various Ultrasonic Modes

Three standard piezocomposite transducers were applied as detectors in this hybrid system. Details of the transducer characteristics are provided in Table 6.1, where Z_{ml} and Z_{bb} are the specific acoustic impedances of the matching layer and backing block respectively. The matching layer material utilised was RTV Silicone Rubber, at a quarter wavelength of the transducer fundamental frequency, with Tungsten loaded hard set epoxy employed as a damped backing medium.

	Transducer #1	Transducer #2	Transducer #3
volume fraction (%)	40	40	40
f_m (kHz)	525	541	1720
f_n (kHz)	643	656	1985
k_t	0.617	0.605	0.538
Z_{ml} (MRayl)	1.0	1.0	1.0
Matching Layer thickness (mm)	0.4	0.4	0.13
Z_{bb} (MRayl)	8.0	none	none
Backing Block thickness (mm)	40	/	/

Table 6.1 Properties of piezcomposite detectors

Experiments were performed to evaluate the laser source/piezoelectric receiver system, both on opposite sides of a sample (in through-transmission), and also on the same side to investigate Rayleigh and Lamb wave performance. A detailed account of the use of these piezocomposite receivers, in this transduction system, can be found in Reference 67. Here, only a selection of these results will be shown. These experiments utilised a Nd:YAG laser to generate ultrasonic transients in various blocks of aluminium.

Longitudinal and shear waves generated in an 86mm thick aluminium sample were detected by the 640kHz receiver, Transducer #1. The waveform recorded by this damped

device is shown in Figure 6.13, where multiple longitudinal reflections (L, 3L) are visible. Rayleigh wave detection was investigated using a combination of the laser-induced source and piezoelectric receiver on the same side of a thick 86mm aluminium block. The detection of the ultrasonic mode was optimised by rotating the air-coupled detector to the critical angle θ_c (6° for aluminium). The experimentally acquired waveform, detected by the undamped Transducer #2, is shown in Figure 6.14. For Lamb wave detection, dispersion causes the wave velocity to vary with frequency, and hence the angle θ has to be chosen carefully. Figure 6.15 shows the waveform detected at θ=12° in a thin aluminium plate (thickness = 0.86mm) by the 2MHz composite receiver, Transducer #3. This transduction system has been optimised for a_0 mode detection, due to its associated large out of plane motion.

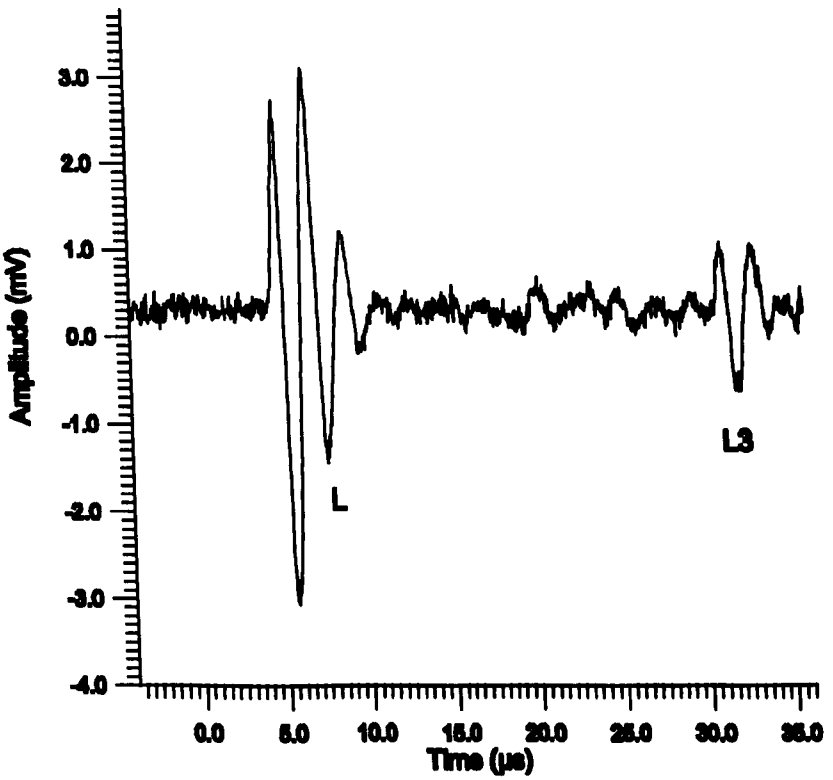

Figure 6.13 Through transmission response for 650kHz damped composite

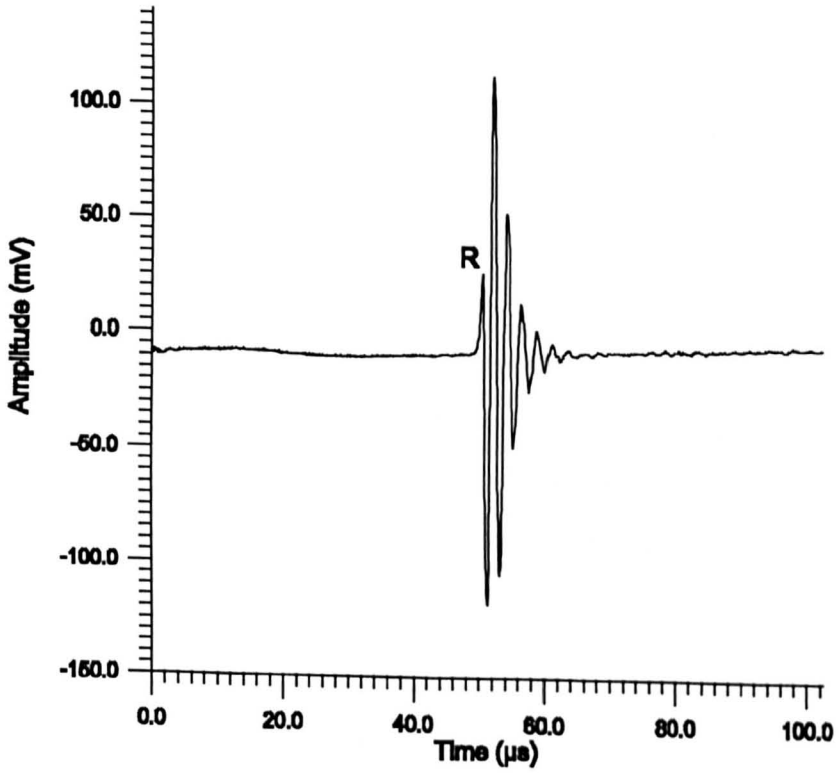

Figure 6.14 Detection of Rayleigh wave on 650Khz undamped composite

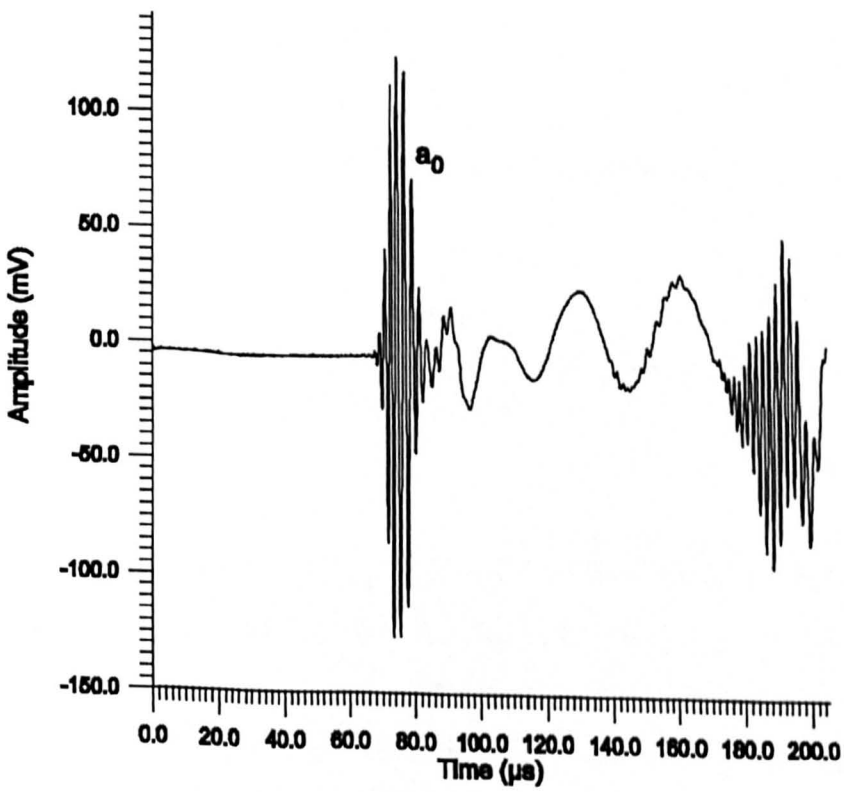

Figure 6.15 Detection of a_o mode lamb wave on 2MHz resonant composite

6.1.4 Application of Laterally Coupled Composite Transducers

(a) Through Transmission

This laser/piezoelectric hybrid system was utilised to evaluate the performance of the laterally coupled composite transducer designs, described in Chapter 5. A high resolution capability is required to detect the laser-induced ultrasonic transients. The contact capacitive transducer was employed to acquire a calibration waveform through which assessment of the wideband composite transducers could be achieved. This calibration waveform, where the ultrasonic signals were generated by a laser pulse in a 12.83mm aluminium block, is shown in Figure 6.16. Multiple acoustic reflections, both longitudinal (L,3L,..) and shear (S,3S,..), within the aluminium may be recognised clearly.

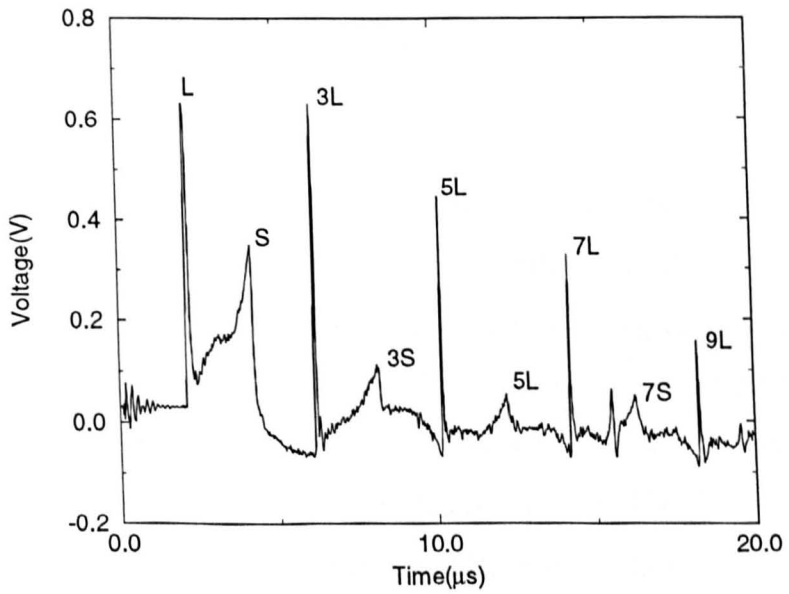

Figure 6.16 Signal received by a capacitive device after laser excitation of a 12.83mm thick aluminium block

A 20% composite transducer was constructed from a 15mm diameter PZT5A disc and hard set epoxy and designed such that the first lateral resonance effectively extended the thickness mode bandwidth of the device. The transducer possessed an aspect ratio of 0.24. A perspex backing block was attached to the rear face of the composite. The experimental impedance profile of the damped transducer is shown in Figure 6.17, where the fundamental mechanical resonace is approximately 1.65MHz.

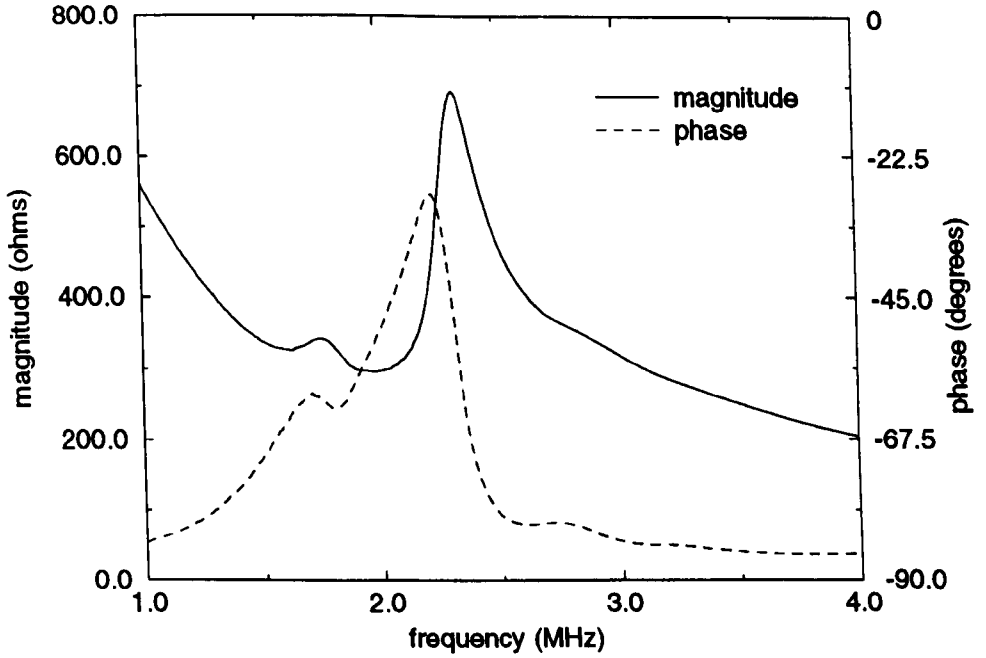

Figure 6.17 Impedance plot of 20% composite transducer

The wideband characteristics of the 20% composite receiver enabled the detection of signals in the 12.83mm aluminium block, where the internal reflections in the block are separated by 4μs. The detected waveform, free of any post signal processing, is shown in Figure 6.18. As can be seen from this Figure, the wide bandwidth allows discrete multiple longitudinal reflections (L, 3L, etc) to be seen, as well as some shear (S, 3S etc) arrivals. To illustrate the operational bandwidth of this device, the frequency spectrum of a single through air longitudinal reflection is shown in Figure 6.19. This constitutes a -6db system bandwidth of approximately 150%, with respect to the 950kHz centre frequency.

This received signal can be compared to the waveform detected by the contacting capacitive transducer, shown in Figure 6.16. The longitudinal echoes are evident in both traces, as are shear modes generated within the test sample. These shear waves are only just visible in the through air detected signal, which relates to mode conversion by shear waves into longitudinal waves at the surface of the aluminium. The presence of this mode conversion could be a problem when signal processing is applied to interpret the NDE information contained in the signal.

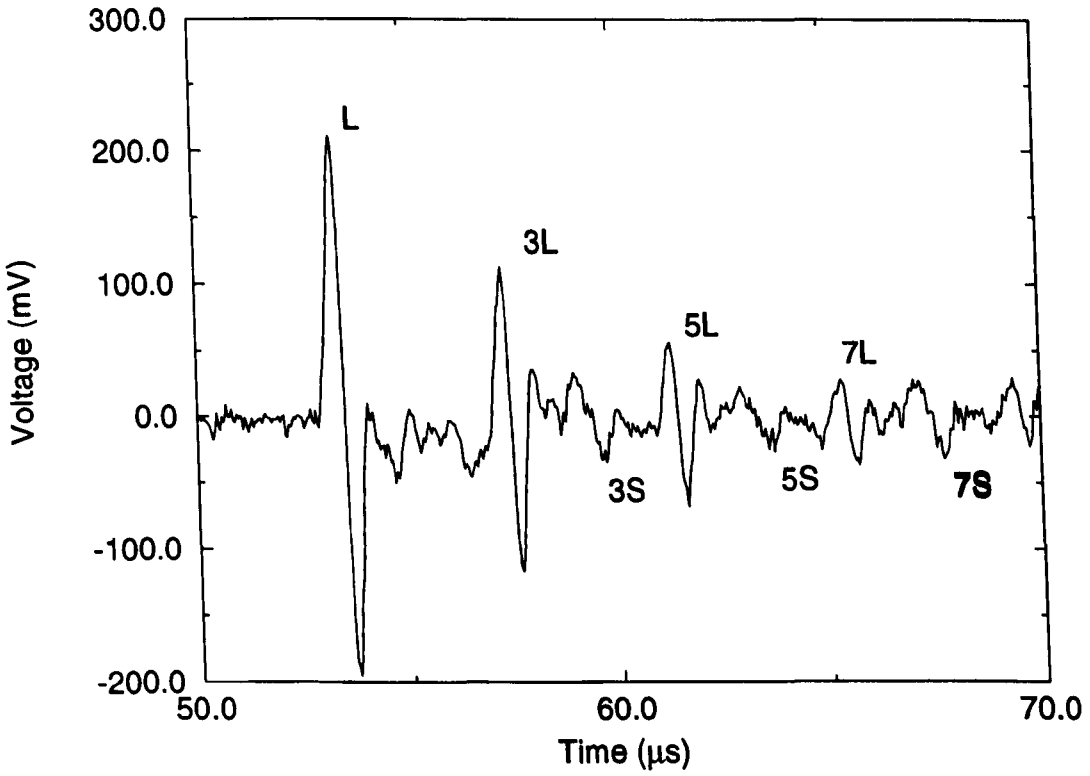

Figure 6.18 Signal received by 20% annular composite transducer after excitation of a 12.83mm thick aluminium block

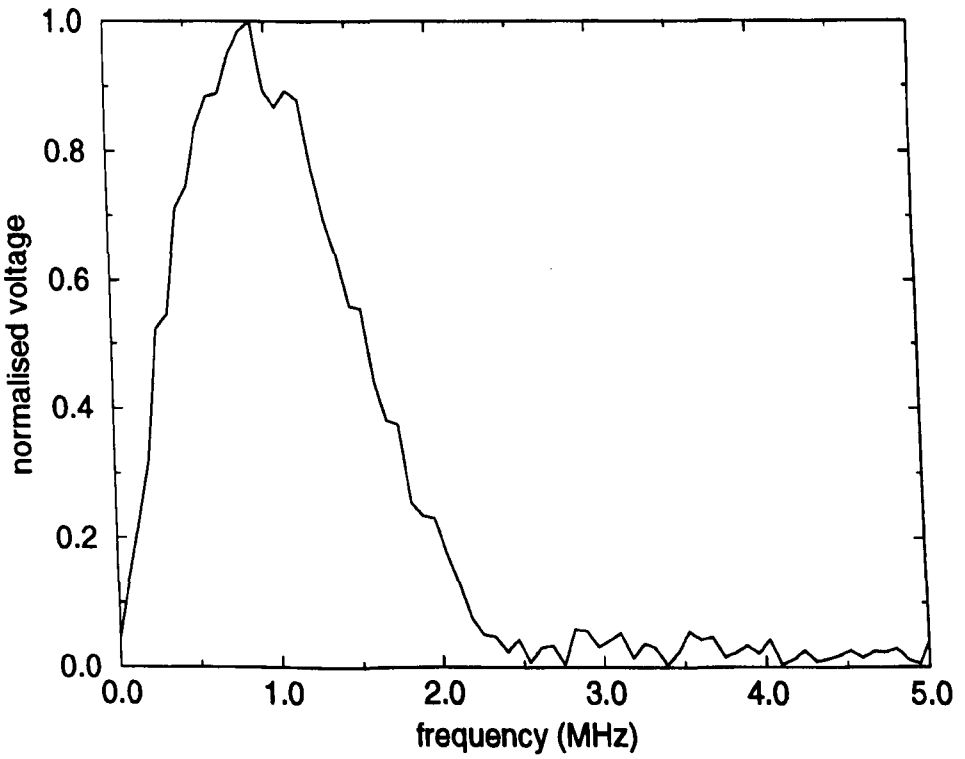

Figure 6.19 Frequency spectrum for signal detected on laterally coupled composite

Figure 6.20 shows waveforms in three thicknesses of quasi-isotropic carbon fibre reinforced polymer composite, where multiple echoes in the thickness direction have been clearly resolved without the need for further processing. As indicated earlier in this Chapter and in [67], the deconvolution approaches were relatively successful, with the adaptive method shown providing good resolution enhancement. However, it is also apparent that there is little benefit to be gained when compared with the performance of the wideband composites presented here. Consequently, deconvolution is expected to be restricted to those applications requiring relatively narrowband transducers, when higher sensitivity is beneficial.

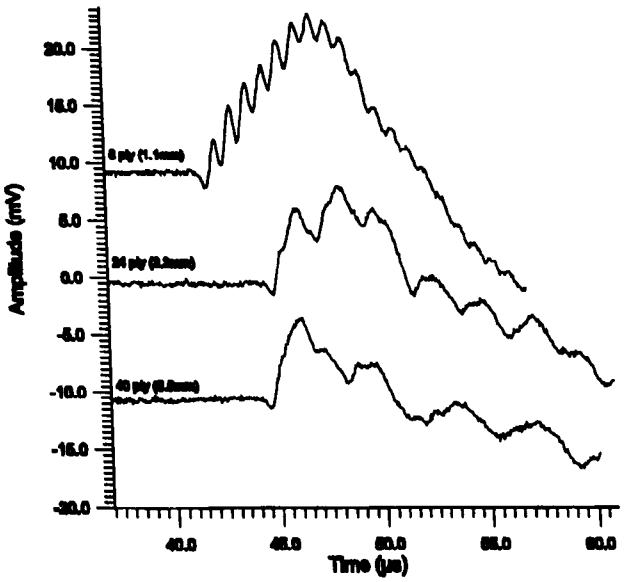

Figure 6.20 Through transmission response for various thicknesses of quasi-isotropic carbon fibre reinforced polymer composite

Sufficient signal exists for imaging in through-transmission by translating the sample on a computer-controlled X-Y stage, with the CO_2 laser source and air-coupled receiver fixed in position. Waveforms were digitised at 1mm intervals, and processed using custom software which could record the maximum amplitude within a chosen window in either the time or frequency domain. Figure 6.21(a) shows the image of a 10mm diameter machined defect in a 9.8mm thick glass fibre pultruded composite. The defect is visible in this highly scattering and attenuating material, together with a resin-rich area immediately above it. Images were also obtained in UD carbon-fibre samples, with Teflon layers inserted during manufacture to simulate delaminations. Figure 6.21(b) shows the image of a 25mm square defect, where both size and shape are reproduced

with some accuracy.

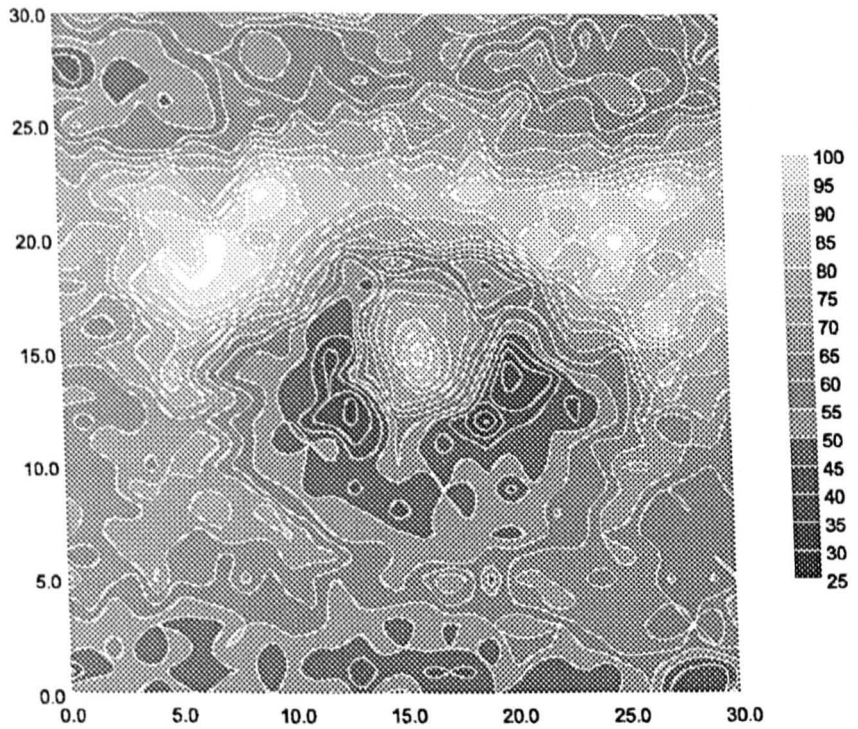

Figure 6.21(a) Image of a 10mm diameter machined defect in a 9.8mm thick glass fibre pultruded composite

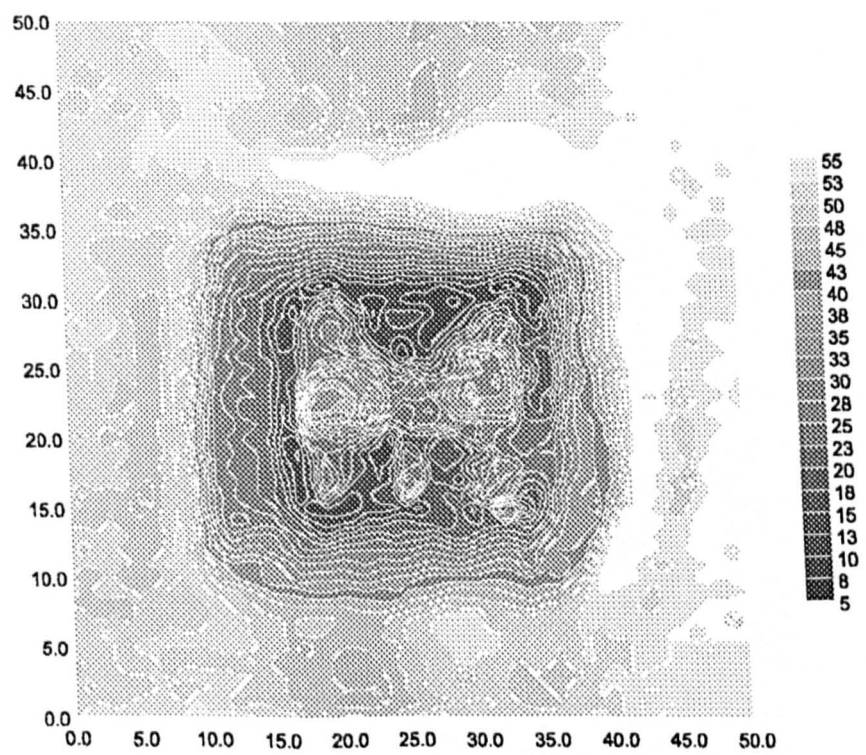

Figure 6.21(b) Image of a 25mm square defect in UD carbon-fibre sample

(b) Lamb Wave Tomographic Imaging

Tomographic images were obtained using the CO_2 laser to propagate Lamb waves in various directions across a defect, and the wideband air-coupled receiver at a fixed distance from the source and angle θ to the plate on the same side of the sample. A computer-controlled translation/rotation stage for the technique was constructed to build up a series of time waveforms taken in the form of projections. Several processing methods were investigated for extracting time of flight variation data suitable for tomographic reconstruction. The most reliable was found to be a cross-correlation of the a_0 mode. Images formed in this way are shown in Figure 6.22 for (a) a 5mm diameter defect in a 1mm thick Perspex sheet, and (b) for a 10mm circular defect in a 32-ply cross-ply carbon fibre plate. In both cases the defect has been located successfully.

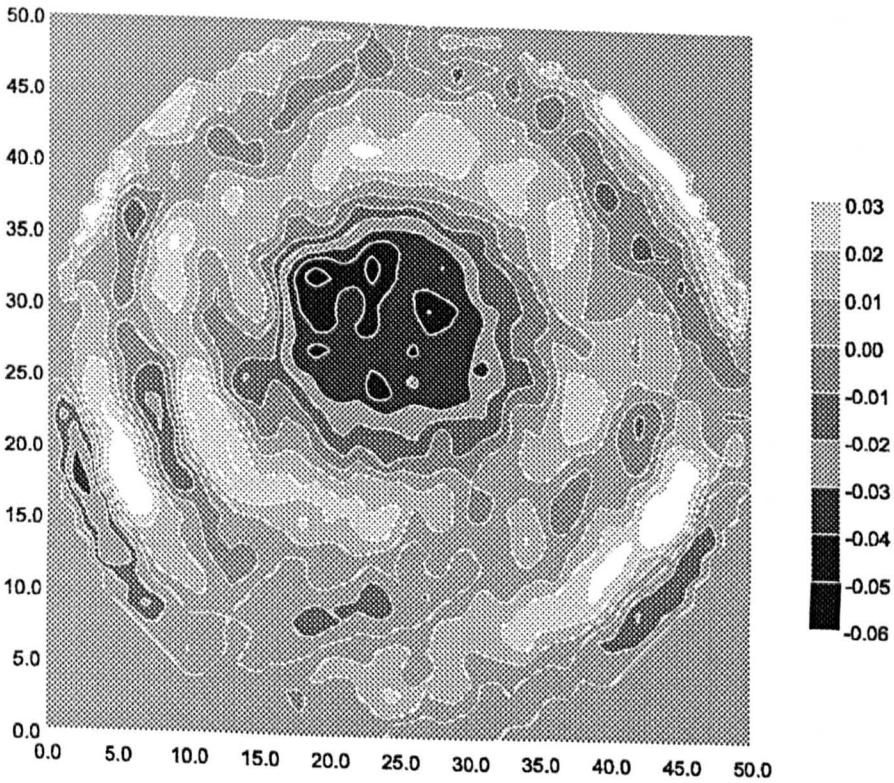

Figure 6.22(a) Tomographic image of 5mm diameter defect in a 1mm thick perspex sheet

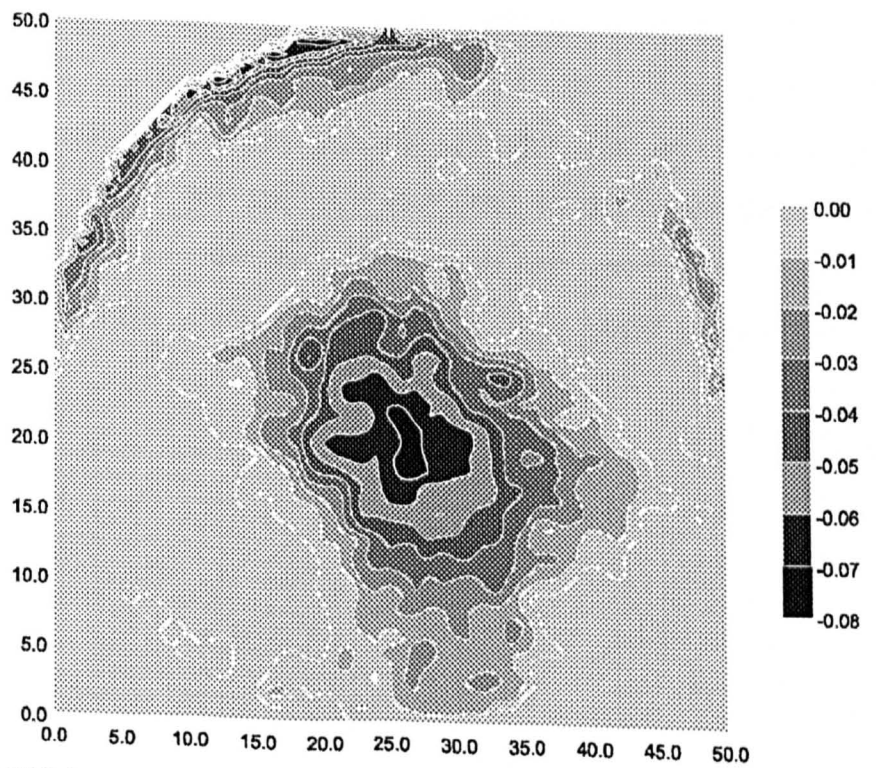

Figure 6.22(b) Tomographic image for a 10mm circular defect in a 32-ply cross-ply carbon fibre plate

6.2 Air-Coupled NDT System utilising Lamb Wave Techniques

Within the laboratory at Strathclyde University, Roger Farlow has employed piezocomposite transducers, designed from this Thesis, in the non-destructive evaluation of thin plates [2,61]. The system was constructed using a pair of frequency matched composite transducers each of which has a ceramic volume fraction of 20%. The transducers were designed to operate at 560kHz. It was envisaged that the final system would utilise single mode Lamb wave propagation and would be suitable for testing in samples less than approximately 2mm in thickness. At this frequency, the influence of airborne attenuation was not considered to be a major restricting factor over short propagation distances.

The configuration of this NDE system is shown in Figure 6.23. Here, both transducers are situated on the same side of the sample. The transducers are driven by a 20-cycle tone burst, at 560kHz, delivered through a 55dB power amplifier. The angles at which the transducers are positioned dictates the type of acoustic wave generated within a sample. Using this approach, shear waves, Rayleigh waves and various Lamb wave modes have been generated and detected. To improve SNR in real-time, the received signal was processed within several analogue stages. The detected signal was initially amplified, in low noise pre-amplifier positioned within the screened housing of the composite receiver, before bandpass filtering and envelope detection were applied. This produced a narrowband operating environment, with a large system SNR.

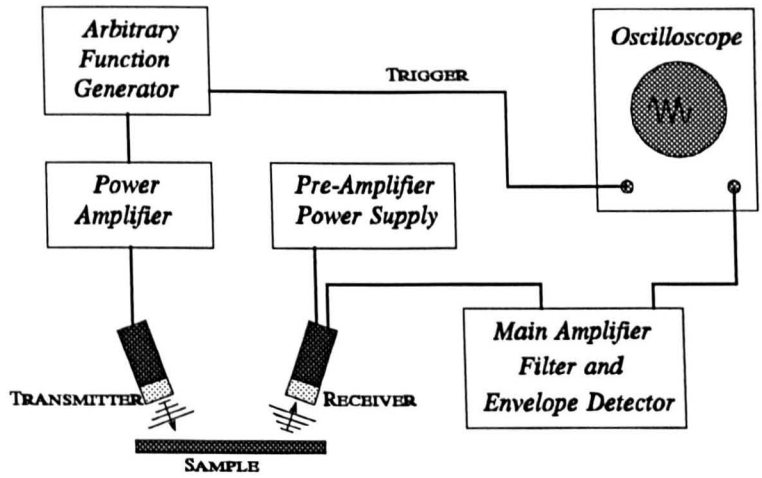

Figure 6.23 Lamb wave NDE experimental layout

The primary application of this NDE system utilises Lamb wave mode propagation in thin plates. Due to its large out of plane motion the a_0 mode was considered the appropriate Lamb wave mode for this system. Using different thicknesses of steel plates, excellent agreement between experimentally acquired data and the theoretical group velocity curve, for the a_0 mode, was observed [2]. The system has used this approach to investigate defects in both aluminium and carbon fibre plates.

A controlled defect, in a 1.1mm thick aluminium plate, was introduced by milling away 50% of the material thickness in a 30mm diameter disc located close to the centre of the plate. This test-piece is illustrated in Figure 6.24. The transducer angles were adjusted to initiate a strong Lamb wave mode (a_0) in an undamaged area of the plate. The test-piece was then scanned with both transducers locked together so that there was a fixed separation between them. When the transmitter was positioned over the defect, the signal amplitude of the Lamb wave mode reduced. By scanning the aluminium in two dimensions, an image of the defect could be generated. Figures 6.25(a) and 6.25(b) illustrate a three dimensional amplitude plot and a grey-scale image of this defect. In this experiment the diameter of each transducer was 30mm and the separation between centres was 40mm. Hence, the effective dimensions of the scanning aperture is 30mm by 70mm, because the signal amplitude drops to zero when either the transmitter or the receiver is over the damaged section. This results in the distortion which can be

observed in both of these Figures.

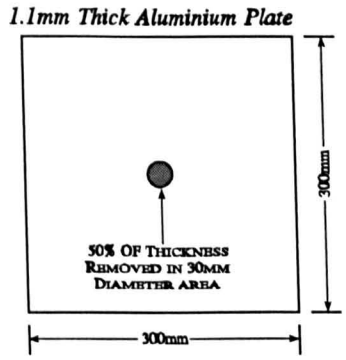

Figure 6.24 Aluminium test-piece, with manufactured defect

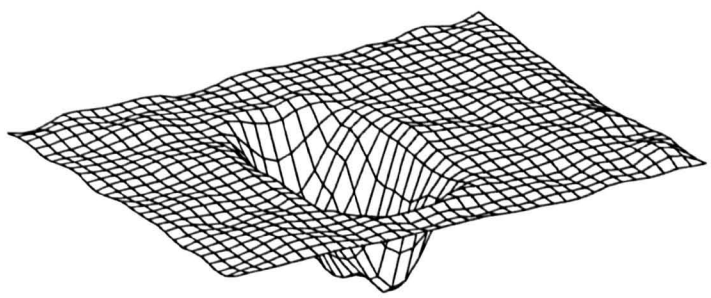

Figure 6.25(a) 3D representation of defect in aluminium test-piece

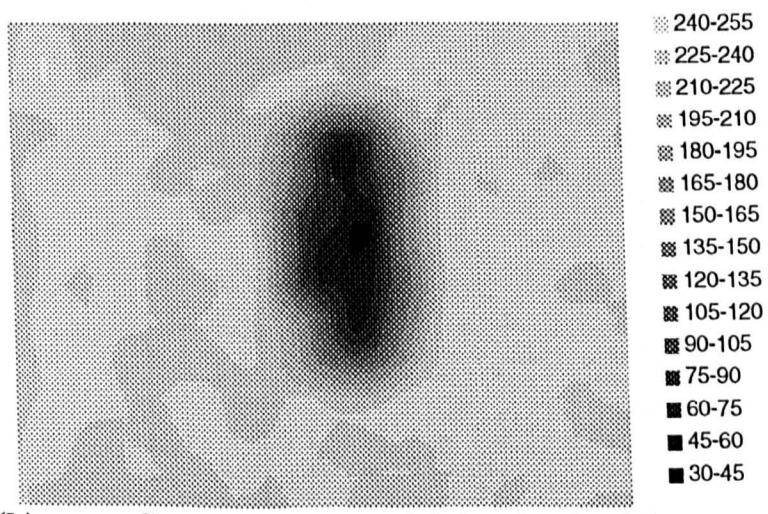

Figure 6.25(b) Grey-scale image of defect in aluminium test-piece

Further experimentation utilised a carbon fibre plate, 1mm thick, in which an area of delamination was present. A sketch of this plate is shown in Figure 6.26. Using the procedure described above, for the aluminium test-piece, it was possible to generate an image of the area containing the defect. The grey-scale image produced using data from this scan is shown in Figure 6.27.

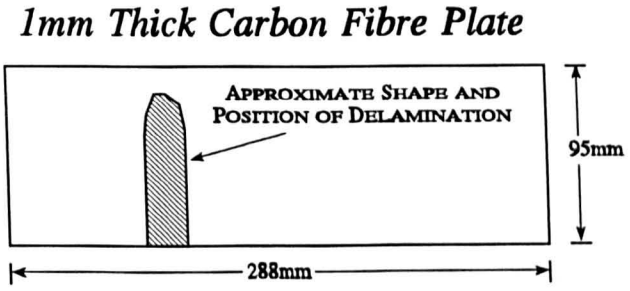

Figure 6.26 Carbon-fibre test-piece containing an area of delamination

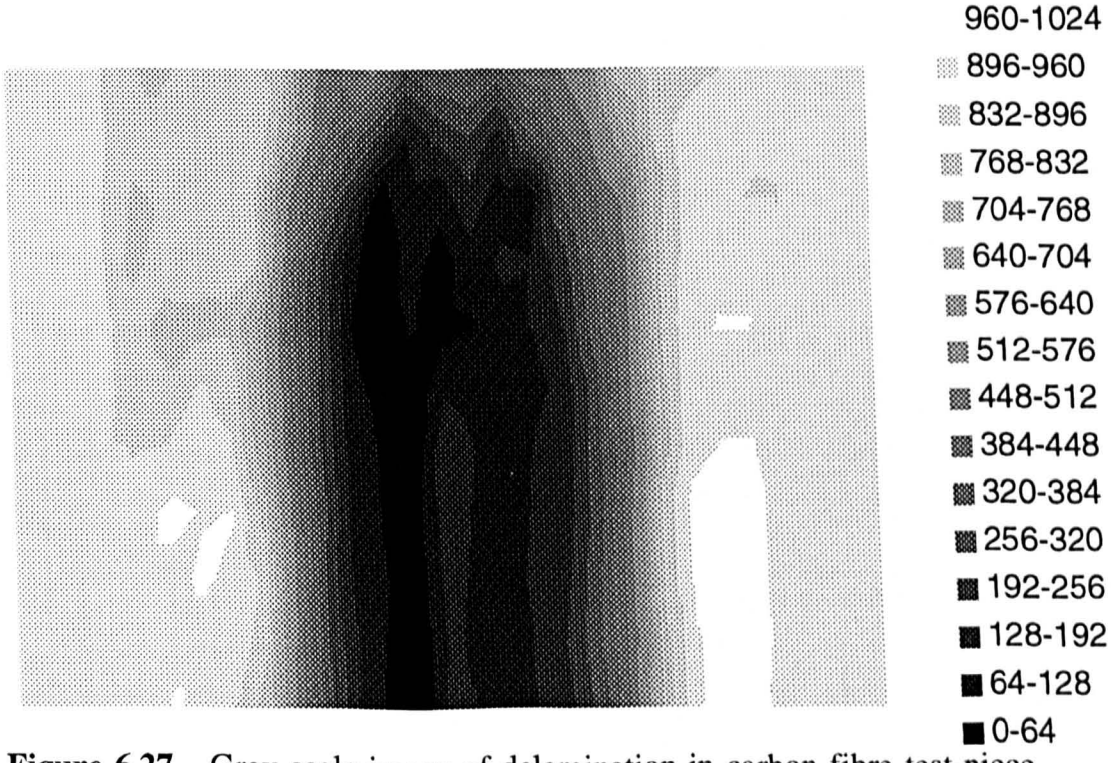

Figure 6.27 Grey-scale image of delamination in carbon fibre test-piece

This transduction system, utilising air-coupled piezocomposite transducers, has been employed to detect shear waves, Rayleigh waves and Lamb waves in real-time [2]. It has been demonstrated that an air-coupled Lamb wave configuration provides an excellent method of detecting and imaging defects in thin sheets of material, such as carbon fibre. Further work will automate the scanning mechanism and determine the resolution capabilities for this NDE system [61].

6.3 Through Transmission Inspection of Composite Sections

The feasibility of using air-coupled ultrasonic transducers in a rapid NDE scanning system has been demonstrated by Stephen Kelly, within the Ultrasonics Research Group at Strathclyde [62]. Here, the set of design guidelines described in Chapter 4 has been utilised by Stephen Kelly to develop a prototype, through transmission, air-coupled NDE system. This system will have to exhibit improved speed and efficiency over current water jet systems used within the aircraft industry. Similar design criteria to the Lamb wave scanner system, described in the previous section, have been implemented, where the piezocomposite transducers will be optimised for narrowband operation and operate with identical receive electronics. Through this approach, signals have been detected in real-time through a number of different materials, including aluminium, carbon fibre and honeycomb structures, where a SNR greater than 20dB has been achieved through a 22mm thick honeycomb sample.

The experimental arrangement shown in Figure 6.23 has been revised with the transducers situated on each side of the test-piece. For this experimentation, the transmit and receive transducer are carefully aligned and positioned normal to the surface of the test-piece. This configuration generates longitudinal waves in the sample.

Using the modelling work described in Chapter 4, an air-coupled through transmission system has been built and evaluated. A frequency matched 60% PZT5H / hard set epoxy transmitter and 30% PZT5A / hard set receiver have been constructed, with an operational frequency of 600kHz. To enhance system resolution and improve sensitivity, both devices have a focused perspex lens, incorporating a loaded Silicone Rubber outer layer, attached to the front face. Using a single 2mm x 30mm reception element, a C-scan of the plate illustrated in Figure 6.28(a) has been acquired. The composite plate is 3.7mm thick and incorporated 9 PTFE inclusions. The resultant C-scan image is presented in Figure 6.28(b). It is apparent that this air-coupled ultrasonic system has successfully detected all 9 defects. Consequently, this air-coupled configuration has sufficient sensitivity and resolution for implementation in practical NDE applications.

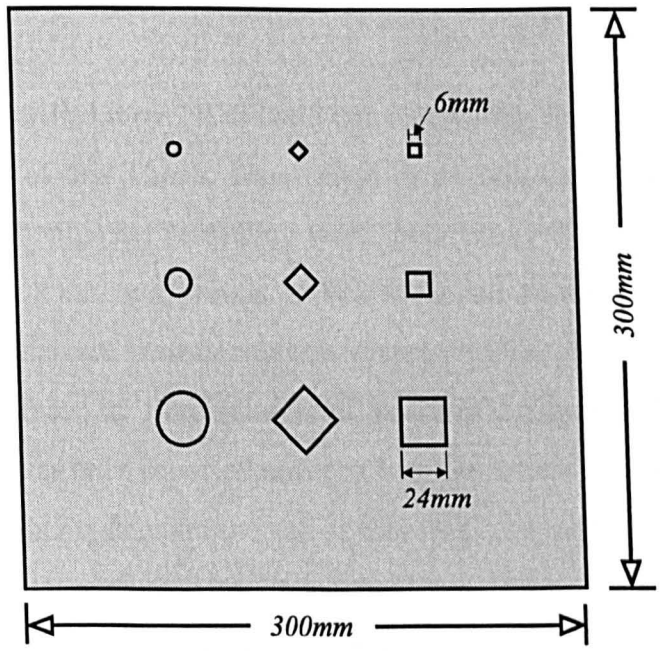

Figure 6.28(a) Carbon fibre reinforced polymer composite plate, 3.7mm thick, including 9 PTFE inclusions of various dimensions

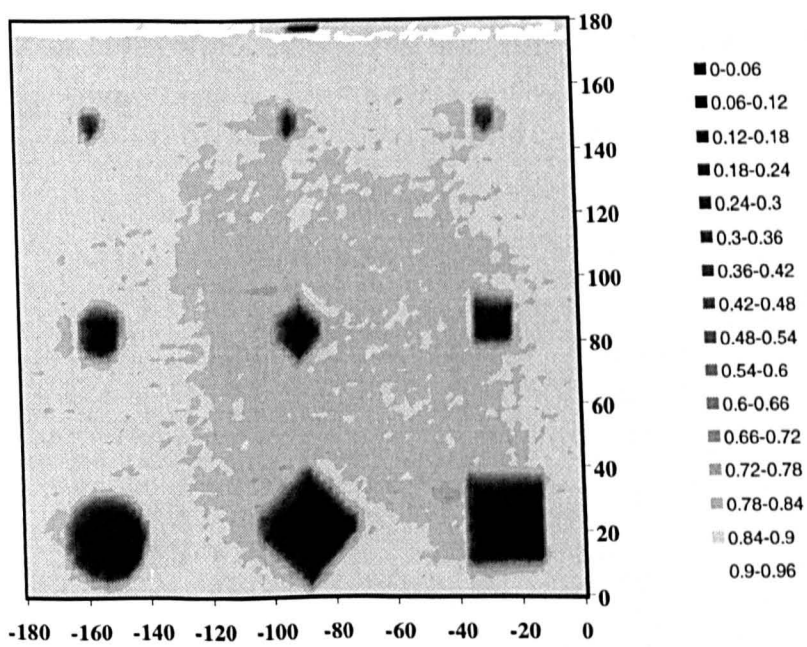

Figure 6.28(b) Air-coupled C-scan of composite plate shown in Figure 6.28(a)

6.4 Conclusions

This Chapter has described three NDE applications utilising the research results reported in Chapters 4 and 5 of this Thesis. From these examples, the practical significance of the 1-3 connectivity composite modelling work, presented earlier, is evident. Firstly, the collaboration between the two groups at Warwick and Strathclyde Universities have developed a new wideband instrumentation system, which has potential application in the detection of defects in fibre-reinforced polymer composites. A high resolution transduction system has been reported utilising laterally coupled composite receivers, but if sensitivity requirements demand the use of standard composite designs, deconvolution techniques have been evaluated to enhance system resolution. Secondly, real-time ultrasonic techniques have been employed in the implementation of non-contact NDE systems. This air-coupled system used a frequency matched composite transducer pair to generate/detect Lamb waves in thin plates. Defect detection has been illustrated in both metallic and carbon fibre composite materials. Finally, a prototype through transmission NDE system has been presented, in which signals have been detected through a 22mm thick honeycomb sample. This response was obtained in real-time, with a SNR greater than 20dB.

CHAPTER 7

CONCLUSIONS AND SUGGESTIONS FOR FURTHER WORK

ABSTRACT

A synopsis of the programme of work documented in this Thesis will be presented. Furthermore, a series of recommendations for further work will be proposed and their significance within the frame of the Thesis will be highlighted.

7.1 CONCLUSIONS

7.1.1 General Overview

Research in the field of air-coupled ultrasound has been established for many years, although recent technology advances have made possible operation in the low Megahertz range. This Thesis has concentrated on two important considerations in the design of an air-coupled ultrasonic system for practical NDE applications. Firstly, a novel and robust characterisation methodology has been developed to facilitate comparison between different transducer technologies for operation in the frequency range 50kHz - 2.0 MHz. Secondly, an evaluation of 1-3 connectivity piezocomposite transducer configurations for practical air-coupled applications was discussed. The contribution of these two considerations for practical NDE applications was presented in Chapter 6. The implementation of the 1-3 connectivity piezocomposite transducer technology in three different application areas highlights the significance of the transducer evaluation work presented in Chapters 3-5. Importantly, the defect resolution illustrated in the Applications Chapter indicates the practical feasibility for air-coupled NDE systems using piezocomposite technology.

7.1.2 Air-Coupled Transducer Characterisation

Novel experimental techniques were adopted to evaluate the wideband impulsive response for air-coupled transducer designs operating in the frequency range 50kHz - 2MHz. Wideband transducers have been designed and constructed using piezopolymer film (PVDF) and employed to characterise air-coupled transducer designs in both transmission and reception modes of operation. Notwithstanding the considerable influence of airborne attenuation, a properly configured PVDF transmitter approximates well to a wideband source for operation in this frequency range. Moreover, a standard PVDF membrane hydrophone, calibrated for operation in water, can be utilised to acquire quantative information for air-coupled ultrasonic transmitters, although SNR is reduced when compared to the water coupled situation.

An experimental comparison involving both electrostatic and 1-3 connectivity

piezocomposite transducer designs was conducted. In addition to the wideband evaluation of the air-coupled transducers, in terms of their through-air system impulse response and insertion loss, the study was complemented through the acquisition of transducer characteristics under narrowband operating conditions. An important consideration of this comparative study is that the narrowband operation of the piezocomposite designs promotes a high sensitivity performance characteristic, under both wideband and narrowband operating conditions, in both transmission and reception. The wideband nature of the electrostatic configurations was demonstrated and it is considered unlikely that standard piezocomposite designs will ever match their gain-bandwidth product figures. For many air-coupled transducer applications, the high sensitivity characteristic associated with 1-3 connectivity piezocomposite transducers may be required to overcome the losses associated with both the acoustic impedance mismatch at each air/solid boundary and airborne attenuation.

It is important to note that, for industrial applications, electrostatic transducers are disadvantaged considerably with regard to operational robustness. Applications in which the Ultrasonics Group (University of Strathclyde) are involved include real time scanning of aerospace components, testing of automobile structures and internal inspection of gas pipelines. In all cases, available electrostatic devices are not sufficiently robust to operate reliably in the industrial environment. This problem was recognised many years ago and the solution was to provide a protective 'guard cage' over the surface of the fragile membrane. This was satisfactory for the relatively low frequencies (~50kHz) involved, but it is not a practical solution for the non-destructive testing applications presently under consideration. Since the location of a thin and fragile vibrating membrane adjacent to the air environment is essential to the successful operation of electrostatic devices, it is difficult to envisage how this difficulty may be resolved successfully. This is a major problem for widespread application of electrostatic technology, although the technology is considered to possess attractive properties for operation within controlled environments and possibly as device standards for laboratory calibration.

Another point of note concerns the general viability of through air ultrasound and in particular, non-contact inspection. Conventionally, ultrasonic inspection of solid components is performed with the aid of a thin layer of couplant material, or alternatively by immersing the test piece and ultrasonic transducer within a water bath. As discussed in Section 1.1, removal of the liquid coupling medium and replacement by air results in a reduction in SNR of approximately 140 dB. This cannot be recovered by transducer technology alone, even by optimisation of the complete system. The difficulties are compounded in those practical applications where real time scanning or imaging of large components is required. In many instances the ultrasonic data must be captured in single shot mode, without recourse to signal averaging or the use of alternative signal processing techniques such as pseudo-random codes and subsequent cross correlation. For such operation, the use of wideband techniques is questionable, due to the resultant low SNR. The solution which the Ultrasonics Group, at Strathclyde University, have been forced to adopt is to design instead extremely narrowband systems, using resonant transducer technology and narrowband filtering at the matched receiver stage [2,62]. Using these methods, it is possible to design and implement rapid through air scanning systems for practical industrial applications.

7.1.3 Optimisation of Air-Coupled 1-3 Connectivity Piezocomposite Transducers

Using the novel calibration techniques, described in Chapter 3, an evaluation of 1-3 connectivity piezocomposite transducer designs for air-coupled operation was presented. A dual modelling strategy, incorporating both uni-dimensional and finite element techniques, was experimentally verified for a range of piezocomposite transducers, including the application of both mechanical matching and damping. The limitation of the uni-dimensional modelling approach was highlighted and consequently, the finite element technique was employed to predict the components necessary for a practical air-coupled composite transducer system. At an operational frequency of 500kHz, the modelling has predicted the following transducer system components :

- *Transmission* — 50-70% PZT5H and CIBA-GEIGY CY1301/HY1300 composite transducer

• *Reception*	10-30% PZT5A and CIBA-GEIGY CY1301/HY1300 composite transducer
• *System Configuration*	A frequency-matched composite transducer pair operating in a through-transmission configuration has a predicted 30dB improvement over a composite transducer operating under pulse-echo conditions
• *Matching Layers*	A double matching layer configuration, consisting of quarter wavelength layers of perspex and membrane filter, is predicted to enhance transducer performance by 16dB
• *Mechanical Damping*	100% mechanical damping, at the transducer rear face, is predicted to provide a 75% -6dB bandwidth characteristic, but with a 17dB reduction is sensitivity for a matched 20% composite transducer pair.

Consequently, an air-coupled 1-3 connectivity piezocomposite transducer system should operate in through-transmission and under narrowband conditions. The transducers require to be frequency-matched and incorporate a double matching layer to improve system sensitivity.

7.1.4 Detection of Wideband Air-Coupled Ultrasound

A comprehensive analysis was carried out in Chapter 5 to evaluate a novel approach to the design of a wideband composite receiver. The technique utilised coupling between the fundamental thickness and first lateral resonances within a 20% composite transducer to effectively extend the operational bandwidth of the device. Initially, verification of the finite element approach utilised both impedance measurements and experimentation under water load, for a range of composite transducer with differing aspect ratio. The finite element model was then extended to simulate the laterally-coupled composite transducer under air-coupled operating conditions. The performance of the laterally-coupled composite, in air, compared favourably with an electrostatic transducer, where the composite transducer demonstrated excellent bandwidth characteristics, but with a lower receive sensitivity.

7.2 SUGGESTIONS FOR FURTHER WORK

7.2.1 Optimising Piezocomposite Designs for Air Operation

The work presented in Chapter 4 addressed only the doubly periodic composite structure, comprising a regular array of square sectioned piezoceramic pillars embedded within a uniform filler material. Several significant improvements have been omitted. Therefore advanced piezocomposite transducers designs are feasible by incorporating the following improvements :

- The advent of injection moulding techniques [89] facilitates the manufacture of ceramic pillars that present an acoustic impedance gradient from the rear to the front face, thereby providing enhanced matching to air. One choice is a pyramid form of pillar with a triangular base [84], thereby minimising inter-pillar resonances and presenting a very low impedance at the front face. Alternatives include horn shaped pillars for power matching and non-uniform spacing for promotion of homogeneous operation.
- The use of loaded fillers [112] for enhancement of transducer sensitivity, particularly important for operation in air.

7.2.2 Comprehensive Beam Profiling Analysis

Experimental acquisation of beam profile characteristics may suffer from problems relating to low sensitivity and the inherent short wavelengths in air. These problems are manifest in the small propagation distances, associated with many standard air-coupled transducer designs, and with the design of a suitable calibrated reception device.

The short wavelengths associated with airborne operation, in the low Megahertz frequency range, will require a reception device comprising a very fine scale active area (e.g. at 500kHz an active area less than 0.3mm diameter is desired). This constraint is further handicapped by a reduction in receive sensitivity when using these dimensions. Standard hydrophone devices are designed to operate under water loading and consequently, their active area could be approximately five times greater than for a

corresponding air-coupled device. The use of such a device would introduce a degree of spatial integration to the received signal. Therefore the design and development of a standard hydrophone for operation in an airborne environment is a necessary tool for the acquisition of experimental beam characteristics.

The inherent low sensitivity, for air-coupled ultrasonic operation, may restrict the range over which the experimental data can be acquired. Thus, the high sensitivity characteristic associated with some piezocomposite transducer designs could enable field profile measurements over greater distances. For piezocomposite designs, there are two aspects that increase the complexity of the theoretical approach. Firstly, the most sensitive piezocomposite transducers incorporate a double mechanical matching layer configuration. Secondly, the behaviour of a piezocomposite transducer can include significant lateral vibrational activity, especially when encased within a screened housing. This housing can also damp the edge components from the transducer as a result of the bonding agent between the casing and the device. Therefore, these elements could be incorporated into a comprehensive modelling approach.

The integration of airborne attenuation [3], as discussed in Section 3.4, into standard beam profiling theory would constitute a powerful software tool for the design of airborne ultrasonic transducers. A comprehensive software package could enable the transducer design process to evaluate the pressure field characteristics from a knowledge of the fundamental transducer construction and external electrical stimulus. Standard software tools for the prediction of acoustic field profile solve the problem using one-dimensional techniques [107]. The results presented in Chapter 4 suggest that a linear systems approach is not suitable across the entire piezocomposite ceramic volume fraction range and hence, finite element techniques would constitute an appropriate approach. A FEA model could predict the variation in the air-coupled field profile for a multiplicity of conditions, including : variation of constituent materials; differing transducer dimensions; apodised electrode configurations; influence of mechanical matching layers or backing materials and the influence of the housing arrangement. A model of this complexity would require an extremely large computing facility, but the

rapid advances in workstation technology could soon enable a suitable extension to the fundamental modelling work presented in Chapter 4 of this Thesis.

7.2.3 Characterisation of Advanced Airborne Transducer Designs

As discussed in Section 7.2.1, there are methods through which the composite transducer performance could be improved. In addition, it should also be noted that for the majority of the experimentation presented in this Thesis, the measured electromechanical coupling efficiency has been lower than predicted by modelling. This was a consequence of depoling, in the ceramic phase, within the manufacturing process at Strathclyde University. Using more advanced dicing machines or injection moulding techniques it should be possible to construct composite devices with a coupling efficiency closer to the predicted values. Thus, it is anticipated that 'improved' 1-3 connectivity piezocomposite transducer designs will provide an enhancement in sensitivity when compared to the devices utilised in the characterisation process, described in Chapter 3.

The current micromachined electrostatic designs reported within the literature differ in design from the devices utilised within the characterisation study, in Chapter 3 [40,44,45,47,51]. These advanced micromachined devices are reported to exhibit a better bandwidth characteristic when compared to the devices employed within this Thesis. Although from the literature, it is not apparent if they also demonstrate an improvement in sensitivity.

The characterisation process should be applied to the advanced designs for both piezocomposite and electrostatic transducers. Thus a true comparison between these prospective transducer designs for airborne applications will be realised. With some of the current electrostatic transducer designs operating beyond 2MHz, the characterisation process could use a different pulser excitation, as described in Section 3.4. Although the practical feasibility of operating beyond 2MHz will have to be considered.

7.2.4 Laterally-coupled wideband composite transmitter

The work presented in Chapter 5 concentrated on extending the bandwidth for piezocomposite receivers. These laterally-coupled composites were also utilised to analyse their transmit performance. The results were poor for both sensitivity and bandwidth measurements. It must be noted that the transducers employed in this investigation were designed to operate efficiently in reception. Hence, this work could be repeated using 1-3 connectivity composite transducers with a ceramic volume fraction of 60%, as discussed in Section 4.5.2. This will certainly improve the transducer sensitivity and therefore enable the influence of mode coupling upon the transducer bandwidth to be analysed. The maximum pillar aspect ratio (MPAR) criteria for a 60% composite is 0.46 [87]. Hence, a completely different transducer construction is required in order to fully appreciate the influence of mode coupling within this transducer structure.

Another approach to improve the performance of a laterally-coupled transmitter would be the addition of a thin stiffening plate to the front face of the transducer. This configuration should demonstrate an improved dilation quality and hence, discourage the resonance mechanisms from acting independently. Consequently, the transducer bandwidth may be improved, but the influence of the stiffening layer upon sensitivity would have to be analysed.

7.2.5 Practical Implementation of an Air-Coupled Ultrasonic NDE System

The work presented in this Thesis is intended to be used as a platform from which practical air-coupled NDE systems can be implemented. This work has described the desired transducer system configuration for airborne operation, in terms of material selection, ceramic volume fraction and incorporation of mechanical matching layers. In order to realise a practical system capable of performing NDE within an industrial environment, the following considerations would have to be addressed :

- dedicated electronics in order to enhance the air-coupled system SNR
- the application of transducer arrays will increase the achievable scanning speed

for an air-coupled NDE system

- the removal of transducers from a controlled laboratory environment :
  - air currents may influence the received signal and some form of mechanical baffle would have to be incorporated into the design
  - the variation in the speed of sound with temperature [12] will have to be included into the data acquisition software
- when operating at elevated temperatures, the radiation of heat from the sample will disturb the acoustic field and consequently, influence the received signal strength

A number of these aspects are currently under consideration within the Ultrasonics Research Group, at the University of Strathclyde, and it is hoped that encouraging results will be published in the near future.

REFERENCES

Acronyms and Abbreviations

IEEE Trans UFFC	IEEE Transactions on Ultrasonics, Ferroelectrics, Frequency and Control
JASA	The Journal of the Acoustical Society of America
Meas Sci Tech	Measurement Science and Technology
Proc IEEE US Symp	Proceedings of the IEEE Ultrasonics Symposium
Review of Progress in QNDE	Review of Progress in Quantitative Nondestructive Evaluation

1. IEEE Standard on Piezoelectricity, Special Issue of Transactions on Sonics and Ultrasonics, Vol Su31-2 ptII, 1984, ANSI-IEEE Std 176, 1987 (IEEE : New York 1987)
2. Farlow R and Hayward G, 'Real-time ultrasonic techniques suitable for implementing noncontact NDT systems employing piezoceramic composite transducers', Insight, Vol 36(12), 1994, pp 926-935
3. Bass HE, Sutherland LC, Piercy J and Evans L, 'Absorption of sound by the atmosphere', Physical Acoustics, XVII, pp 145-232
4. Deka M, 'Air-coupled ultrasonic transducer for NDE', Proc IEEE US Symp 1987, pp 543-546
5. Yang SK, Varadan VV and Varadan VK, 'Noncontact thickness measurements of wet/dry paint coating using an air-coupled transducer', Materials Evaluation, Vol 48(4), 1990, pp 471-474
6. Rogovsky AJ, 'Development and application of ultrasonic dry-contact and air-contact C-scan systems for nondestructive evaluation of aerospace composites', Materials Evaluation, Vol 49, 1991, pp 1491-1497
7. Chimenti DE and Fortunko CM, 'Characterisation of composite prepreg with gas-coupled ultrasonics', Ultrasonics, Vol 32(4), 1994, pp 261-264

8. Stor-Pellinen J and Luukkala M, 'Paper roughness measurement using airborne ultrasound', Sensors and Actuators A-Physical, Vol 49, 1995, pp 37-40

9. Jackson MN, 'Simulation and control of thickness-mode piezoelectric transducers', University of Strathclyde, Phd Thesis, 1984

10. Schiller C, Hsieh C-K, Chou C-H and Khuri-Yakub BT, 'Novel high-frequency air transducers', Review of Progress in QNDE, edited by Thomson DO and Chimenti DE, Plenum Press, New York, Vol 9, 1990, pp 795-798

11. Fox JD, Khuri-Yakub BT and Kino GS, 'High frequency acoustic wave measurements in air', Proc IEEE US Symp 1983, pp 581-584

12. Fox JD, Khuri-Yakub BT and Kino GS, 'Excitation and detection of 8MHz acoustic waves in air', Proc IEEE US Symp 1984, pp 475-479

13. Hickling R and Marin SP, 'The use of ultrasonics for gauging and proximity sensing in air', JASA, Vol 79(4), 1986, pp 1151-1160

14. Yano T, Tone M and Fukumoto A, 'Range finding and surface characterisation using high-frequency air transducers', IEEE Trans UFFC, Vol 34(2), 1987, pp 232-236

15. Khuri-Yakub BT, Kim JH, Chou C-H, Parent P and Kino GS, 'A new design for air transducers', Proc IEEE US Symp 1988, pp 503-506

16. Gerlach R, Kraus O, Fricke J, Eccardt P-Ch, Kroemer N and Mágori V, 'Modified SiO_2 aerogels as acoustic impedance matching layers in ultrasonic devices', Journal of Non-Crystalline Solids, Vol 145, 1992, pp 227-232

17. Stor-Pellinen J, Oksanen M, Vuohelainen R, Rantala J, Hartikainen and Luukkala M, 'Photoacoustic inspection of matching layers of ultrasonic air-coupled transducers', IEEE US Symp, 1989, pp 665-668

18. Fletcher NH and Thwaites S, 'Multi-horn matching plate for ultrasonic transducers', Ultrasonics, Vol 30(2), 1992, pp 67-75

19. Haller MI and Khuri-Yakub BT, 'Micromachined 1-3 composites for ultrasonic air transducers', Review of Scientific Instruments, Vol 65(6), 1994, pp 2095-2098

20. Kiełczyński PJ, Pajewski W and Szalewski M, 'Ring piezoelectric transducers radiating ultrasonic energy into the air', IEEE Trans UFFC, Vol 37(1), 1990, pp

38-43

21. Babič M, 'A 200kHz ultrasonic transducer coupled to the air with a radiating membrane', IEEE Trans UFFC, Vol 38(3), 1991, pp 252-255
22. Okada H, Kurosawa M, Ueha S and Masuda M, 'New airborne ultrasonic transducer with high output sound pressure level', Japanese Journal of Applied Physics, Vol 33(5B), 1994, pp 3040-3044
23. Dabirikhah H and Turnet CW, 'Leaky plate wave airborne ultrasonic transducer', Electronics Letters, Vol 30(18), 1994, pp 1549-1550
24. Seyed-Bolorforosh MS, 'Novel integrated impedance matching layer', IEEE Trans UFFC, Vol 42(5), pp 809-811
25. Schoenwald JS and Martin JF, 'PVF_2 transducers for acoustic ranging and imaging in air', IEEE US Symp 1983, pp 577-580
26. Fiorillo A, 'Design and characterisation of a PVDF ultrasonic range sensor', IEEE Trans UFFC, Vol 39(6), 1992, pp 688-692
27. Fiorillo A, 'Layered PVDF transducers for in-air US applications', IEEE US Symp 1993, pp 663-666
28. Capineri L, Fiorillo AS, Masotti L and Rocchi S, 'Array of PVDF sensors for ultrasonic imaging in air', IEEE US Symp 1994, Cannes, pp 487-490
29. Hutchins DA, 'Ultrasonic generation by pulsed lasers', Physical Acoustics, edited by WP Mason and RN Thurston, (Academic Press, New York, 1988), VolXVIII, pp 21-123
30. Davies SJ, Edwards C, Taylor GS and Palmer SB, 'Laser-generated ultrasound : its properties, mechanisms and multifarious applications', Journal of Physics D : Applied Physics, Vol 26, 1993, pp 329-348
31. Wagner JW, 'Optical detection of ultrasound', Physical Acoustics, edited by WP Mason and RN Thurston, (Academic Press, New York, 1990), VolXIX, pp 201-266
32. Monchalin JP, "Optical detection of ultrasound", IEEE Trans. UFFC, Vol 33, 1986, pp 485-499
33. Huber RD and Green RE, 'Noncontact acousto-ultrasonics using laser generation and laser interferometric detection', Materials Evaluation, Vol 49(5), 1991, pp

613-618

34. Monchalin JP, 'Progress towards the application of laser-ultrasonics in industry', Review of Progress in QNDE, Vol 12A, edited by Thomson DO and Chimenti DE, Plenum Press, New York, 1993, pp 495-506

35. Dewhurst RJ, He R and Qing S, 'Defect visualisation in carbon fiber composite using laser ultrasound', Materials Evaluation, Vol 51(8), 1993, pp 935-940

36. Wagner JW, Deaton JB, Spicer JB and McKie ADW, 'Laser generation of narrowband and directed ultrasound for noncontact ultrasonic testing', IEEE US Symp 1990, pp 661-665

37. Yang J, DeRidder N, Ume C and Jarzynski J, 'Non-contact optical fibre phased array generation of ultrasound for non-destructive evaluation of materials and processes', Ultrasonics, Vol 31(6), 1993, pp 387-394

38. Hoyes JB, Shan Q and Dewhurst RJ, 'A non-contact scanning system for laser ultrasonic defect imaging', Meas Sci Tech, Vol 2, 1991, pp 628-634

39. McKie ADW, McKie DW and Addison RC, 'Practical considerations for the rapid inspection of composite-materials using laser-based ultrasound', Ultrasonics, Vol 32(5), 1994, pp 333-345

40. Schindel DW, Hutchins DA, Zou 1 and Sayer M, 'The design and characterisation of micromachined air-coupled capacitance transducers', IEEE Trans UFFC, Vol 42(1), 1995, pp 42-50

41. Carr H and Wykes C, 'Diagnostic measurements in capacitive transducers', Ultrasonics, Vol 31(1), 1993, pp 13-20

42. Mattila P, Tsuzuki F, Väätäjä H and Sasaki K, 'Electroacoustic model for electrostatic ultrasonic transducers with v-grooved backplates', IEEE Trans UFFC, Vol 42(1), 1995, pp 1-7

43. Adamowski JC, Silva ECN, Simon C, Buiochi F and Higuti RT, 'Finite element modelling of an ultrasonic capacitive transducer', IEEE US Symp 1994, Cannes, pp 1261-1264

44. Haller MI and Khuri-Yakub BT, 'A surface micromachined electrostatic ultrasonic air transducer', IEEE Trans UFFC, Vol43(1), 1996, pp 1-6

45. Anderson MJ, Hill JA, Fortunko CM, Dogan NS and Moore RD, 'Broadband

electrostatic transducers: modelling and experiments', JASA, Vol 97(1), 1995, pp 262-272

46. Rafiq M and Wykes C, 'The performance of capacitive ultrasonic transducers using v-grooved backplates', Meas Sci Tech, Vol 2, 1991, pp 168-174

47. Suzuki K, Higuchi K and Tanigana H, 'A silicon electrostatic ultrasonic transducer', IEEE Trans UFFC, Vol 36(6), 1989, pp 620-627

48. Hutchins DA, Bashford AG, Wright WMD and Schindel DW, 'Advances in wide bandwidth air-coupled capacitive transducers', IEEE US Symp 1995, Seattle, 981-984

49. Hutchins DA, Wright WMD and Schindel DW, 'Ultrasonic measurements in polymeric materials using air-coupled capacitance transducers', JASA, Vol 96(3), 1994, pp 1634-1642

50. Schindel DW and Hutchins DA, 'Applications of micromachined capacitance transducers in air-coupled and nondestructive evaluation', IEEE Trans UFFC, Vol 42(1), 1995, pp 51-58

51. Ladabaum I, Khuri-Yakub and Spoliansky, 'Micromachined ultrasonic transducers : 11.4MHz transmission in air and more', Applied Physics Letters, Vol 68(1), 1996, pp 7-9

52. Bond LJ, Chiang CH and Fortunko CM, 'Absorption of ultrasonic waves in air at high frequencies (10-20MHz)', JASA, Vol 92(4), 1992, pp 2006-2015

53. Luukkala M and Meriläinen P, 'Metal plate testing using airborne ultrasound', Ultrasonics, Vol 11, 1973, pp 218-221

54. Schindel DW and Hutchins DA, 'Through-thickness characterisation of solids by wideband air-coupled ultrasound', Ultrasonics, Vol 33(1), 1995, pp 11-17

55. Möckl T, Mágori V and Eccardt C, 'Sandwich-layer transducer - a versatile design for ultrasonic transducers operating in air', Sensors and Actuators A-Physical, Vol 21-23, 1990, pp 687-692

56. Ermert H, Schmokle J and Weth G, 'An adaptive ultrasonic sensor for object identification', IEEE US Symp 1986, pp 555-558

57. Manthey W, Kroemer N and Mágori V, 'Ultrasonic transducers and transducer arrays for applications in air', Meas Sci Tech, Vol 3, 1992, pp 249-261

58. Smith WA and Auld BA, 'Modelling 1-3 composite piezoelectric : thickness mode oscillations', IEEE Trans UFFC, Vol 38, 1990, pp 40-47

59. Hayward G and Gorfu Y, 'Performance assessment of ultrasonic NDT through an intermediate airgap' RAE Farnborough MOD Contract 2065/058, 1988

60. Reilly D and Hayward G, 'Through air transmission for ultrasonic non-destructive testing', IEEE US Symp 1991, pp 763-766

61. Farlow R and Hayward G, 'An automated ultrasonic NDT scanner employing advanced air-coupled 1-3 connectivity composite transducers', Insight, Vol 38(1), pp 41-50

62. Kelly SP, Farlow R and Hayward G, 'Applications of through-air ultrasound for rapid NDE scanning in the aerospace industry', IEEE Trans UFFC, Vol 43(4), 1996, pp 581-591

63. Thomson RB, 'Physical principles of measurement with EMAT transducers', Physical Acoustics, edited by WP Mason and RN Thurston, (Academic Press, New York, 1990), Vol XIX, pp 179-275

64. Maxfield BW, Kuramoto A and Hulbert JK, 'Evaluating EMAT designs for selected applications', Materials Evaluation, Vol 45(10), 1987, pp 1166-1183

65. Hirao M, Ogi H and Fukouka H, 'Resonance EMAT system for acoustoelastic stress measurement in sheet metals', Review of Scientific Instruments, Vol 64(11), 1993, pp 3198-3204

66. Wang Z, Zhang S and Lu Z, 'High frequency photoacoustic measurements in air', Science in China (Series A), Vol 34(10), 1991, pp 1273-1280

67. Hutchins DA, Wright WMD, Hayward G and Gachagan A, 'Air-coupled piezoelectric detection of laser generated ultrasound', IEEE Trans UFFC, 1994, Vol 41(6), pp 796-805

68. Wright WMD, Hutchins DA, Gachagan A and Hayward G, 'Evaluation of fiber-reinforced composites using a non-contact laser/air-transducer system', Review of Progress in QNDE, Vol 14(B), Plenum Press, New York, edited Thomson DO and Chinemti DE, 1994, pp 1333-1340

69. Gachagan A, Hayward G, Wright WMD and Hutchins DA, 'Air-coupled piezoelectric detection of laser generated ultrasound', IEEE US Symp 1993,

Baltimore, pp 651-654

70. Wright WMD, Schindel DW and Hutchins DA, 'Studies of laser-generated ultrasound using a micromachined silicon electrostatic transducer in air', JASA, Vol 95(5), 1994, pp 2567-2575

71. Taylor GS, Hutchins DA and Palmer SB, 'Non-contact ultrasonic inspection of diffusion bonds in Titanium', IEEE US Symp 1989, pp 1113-1115

72. Edwards C, Nurse G, Palmer SB and Dewhurst RJ, 'An integrated optical fibre-EMAT device for applications in ultrasonic NDT', British Journal of NDT, Vol 32(2), 1990, pp 76-78

73. Hutchins DA, Jansen DP and Edwards C, 'Lamb-wave tomography using non-contact transduction', Ultrasonics, 1993, Vol 31(2), pp 97-103

74. Safaeinili A, Lobkis OI and Chimenti DE, 'Air-coupled ultrasonic estimation of viscoelastic stiffness in plates', IEEE Trans UFFC, Vol 43(6), 1996, pp 1171-1179

75. Hutchins DA and Schindel DW, 'Advances in non-contact and air-coupled transducers', IEEE US Symp, 1994, Cannes, pp 1245-1254

76. Grandia WA and Fortunko CM, 'NDE applications of air-coupled ultrasonic transducers', IEEE US Symp, 1995, Seattle

77. Hossack JA, 'Modelling techniques for 1-3 composite transducers', Phd Thesis, University of Strathclyde, 1990

78. Ting RY, 'Composite piezoelectric materials for transduction', Applied Acoustics, Vol 41(4), 1994, pp 325-335

79. Smith WA, 'Composite piezoelectric materials for medical ultrasonic imaging transducers - A review', Proceedings of the 6th IEEE International Symposium on Applications of Ferroelectrics, 1986, pp 249-256

80. Hall DDN, Hayward G and Gorfu Y, 'Theoretical and experimental evaluation of 2-dimensional composite matrix array', IEEE Trans UFFC, Vol 40(6), 1993, pp 704-709

81. Hayward G, Pearson J and Stirling G, 'An intelligent ultrasonic inspection system for flooded member detection in offshore structures', IEEE Trans UFFC, Vol 40(5), 1993, pp 512-521

82. Yi-quan Y, 'The performance and applications of PZT composite transducer with 3-3 connectivity', IEEE Trans UFFC, Vol 38(6), 1991, pp 712-714

83. Smith WA, Shaulov A and Auld BA, 'Tailoring the properties of composite piezoelectric materials for medical ultrasound transducers', IEEE US Symp, 1985, pp 642-647

84. Hossack J and Hayward G, 'Finite element analysis of 1-3 composite transducers', IEEE Trans UFFC, Vol 38(6), 1991, pp 618-629

85. Hayward G and Hossack J, 'Unidimensional modelling of 1-3 composite transducers', JASA, Vol 88(2), 1990, pp 599-608

86. Hayward G, MacLeod CJ and Durrani TS, 'A systems model of the thickness mode piezoelectric transducer', JASA, 1984, Vol 76(2), pp 369-382

87. Hayward G and Bennett J, 'Assessing the influence of pillar aspect ratio on the behaviour of 1-3 connectivity composite transducers', IEEE Trans UFFC, Vol 43(1), 1996, pp98-108

88. Savakus HP, Klicker KA and Newnham RE, 'PZT epoxy piezoelectric transducers : a simplified fabrication process', Materials Research Bulletin, Vol 16, 1980, pp 667-680

89. Bowen LJ, Gentelman RL, Pham HT, Fiore DF and French KW, 'Injection-moulded fine-scale piezoelectric composite transducers', IEEE US Symp 1993, pp 499-503

90. Lubitz K, Wolff A and Preu G, 'New piezoelectric composites for ultrasonic transducers', Ferroelectrics, Vol 133, 1992, pp 21-26

91. Erikson KR, 'Tone-burst testing of pulse echo transducers', IEEE Transactions on Sonics and Ultrasonics, Vol SU-26(1), Jan 1979, pp 7-14

92. Miller EB and Eitzen DG, 'Ultrasonic characterisation at the NBS', IEEE Transactions on Sonics and Ultrasonics, Vol SU-26(1), Jan 1979, pp 28-36

93. Pedersen PC, Lewin PA and Bjørnø L, 'Application of time-delay spectrometry for calibration of ultrasonic transducers', IEEE Transactions on Sonics and Ultrasonics, Vol 35(2), March 1988, pp 185-205

94. Fay B and Reinmann H-P, 'Reciprocity calibration of ultrasonic contact transducers', IEEE Trans. UFFC, 41(1), 1994, pp 123-129

95. Simmons JA, Turner CD and Wadley HNG, 'Vector calibration of ultrasonic and acoustic emission transducers', JASA, 82(4), 1987, pp 1122-1130

96. Damion JP, 'Means of dymanic calibration for pressure transducers', Metrologia, Vol30(6), 1994, pp 743-746

97. Wang T, Cheung F and Butera M, 'An automated digital beam profile system for ultrasonic transducer characterisation', NDT&E International, Vol 25(4-5), 1992, pp 171-176

98. Hientanen J and Oksanen M, 'Photoacoustic testing of ultrasonic air transducers', Meas Sci and Tech, Vol 5, 1994, pp 960-963

99. Hutchins DA and Hayward G, 'Radiated fields of ultrasonic transducers', Physical Acoustics, Vol XIX, Academic Press, 1990, pp 1-80

100. Bacon DR, 'Characterisation of a PVDF membrane hydrophone for use in the Range 1-100MHz', IEEE Transactions on Sonics and Ultrasonics, Vol SU-29(1), Jan 1982, pp 18-25

101. Membrane Hydrophone Calibration Datasheet, Y34-6543, GEC-Marconi Research Centre, Chelmsford, England, 1993

102. Hayward G, 'The influence of pulser parameters on the transmission response of piezoelectric transducers', Ultrasonics, Vol 23(3), May 1985, pp 103-112

103. Kino GS, 'Acoustic Waves', Prentice Hall, pp 557

104. Wurster C, Staudenraus J and Eisenmenger W, 'The fibre optic hydrophone', Proc IEEE US Symp, 1994, Cannes, Vol 2, pp 941-944

105. Galbraith W, Hayward G and Benny G, 'Development of a PVDF membrane hydrophone for use in air-coupled ultrasonic transducer calibration', Proc IEEE US Symp, 1996, San Antonio, Vol 2, pp 917-920

106. Krautkrämer J and Krautkrämer H, 'Ultrasonic tesing of materials', Fourth fully revised edition, Springer-Verlag, 1990, pp 70-76

107. Stepanishen P.R., 'Transient Radiation from pistons in an infinite planar baffle', JASA, 49(5), 1971, pp 1629-1638

108. Smith RA and Bacon DR, 'A multiple-frequency hydrophone calibration technique', JASA, Vol 85(5), 1990, pp 2231-2243

109. Hayward G, 'Using a block diagram approach for the evaluation of electrical

loading effects on piezoelectric reception', Ultrasonics, Vol 24(3), 1986, pp 156-163

110. Montgomery CG, 'Technique of microwave measurements', McGraw-Hill Book Company, New York and London, 1947

111. Selfridge AR, 'The design and fabrication of ultrasonic transducers and transducer arrays', PhD Thesis, Stanford University, 1982

112. Hayward G, Bennett J and Hamilton R, 'A theoretical study on the influence of some consituent material properties on the behaviour of 1-3 connectivity composite transducers', JASA, 1995, Vol 98(4), pp 2187-2196

113. Swanson Analysis Systems, 'ANSYS User's Manual for Revision 5.0 Vol III : Elements', DN-R300:50-3, Dec 1992

114. Bennett JT, 'Development of finite element modelling system for 1-3 piezocomposites', Phd Thesis, University of Strathclyde, 1995

115. Selfridge AR, 'Approximate material properties in isotropic materials', IEEE Transactions on Sonics and Ultrasonics, Vol SU-32(3), 1985, pp 381-394

116. Fisons Apparatus Catalogue 1993, Whatman Scientific Ltd, Maidstone, U.K.

117. Gururaja TR, Schulze WA, Cross LE, Newham RE, Auld BA and Wang YJ, 'Piezoelectric composite materials for ultrasonic transducer applications. Part I: Resonant modes of vibration of PZT rod-polymer composites', IEEE Transactions on Sonics and Ultrasonics, Vol SU-32(4), July 1985, pp 481-498

118. Auld BA and Wang YJ, 'Acoustic wave vibrations in periodic composite plates', Proc IEEE US Symp, Dallas, 1984, pp 528-532

119. Auld BA, 'Waves and vibrations in periodic piezoelectric composite materials', Materials Science and Engineering, Vol A122, 1989, pp 65-70

120. Chan HLW, Unsworth J and Bui T, 'Mode coupling in modified lead titanate/polymer 1-3 composites', Journal of Applied Physics, Vol 65(4), 1989, pp 1754-1758

121. Hossack JA, Auld BA and Batha HD, 'Techniques for suppressing spurious resonant modes in 1:3 composite transducers', Proc IEEE US Symp, 1991, pp 651-655

122. Sherrit S, Wiederick HD, Mukherjee BK and Prasad SE, 'Stree isolation in PZT-

air composites', Ferroelectrics, Vol 132, 1992, pp 61-68

123. Oakley C and Marsh P, 'Development of 1-3 ceramic-air composite transducers', New Developments in Ultrasonic Transducers and Transducer Systems, 1992, Ch. 29, pp 272-283

124. Bui T, Chan HLW and Unsworth J, 'Development of a multifrequency ultrasonic transducer using PZT/polymer 1-3 composite', Ferroelectrics Letters, Vol 10, 1989, pp 97-106

125. Kossoff G, 'The effects of backing and matching on the performance of piezoelectric ceramic transducers', IEEE Transactions on Sonics and Ultrasonics, Vol SU-13(1), 1966, pp 20-30

126. Desilets CS, Fraser JD and Kino GS, 'The design of efficient broad-band piezoelectric transducers', IEEE Transactions on Sonics and Ultrasonics, Vol SU-25(3), 1978, pp 115-125

127. Hutchins DA and Macphail JP, 'A new design of capacitive transducer for ultrasonic displacement detection', Journal of Physics E : Science and Instrumentation, Vol 18, 1985, pp 69-72

128. Perrot P, 'Deconvolution of Ultrasonic Signals', Internal Report, University of Strathclyde, March 1994

129. Hayward G and Lewis J, "Comparison of some non-adaptive deconvolution techniques for resolution enhancement of ultrasonic data", Ultrasonics, Vol 27, pp 155-164 (1989)

130. B Widrow and SD Stearns, "Adaptive Signal Processing", Englewood Cliffs, New Jersey, Prentice Hall, 1985

131. Wiggins RA, 'Minimum entropy decovolution (MED)', Geophysical Exploration, Vol 16(1), 1978, pp 21-35

132. Hayward G, Hamilton R, Kanani B and Reilly DA, 'A thin film technique for spatial apodisation of disk-shaped piezoceramic transducers', JASA, Vol 89(4), 1991, pp 1808-1815

133. ANSI S1.26-1978, 'American national standard method for the calculation of the absorption of sound by the atmosphere', American National standards Institute, New York, 1978

134. Bass HE, Sutherland LC and Zuckerwar AJ, 'Absorption of sound by the atmosphere : Update', JASA, 1990, Vol 88(4), pp 2019-2021

135. Bass HE, Sutherland LC, Zuckerwar AJ, Blackstock DT and Hester DM, 'Absorption of sound by the atmosphere : Further developments', JASA, 1995, Vol 97(1), pp 680-683

136. Bass HE, Sutherland LC, Zuckerwar AJ, Blackstock DT and Hester DM, 'Erratum : Absorption of sound by the atmosphere : Further developments', JASA, 1996, Vol 99(2), pp 1259

137. Widrow B, "Adaptive noise cancelling: Principles and Applications", Proc. IEEE, Vol 63, 1972, pp 926-935

APPENDIX A

Material Parameters

A detailed description of the physical properties of the materials used for this Thesis is presented. This Appendix is divided into four categories : piezoceramic, polymer and mechanical matching/damping materials and load media.

Piezoceramic Materials

The piezoceramic parameters utilised in this Thesis are defined in Table A-1. The ceramics were used for both finite element analysis and linear systems modelling and a comprehensive inventory of parameters are shown. The ceramics were supplied by Morgan-Matroc and the Table presents the manufacturers specified properties. All piezoceramic used has been tested according to the IEEE standard [1] and rejected, if the properties deviated by more than 10% from manufacturers specifications.

Polymer Materials

Two types of polymer material are specified in Table A-2, the piezoelectric Polyvinylene-Flouride and passive filler materials used in the manufacture of 1-3 connectivity composites. The uni-axially poled piezopolymer was used only with the linear systems model and hence, only the equivalent thickness mode parameters, calculated from the manufacturers specifications, are presented here. The parameters for the filler materials have been measured experimentally, or derived from experimental figures. The epoxies are produced by combining a specified ratio of epoxy resin and hardener and consequently, accurate measurement and thorough mixing of these constituent materials is essential. The final product may vary in every case, but during manufacture care was taken to follow the supplier's instructions precisely and a 10% tolerance in these parameters was observed.

Matching / Backing Materials

The materials described here, in Table A-3, can be split into two categories, those used in either the experimental or simulated phases. The properties for the experimental materials, numbers 1-5, have been calculated from velocity and density measurements to enhance the accuracy of the modelling. Whereas, parameters for materials 6 and 7 have been extracted from Selfridge [115]. Data for materials 8 and 9 were estimated using standard theory.

Load Media

Two load media were used in this Thesis, as detailed in Table A-4, : air and water. Water loading was employed on several occasions in order to validate the modelling before extending the theory into an air environment. The properties for water are extracted from Kino [103] and standard conditions of temperature, 20°C, and pressure, 1.013×10^5Pa, are assumed. In an airborne environment there is a requirement to ensure consistency, with regard to air temperature, pressure and humidity [3]. Variations in these parameters result in different values for principally both sound velocity and attenuation. Hence, all experiments were performed in a constrained environment at standard atmospheric pressure, where the temperature was maintained around 20°C and relative humidity remained reasonably constant around 40%.

Material	Compliance, s_{ij}^E, and stiffness, c_{ij}^E, under constant electric field												Loss coefficients	
	s_{11}^E	s_{12}^E	s_{13}^E	s_{33}^E	s_{44}^E	s_{66}^E	c_{11}^E	c_{12}^E	c_{13}^E	c_{33}^E	c_{44}^E	c_{66}^E	$tan\delta$	Q_m
PZT5A	16.4	-5.74	-7.22	18.8	47.5	44.3	12.1	7.54	7.52	11.1	2.11	2.26	0.02	75
PZT5H	10.7	-3.2	-4.6	13.9	39.5	29.7	14.8	7.62	7.42	13.1	2.53	3.37	0.02	65

Material	Piezoelectric Coefficients, d_{ij}, e_{ij} and h_{ij}									Dielectric Constants, ε_{ij} (T-constant stress ; S - constant strain)				Density
	d_{31}	d_{33}	d_{15}	e_{31}	e_{33}	e_{15}	h_{31}	h_{33}	h_{15}	$\varepsilon_{11}^T/\varepsilon_o$	$\varepsilon_{33}^T/\varepsilon_o$	$\varepsilon_{11}^S/\varepsilon_o$	$\varepsilon_{33}^S/\varepsilon_o$	ρ
PZT5A	-171	374	584	-5.4	15.8	12.3	-7.3	21.5	15.2	1730	1700	916	830	7750
PZT5H	-274	593	741	-6.5	23.3	17.0	-5.0	18.0	11.3	3130	3400	1700	1470	7500

Units :
- s_{ij}^E : $10^{-12}m^2/N$
- c_{ij}^E : $10^{10}N/m^2$
- d_{ij} : $10^{-12}C/N$
- e_{ij} : C/m
- h_{ij} : $10^8V/m$
- ε_o : dielectric constant of free space, 8.85×10^{-12} F/m
- ρ : Kg/m^3

Table A-1 Properties of piezoceramic materials

Materials	Dielectric Constant $\varepsilon_{33}/\varepsilon_o$	Youngs Modulus Y	Poisson Ratio, σ	Density ρ	Elastic Stiffness C_{33}^D	Piezoelectric constant h_{33}	Acoustic Impedance Z_{AC}	Attenuation α
CIBA-GEIGY CY1301/HY1300	4.0	4.1	0.37	1132	7.177	0	2.85	1.25
CIBA-GEIGY CY208/HY956	4.0	1.8	0.41	1180	4.125	0	2.23	1.5
Polyvinylene Flouride (PVDF)	8.4	N/A	N/A	1760	8.713	2.045	3.92	6.5

Units :
- ε_o : dielectric constant of free space, 8.85 x 10^{-12} F/m
- Y : x 10^9 N/m^2
- ρ : kg/m^3
- C_{33}^D : x 10^9 N/m^2
- h_{33} : x 10^9 V/m
- Z_{AC} : MRayl
- α : dB/cm @ 1MHz

Note : N/A : Material parameters are not required for linear systems model

Table A-2 Properties of selected polymers

Material	Nemonic	Number	Z (MRayl)	C_{33}^{D} (x10^9) (Nm^{-2})	ρ (kgm^{-3})	c (ms^{-1})	α ($dBcm^{-1}$)	Y (x10^9) (Nm^{-2})	σ
CY208/HY956	SS	1	2.23	4.215	1180	1890	1.5	1.806	0.41
CY1301/HY1300	HS	2	2.85	7.177	1132	2520	1.25	4.056	0.37
Perspex	PX	3	3.29	9.1154	1188	2770	0.75	5.926	0.34
Silicone Rubber	SR	4	1.05	1.053	1053	1000	5	0.4212	0.42
Membrane Filter	MF	5	0.5125	0.6406	410	1250	2.5	0.2563	0.42
Tracon 401ST	TR	6	4.81	14.29	1620	2970	2.5	10.00	0.32
Epon	EP	7	3.4	9.691	1210	2830	1.25	6.008	0.35
optimum layer #1	O1	8	0.1	0.05	200	500	2.5	0.0113	0.45
optimum layer #2	O2	9	0.07	0.0365	180	450	3.0	0.00866	0.45

Table A-3 Properties of materials used as mechanical matching layers and backing blocks

Load Media	Density, ρ, Kg/m^3	Velocity, *c*, m/s	Acoustic Impedance, *Z*, MRayl
Air, @20°C	1.24	343	4.26×10^{-4}
Water	1000	1483	1.483

Table A-4 Properties for ultrasound propagation channels

APPENDIX B

Linear Systems Model Theory

The Linear Systems Approach

The methodology utilised for the uni-dimensional modelling employed throughout this Thesis represents the primary and secondary piezoelectric mechanisms in a block diagram format [86]. This approach presents a physically meaningful tool through which analysis of the transducer behaviour can be predicted. This modelling technique has the facility to investigate the influence of electrical stimulation in transmission, electrical loading in reception and the inclusion of mechanical matching and/or damping, to predict impedance, transmission, reception and pulse-echo characteristics for piezoceramic, piezocomposite and piezopolymer transducer performance as a function of the operating environment. Hence, the model can be used to produce transducer characteristics such as centre frequency, bandwidth and sensitivity and present this information as either the time or frequency domain plots. The following sections will describe the block diagram approach for both transmission and reception modes of operation, where the relevant symbol list is given below :

C_0 Transducer static capacitance

h Piezoelectric charge constant

K_B Back face reverberation factor

K_F Front face reverberation factor

R_B Back face reflection coefficient (force)

R_F Front face reflection coefficient (force)

T Transit time for mechanical waves to cross the transducer thickness

T_B Back face transmission coefficient (force)

T_F Front face transmission coefficient (force)

Z_C Specific acoustic impedance of transducer

Z_1 Specific acoustic impedance of front face medium

Z_2 Specific acoustic impedance of rear face medium

The Piezoelectric Transmitter

The basic configuration for the transmission model is illustrated in Figure B.1. Here the transducer electrical load is represented by the lumped impedance Z_E, which is connected across the terminals of the transducer. The transducer is driven by a non ideal voltage source, e, having an output impedance, Z_O. F_F relates to the force generated at the transducer front face.

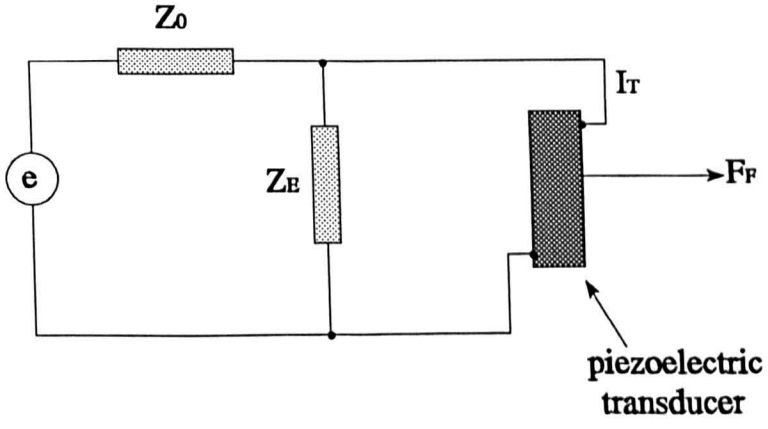

Figure B.1 Basic configuration for the transmit model

The relationship between the output force and the excitation voltage may be expressed as a Laplace transfer function, as shown in Equation B.1 [102]. The bar symbol denotes Laplace transformation.

$$\frac{\overline{F_F}}{\overline{e}} = \frac{-hC_O\overline{Z_I}\overline{K_F}A_F/2}{1-k^2\overline{Z_F}(\overline{K_F}T_F/2+\overline{K_B}T_B/2)/sT} \qquad \textbf{(B.1)}$$

where :

$$\overline{Z_I} = \overline{Z_E}/(\overline{Z_O}+\overline{Z_E}+\overline{Z_O}\,\overline{Z_E}\,s\,C_O)$$

$$\overline{Z_F} = (\overline{Z_E}+\overline{Z_O})/(\overline{Z_O}+\overline{Z_E}+\overline{Z_O}\,\overline{Z_E}\,s\,C_O)$$

$$\overline{K_F} = (1-e^{-sT})(1-R_B\,e^{-sT}) / (1-R_F R_B\,e^{-2sT})$$

$$\overline{K_B} = (1-e^{-sT})(1-R_F\,e^{-sT}) / (1-R_F R_B\,e^{-2sT}) \qquad \textbf{(B.2)}$$

$$T_F = 2\,Z_C / (Z_C+Z_1)$$

$$T_B = 2\,Z_C / (Z_C+Z_2)$$

$$A_F = 2\,Z_1 / (Z_C+Z_1)$$

$$R_F = (Z_C-Z_1) / (Z_C+Z_1)$$

$$R_B = (Z_C-Z_2) / (Z_C+Z_2)$$

The mechanical reverberation factors, at the transducer front and rear faces, are represented by K_F and K_B respectively. Transmission and reflection coefficients for waves of force at the front and rear faces are represented by the terms T_F, T_B, A_F, R_F and R_B respectively.

Using the positive feedback transfer function shown in Equation B.1, a systems feedback configuration can be described in block diagram format. This approach is illustrated in Figure B.2.

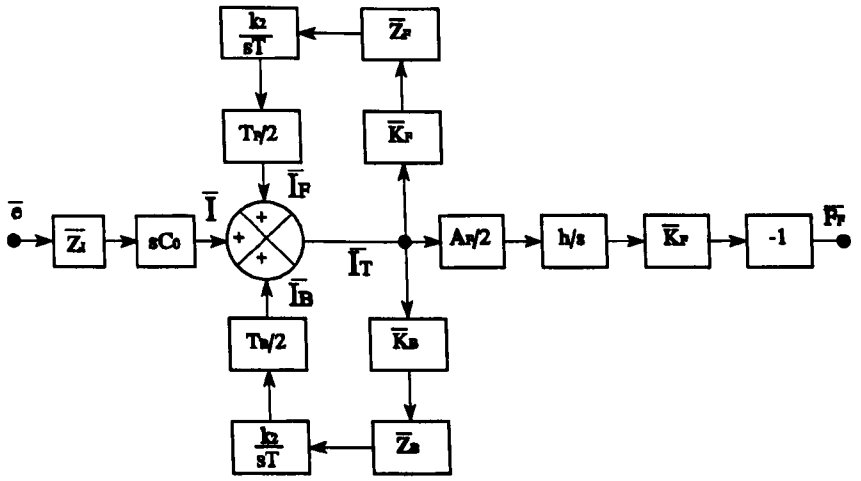

Figure B.2 Block diagram system feedback model in transmission

Secondary feedback mechanisms are described by the front and rear feedback loops and their associated secondary currents, I_F and I_B, respectively. The total current flowing through the transducer, I_T, comprises the vector sum of the two secondary currents and the current, I, flowing through the transducer static capacitance, C_O. From Figure B.2 it can be seen that in addition to the piezoelectric properties of the transducer, the transmitted wave force is highly dependent on both electrical and mechanical loading factors. The electrical load directly influences the output force via the forward loop parameter, Z_I, which is dependent on the exact form of generator, Z_E, and coupling , Z_O, impedances, shown in Figure B.1. The front and rear reflection coefficients, R_F and R_B respectively, and hence, the reverberation factors, K_F and K_B, are dependant upon the mechanical load conditions. The amount of feedback can also be seen to be directly proportional to the square of the coupling coefficient and inversely proportional to frequency. Under conditions of zero feedback, the transducer impedance is represented electrically as a pure capacitance of value C_O.

The Piezoelectric Receiver

The complex electromechanical operation of a piezoelectric reception element has been successfully analysed using a physically meaningful block diagram format [109]. This approach is illustrated in Figure B.3 and demonstrates the factors which influence both primary and secondary piezoelectric action. This representation follows the piezoelectric action after the front face of the transducer has been subject to an incident force, F_I, and develops a voltage, V_0, across a load Z_E, as shown in Figure B.4. The primary piezoelectric action combines the transmission coefficient at the transducer front face (T_F), the transduction transfer block (h/sZ_C), mechanical reverberation factor at the front face (K_F), the forward loop voltage attenuation factor (U) and phase inversion at the transducer front face (-1). The secondary piezoelectric mechanism are represented by positive feedback loops, from the transducer front and rear faces. This secondary action combines the mechanical reverberation factor (K_F and K_B), external loading effects (Z_F and Z_B), electromechanical coupling (k^2/sT) and the transmission coefficients (T_F and T_B). The external loading effects, Z_F and Z_B, are critical to the secondary regeneration due to the influence of the finite electrical load, Z_E. Here, under open circuit conditions, $Z_E \rightarrow \infty$, no current can flow and consequently, no secondary piezoelectric action is produced.

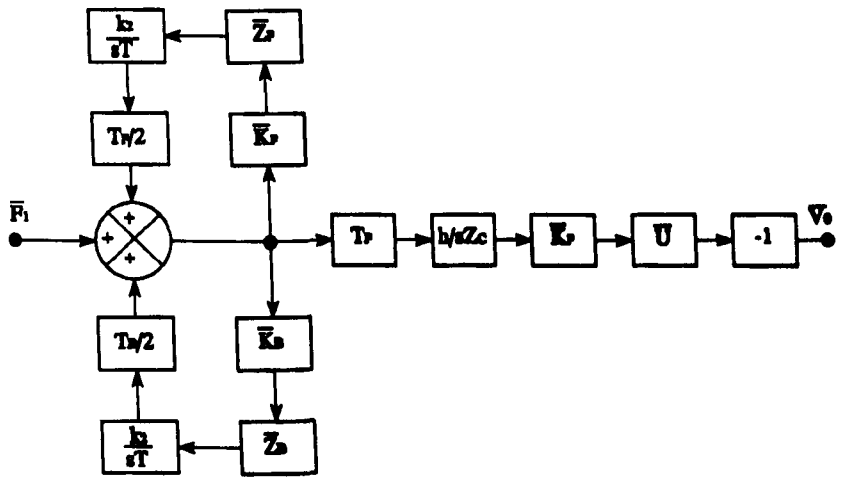

Figure B.3 Block diagram representation of the piezoelectric receiver

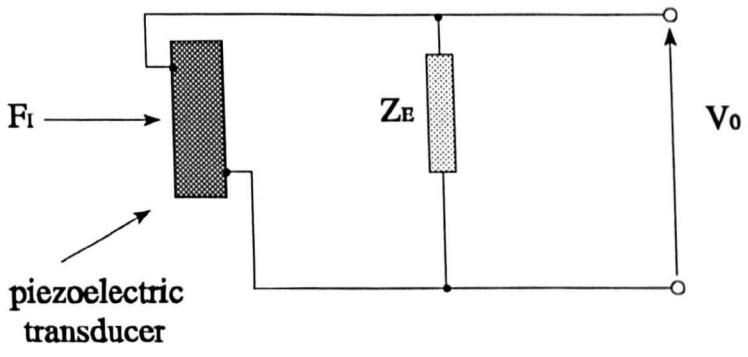

Figure B.4 Basic transducer configuration in reception

The Laplace transfer function relating the received voltage, V_0, to the excitation force is given in Equation B.1.

$$\frac{\overline{V_0}}{\overline{F_1}} = \frac{-hT_F\overline{K_F}\,\overline{U}/sZ_C}{1-\overline{Z_F}(\overline{K_F}T_F/2+\overline{K_B}T_B/2)k^2/sT} \qquad \textbf{(B.1)}$$

The primary piezoelectric mechanism is fully described in the following Equations B.2:

$$T_F = 2Z_C/(Z_C+Z_1)$$

$$K_F = (1-e^{-sT})(1-R_B e^{-sT})/(1-R_F R_B e^{-2sT}) \qquad \textbf{(B.2)}$$

$$\overline{U} = sC_0\overline{Z_E}/(1+sC_0\overline{Z_E})$$

The positive feedback mechanisms from the front face use the same formulae as described for the primary actions. The secondary action from the rear face of the transducer are described by the following Equations B.3 :

$$K_B = (1 - e^{-sT})(1 - R_F e^{-sT}) / (1 - R_F R_B e^{-2sT})$$

$$T_B = 2Z_C / (Z_C + Z_2) \qquad \textbf{(B.3)}$$

$$\overline{Z_F} = \overline{Z_B} = 1 / (1 + sC_0 \overline{Z_E})$$

The reverberation factors are each dependant upon the reflection coefficients from the front face (R_F) and rear face (R_B) of the transducer. Equations B.4 and B.5 describe the formulae for each reflection coefficient.

$$R_F = (Z_C - Z_1) / (Z_C + Z_1) \qquad \textbf{(B.4)}$$

$$R_R = (Z_C - Z_2) / (Z_C + Z_2) \qquad \textbf{(B.5)}$$

APPENDIX C

Airborne Attenuation Theory

The absorption of acoustic energy in air is of critical importance in the design of an air-coupled ultrasonic system. The attenuation in air is particularly high at ultrasonic frequencies and therefore, must be incorporated into the design process. Bass et al presented a comprehensive analysis of the fundamental mechanisms through which airborne attenuation is realised [3]. This work collated previous publications in this field, including the ANSI Standard [133]. Since the initial publication in 1985, Bass et al have published three updates, through which several corrections have been presented [134, 135, 136]. These further developments have been included into the software models utilised for this Thesis. The following work will describe the approach adopted, for this Thesis, to predict the influence of airborne attenuation.

Air is a mixture of several gases (oxygen, nitrogen, water vapour, carbon dioxide, etc.) and hence, prediction of attenuation is a complex process. There are two fundamental attenuation mechanisms : "classical" losses (associated with the conversion of kinetic, acoustic energy into thermal energy by viscous and thermal conduction processes) and "relaxation" losses (related to the redistribution of internal, rotational and vibrational energy in the molecules) [3]. A further classification enables the dependence of each loss mechanism on the individual gas components for air. Both classical and rotational losses are dependant upon the overall properties of the air medium and are computed from values for pressure, temperature and frequency. Vibrational loss mechanisms are dependant upon the individual gas components and therefore, must be considered separately. Many of the vibrational loss mechanisms are insignificant and Bass et al have incorporated only the losses from oxygen and water. The overall air attenuation factor is calculated from the sum of these individual components.

The following parameters are required in order to calculate the air attenuation factor, as described in Equations C.1 - C.5 :

T temperature (K)

T_0 reference temperature (293.15K)

P pressure (Nm^{-2})

P_0 standard pressure (1.01325×10^5 Nm^{-2})

f frequency (Hz)

h_r relative humidity (%)

The classical and rotational attenuation components are combined, α_{cr}, and calculated as shown in equation C.1 :

$$\alpha_{cr} = 1.84e^{-11} f^2 (P/P_0) (\sqrt{T/T_0}) \qquad \textbf{(C.1)}$$

The vibrational losses are calculated for both oxygen, $\alpha_{vib,O}$, and nitrogen, $\alpha_{vib,N}$ as follows :

$$\alpha_{vib,O} = f^2 (T_0/T)^{5/2} (1.275e^{-2} \frac{e^{-2239.1/T}}{f_{r,O} + (f^2/f_{r,O})})$$

$$\alpha_{vib,N} = f^2 (T_0/T)^{5/2} (1.068e^{-1} \frac{e^{-3352/T}}{f_{r,N} + (f^2/f_{r,N})}) \qquad \textbf{(C.2)}$$

where $f_{r,O}$ and $f_{r,N}$ are the oxygen and nitrogen relaxation frequencies (Hz) and are calculated as shown in Equation C.3 :

$$f_{r,O} = (P/P_0) (24 + (4.04e^4 h (\frac{0.02+h}{0.391+h})))$$

$$f_{r,N} = (P/P_0) (\sqrt{T_0/T}) (9 + (280 h e^{-4.17((T_0/T)-1)^{1/3}})) \qquad \textbf{(C.3)}$$

The water mole fraction, h (%), is calculated from the relative humidity, h_r (%), and the saturation vapour pressure of pure water over liquid water, P_{sat} (Nm^{-2}) :

$$h = h_r (P_{sat}/P_0) / (P/P_0)$$

$$\begin{aligned} \log_{10}(P_{sat}/P_0) = {} & 10.79586\,(1-(T_{01}/T)) \\ & - 5.02808 \log_{10}(T/T_{01}) \\ & + 1.50474e^{-4}\,(1-10^{-8.29692((T/T_0)-1)}) \\ & - 0.42873e^{-3}\,(10^{4.76955(1-(T_{01}/T))}-1) \\ & - 2.2195983 \end{aligned} \qquad \textbf{(C.4)}$$

where T_{01} is the triple-point isotherm temperature with the exact, internationally agreed value of 273.16K.

The overall attenuation factor, α (Npm $^{-1}$), is calculated from the addition of Equations C.1 and C.2 :

$$\alpha = \alpha_{cr} + \alpha_{vib,O} + \alpha_{vib,N} \qquad \textbf{(C.5)}$$

$$\begin{aligned} \alpha = {} & f^2 \{1.84e^{-11}(P_0/P)(T/T_0)^{1/2} \\ & + (T_0/T)^{5/2} [\, (1.278e^{-2} \frac{e^{-2239.1/T}}{f_{r,O}+(f^2/f_{r,O})}) \\ & + (1.068e^{-1} \frac{e^{-3352/T}}{f_{r,N}+(f^2/f_{r,N})}) \,] \} \end{aligned} \qquad \textbf{(3.3)}$$

Bass et al have stated that the algorithm is accurate to +/- 5% over the temperature range 273.15°K-313.15°K; the range of relative humidity 0-100%; the range of frequencies from 50Hz to 10MHz when the pressure is 1 atm; and for pressure from 1 atm down to a few hundredths of an atmosphere [3].

APPENDIX D

Finite Element Analysis Interface

General Overview

This appendix describes the basic input and output software routines, written by Bennett [114], which act as an interface to the finite element analysis code. The finite element package employed to investigate the different aspects of behaviour for 1-3 piezocomposite transducer structures is ANSYS [113]. The package was run on a SUN Sparc 10/51 workstation, running Solaris 1.1. Bennett has developed software processing routines for static, modal and harmonic analysis. This Thesis has exclusively used harmonic analysis and the following discussion applies only to this type of analysis.

The software interface comprises of three parts : a standard file which contains all the possible composite transducer structures available for analysis; a user defined input file to select the transducer components from the standard file; and a standard output file. Each of these components will be discussed in the following sections.

Standard Input File

This file must have the extension '*.tharm*' to designate that it is to be used in harmonic analysis. The layout of the file can be split into three sections : basic composite transducer structure; matching layer components and backing block parameters. The basic composite transducer block must always be accessed, but the remaining two sections are options. Each of these sections contains a selection of user definable parameters, with each having a pre-defined default value. An example of this file structure is shown in Example D-1.

The initial section, preceding '*>matching layer*' enables the user to define the basic composite transducer structure. The fundamental components for this part enable the

user to input the following information :

mc - ceramic material
mp - polymer material
md - damping within polymer
sf - start frequency (MHz)
ef - end frequency (MHz)
nf - number of frequency steps
im - meshing
ir - source/load resistance

Input from the user defined file, detailed later, will define the height, ceramic pillar width and width of quarter symmetry cell. From this information the basic quarter symmetry section of the 1-3 piezocomposite will be defined.

The matching layer section consists of two sections : for either a single or double matching layer combination. '*>matching layer*' defines the first layer, that is the layer bonded onto the transducer front face. '*>double layer*' defines the outer second layer if required. For both layers the user has three parameters to define :

ml - thickness of first layer
mm - material type for first layer
dm - damping in layer
dl - thickness of second layer
md - material type for second layer
dd - damping in layer

The section, '*>backing block*', enables the damping at the rear face of the transducer to be defined. Again the user must supply information regarding the backing block :

bb - backing block thickness
mb - backing block material
db - level of damping in backing material

The final section initiates the ANSYS code and defines the frequency range and source/load resistance for the analysis.

```
/title, VF %vf% AR %ar% MC %mc% MP %mp%
#mc 1
#mp 1
#nf 170
#sf 0.1e6
#ef 1.8e6
#md 1e-8
#im 2
#ir 50

ceramic,1,mc
ancilly,2,mp
mp,damp,mp,md
k
k,2,,c2
k,3,,t2
kgen,2,all,,,c2
kgen,2,1,3,1,t2

<complete height
height=h2
/com,Defining half-height model
imesh=im*2
<end
>complete height
height=h2*2
imesh=im*2
/com,Defining complete-height model
>end

kgen,2,all,,,,,height
l,5,14,imesh
esiz,,im
cvol,1
vatt,1,,1
vmesh,1
cvol,2
cvol,4
cvol,5
vatt,2,,2
vmesh,2,4
vnext=5
knext=19

>matching layer
/com,Defining the matching layer
#ml 0.1e-3
#mm 2
#dm 4.0e-7
height=height+ml
ancilly,3,mm
mp,damp,3,dm
kgen,2,10,18,1,,,ml
cvol,10
cvol,11
cvol,13
cvol,14
vatt,3,,3
vmesh,5,8
knext=28
vnext=9
cmu=amu
>end

>double layer
/com,Defining the second (outer) matching layer
#dl 0.1e-3
#md 2
#dd 4.0e-7
height=height+dl
ancilly,8,md
mp,damp,8,dd
kgen,2,19,27,1,,,dl
cvol,19
cvol,20
cvol,22
cvol,23
vatt,8,,8
vmesh,9,12
knext=37
vnext13
cmu=amu
>end

>backing block
/com,Defining the backing block
#bb      1.0e-3
#mb      1
#db      1.0e-3
ancilly,4,mb
mp,damp,4,db
*set,bade,bz*bz*250.0
mp,dens,4,bade
kgen,2,1,9,1,,,-bb
l,knext+4,5,eb
bvol,knext,1
bvol,knext+1,2
bvol,knext+3,4
bvol,knext+4,5
vatt,4,,4
vmesh,vnext,vnext+3
>end

nsel,s,loc,x,0.0
nsel,a,loc,x,t2
dsym,symm,x,0
nsel,s,loc,y,0.0
nsel,a,loc,y,t2
dsym,symm,y,0

stan,1,10,height
fharm,nf,sf,ef,ir
```

Example D-1 : Standard Input File Structure

User Defined Input File

This file contains the name of the '*.tharm*' file to be used, the output file name and the specifications of the composite transducer to be analysed. The structure of the file is demonstrated in Example D-2, where four consecutive runs have been defined. The '*&*' command signifies the end of the user parameters for one run. The runs defined in this Example are for an unmatched and unbacked composite, '*comp*', for a double matching layer, '*double*', a single matching layer, '*match*', and for a damped device, '*back*'. The mnemonics correspond with inputs in standard input file.

```
t h sqrcmp
        comp
        pa 3
        vf 10
        ar 0.07
        he 2.56e-3
        mc 1
        mp 1
        nf 60
        sf 0.2e6
        ef 1.0e6
        tm complete height
        &
 t h sqrcmp
        double
        pa 3
        vf 20 40 10
        ar 0.088
        he 2.73e-3
        mc 1
        mp 1
        nf 60
        sf 0.2e6
        ef 1.0e6
        tm complete height
        tm matching layer
        ml 0.5e-3
        mm 10
        dm 4.0e-7
        tm double layer
        dl 0.2e-3
        md 16
        dd 8.0e-7
        &
```

```
t h sqrcmp
        match
        pa 3
        vf 10
        ar 0.19
        he 2.5e-3 3.0e-3 0.25e-3
        mc 1
        mp 1
        nf 60
        sf 0.2e6
        ef 1.0e6
        tm complete height
        tm matching layer
        ml 0.5e-3
        mm 10
        dm 4.0e-7
        &
 t h sqrcmp
        back
        pa 3
        vf 30
        ar 0.098
        he 2.80e-3
        mc 1
        mp 1
        nf 60
        sf 0.2e6
        ef 1.0e6
        tm complete height
        tm backing block
        bb 40e-3
        mb 4
        db 1e-8
        &
```

Example D-2 : Example of a user defined input file

The command '*tm*' enables the chosen option from the standard file. The user must then set the parameters for their chosen option as defined in the standard input file. In the

second and third runs two parameters have been defined by three values, where these correspond to a start value, end value and step size. The software will generate a loop and sequentially initiate ANSYS for each value in the range. The file begins by defining six primary parameters for use by the software program which will produce the ANSYS code:

t h filename	defines harmonic analysis using the '*.tharm*' file defined by filename as the standard input file
filename	six character results filename
vf	volume fraction (%)
pa	defines how the quarter symmetry section is to be defined, in this case '3' requires the height and aspect ratio as inputs
he	height (mm)
ar	aspect ratio (ceramic pillar width-to-height)

A software program, '*probat*', must be called to produce the ANSYS code from the user defined parameters. This file is simply called through the command :

probat 'user defined input file'

This program will sequentially run through the commands in the '***user defined input file***' and initiate each ANSYS run.

Standard Output File

The results from the finite element analysis will be processed into column format. The results filename has been defined by the user. The structure of the output file is given in Example D-3, where the first 7 lines are comments to enable the user to identify the particular ANSYS run. The second line states the volume fraction, aspect ratio and constituent materials used in the analysis. Lines 4 - 7 enable the user to identify the prominent features predicted by the analysis : maximum impedance, minimum insertion loss, maximum transmission sensitivity and maximum reception sensitivity. The column format adopted for the results file enables simple integration of the data into graphical packages.

```
# Impedance analysis produced by ANSYS 5.0A
# Processing Square VF 50 AR 0.185 MC 1 MP 1
# Complete sensitivity and efficiency measurement
# Maximum Impedance =  124.05
# Minimum Insertion Loss =  66.16
# Maximum TX Sensitivity =  130.69
# Maximum RX Sensitivity =  62.07
 0.200  110.05  -89.3   0.914  1.55e-01        178.6   67.15  98.43  35.88
 0.227  108.77         -89.2  0.916  1.63e-01         178.3  68.03  99.94  36.11
 0.253  107.57         -89.0  0.919  1.73e-01         178.0  68.90  101.4  36.39
 0.280  106.42         -88.8  0.921  1.85e-01         177.6  69.79  102.8  36.70
 0.307  105.27         -88.5  0.925  2.01e-01         177.2  70.73  104.3  37.06
 0.333  104.10         -88.1  0.928  2.22e-01         176.6  71.73  105.9  37.48
 0.360  102.86         -87.6  0.932  2.51e-01         175.9  72.82  107.6  37.95
 0.387  101.49  -86.9  0.937  2.91e-01        174.9   74.06  109.6  38.50
 0.413  99.89          -85.7  0.941  3.52e-01         173.4  75.49  111.8  39.14
 0.440  97.89          -83.6  0.947  4.54e-01         171.0  77.23  114.5  39.87
 0.467  95.08          -79.3  0.952  6.53e-01         166.1  79.49  118.2  40.73
 0.493  90.46          -66.5  0.959  1.18e+00         152.8  82.83  123.9  41.76
 0.520  84.91          -0.1   0.965  2.46e+00         85.5   86.85  130.6  43.00
 0.547  93.49           58.0  0.973  1.04e+00         26.2   84.11  123.6  44.55
 0.573  100.53  68.0   0.981  5.56e-01        14.3   82.60  118.6  46.56
 0.600  106.49  69.0   0.990  3.68e-01        9.8    82.40  115.4  49.34
 0.627  113.07  63.1   0.998  2.71e-01        7.5    83.40  113.1  53.63
 0.653  122.31  28.5   0.977  2.12e-01        6.0    86.23  111.3  61.08
 0.680  120.47  -58.9  0.954  1.72e-01        5.1    83.85  109.9  57.79
 0.707  115.02  -77.8  0.930  1.43e-01        4.4    79.90  108.6  51.11
 0.733  112.00  -83.1  0.906  1.22e-01        3.8    77.32  107.6  47.02
 0.760  110.02  -85.4  0.881  1.06e-01        3.4    75.38  106.6  44.09
 0.787  108.58  -86.7  0.856  9.24e-02        3.0    73.81  105.8  41.80
 0.813  107.45  -87.4  0.830  8.17e-02        2.8    72.48  105.0  39.90
 0.840  106.53  -87.9  0.804  7.28e-02        2.5    71.31  104.3  38.27
 0.867  105.76  -88.3  0.778  6.52e-02        2.3    70.26  103.6  36.84
 0.893  105.08  -88.5  0.752  5.88e-02        2.1    69.31  103.0  35.55
 0.920  104.48  -88.7  0.725  5.33e-02        1.9    68.44  102.5  34.38
 0.947  103.95  -88.8  0.698  4.84e-02        1.8    67.63  101.9  33.30
 0.973  103.46  -88.9  0.671  4.42e-02        1.7    66.87  101.4  32.30
 1.000  103.01  -89.0  0.644  4.04e-02        1.5    66.16  100.9  31.36
```

Example D-3 : Column format of the standard output file

There are nine columns which contain results generated by the finite element analysis:

Column 1	frequency (MHz)
Column 2	magnitude of the impedance in decibels relative to 1 $\Omega.mm^2$
Column 3	phase angle of the impedance in degrees from -180° to 180°
Column 4	surface dilation quality
Column 5	magnitude of the average displacement in nanometers at the surface plane per unit volt that exists between the electrodes
Column 6	angle of the average displacement at the surface plane in degrees -180° to 180°
Column 7	reciprocity parameter of the transducer in decibels relative to 1.0
Column 8	transmit sensitivity (S_{TX}) in decibels relative to 1$\mu Pa.V^{-1}$
Column 9	receive sensitivity (S_{RX}) in decibels relative to 1$\mu Pa.V^{-1}$

APPENDIX E

Deconvolution Algorithms Implemented

Minimum Delay Wavelets

The minimum delay wa*velet theorem* states that the energy of a minimum delay wavelet is more concentrated at the 'front end' than any other wavelet in *the class of all* wavelets with the same autocorrelation [137]. That is, the major concentration of energy in a minimum delay sequence occurs as early as possible in the sequence and is not delayed any more than necessary to fit the given autocorrelation. For that reason, a minimum delay sequence is often called a 'front loaded' sequence. Figure E-1 illustrates a digital sequence which represents a minimum delay wavelet. Here, as the sequence progresses the magnitude of each successive term is reduced, i.e. $|a_0| > |a_1| > |a_2|$ etc.

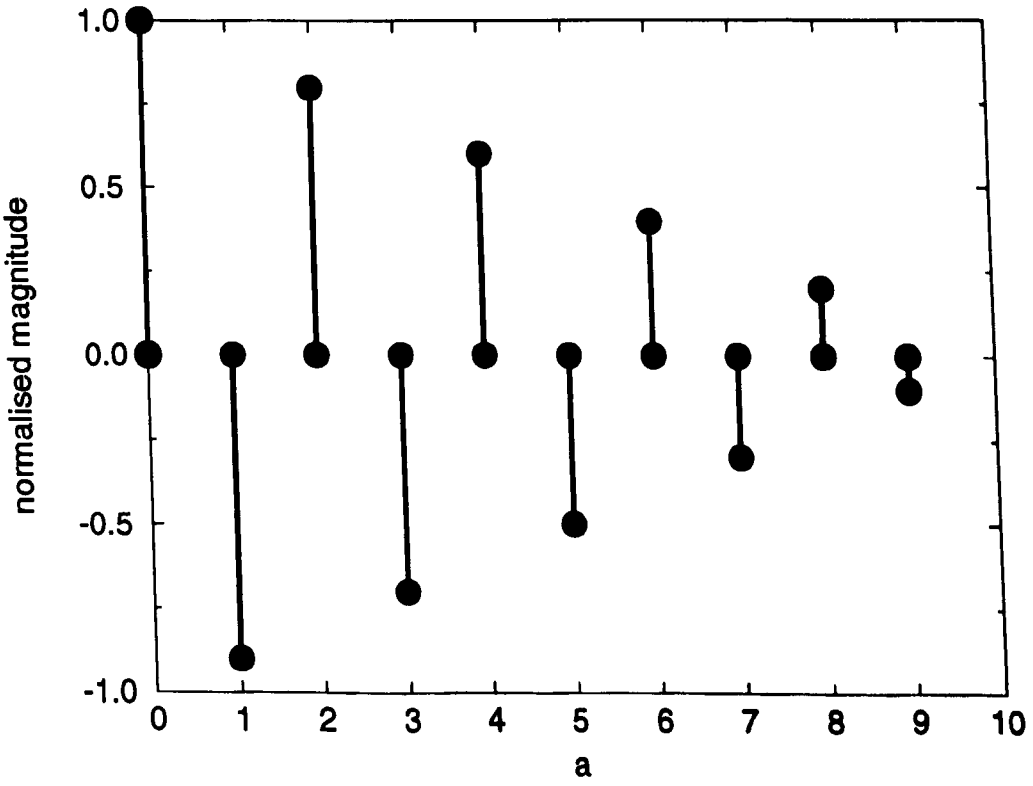

Figure E-1 Digital waveform sequence depicting minimum delay characteristics

The Linear Model of Deconvolution

The two deconvolution algorithms [128] applied to produce the desired pulse compression from the laser generation / piezocomposite detection hybrid system, utilised in Chapter 6, are described. The adaptive approach selected was the 1D Modified Least Means Squared (MLMS) algorithm, which is based on the Adaptive Line Enhancer (ALE) configuration [130]. The nonadaptive technique chosen was the Minimum Entropy Deconvolution (MED) algorithm [131]. This is an iterative algorithm, which is computationally excessive and consequently very slow. In the following discussion, the linear model of the deconvolution shown in Equation E.1 will be utilised. Where, $y(t)$ represents the real signal, $h(t)$ is the impulse response of the system, $x(t)$ is the reflectivity function and $b(t)$ is additive white Gaussian noise. The deconvolution operation attempts to recover the reflectivity function, containing information concerning the internal structure of the sample under investigation, from the acquired real signal.

$$y(t) = h(t) * x(t) + b(t) \tag{E.1}$$

Modified Least Means Squared (MLMS)

The MLMS algorithm is an adaptive technique in which $h(t)$ is not known [130]. The ultrasonic waveform is assumed to be the result from an auto-regressive (AR) system, where the innovation series is represented by the reflectivity signal. A white Gaussian nature for the reflectivity function is assumed. The mathematical model for this technique is shown in Equation E.2, where p is the order of the model and d is called the prediction delay.

$$y_{n+d} = -\sum_{i=1}^{p} a_i y_{n-i} + x_n \tag{E.2}$$

The chosen AR model assumes that the unknown wavelet is minimum phase, where the a_i terms correspond to the AR parameters that describe this unknown wavelet. The objective of the adaptive predictive algorithm is to predict the AR parameters as the wave evolves inside the sample. Once achieved, the algorithm will be able to compute both the estimated and reflectivity signals.

The least means squared technique will be utilised to estimate the AR vector. From Equation E.2 the autocorrelation matrix of the real signal, R_{yy}, can be described by Equation E.3. A represents the autoregressive vector and $P_y(d)$ is given by Equation E.4.

$$R_{yy}A = P_y(d) \tag{E.3}$$

$$p_y(d) = E(y_{k+d}\,Y(k)) \quad with \quad Y'(k) = [y_k, y_{k-1}, \ldots, y_{k-p+1}] \tag{E.4}$$

The autoregressive vector, A, can then be determined in an iterative manner with the use of a gradient-type algorithm. If an arbitrary vector is chosen for the first AR vector, A_0, then $A(k)$ can be given by Equation E.5, where μ is called the convergence parameter and lies between 0 and 1.

$$A(k+1) = A(k) + \mu[y_{k+d} - \hat{y}_{y+d}]\,Y(k) \tag{E.5}$$

The performance of this algorithm depends upon the correct selection of the order, p, and the convergence parameter, μ. These parameters are entirely dependant on the data, although algorithms exist to assist in the choice of these values [137].

Minimum Entropy Deconvolution (MED)

This algorithm is adaptive, computationally fast and requires no apriori knowledge of the waveform. If the wavelet exhibits a minimum phase characteristics, good resolution performance can be achieved. The algorithm is relatively straightforward to use and requires only precise adjustment of the convergence parameter.

The nonadaptive MED technique, proposed by Wiggins, assumes a non-Gaussian reflectivity function and utilises an optimisation technique to recover both the amplitude and phase information [131]. For this reason the algorithm is more robust to non-minimum phase wavelets, when compared to most of the classical deconvolution algorithms. The algorithm requires the spatial invariance assumption to obtain the best resolution along the wavelet. This approach will produce a solution when the desired signal consists of a few large spikes (delta functions) and an group of sample signals exists for which the time separations between the spikes differ while the source wavelet shape remains constant. One significant advantage of the MED approach is that is addition to providing signal compression, the noise components are reduced. As the MED operator maximises the spikiness of the output traces, it selectively suppresses frequency bands over which the ratio of coherent signal-to-random noise is lowest and thereby emphasizes those bands in which coherent signals dominate.

The technique obtains the simplest signal which is consistent with the acquired real data signal. The process seeks the smallest number of large spikes separated by near-zero terms, which is equivalent to minimising entropy or maximising the order of the data. This technique does not require a reference wavelet and its solution is computed as the coefficients of an inverse filter of the ultrasonic wavelet. The form of this inverse filter is shown in Equation E.6, where a_k is an approximation to a delta function.

$$\begin{aligned} f_k * y_k &= (f_k * h_k) * x_k + f_k * b_k \\ &= x_k + (a_k - \delta_k) * x_k + f_k * b_k \\ &= \hat{x}_k \end{aligned} \qquad \textbf{(E.6)}$$

Wiggins proposed that the solution for the coefficients of the inverse filter, length of $L+1$, is when the objective function, described in Equation E.7, is maximised. N represents the length of the data set.

$$\frac{\sum_{k=1}^{N} \hat{x}_k^4}{(\sum_{k=1}^{N} \hat{x}_k^2)^2} \qquad \textbf{(E.7)}$$

Maximising this criterion yields the system shown in Equation E.8.

$$\sum_j f_j \sum_k y_{k-j} y_{k-i} = \sum_k u_1(\hat{x}_k) y_{k-i} \quad for\ i = 0,....,L \qquad \textbf{(E.8)}$$

where

$$u_1(\hat{x}_k) = \frac{\frac{1}{N}\sum_m \hat{x}_m^2}{\frac{1}{N}\sum_m \hat{x}_m^4} \hat{x}_k^3 \qquad \textbf{(E.9)}$$

This system is solved in an iterative manner through the computation of $u_1(\hat{x}_k)$. The solution is not necessarily unique, but Wiggins maintains that a useful maximum is always reached.

The MED technique is a nonadaptive approach in the sense that it cannot follow the evolution of the distortion wavelet. An optimum inverse filter is built for each processed signal. They do not require to operate on minimum phase signals. The implementation is very slow, but only requires the adjustment of two parameters : the length of the filter, L, and the number of iterations.